An exploration of host responses to oral and chronic *Toxoplasma gondii* infection

By

Patrick W. Cervantes

A dissertation submitted in partial fulfillment of the requirements for the degree of

Doctor of Philosophy

(Cellular and Molecular Biology)

at the University of Wisconsin-Madison, 2020

Date of final oral examination: 09/18/2020

This dissertation is approved by the following members of the Final Oral Committee:

Laura J. Knoll, Professor of Medical Microbiology and Immunology
Timothy Yoshino, Professor of Parasitology
Nancy Keller, Professor of Medical Microbiology and Immunology
John-Damian Sauer, Associate Professor of Medical Microbiology and Immunology
Andrew Mehle, Associate Professor of Medical Microbiology and Immunology

An exploration of host responses to oral and chronic *Toxoplasma gondii* infection

By Patrick W. Cervantes

Under the supervision of Professor Laura J. Knoll

At the University of Wisconsin-Madison

Thesis abstract

Toxoplasma gondii is a global public health concern and poses a significant health threat as a foodborne illness to humans and animals. Upon exposure, *T. gondii* parasites replicate quickly and disseminate from the intestine throughout the body over acute infection. Host immune pressure causes acute infection parasites to differentiate into slow growing cysts that establish a persistent chronic infection in the brain and muscle tissue of the host. This thesis explores the role of programmed cell death as a host response to a natural acute oral infection, and this thesis measures the host transcriptional response to long-term chronic infection in the brain. We identified the receptor-interacting serine/threonine-protein kinase 3 (RIPK3), an essential component to necroptosis mediated programmed cell death pathway, to have negative impacts on host survival to oral *T. gondii* infection. The detrimental effects of RIPK3 activity on host survival to oral infection were attributed to necroptosis-independent roles. Host survival to an oral *T. gondii* exposure potentially gives rise to chronic infection cysts if parasites are not completely cleared. These chronic infection cysts are thought to reside in the host for its lifetime. We measured the host transcriptional response to long-term chronic infection in the brain and discovered sex specific gene expression responses. Both male and females has similar levels of more abundant gene expression with immune related functions. Interestingly, infected male mice have significantly more less-abundant gene expression compared to infected female mice, but these differences do not result in biological changes to the way the host responds to *T. gondii* infection.

Acknowledgments

I am grateful to my family, friends, and academic advisors who have supported and shared experiences with me throughout my academic career. Without this network, none of my accomplishments would have been possible. There are several individuals and groups that I would like to thank.

First, I would like to thank my graduate advisor Laura Knoll and the Knoll lab members. As a mentor, Laura has encouraged my creativity, supported my ideas, and challenged my abilities as a scientist. I have learned a tremendous amount being a part of your lab, and the environment you create motivates me to inspire others throughout my future career as a scientist. Thank you, Laura. To all of the past and present Knoll lab members. Thank you for being the best colleagues and friends I could have asked for. The sense of community and free exchange of ideas with the Knoll group is the type of atmosphere I wish to foster in my workplace. Thank you, Knoll lab group.

Second, I would like to thank my family for believing in me and giving me the confidence to pursue my dreams. My dad, Ron, has been a source of intellectual and philosophical stimulation. My mom, Sherry, has reinforced my pursuit of happiness even though it has taken me away from home. My siblings – Adam, Erica, and Katie – for being there through thick and thin. I am also thankful for Mario, Jenny, and their children, Liora and Marc, for being a part of my life.

Finally, I would like to thank Rachel and our dogs, Bruce and Milo. I am so grateful Bruce introduced me to Rachel and Milo. Rachel is the most thoughtful, selfless, and patient person I have ever met. Rachel and our dogs inspire me to be a better person.

Table of contents

List of figures

List of tables

Chapter 1

Overview of host responses to oral *Toxoplasma gondii* infection and the effects of chronic infection

Patrick W. Cervantes[1] and Laura J. Knoll[1]*

[1]Department of Medical Microbiology and Immunology, University of Wisconsin-Madison, Madison, WI

* Corresponding author ljknoll@wisc.edu

Running title: Acute oral and chronic *T. gondii* infection

This chapter will be submitted for publication in the Journal of Microbiology and Molecular Biology Reviews

Author contributions: PWC wrote the manuscript and designed the figures.

Abstract

Toxoplasma gondii is naturally acquired by consuming food or water contaminated with infectious tissue cysts or oocysts. Toxoplasmosis poses a significant health threat as a foodborne illness to humans and animals. The gut mucosal immune system must form a robust and balanced pro-inflammatory response to protect the host throughout acute infection and facilitate host survival into a chronic infection. If the acute pro-inflammatory response is too weak or too strong, then the host will succumb to parasite overgrowth or severe tissue immunopathology, respectively. The host response to acute infection causes *T. gondii* parasites to differentiate into chronic cysts that reside in muscle and brain tissue. Once chronic infection is reached, host inflammatory responses must be maintained above a normal baseline to prevent host death from cyst reactivation and uncontrolled parasite replication. As a consequence, a host with a latent *T. gondii* infection displays a state of chronic inflammation. This review highlights the protective host response, coordinated by the gut mucosal immune system from a natural oral *T. gondii* exposure. In addition, this review discusses the physiological impacts of chronic inflammation on the host with a latent *T. gondii* infection.

Introduction

Toxoplasma gondii infection is a global public health concern, with an average prevalence estimated at 30% among the entire human population (1). The three most common routes of *T. gondii* transmission are: i.) congenital infection from mother to fetus, ii.) ingestion of tissue cysts from undercooked meat, iii.), and consumption of oocysts from contaminated food or water (2). The impact of natural oral exposure to *T. gondii* in susceptible humans makes it the second leading cause of death among foodborne illnesses and is estimated to cost $3 billion dollars annually, with 11,000 quality-adjusted life-years lost per year in the United States (1). Beyond humans, *T. gondii* poses a significant health threat to domestic animals, wildlife, and livestock through economic losses (1). Typically, a healthy host is asymptomatic after infection,

with occasional flu-like symptoms, but congenital or immunocompromised individuals can have more severe disease outcomes, like stillbirths and fatal encephalitis (3) Currently, there are no vaccines to protect against acute toxoplasmosis or treatments for chronic infection (4).

Felines are the definitive host of *T. gondii* and facilitate completion of the parasite's sexual life cycle by shedding environmentally resistant and highly infectious oocysts. All other warm-blooded animals, including humans, are *T. gondii* intermediate hosts (1). In an intermediate host, *T. gondii* can differentiate into two distinct developmental stages. In the acute infection stage, parasites replicate asexually as a rapidly dividing tachyzoite. In the chronic infection stage, parasites replicate slowly as a bradyzoite, forming a chronic tissue cyst. Acute parasites are naturally exposed to the host in the intestine following a natural oral route of infection. There are three models that *T. gondii* uses to cross the intestine epithelium and disseminate throughout the body: i.) passage between tight junctions, ii.) transcellular crossing, and iii.) a "trojan horse" mechanism where immune cells are actively infected or phagocytose parasites and travel throughout the body (5). From the moment of exposure, the gut mucosal immune system mounts a protective innate immune response that causes *T. gondii* to differentiate from tachyzoites to bradyzoite cysts, a transition that can be measured by transcriptional and epigenetic changes (3, 6, 7). Bradyzoite cysts reside in immune-privileged sites like muscle and the central nervous system (CNS), which includes the retina, spinal cord, and brain (6, 7). The central dogma of chronic *T. gondii* infection speculates that bradyzoite cysts are quiescent and reside in the host for its lifetime (8).

The goal of this review is to summarize our current understanding of the physiological effects of acute oral and chronic *T. gondii* infection on the host. This review will focus on the fine-tuned process of the gut mucosal immune response and its role in supporting host survival through the acute phase of oral infection and into a chronic infection. The review will conclude with the impacts of chronic infection on the host.

Parasite dissemination and intestine mucosal immune system

The precise mechanisms and cues for *T. gondii* parasites to exit infectious bradyzoite cysts or oocysts after consumption remain unknown. It is known that following ingestion, *T. gondii* uses gliding motility to propel itself between and within intestinal epithelial cells (IECs) to establish infection in the underlying lamina propria (LP) tissue of the distal small intestine (5). Parasite dissemination throughout the body is facilitated by entry into blood and lymph vessels within the intestine. Alternatively, *T. gondii* can reach other organs by the "trojan horse" mechanism. Parasites can be found in IECs 30 minutes post oral infection, but quickly reside in the LP thereafter (9). Within 2 to 3 days, parasites have spread from the LP to peripheral lymphatic tissue. By 1 week, parasites can be found in the lung, liver, heart, and the CNS (10). Mechanisms of *T. gondii* mobility and dissemination have been extensively reviewed elsewhere (10).

The gut mucosal immune system is the first to interact with *T. gondii* upon peroral exposure with tissue cysts or oocysts. The IEC layer is composed of a variety of cell types (e.g. enterocytes, Paneth cells, microfold cells, and goblet cells) that create a physical and chemical barrier between the host and the intestinal lumen (11, 12). Within the IEC layer resides intraepithelial lymphocytes that are responsible for intestine homeostasis and inflammatory responses to infection (13). The IECs are supported by the LP which is composed of connective tissue, blood vessels, lymphatic ducts, and a myriad of resident immune cells that mediate innate and adaptive immunity. These include dendritic cells (DCs), macrophages, conventional CD4+ and CD8+ T cells, B lymphocytes, and innate lymphoid cells (ILCs) (14, 15). Peyer's patches are spread throughout the intestinal LP and contain germinal centers for T and B cells (16). These elements make up the gut mucosal immune system responsible for host protection against oral *T. gondii* infection (Fig. 1).

Recognition and host survival

Host survival to oral *T. gondii* infection depends on a robust and balanced innate immune response. Pattern recognition receptors (PRRs) in the gut mucosal immune system are an essential component to host resistance. These receptors identify pathogen- or damage-associated molecular compounds (PAMPs or DAMPs, respectively) and trigger inflammatory signaling cascades that activate and recruit immune cells in a coordinated effort to curb infection. The pro-inflammatory consequences of *T. gondii* infection must be regulated in order to prevent severe tissue damage and host death. The following section will focus on the molecular mechanisms that promote host survival, the cell types that induce a protective innate immune response, and the factors that prevent inflammatory-mediated pathology after oral *T. gondii* infection.

Molecular mechanisms of survival

The intestine epithelium and mucosal immune system are the first to interact with *T. gondii* parasites after ingestion. These cells harbor toll-like receptors (TLRs) which are a family of PRRs that recognize PAMPs and stimulate innate immunity as a consequence. One TLR that is particularly relevant for the discussion of *T. gondii* infection is TLR-11/12. Unlike humans, mice have functional TLR-11/12 genes that specifically recognize *T. gondii* profilin, a surface protein critical to parasite invasion. Activation of TLR-11/12 recruits the signaling adaptor, myeloid differentiation primary response 88 (MYD88), to induce interleukin 12 (IL-12) which stimulates interferon-gamma (IFN-γ) expression. The MYD88, IL-12, and IFN-γ signaling axis is vital to host survival. Hosts deficient in MYD88 or IL-12 fail to control parasite replication and die from sublethal *T. gondii* infections (17-20). IFN-γ is also an important molecule in host survival because it is the downstream product of MYD88 signaling, and IFN-γ perturbations lead to uncontrolled parasite replication and host death to sublethal infections (21, 22). The power of IFN-γ-mediated host protection rests in its ability to stimulate a multitude of host genes that

activate immune cells, promote cell proliferation, and induce mechanisms that clear intracellular pathogens (23-25).

Multiple cell types, including non-immune cells, contribute to pathogen clearance through IFN-γ stimulated pathways (23). The precise mechanisms that regulate intracellular defenses to *T. gondii* have been described elsewhere (24, 25). Briefly, IFN-γ can stimulate cells to produce immunity-related GTPases (IRGs) and guanylate-binding proteins (GBPs) that disrupt *T. gondii* membranes and facilitate pathogen clearance. The molecular mechanisms of IRG and GBP localization to parasite membranes remains unclear, but ubiquitination is likely one tool to distinguish *T. gondii* from the host. In addition, IFN-γ signal transduction causes resident intestine macrophages and circulating monocytes to differentiate into an inflammatory subtype. These immune effectors can produce nitric oxide (NO) to increase parasite degradation. Interestingly, mice lacking NO have significantly improved acute survival, even with a higher parasite burden relative to wild type mice, after a lethal oral *T. gondii* infections (26, 27). An increase in host fitness in NO deficient mice was attributed to reduced tissue pathology, but these mice succumb to parasite burden in the early stages of chronic infection (28). Two conclusions can be drawn from these data: first, NO overproduction causes detrimental immunopathology, and second, the pleiotropic effects of IFN-γ that are NO-independent are sufficient for host protection over acute infection but are necessary during chronic infection. The protective effect of IFN-γ signaling in chronic infection is evident in infected mice treated with anti-IFN-γ antibodies. After antibody assisted depletion of IFN-γ, chronically infected mice die from complications due to cyst reactivation and uncontrolled parasite replication in CNS (29). Control of parasite replication during acute infection is also enhanced by the inflammatory cytokine, tumor necrosis factor-alpha (TNF-α), in combination with IFN-γ (30, 31). Similar to NO, TNF-α is dispensable during acute infection, but required for host survival in chronic infection (32). These studies provide strong evidence for the essential role IFN-γ plays in host defense.

The gut microbiome also plays a critical role in host survival by promoting a protective innate immune response through the MYD88, IL-12, and IFN-γ axis. The inflammatory response generated upon oral *T. gondii* infection reduces the intestinal antimicrobial barrier and creates a shift in gut bacteria from a mostly gram-positive, non-pathogenic species to a largely gram-negative, pathogenic species (33, 34). This process of gut dysbiosis increases intestine permeability and allows pathogenic gut bacteria to interact with mucosal PRRs to promote a protective immune response. The protective effect of gut bacteria was highlighted in a study that compared the survival of TLR-11/12 null (TLR-11/12$^{-/-}$) mice when challenged with oral or intraperitoneal (IP) *T. gondii* infections. Gut bacteria improved mouse survival in oral, but not IP infection (35). This observation demonstrated how the microbiome promotes a protective immune response in a TLR-11/12-independent manner, which is particularly relevant to humans who have a pseudo TLR-11/12 gene. Moreover, gut bacteria failed to direct its protective effects in MYD88$^{-/-}$ mice after oral infection (35). This establishes MYD88 as a central mediator to protective host immunity against oral *T. gondii* exposures through multiple TLRs. The molecular mechanisms of host survival are summarized in Figure 2.

Immune cell effectors

Host survival to *T. gondii* infection is a coordinated response from a variety of cell types to generate IFN-γ-dependent resistance. Macrophages, IECs, and DCs produce IL-12 which polarizes CD4+ T cells to a T helper type 1 (Th1) subset that express IFN-γ. Stimulation with IL-12 also activates CD8+ T cells and ILCs to upregulate IFN-γ (36-39). Both Th1 and activated CD8+ T cells play complementary roles in IFN-γ production and host protection. However, dual deletion of these activated T cells is detrimental to host survival during acute infection because IFN-γ is severely limited (40). The function of ILCs in oral *T. gondii* infection is complex, unclear,

and reviewed extensively by another group (15). Importantly, ILCs overlap with the function of Th1 and effector CD8+ T cells, which provides the host with multiple layers of protection.

Inflammatory monocytes are a multifaceted group of cells important in acute oral *T. gondii* infection. They have the potential to serve a pro- or anti-inflammatory role (41). Along with neutrophils, inflammatory monocytes are among the first immune cells recruited to the LP after *T. gondii* recognition (42, 43). Inflammatory monocytes can differentiate into macrophages and dendritic cells upon localization to sites of infection (44-46). Dendritic cells are considered to be the primary producers of IL-12, but their deletion results in delayed IFN-γ kinetics and host survival (42, 47, 48). Mouse models that lack inflammatory monocyte recruitment fail to control *T. gondii* infection and die from severe tissue damage after a sublethal oral dose (46, 49, 50). However, the increase in susceptibility was credited to neutrophil-mediated tissue damage, because wild type (WT) mice with neutrophil depletion survive after the same sublethal dose (49). Neutrophils produce other pro-inflammatory cytokines, like IL-1β, IL-18, and IL-17, which can enhance immune activity and cause tissue damage (51). The consequences of IL-1β, IL-18, and IL-17 on host survival to acute *T. gondii* infection are discussed below. Interestingly, after a lethal high dose oral infection, inflammatory monocytes display anti-inflammatory elements through neutrophil modulation and tissue preservation (50). These results illustrate a twofold nature of inflammatory monocytes: one that degrades parasites and another that mediates tissue pathology. A more detailed account of the molecular mechanisms used by inflammatory monocytes in the context of *T. gondii* infection is comprehensively reviewed elsewhere (42).

The cellular responses to *T. gondii* infection form a positive feedback loop that circulates between recognition, immune effector activation, and inflammatory outputs (Fig. 3). Under normal circumstances, a healthy host generates a pro-inflammatory response that curbs parasite growth and enables host survival. However, immune regulation is critical in this process to avoid severe tissue damage and death.

Immune regulation and pathology

The gut mucosal immune system is constantly challenged by non-self-antigens, so immune tolerance mechanisms must be in place to prevent a state of perpetual immune activation. Regulatory T cells (Tregs) are an essential component of immune tolerance and tissue homeostasis. They limit excessive inflammatory responses in antigen presenting cells and effector T cells (52). Immune tolerance must be broken in order to produce a protective immune response against pathogens. In *T. gondii* infection, Tregs are downregulated from inflammatory responses, Th1 expansion, and subsequent IL-2 deprivation (53, 54). This process is vital to induce optimal host defenses. For example, when Treg populations are upheld by IL-2 supplementation, the host is unable to produce effective IFN-γ resistance and dies due to parasite burden (53). In a healthy host, Treg population loss is transient and repopulation is necessary to prevent lethal pathology from excessive pro-inflammatory responses (53, 55).

Several cellular mechanisms are in place to repopulate Tregs. Retinoic acid (RA), a Vitamin A metabolite, and transforming growth factor-beta (TGF-β) are two molecules expressed by a variety of cell types that regenerate Tregs and restores immune tolerance (56, 57). However, RA and TGF-β are also capable of inducing effector T cell populations (57, 58). The duality of these molecules complicates their function in *T. gondii* infection, but Treg populations are clearly an important cell type that helps the host recover from the pro-inflammatory responses in acute infection.

The anti-inflammatory nature of Tregs is accomplished, in part, by IL-10 (59). As an inhibitor of effector immune cell stimulation and inflammatory cytokines production, IL-10 expression is required to prevent catastrophic immunopathology during acute *T. gondii* infection (60, 61). In addition to Tregs, inflammatory monocytes can be programmed into regulatory macrophages that also express IL-10 as well as prostaglandin E2 (PGE2), another molecule

shown to limit effector immune cell activation (42, 62). Specifically, PGE2 from inflammatory monocytes could play a significant role in host protection from neutrophil-mediated damage after oral *T. gondii* infection (49). These results demonstrate there is a delicate balance between a safe and harmful host response.

The early studies of peroral *T. gondii* administration established the factors responsible for generating a pathogenic response that causes severe tissue damage and host death. These detrimental effects were credited to uncontrolled Th1 effector responses and unrestrained expression of IL-12, IFN-γ, TNF-α, or NO (27, 63, 64). Blocking any of these factors significantly improved tissue pathology scores and extended host life. However, the shift to a pathogenic immune response can be more directly attributed to advanced immune stimulation by bacterial imbalances in the gut after an oral *T. gondii* infection. This is most clearly represented in gnotobiotic mice and mice pre-treated with antibiotics before an oral infection (65, 66). These gut-bacteria-free mice had reduced intestine pathology and significantly lower IFN-γ and TNF-α levels. Consequently, host survival was improved even though there was no difference in parasite burden. This suggests the fatal immune pathogenesis that occurs in colonized mice is independent of parasite control and a consequence of unregulated immune stimulation from intestine dysbiosis.

The peroral route of *T. gondii* infection is a unique model to study the cellular and molecular mechanisms that trigger a break in immune tolerance and the methods that assist immune recovery. Interestingly, the physiological consequences of an oral *T. gondii* challenge cause similar gut dysbiosis and pathological responses observed in inflammatory bowel diseases (67). This highlights the value of oral *T. gondii* infection as a model to study autoimmune disorders that are particularly relevant to humans.

Programmed cell death and inflammation

Lytic programmed cell death pathways could augment host immunity out of tolerance and into the realm of disease. Necroptosis and pyroptosis are two lytic programmed cell death pathways that release DAMPs, which promote inflammation (68). The molecular mechanisms of necroptosis and pyroptosis are briefly described below, and more detailed analyses have been extensively reviewed (69, 70). These pathways have evolved to control viral, bacterial, and parasitic infections by destroying replicative niches (68). However, when unregulated, these lytic cell death pathways have the potential to be the tipping point that suddenly brings about catastrophic host pathology.

Central to necroptosis is the receptor-interacting serine/threonine-protein kinase 3 (RIPK3) and its downstream substrate, mixed lineage kinase domain-like pseudokinase (MLKL), which ultimately compromises cellular integrity and DAMPs are released to promote inflammation. Without RIPK3 or MLKL, the necroptosis pathway is inhibited (71-73). There are several lines of evidence that support the detrimental role of necroptosis in host physiology. These come from the observations that RIPK3$^{-/-}$ mice have reduced pathology and organ injury after viral or bacterial ligand exposure (71, 72, 74, 75). However, the direct effects of necroptosis in these studies can be difficult to interpret because RIPK3 has necroptosis-independent functions in the pyroptosis pathway and kinase-independent activity in inflammatory gene induction (76). The direct impact of necroptosis on host physiology, tissue damage, and survival could be more clearly demonstrated in MLKL$^{-/-}$ mice. This approach is demonstrated in Chapter 3 with MLKL$^{-/-}$ mice, and our evidence suggests that necroptosis does not impact host survival to *T. gondii* infection.

The core inflammatory mediators of pyroptosis are IL-1β and IL-18. A more thorough background on pyroptosis has been described elsewhere (70). Concisely, PRR sense specific PAMPs or DAMPs and assemble a multi-protein complex called the inflammasome. The

inflammasome recruits the enzymes, Caspase 1 and 11 to cleave Gasdermin D, which causes cell permeability. Activation of Caspase 1 and 11 also leads to the cleavage of IL-1β and IL-18 into mature and active forms. Upon release, IL-1β and IL-18 mediate pro-inflammatory cellular responses. The host genes involved in pyroptosis have been studied recently in the context of *T. gondii* infection. Exposure to *T. gondii* has been reported to activate the pyroptosis pathway which controls parasite burden in *in vivo* and *in vitro* models (77, 78). Although there appears to be some controversy over the implications of pyroptosis on host survival to different *T. gondii* infection models. For instance, genetic knockout models and inhibition of pyroptosis effectors, like IL-18, the IL-1β receptor, and its IL-17 product show improved host survival compared to WT mice after oral infection (64, 79-81). On the other hand, mice with deletions in various components of the inflammasome show reduced host survival after IP infection (82-84). The host responses of any given genetic mouse model, like the TLR-11/12$^{-/-}$ mice described above, can show drastically different effects that are dependent on the route of infection. The individual inputs of the genes along the pyroptosis pathway and the effects of pyroptosis on the host could be clarified with the oral infection model, which is biologically relevant and would account for the impact of gut bacteria on mucosal immunity.

There are other cell death pathways, like apoptosis and autophagy, that are also important in pathogen control, but these pathways are considered non-immunogenic. Interestingly, *T. gondii* has developed specific mechanisms to circumvent apoptosis and autophagy pathways to establish infection (85, 86). The majority of studies that investigate apoptosis in relation to *T. gondii* infection occur *in vitro,* and investigation of apoptosis *in vivo* is difficult since genetic knockouts in essential apoptosis genes, like Caspase-3, are developmentally lethal (87). Recent advancements have been made in understanding the effects of autophagy *in vivo* after oral *T. gondii* infection. Autophagy was shown to be an essential process in intestine Paneth cells for tissue homeostasis and host defense to oral *T.*

gondii infection (33). Disruption of the autophagy pathway results in increased host susceptibility and intestine pathology after oral infection. The requirement of autophagy in Paneth cells has significant clinical relevance in humans, observed by correlations between autophagy gene mutations and inflammatory bowel disease occurrences (88).

Chronic infection

The host immune response to acute *T. gondii* infection enables parasite differentiation into bradyzoite cysts that establish a chronic infection. The process of parasite differentiation, from tachyzoites to bradyzoite tissue cysts, can be measured by alternate gene expression profiles and epigenetic changes (6, 7). Bradyzoites produce a highly glycosylated cyst wall, approximately 240 nm thick and between 20 – 70 μm in diameter, that protects the internal parasites against cell-mediated responses (89). Chronic cysts form in smooth muscle tissue and in the CNS, but the majority of chronic infection studies have focused on host-pathogen interactions in the brain. The idea that bradyzoite cysts reside for the lifetime of the host and offer protective immunity from secondary infection has been challenged (8). In addition, it is also believed that bradyzoite cysts are dormant because a healthy host shows no overt symptoms, but it was recently revealed that chronic cysts are dynamic entities (90, 91). The following section will discuss the physiological impacts of chronic *T. gondii* infection on the host.

The CNS is a complicated and vital organ composed of neurons and glial cells. Neurons are primarily responsible for signal transduction, while glial cells offer neuronal support and contribute to innate and adaptive immune responses (5, 92). *T. gondii's* access to the brain is similar to the mechanisms of parasite dissemination during acute infection. *T. gondii* passes the blood-brain barrier through cellular tight junctions, by transcellular crossing, or via the "trojan horse" mechanism. Bradyzoite cysts primarily reside in neurons because they are unable to mount intracellular defenses (93, 94). The CNS was thought of as an immune-privileged site, but glial cells within the CNS are capable of clearing intracellular parasites through innate immune responses, which support the observation that *T. gondii* selectively inhabit neurons (94-

97). The innate immune responses generated from IFN-γ must be maintained throughout chronic infection or else the host dies from uncontrolled parasite growth, cell lysis, and encephalitis (29). The host transcriptional response in the brain shows elevated immune genes throughout acute and long-term chronic infection, which is further discussed in Chapter 2 (6, 98). An elevated immune response that is prolonged for extended periods of time defines chronic inflammation. Generally, chronic inflammation is thought to have negative impacts on host health.

Cachexia is a syndrome defined as a metabolic disorder associated with chronic inflammation that results in muscle and fat loss (99). Mice have higher levels of immune gene transcripts in the brain as well as an elevated, local and systemic, production of inflammatory cytokines throughout chronic *T. gondii* infection (6, 98). Cachexia is a result of *T. gondii* induced chronic inflammation on the mouse host (79, 100, 101). In addition, chronic infection and inflammation trigger prolonged intestinal dysbiosis (100, 102). Considering the fact that the intestinal dysbiosis observed in acute oral *T. gondii* infection leads to intestine pathology, it would be interesting to determine if chronically infected mice with gut microbial imbalances also suffer from intestine pathology. The chronic infection phenotypes on the mouse host are particularly interesting because this is a latent infection that primarily occurs in the brain and has profound effects on host metabolism and gut physiology. This summons the idea of the gut-brain-axis.

The gut-brain-axis entails a bidirectional line of communication between the intestine and CNS. This relationship provides a feedback mechanism when alterations occur in the intestine or brain. For instance, alterations in gut composition have been linked to behavioral changes, like stress or psychological disorders, and vice versa (103, 104). Chronic *T. gondii* infection is associated with behavioral changes, mental disorders, and cognitive diseases (105). However, many of these studies that investigate *T. gondii* effects on the brain are riddled with design limitations and experimental caveats. Since neurons are the primary source of

communication in the brain and most bradyzoite cysts are found within the cerebral cortex and basal ganglia, two regions with executive functions in perception, memory, and behavior (5), it is interesting to speculate the consequences of altered signal transduction in the brain by chronic *T. gondii* cysts.

Conclusion

Toxoplasmosis is a significant health concern for humans, wildlife, domestic animals, and livestock. Although, *T. gondii* infection mainly poses an imminent threat to the immune-compromised or developing fetus. The host response that promotes survival to an acute oral infection is a coordinated response between the gut mucosal immune system and the gut microbiome. This process requires adequate pathogen recognition, immune activation, and pro-inflammatory responses to control parasite replication and promote host survival. Immune regulation is critical to prevent unnecessary tissue damage and host death. The line between a sufficient and disadvantageous immune response is narrow. Uncontrolled lytic cell death pathways could tilt the scales of immune tolerance into disease associated with intestine inflammation and host death after oral *T. gondii* infection
n. However, a balanced immune response enables parasite dissemination and transition to bradyzoite cysts, which promote a chronic inflammatory phenotype that could have negative consequences on host physiology. Ultimately, oral *T. gondii* infection is the biologically relevant model to study the cellular and molecular mechanisms of host innate and adaptive immunity.

References

1. Aguirre AA, Longcore T, Barbieri M, Dabritz H, Hill D, Klein PN, Lepczyk C, Lilly EL, McLeod R, Milcarsky J, Murphy CE, Su C, VanWormer E, Yolken R, Sizemore GC. 2019. The One Health Approach to Toxoplasmosis: Epidemiology, Control, and Prevention Strategies. Ecohealth 16:378-390.
2. Tenter AM, Heckeroth AR, Weiss LM. 2000. Toxoplasma gondii: from animals to humans. Int J Parasitol 30:1217-58.
3. Pittman KJ, Knoll LJ. 2015. Long-Term Relationships: the Complicated Interplay between the Host and the Developmental Stages of Toxoplasma gondii during Acute and Chronic Infections. Microbiol Mol Biol Rev 79:387-401.
4. Konstantinovic N, Guegan H, Stäjner T, Belaz S, Robert-Gangneux F. 2019. Treatment of toxoplasmosis: Current options and future perspectives. Food Waterborne Parasitol 15:e00036.
5. Mendez OA, Koshy AA. 2017. Toxoplasma gondii: Entry, association, and physiological influence on the central nervous system. PLoS Pathog 13:e1006351.
6. Pittman KJ, Aliota MT, Knoll LJ. 2014. Dual transcriptional profiling of mice and Toxoplasma gondii during acute and chronic infection. BMC Genomics 15:806.
7. Dixon SE, Stilger KL, Elias EV, Naguleswaran A, Sullivan WJ. 2010. A decade of epigenetic research in Toxoplasma gondii. Mol Biochem Parasitol 173:1-9.
8. Rougier S, Montoya JG, Peyron F. 2017. Lifelong Persistence of Toxoplasma Cysts: A Questionable Dogma? Trends Parasitol 33:93-101.
9. Gregg B, Taylor BC, John B, Tait-Wojno ED, Girgis NM, Miller N, Wagage S, Roos DS, Hunter CA. 2013. Replication and distribution of Toxoplasma gondii in the small intestine after oral infection with tissue cysts. Infect Immun 81:1635-43.
10. Drewry LL, Sibley LD. 2019. The hitchhiker's guide to parasite dissemination. Cell Microbiol 21:e13070.

11. Okumura R, Takeda K. 2017. Roles of intestinal epithelial cells in the maintenance of gut homeostasis. Exp Mol Med 49:e338.
12. Hooper LV. 2015. Epithelial cell contributions to intestinal immunity. Adv Immunol 126:129-72.
13. Olivares-Villagómez D, Van Kaer L. 2018. Intestinal Intraepithelial Lymphocytes: Sentinels of the Mucosal Barrier. Trends Immunol 39:264-275.
14. Cohen SB, Denkers EY. 2015. The gut mucosal immune response to Toxoplasma gondii. Parasite Immunology 37:108-117.
15. Dunay IR, Diefenbach A. 2018. Group 1 innate lymphoid cells in Toxoplasma gondii infection. Parasite Immunol 40.
16. Jung C, Hugot JP, Barreau F. 2010. Peyer's Patches: The Immune Sensors of the Intestine. Int J Inflam 2010:823710.
17. Scanga CA, Aliberti J, Jankovic D, Tilloy F, Bennouna S, Denkers EY, Medzhitov R, Sher A. 2002. Cutting edge: MyD88 is required for resistance to Toxoplasma gondii infection and regulates parasite-induced IL-12 production by dendritic cells. J Immunol 168:5997-6001.
18. Plattner F, Yarovinsky F, Romero S, Didry D, Carlier MF, Sher A, Soldati-Favre D. 2008. Toxoplasma profilin is essential for host cell invasion and TLR11-dependent induction of an interleukin-12 response. Cell Host Microbe 3:77-87.
19. Koblansky AA, Jankovic D, Oh H, Hieny S, Sungnak W, Mathur R, Hayden MS, Akira S, Sher A, Ghosh S. 2013. Recognition of profilin by Toll-like receptor 12 is critical for host resistance to Toxoplasma gondii. Immunity 38:119-30.
20. Sukhumavasi W, Egan CE, Warren AL, Taylor GA, Fox BA, Bzik DJ, Denkers EY. 2008. TLR adaptor MyD88 is essential for pathogen control during oral toxoplasma gondii infection but not adaptive immunity induced by a vaccine strain of the parasite. J Immunol 181:3464-73.

21. Scharton-Kersten TM, Wynn TA, Denkers EY, Bala S, Grunvald E, Hieny S, Gazzinelli RT, Sher A. 1996. In the absence of endogenous IFN-gamma, mice develop unimpaired IL-12 responses to Toxoplasma gondii while failing to control acute infection. J Immunol 157:4045-54.

22. Deckert-Schlüter M, Rang A, Weiner D, Huang S, Wiestler OD, Hof H, Schlüter D. 1996. Interferon-gamma receptor-deficiency renders mice highly susceptible to toxoplasmosis by decreased macrophage activation. Lab Invest 75:827-41.

23. Yap GS, Sher A. 1999. Effector cells of both nonhemopoietic and hemopoietic origin are required for interferon (IFN)-gamma- and tumor necrosis factor (TNF)-alpha-dependent host resistance to the intracellular pathogen, Toxoplasma gondii. J Exp Med 189:1083-92.

24. Sasai M, Pradipta A, Yamamoto M. 2018. Host immune responses to Toxoplasma gondii. Int Immunol 30:113-119.

25. Yarovinsky F. 2014. Innate immunity to Toxoplasma gondii infection. Nat Rev Immunol 14:109-21.

26. Khan IA, Schwartzman JD, Matsuura T, Kasper LH. 1997. A dichotomous role for nitric oxide during acute Toxoplasma gondii infection in mice. Proc Natl Acad Sci U S A 94:13955-60.

27. Liesenfeld O, Kang H, Park D, Nguyen TA, Parkhe CV, Watanabe H, Abo T, Sher A, Remington JS, Suzuki Y. 1999. TNF-alpha, nitric oxide and IFN-gamma are all critical for development of necrosis in the small intestine and early mortality in genetically susceptible mice infected perorally with Toxoplasma gondii. Parasite Immunol 21:365-76.

28. Scharton-Kersten TM, Yap G, Magram J, Sher A. 1997. Inducible nitric oxide is essential for host control of persistent but not acute infection with the intracellular pathogen Toxoplasma gondii. J Exp Med 185:1261-73.

29. Suzuki Y, Joh K. 1994. Effect of the strain of Toxoplasma gondii on the development of toxoplasmic encephalitis in mice treated with antibody to interferon-gamma. Parasitol Res 80:125-30.

30. Sibley LD, Adams LB, Fukutomi Y, Krahenbuhl JL. 1991. Tumor necrosis factor-alpha triggers antitoxoplasmal activity of IFN-gamma primed macrophages. J Immunol 147:2340-5.

31. Langermans JA, Van der Hulst ME, Nibbering PH, Hiemstra PS, Fransen L, Van Furth R. 1992. IFN-gamma-induced L-arginine-dependent toxoplasmastatic activity in murine peritoneal macrophages is mediated by endogenous tumor necrosis factor-alpha. J Immunol 148:568-74.

32. Yap GS, Scharton-Kersten T, Charest H, Sher A. 1998. Decreased resistance of TNF receptor p55- and p75-deficient mice to chronic toxoplasmosis despite normal activation of inducible nitric oxide synthase in vivo. J Immunol 160:1340-5.

33. Burger E, Araujo A, López-Yglesias A, Rajala MW, Geng L, Levine B, Hooper LV, Burstein E, Yarovinsky F. 2018. Loss of Paneth Cell Autophagy Causes Acute Susceptibility to Toxoplasma gondii-Mediated Inflammation. Cell Host Microbe 23:177-190.e4.

34. Craven M, Egan CE, Dowd SE, McDonough SP, Dogan B, Denkers EY, Bowman D, Scherl EJ, Simpson KW. 2012. Inflammation drives dysbiosis and bacterial invasion in murine models of ileal Crohn's disease. PLoS One 7:e41594.

35. Benson A, Pifer R, Behrendt CL, Hooper LV, Yarovinsky F. 2009. Gut commensal bacteria direct a protective immune response against Toxoplasma gondii. Cell Host Microbe 6:187-96.

36. Vallon-Eberhard A, Landsman L, Yogev N, Verrier B, Jung S. 2006. Transepithelial pathogen uptake into the small intestinal lamina propria. J Immunol 176:2465-9.

37. Muller PA, Matheis F, Mucida D. 2020. Gut macrophages: key players in intestinal immunity and tissue physiology. Curr Opin Immunol 62:54-61.

38. Zhou L, Sonnenberg GF. 2018. Essential immunologic orchestrators of intestinal homeostasis. Sci Immunol 3.

39. Agalioti T, Villablanca EJ, Huber S, Gagliani N. 2018. TH17 cell plasticity: The role of dendritic cells and molecularmechanisms. J Autoimmun 87:50-60.

40. Gazzinelli R, Xu Y, Hieny S, Cheever A, Sher A. 1992. Simultaneous depletion of CD4+ and CD8+ T lymphocytes is required to reactivate chronic infection with Toxoplasma gondii. J Immunol 149:175-80.

41. Detavernier A, Azouz A, Shehade H, Splittgerber M, Van Maele L, Nguyen M, Thomas S, Achouri Y, Svec D, Calonne E, Fuks F, Oldenhove G, Goriely S. 2019. Monocytes undergo multi-step differentiation in mice during oral infection by Toxoplasma gondii. Commun Biol 2:472.

42. Park J, Hunter CA. 2020. The role of macrophages in protective and pathological responses to Toxoplasma gondii. Parasite Immunol 42:e12712.

43. Bliss SK, Butcher BA, Denkers EY. 2000. Rapid recruitment of neutrophils containing prestored IL-12 during microbial infection. J Immunol 165:4515-21.

44. Ruiz-Rosado JeD, Olguín JE, Juárez-Avelar I, Saavedra R, Terrazas LI, Robledo-Avila FH, Vazquez-Mendoza A, Fernández J, Satoskar AR, Partida-Sánchez S, Rodriguez-Sosa M. 2016. MIF Promotes Classical Activation and Conversion of Inflammatory Ly6C(high) Monocytes into TipDCs during Murine Toxoplasmosis. Mediators Inflamm 2016:9101762.

45. Goldszmid RS, Caspar P, Rivollier A, White S, Dzutsev A, Hieny S, Kelsall B, Trinchieri G, Sher A. 2012. NK cell-derived interferon-γ orchestrates cellular dynamics and the differentiation of monocytes into dendritic cells at the site of infection. Immunity 36:1047-59.

46. Dunay IR, Damatta RA, Fux B, Presti R, Greco S, Colonna M, Sibley LD. 2008. Gr1(+) inflammatory monocytes are required for mucosal resistance to the pathogen Toxoplasma gondii. Immunity 29:306-17.

47. Mashayekhi M, Sandau MM, Dunay IR, Frickel EM, Khan A, Goldszmid RS, Sher A, Ploegh HL, Murphy TL, Sibley LD, Murphy KM. 2011. CD8α(+) dendritic cells are the critical source of interleukin-12 that controls acute infection by Toxoplasma gondii tachyzoites. Immunity 35:249-59.

48. Liu CH, Fan YT, Dias A, Esper L, Corn RA, Bafica A, Machado FS, Aliberti J. 2006. Cutting edge: dendritic cells are essential for in vivo IL-12 production and development of resistance against Toxoplasma gondii infection in mice. J Immunol 177:31-5.

49. Dunay IR, Fuchs A, Sibley LD. 2010. Inflammatory monocytes but not neutrophils are necessary to control infection with Toxoplasma gondii in mice. Infect Immun 78:1564-70.

50. Egan CE, Craven MD, Leng J, Mack M, Simpson KW, Denkers EY. 2009. CCR2-dependent intraepithelial lymphocytes mediate inflammatory gut pathology during Toxoplasma gondii infection. Mucosal Immunol 2:527-35.

51. Tecchio C, Micheletti A, Cassatella MA. 2014. Neutrophil-derived cytokines: facts beyond expression. Front Immunol 5:508.

52. Sakaguchi S, Yamaguchi T, Nomura T, Ono M. 2008. Regulatory T cells and immune tolerance. Cell 133:775-87.

53. Benson A, Murray S, Divakar P, Burnaevskiy N, Pifer R, Forman J, Yarovinsky F. 2012. Microbial infection-induced expansion of effector T cells overcomes the suppressive effects of regulatory T cells via an IL-2 deprivation mechanism. J Immunol 188:800-10.

54. Iwasaki A, Medzhitov R. 2004. Toll-like receptor control of the adaptive immune responses. Nat Immunol 5:987-95.

55. Oldenhove G, Bouladoux N, Wohlfert EA, Hall JA, Chou D, Dos Santos L, O'Brien S, Blank R, Lamb E, Natarajan S, Kastenmayer R, Hunter C, Grigg ME, Belkaid Y. 2009.

Decrease of Foxp3+ Treg cell number and acquisition of effector cell phenotype during lethal infection. Immunity 31:772-86.

56. Hall JA, Grainger JR, Spencer SP, Belkaid Y. 2011. The role of retinoic acid in tolerance and immunity. Immunity 35:13-22.

57. Zare-Bidaki M, Assar S, Hakimi H, Abdollahi SH, Nosratabadi R, Kennedy D, Arababadi MK. 2016. TGF-β in Toxoplasmosis: Friend or foe? Cytokine 86:29-35.

58. Hall JA, Cannons JL, Grainger JR, Dos Santos LM, Hand TW, Naik S, Wohlfert EA, Chou DB, Oldenhove G, Robinson M, Grigg ME, Kastenmayer R, Schwartzberg PL, Belkaid Y. 2011. Essential role for retinoic acid in the promotion of CD4(+) T cell effector responses via retinoic acid receptor alpha. Immunity 34:435-47.

59. Kumar P, Saini S, Khan S, Surendra Lele S, Prabhakar BS. 2019. Restoring self-tolerance in autoimmune diseases by enhancing regulatory T-cells. Cell Immunol 339:41-49.

60. Suzuki Y, Sher A, Yap G, Park D, Neyer LE, Liesenfeld O, Fort M, Kang H, Gufwoli E. 2000. IL-10 is required for prevention of necrosis in the small intestine and mortality in both genetically resistant BALB/c and susceptible C57BL/6 mice following peroral infection with Toxoplasma gondii. J Immunol 164:5375-82.

61. Roers A, Siewe L, Strittmatter E, Deckert M, Schlüter D, Stenzel W, Gruber AD, Krieg T, Rajewsky K, Müller W. 2004. T cell-specific inactivation of the interleukin 10 gene in mice results in enhanced T cell responses but normal innate responses to lipopolysaccharide or skin irritation. J Exp Med 200:1289-97.

62. Grainger JR, Wohlfert EA, Fuss IJ, Bouladoux N, Askenase MH, Legrand F, Koo LY, Brenchley JM, Fraser ID, Belkaid Y. 2013. Inflammatory monocytes regulate pathologic responses to commensals during acute gastrointestinal infection. Nat Med 19:713-21.

63. Liesenfeld O, Kosek J, Remington JS, Suzuki Y. 1996. Association of CD4+ T cell-dependent, interferon-gamma-mediated necrosis of the small intestine with genetic

susceptibility of mice to peroral infection with Toxoplasma gondii. J Exp Med 184:597-607.

64. Vossenkämper A, Struck D, Alvarado-Esquivel C, Went T, Takeda K, Akira S, Pfeffer K, Alber G, Lochner M, Förster I, Liesenfeld O. 2004. Both IL-12 and IL-18 contribute to small intestinal Th1-type immunopathology following oral infection with Toxoplasma gondii, but IL-12 is dominant over IL-18 in parasite control. Eur J Immunol 34:3197-207.

65. Heimesaat MM, Bereswill S, Fischer A, Fuchs D, Struck D, Niebergall J, Jahn HK, Dunay IR, Moter A, Gescher DM, Schumann RR, Göbel UB, Liesenfeld O. 2006. Gram-negative bacteria aggravate murine small intestinal Th1-type immunopathology following oral infection with Toxoplasma gondii. J Immunol 177:8785-95.

66. Heimesaat MM, Fischer A, Jahn HK, Niebergall J, Freudenberg M, Blaut M, Liesenfeld O, Schumann RR, Göbel UB, Bereswill S. 2007. Exacerbation of murine ileitis by Toll-like receptor 4 mediated sensing of lipopolysaccharide from commensal Escherichia coli. Gut 56:941-8.

67. Egan CE, Cohen SB, Denkers EY. 2012. Insights into inflammatory bowel disease using Toxoplasma gondii as an infectious trigger. Immunol Cell Biol 90:668-75.

68. Jorgensen I, Rayamajhi M, Miao EA. 2017. Programmed cell death as a defence against infection. Nat Rev Immunol 17:151-164.

69. Dhuriya YK, Sharma D. 2018. Necroptosis: a regulated inflammatory mode of cell death. J Neuroinflammation 15:199.

70. Man SM, Karki R, Kanneganti TD. 2017. Molecular mechanisms and functions of pyroptosis, inflammatory caspases and inflammasomes in infectious diseases. Immunol Rev 277:61-75.

71. Cho YS, Challa S, Moquin D, Genga R, Ray TD, Guildford M, Chan FK. 2009. Phosphorylation-driven assembly of the RIP1-RIP3 complex regulates programmed necrosis and virus-induced inflammation. Cell 137:1112-23.

72. He S, Wang L, Miao L, Wang T, Du F, Zhao L, Wang X. 2009. Receptor interacting protein kinase-3 determines cellular necrotic response to TNF-alpha. Cell 137:1100-11.

73. Wang H, Sun L, Su L, Rizo J, Liu L, Wang LF, Wang FS, Wang X. 2014. Mixed lineage kinase domain-like protein MLKL causes necrotic membrane disruption upon phosphorylation by RIP3. Mol Cell 54:133-146.

74. Hansen LW, Jacob A, Yang WL, Bolognese AC, Prince J, Nicastro JM, Coppa GF, Wang P. 2018. Deficiency of receptor-interacting protein kinase 3 (RIPK3) attenuates inflammation and organ injury in neonatal sepsis. J Pediatr Surg 53:1699-1705.

75. Chen J, Wang S, Fu R, Zhou M, Zhang T, Pan W, Yang N, Huang Y. 2018. RIP3 dependent NLRP3 inflammasome activation is implicated in acute lung injury in mice. J Transl Med 16:233.

76. Moriwaki K, Chan FK. 2017. The Inflammatory Signal Adaptor RIPK3: Functions Beyond Necroptosis. Int Rev Cell Mol Biol 328:253-275.

77. Ewald SE, Chavarria-Smith J, Boothroyd JC. 2014. NLRP1 is an inflammasome sensor for Toxoplasma gondii. Infect Immun 82:460-8.

78. Chu JQ, Shi G, Fan YM, Choi IW, Cha GH, Zhou Y, Lee YH, Quan JH. 2016. Production of IL-1β and Inflammasome with Up-Regulated Expressions of NOD-Like Receptor Related Genes in *Toxoplasma gondii*-Infected THP-1 Macrophages. Korean J Parasitol 54:711-717.

79. Melchor SJ, Saunders CM, Sanders I, Hatter JA, Byrnes KA, Coutermarsh-Ott S, Ewald SE. 2020. IL-1R Regulates Disease Tolerance and Cachexia in *Toxoplasma gondii* Infection. J Immunol 204:3329-3338.

80. Villeret B, Brault L, Couturier-Maillard A, Robinet P, Vasseur V, Secher T, Dimier-Poisson I, Jacobs M, Zheng SG, Quesniaux VF, Ryffel B. 2013. Blockade of IL-1R signaling diminishes Paneth cell depletion and Toxoplasma gondii induced ileitis in mice. Am J Clin Exp Immunol 2:107-16.

81. Guiton R, Vasseur V, Charron S, Arias MT, Van Langendonck N, Buzoni-Gatel D, Ryffel B, Dimier-Poisson I. 2010. Interleukin 17 receptor signaling is deleterious during Toxoplasma gondii infection in susceptible BL6 mice. J Infect Dis 202:427-35.

82. Gorfu G, Cirelli KM, Melo MB, Mayer-Barber K, Crown D, Koller BH, Masters S, Sher A, Leppla SH, Moayeri M, Saeij JP, Grigg ME. 2014. Dual role for inflammasome sensors NLRP1 and NLRP3 in murine resistance to Toxoplasma gondii. mBio 5.

83. Coutermarsh-Ott SL, Doran JT, Campbell C, Williams TM, Lindsay DS, Allen IC. 2016. Caspase-11 Modulates Inflammation and Attenuates Toxoplasma gondii Pathogenesis. Mediators Inflamm 2016:9848263.

84. López-Yglesias AH, Camanzo E, Martin AT, Araujo AM, Yarovinsky F. 2019. TLR11-independent inflammasome activation is critical for CD4+ T cell-derived IFN-γ production and host resistance to Toxoplasma gondii. PLoS Pathog 15:e1007872.

85. Mammari N, Halabi MA, Yaacoub S, Chlala H, Dardé ML, Courtioux B. 2019. *Toxoplasma gondii* Modulates the Host Cell Responses: An Overview of Apoptosis Pathways. Biomed Res Int 2019:6152489.

86. Subauste CS. 2019. Interplay Between *Toxoplasma gondii*, Autophagy, and Autophagy Proteins. Front Cell Infect Microbiol 9:139.

87. Kuida K, Zheng TS, Na S, Kuan C, Yang D, Karasuyama H, Rakic P, Flavell RA. 1996. Decreased apoptosis in the brain and premature lethality in CPP32-deficient mice. Nature 384:368-72.

88. Cadwell K, Patel KK, Komatsu M, Virgin HW, Stappenbeck TS. 2009. A common role for Atg16L1, Atg5 and Atg7 in small intestinal Paneth cells and Crohn disease. Autophagy 5:250-2.

89. Lemgruber L, Lupetti P, Martins-Duarte ES, De Souza W, Vommaro RC. 2011. The organization of the wall filaments and characterization of the matrix structures of Toxoplasma gondii cyst form. Cell Microbiol 13:1920-32.

90. Sinai AP, Watts EA, Dhara A, Murphy RD, Gentry MS, Patwardhan A. 2016. Reexamining Chronic *Toxoplasma gondii* Infection: Surprising Activity for a "Dormant" Parasite. Curr Clin Microbiol Rep 3:175-185.

91. Watts E, Zhao Y, Dhara A, Eller B, Patwardhan A, Sinai AP. 2015. Novel Approaches Reveal that Toxoplasma gondii Bradyzoites within Tissue Cysts Are Dynamic and Replicating Entities In Vivo. mBio 6:e01155-15.

92. Ginhoux F, Lim S, Hoeffel G, Low D, Huber T. 2013. Origin and differentiation of microglia. Front Cell Neurosci 7:45.

93. Cabral CM, Tuladhar S, Dietrich HK, Nguyen E, MacDonald WR, Trivedi T, Devineni A, Koshy AA. 2016. Neurons are the Primary Target Cell for the Brain-Tropic Intracellular Parasite Toxoplasma gondii. PLoS Pathog 12:e1005447.

94. Schlüter D, Deckert M, Hof H, Frei K. 2001. Toxoplasma gondii infection of neurons induces neuronal cytokine and chemokine production, but gamma interferon- and tumor necrosis factor-stimulated neurons fail to inhibit the invasion and growth of T. gondii. Infect Immun 69:7889-93.

95. Louveau A, Harris TH, Kipnis J. 2015. Revisiting the Mechanisms of CNS Immune Privilege. Trends Immunol 36:569-577.

96. Halonen SK, Taylor GA, Weiss LM. 2001. Gamma interferon-induced inhibition of Toxoplasma gondii in astrocytes is mediated by IGTP. Infect Immun 69:5573-6.

97. Peterson PK, Gekker G, Hu S, Chao CC. 1995. Human astrocytes inhibit intracellular multiplication of Toxoplasma gondii by a nitric oxide-mediated mechanism. J Infect Dis 171:516-8.

98. Garfoot AL, Cervantes PW, Knoll LJ. 2019. Transcriptional Analysis Shows a Robust Host Response to *Toxoplasma gondii* during Early and Late Chronic Infection in Both Male and Female Mice. Infect Immun 87.

99. Evans WJ, Morley JE, Argilés J, Bales C, Baracos V, Guttridge D, Jatoi A, Kalantar-Zadeh K, Lochs H, Mantovani G, Marks D, Mitch WE, Muscaritoli M, Najand A, Ponikowski P, Rossi Fanelli F, Schambelan M, Schols A, Schuster M, Thomas D, Wolfe R, Anker SD. 2008. Cachexia: a new definition. Clin Nutr 27:793-9.

100. Hatter JA, Kouche YM, Melchor SJ, Ng K, Bouley DM, Boothroyd JC, Ewald SE. 2018. Toxoplasma gondii infection triggers chronic cachexia and sustained commensal dysbiosis in mice. PLoS One 13:e0204895.

101. Melchor SJ, Ewald SE. 2019. Disease Tolerance in *Toxoplasma* Infection. Front Cell Infect Microbiol 9:185.

102. Prandovszky E, Li Y, Sabunciyan S, Steinfeldt CB, Avalos LN, Gressitt KL, White JR, Severance EG, Pletnikov MV, Xiao J, Yolken RH. 2018. Induced Long-Term Changes in the Upper Intestinal Microflora during the Chronic Stage of Infection. Scientifica (Cairo) 2018:2308619.

103. Johnson KV, Foster KR. 2018. Why does the microbiome affect behaviour? Nat Rev Microbiol 16:647-655.

104. Vuong HE, Yano JM, Fung TC, Hsiao EY. 2017. The Microbiome and Host Behavior. Annu Rev Neurosci 40:21-49.

105. Johnson HJ, Koshy AA. 2020. Latent Toxoplasmosis Effects on Rodents and Humans: How Much is Real and How Much is Media Hype? mBio 11.

Figures

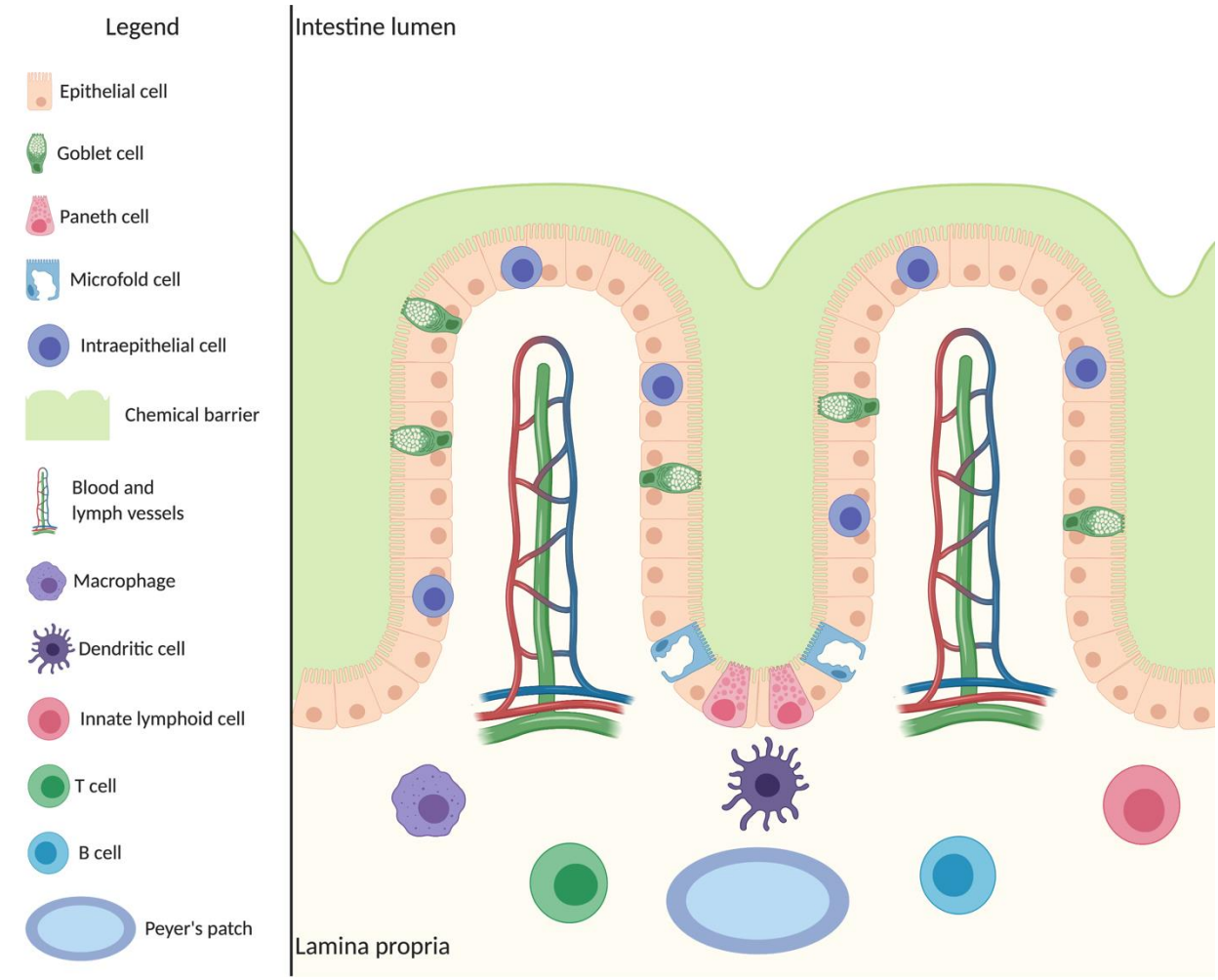

Figure 1. *Gut mucosal immune system.* The intestine epithelium and gut mucosal immune system provide a physical and chemical barrier against luminal contents. Collectively, these features are poised to induce a rapid and coordinated response against pathogens. The gut mucosal immune system generates a protective innate pro-inflammatory response that facilitates host survival to oral *T. gondii* infection.

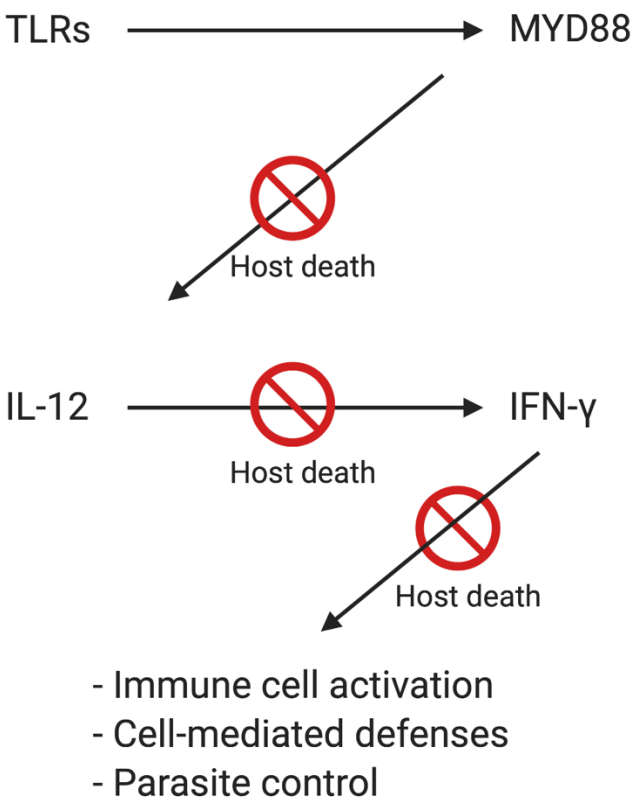

Figure 2. *Molecular mechanisms of host survival against T. gondii infection.* Multiple TLRs can stimulate MYD88-mediated IL-12 production and subsequent IFN-γ expression after oral *T. gondii* infection. The IFN-γ signaling pathway is vital for immune cell stimulation and cell-mediated defenses that control parasite burden. The MYD88, IL-12, and IFN-γ pathway is essential to host survival. Any deficiency in this pathway results in host death from an inadequate pro-inflammatory response and uncontrolled parasite replication.

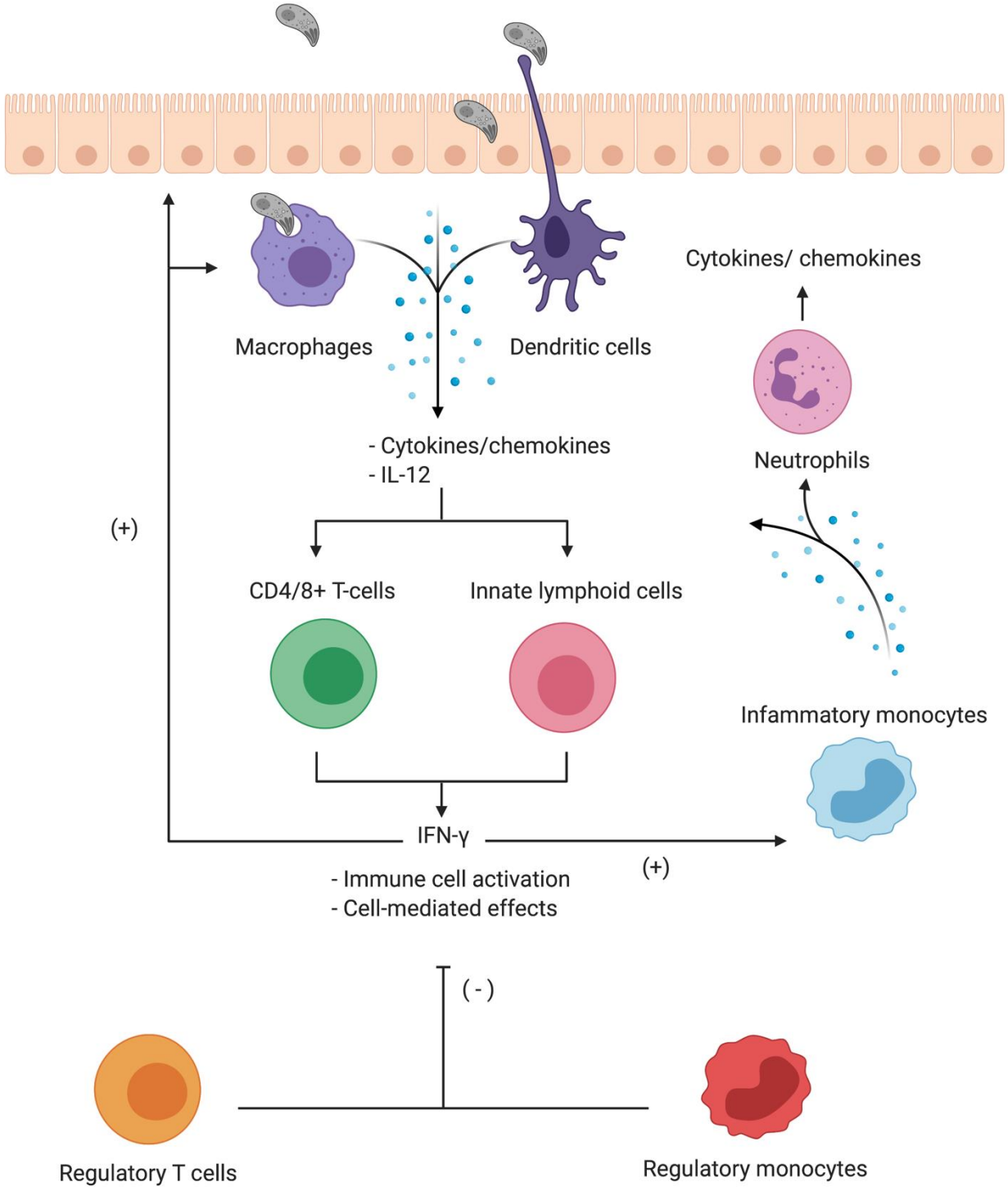

Figure 3. *Immune cell effectors to oral T. gondii infection.* Intestine epithelial cells and resident immune cells initially recognize *T. gondii* infection and secrete inflammatory cytokines and chemokines. These molecules activate and recruit additional immune cells. Production of IL-12

is critical to activate T cells and ILCs, as well as other inflammatory immune cells to produce IFN-γ. Subsequently, IFN-γ drives immune cell activation, pro-inflammatory responses, and mechanisms of *T. gondii* degradation. This process forms a positive feedback loop that amplifies host defenses against *T. gondii* infection. To prevent excessive inflammation and tissue damage, Tregs and regulatory monocytes inhibit further immune cell activation and stimulation. These mechanisms provide a protective host response that is robust and balanced.

Chapter 2

Transcriptional analysis shows a robust host response to *Toxoplasma gondii* during early and late chronic infection in both male and female mice

Andrew L. Garfoot[1]*, Patrick W. Cervantes[1]*, and Laura J. Knoll[1]

[1]Department of Medical Microbiology and Immunology, University of Wisconsin - Madison, 1550 Linden Drive, Madison, WI 53706

* Authors contributed equally to the work

This chapter was accepted for publication in the Journal of Infection and Immunity on March 1, 2019.

Garfoot AL, Cervantes PW, Knoll LJ. Transcriptional Analysis Shows a Robust Host Response to *Toxoplasma gondii* during Early and Late Chronic Infection in Both Male and Female Mice. *Infect Immun*. 2019;87(5):e00024-19. Published 2019 Apr 23. doi:10.1128/IAI.00024-19

Author contributions: PWC designed and performed the RNA-seq experiment. PWC and ALG: analyzed the RNA-seq results, generated the differential gene expression graphs, measured serum cytokine levels, performed gene ontology, and compared sex-specific responses to *T. gondii* infections and *L. monocytogenes* as a secondary infection.

Abstract

The long-term host effects caused by the protozoan parasite *Toxoplasma gondii* are poorly understood. RNA-seq analysis previously determined that the host response in the brain was higher and more complex at 28 versus 10 days postinfection. Here, we analyzed the host transcriptional profile of age- and sex- matched mice during very early (21 days), early (28 days), mid (3 months) and late (6 months) chronic infection. We found that a majority of the host genes which increase in abundance at day 21 postinfection are still increased 6 months postinfection for both male and female mice. While most of the differentially expressed genes were similar between sexes, females have far fewer genes that are significantly less abundant, which may lead to the slight increased cyst burden in males. Transcripts for C-X-C Motif Chemokine Ligand 13 and a C-C Motif Chemokine Receptor 2 (CCR2) were significantly higher in females compared to males during infection. As *T. gondii* chronic infection and profilin (PRF) confer resistance to *Listeria monocytogenes* infection in a CCR2 dependent manner, the differences in CCR2 expression lead us to re-test the protection of PRF in both sexes. Chronic infection as well as PRF were nearly as effective at reducing the bacterial burden in male versus female mice. These data show that most of the host genes differentially expressed in response to *T. gondii* infection are similar between males and females. While differences exist between sexes, these differences do not result in biological changes to the way the host responds to *T. gondii* infection.

Introduction

The parasitic protozoan *Toxoplasma gondii* has the unique ability to form long-lasting chronic infections in the central nervous system (CNS) of humans and other mammals. After the initial infection through ingestion of either *T. gondii* oocysts or tissues cysts, the fast-growing tachyzoite form travels into the CNS and transitions into the slow-growing bradyzoite. These bradyzoites form cysts in the brain, primarily within neurons (1), and reside there presumably for the lifetime of the host. The long-term effects of chronic *T. gondii* infection on the body and brain are poorly understood, and current antiparasitic drugs are ineffective against this chronic form. Although otherwise healthy individuals chronically infected with *T. gondii* are clinically asymptomatic, the risk of cyst reactivation is inherent when an infected person becomes immunocompromised.

In chronically infected mice, *T. gondii* provides protection against lethal pathogens (2–7), largely through a strong immune response against the immunodominant antigen profilin (PRF, (8)). PRF binds the murine Toll-like receptors 11 and 12 (TLR11/12) which leads to an interleukin-12 (IL-12) dependent interferon gamma (IFNγ) response (9–12). Continual IFNγ production is required to suppress chronic *T. gondii* infection, as reduction of IFNγ in chronically infected mice results in tissue cyst reactivation and host death (13, 14). Although the immune mechanism is different in humans, a continuous suppression of *T. gondii* by the immune system is required for survival (15). This effect is evident in patients with chronic *T. gondii* infection who become immune compromised by an immunosuppressive disease or chemotherapeutic treatment. These patients suffer from encephalitis when brain cysts reactivate into tachyzoites.

The immune response to parasitic protozoans, like *T. gondii, Leishmania,* and *Plasmodium,* vary between male and female hosts. During acute *T. gondii* infection, females show reduced survival rates and lower cytokine levels compared to males (16). Innate and adaptive immune cells are influenced by sex hormones that impact the immune response to

protozoan infections (17). Treatment with sex hormones, like estradiol and estrogen, increase acute pathogenesis (18) and increase the number of brain cysts in both male and female mice (19, 20). Although the effects of sex hormones on acute *T. gondii* infection have been well studied, comparisons between male and females during chronic infection have varied depending on mouse genotypes. Cyst counts between male and female outbred mice show no difference between sexes (19), whereas inbred B6 female mice have slightly more brain cyst compared to male during early chronic infection (16).

To start understanding the long-term interactions between the parasite and host, the host/parasite transcriptomic profile was compared at the peaks of acute and chronic mouse infection (21). The number of highly expressed host genes specific to chronic infection was striking and required further investigation. In this manuscript, we used high throughput RNA sequencing (RNAseq) to examine the host response late into chronic *T. gondii* infection. Brain tissue of CBA/J mice infected from 21 days through 6 months of infection was analyzed, and both male and female mice were included to account for sex dependent responses to chronic *T. gondii* infection. We found that a majority of the host genes which are increased in abundance at 21 days postinfection are still more abundant at 6 months postinfection in both sexes. While most of the host response is similar between sexes, females have far fewer genes that are significantly less abundant. Also, the B-cell chemoattractant C-X-C Motif Chemokine Ligand 13 (CXCL13) and a C-C Motif Chemokine Receptor 2 (CCR2) for Monocyte Chemoattractant Protein 1 (MCP1) are higher in females compared to males during infection. These results highlight that studies of the host immune response against *T. gondii* should include both males and females, especially when examining responses to the chemokines and their receptors.

Materials and methods

Mouse infection with T. gondii. The ME49 strain of *T. gondii* was cultured as tachyzoites in human foreskin fibroblast cells. 6-10 week-old CBA/J male and female mice (JAX) were infected intraperitoneally with $1x10^5$ tachyzoites for studies of acute toxoplasmosis and $1x10^4$ tachyzoites to establish chronic toxoplasmosis. Animal survival curves were produced and analyzed using Prism software (v5; GraphPad). Animals were treated in compliance with the guidelines set by the Institutional Animal Care and Use Committee (IACUC) of the University of Wisconsin School of Medicine and Public Health (protocol #M005217), which adheres to the regulations and guidelines set by the National Research Council. The University of Wisconsin is accredited by the International Association for Assessment and Accreditation of Laboratory Animal Care.

Generation of RNA and RNAseq. The cerebral cortex of infected mice at 21, 28, 90, and 180 days postinfection, along with aged-matched uninfected control mice, was harvested. Brain tissue from three mice were processed for RNAseq for each condition and sex for the 21, 28, and 90 day timepoints, and two mice were used for each condition for the 180 day timepoint, except the infected female 180 day timepoint group in which three mice were used. Tissue was immediately homogenized in Trizol (Ambion) using a pellet pestle (Kontes), and RNA extracted using phenol/chloroform separation and ethanol precipitation. RNA libraries were prepared using TruSeq RNA Library Prep Kit v2 set A (Illumina), according to the manufacturers protocol. RNA libraries were multiplexed and run across 9 lanes (infected tissues) or 3 lanes (uninfected tissues) for paired end sequencing by Illumina HiSeq 2500 at the University of Wisconsin Biotechnology Center, generating approximately 5.7 billion total paired-end 125 base pair reads.

Differential Expression Analysis. The sequenced reads were aligned to the *Mus musculus* genome (GRCm38; database v87; Ensembl), using the Spliced Alignment to a Reference (STAR; v2.5.2b) program (40). Alignment parameters for STAR were kept at default except for the following: 2 base pair maximum mismatch, 70 base pair minimum intron length, and a 500,000 base pair maximum intron length. Gene expression levels were then estimated using the program RNA-seq by Expectation-Maximization (RSEM v1.2.31) (41). Differential analysis was calculated using the DESeq2 (v1.14.1) program, analyzing genes with ≥10 raw counts (calculated by RSEM) for at least one sample. Fold change was calculated using the geometric mean values for the infected samples relative to their matching uninfected samples. The rlog transformed DESeq2 values were used for the PCA plot and PCA calculated using "plotPCA" function of the DESeq2 package. The $\log_2$ transformed DESeq2 values were used to calculate Pearson's correlation coefficients and coefficients were calculated using the corrgram package. The Database for Annotation, Visualization and Integrated Discovery (DAVID v6.8) was used as a functional annotation tool to identify enriched biological gene ontology (GO) terms among genes commonly differentially expressed between timepoints. A list of mouse genes with at least 10 RSEM gene counts was used as background for enrichment analysis in DAVID. All raw sequencing data and differential expression values have been deposited in NCBI's Gene Expression Omnibus (GEO) (42) and are accessible through GEO Series accession number GSE117504 (https://www.ncbi.nlm.nih.gov/geo/query/acc.cgi?acc=GSE117504). Heat maps were generated using the Multi Experiment Viewer program.

qPCR. RNA from isolated from the RNAseq experiment was reverse transcribed to synthesize cDNA using SuperScript III polymerase (Invitrogen). Amplification of target genes was quantified using SYBR Green Supermix (Bio-Rad) with primers directed to the mouse genes GAPDH, TUBα1a, Cxcl13, Ccr2, Cd74, Fcrls, TNFα, and IFNγ. Primers were designed using the

Integrated DNA Technologies RealTime PCR Tool. Expression was calculated by normalizing the cycle threshold values (C_t) to that of GAPDH for each sample (ΔC_t). The ΔC_t value was then used to calculate either the fold change by dividing the ΔC_t of each gene in infected mice from the average ΔC_t of the gene in uninfected mice, or the $\log_2$ fold change using the ΔΔCt method (43) relative to uninfected for each sample.

Listeria monocytogenes infection. C57BL/6 mice were either infected peritoneally with 250 ME49 tachyzoites or treated retro-orbitally with 10 ng *T. gondii* PRF (8, 10) or PBS as control treatment. Purified recombinant his-tagged *T. gondii* PRF was a kind gift from F. Yarovinsky which consistently yields near endotoxin-free protein (10). Mice were infected with approximately $6x10^4$ *L. monocytogenes* colony forming units (CFU) retro-orbitally either 28 days post *T. gondii* infection or four hours post-PRF treatment. Bacterial culture was grown to mid-log growth stage at 37°C in LB medium prior to infection. At 3 days post *L. monocytogenes* infection, spleen tissue was harvested and homogenized in 1 mL PBS using a pellet pestle (Kontes). Homogenate was plated on LB agar plates to quantify viable *L. monocytogenes* CFU for each condition.

Quantitation of brain cyst burden. Whole brain tissue was homogenized using a pellet pestle (Kontes) in PBS. Homogenate was fixed in 4% paraformaldehyde, then blocked and permeabilized in PBS with 3% BSA and 0.2% Triton X-100. Biotinylated *Dolichos biflorus* agglutinin (DBA; Vector Laboratories) was used to mark the surface of the *T. gondii* cyst and was visualized using Alexaflour-594 conjugated streptavidin (Thermo Scientific). Cysts were counted by microscopy to calculate cyst burden for each brain.

Quantitation of serum cytokines. Blood was harvested from the mice used for RNAseq analysis via cardia puncture. Samples were incubated on ice, and serum was separated from the coagulated clot by centrifugation (10 minutes at 14000xg). 25 µL of serum was used for cytokine quantification using a cytometric bead array (BD Biosciences). Serum cytokine concentrations were calculated based on a standard curve of known concentrations.

Results

Host response to T. gondii throughout chronic infection

When we previously compared host transcript abundance during *T. gondii* infection, we were surprised to see many more highly abundant transcripts at day 28 than day 10 (21). For this study, our goal was to investigate the temporal nature of this chronic infection gene induction by examining early (21 day), mid (90 day) and late (180 day) chronic infection timepoints. Because sex as a biological variable has not been previously explored by RNAseq during *T. gondii* chronic brain infection, we also examined infected male mice brains at early and late chronic infection. Uninfected age- and sex-matched control mice were sequenced at every timepoint (n=2-3) to account for any age- and sex-related changes independent of infection (Fig. 1A). For this study we used CBA/J mice to be consistent with the previous study (21) and for their ability to survive late into chronic infection.

To reduce sequencing bias, RNA libraries were multiplexed and run across 6 lanes for infected tissues and 2 lanes for uninfected tissues. Sequencing generated approximately 46 million paired-end, 125 base pair reads per lane for each sample, providing approximately 270 million reads for each infected tissue sample and 100 million reads for uninfected tissue sample. Reads were aligned to the *Mus musculus* genome (normalized expression values are listed in Table S1) for analysis. Reads were also aligned to *T. gondii* (normalized values in Table S2); however, the RNA processing methods used did not allow for efficient RNA extraction from the cysts, so no comparisons were performed with the *T. gondii* transcripts. Analyzing the similarity of samples using the mouse alignment data through a principle component analysis showed distinct grouping between male and female groups as well as infected and uninfected samples (Fig. 1B). Within each group, separation of the 180 day samples is seen, likely due to age related changes in the mice since this happens in both uninfected and infected samples. Pearson's correlation coefficients show high similarity among all samples (ranging from 84-99%

similar; Table S3), with the greatest difference between infected and uninfected samples of either sex.

We first compared the differential expression of host genes from infected female cerebral cortex to their corresponding uninfected controls (Table S4). A statistical cutoff of an adjusted p-value or false discovery rate (FDR) of <0.05 was used for all analyses, and genes with >2-fold change from uninfected mice were identified to increase the likelihood of biological significance. This threshold identified 1660, 1369, 745, and 1256 genes differentially expressed in female mice at 21, 28, 90, and 180 days postinfection, respectively. Nearly all these genes were higher in abundance, as only 110, 28, 6, and 52 genes were less abundant at 21, 28, 90, and 180 days postinfection, respectively. This result was similar to that seen in the previous chronic transcriptional analysis of *T. gondii* infection (21). Of the significantly less abundant genes, the average change was approximately 2.5-fold for all timepoints expect for the 90-day timepoint which averaged 5.0-fold reduction. No gene was >10-fold reduced for any of the female timepoints.

Host genes with greater abundance are shared between early and late chronic infection

Among female genes with greater abundance, 710 are shared between all timepoints (Fig. 2A), which represents approximately half of all differentially expressed genes at 21, 28, and 180 days postinfection and 95% at 90 days. The results were similar for male mice, with 609 shared genes between days 28 and 180 (Fig. 2B), out of 2009 and 1014 genes more abundant at 28 and 180 days postinfection, respectively, for males. The number of unique female genes is drastically reduced from 21 to 28 days postinfection (322 to 48, respectively). This large set of 21 day unique genes suggests these genes may be either acute stage specific genes or genes required for the onset and establishment of chronic infection. As evidence for

both scenarios, 193 of the 322 genes specific for 21-days are also differentially expressed when comparing chronic transcripts at 28 days to acute transcripts at 10 days postinfection (21).

To understand which host genes were the most responsive to infection, we sorted for genes with a 20-fold or greater abundance in infected versus uninfected mice. 92 female genes met these criteria in both early (28-days) and late (6 months) chronic infection (Fig. 3A). Similarly, male mice have several genes (42 genes) greater in abundance both early and late into infection (Fig. 3B). 153 male genes were at least 20-fold differentially expressed during infection at 28 days, 148 of which were more abundant. At 180 days 43 male genes are differentially expressed using the 20-fold cutoff, all of which are more abundant and 42 are shared between both timepoints. Moreover, 40 of the 42 shared male genes are also shared with females at both 28 and 180 days postinfection (Fig. 3C). All but six of these 40 shared genes contain a gene ontology (GO) term linked with the immune response, demonstrating that the host continues to robustly respond to *T. gondii* months after initial infection and genes with greater abundance are shared between sexes during chronic infection (Fig. 3D).

Male mice have vastly more genes that are less abundant

The number of less abundant genes was strikingly different between males and females (Fig. 4A). Only 28 and 52 female genes were less abundant at 28 and 180 days postinfection, respectively. In males, 2290 genes were less abundant at 28 days and 970 at 6 months postinfection using a 2-fold cutoff, with 328 shared between both timepoints. Of these, 40 are >10-fold reduced at 28 days and 3 genes reduced at 6-months postinfection, none of which are common between the two timepoints (Table S5).

One host gene less abundant in both males (28-fold at 28 days) and females (8-fold at 28 days) is Fc receptor-like S scavenger receptor (FCRLS), a protein with unknown function that is highly expressed on microglia (22). FCRLS resembles an Fc receptor but does not bind

antibodies. It is interesting to notice that other microglial-specific markers, such as P2ry12, Mertk and Gas6, have similar transcript levels in infected and uninfected males, while C1qa and Pros1 are significantly more abundant in infected versus uninfected males (Table S3). These results point to a specific downregulation of FCRLS in microglia by *T. gondii*, and not a global downregulation or lysis of microglia cells by *T. gondii*. We confirmed that FCRLS was less abundant by quantitative (qPCR) in both male and female mice (Fig. 4B).

Gene ontology analysis shows immune response late into infection

To understand the roles for these common genes during in infection, we analyzed the sets of shared genes for GO enrichment. Using the 710 genes with 2-fold greater abundance shared among the female timepoints, 370 GO terms were significantly enriched (Table S6). Similarly, from the 609 genes with 2-fold greater abundance shared in the male timepoints, 291 GO terms were identified (Table S6). All the most enriched GO terms related to immune responses or other responses to infection and were the same for both males and females (Fig. 5A). This immunological GO term enrichment is also found among the >20-fold more abundant genes (Fig. 5B), using the 92 greater abundant genes shared among the female timepoints and the 42 greater abundant genes shared in the male timepoints. These results show that *T. gondii* continuously induces immunological responses during late chronic infection.

Serum cytokines are elevated throughout the course of infection

We quantified serum cytokines to determine whether the increased transcriptional abundance of immunological factors translated into a physiological response. Serum cytokines important for control of *T. gondii* include tumor necrosis factor alpha (TNFα), IFNγ, IL-12, IL-6, IL-10 and MCP1 (Fig. 6A-F, respectively). TNFα, IFNγ, MCP1, and IL-12 were highest in infected male and female mice at the earliest timepoint tested (21-days postinfection) and

decrease as the infection continued. By 6 months postinfection, TNFα, IFNγ, MCP1, and IL-12 were all decreased by approximately 70% from the levels at 21 days postinfection; however, levels at 6-months were still significantly higher than uninfected. These decreases over time were also seen when analyzing transcript abundance either by RNAseq (Fig. 6G) or by qPCR (Fig. 6H). These results were similar to the decrease in serum cytokines seen in C57BL/6 mice at 8-weeks post *T. gondii* infection (23). While IL-6 and IL-10 both showed a trend of elevated serum concentration compared to uninfected, not all timepoints reached statistical significance. Comparing cytokines from male to female, we found the same trend of decreasing concentrations for TNFα, IFNγ, MCP1, and IL-12 for both sexes. In addition, IL-6 and IL-10 were variably significant for both sexes throughout infection compared to uninfected. Although some cytokines tended to be lower in males, these differences were not statistically different.

The cytokine concentrations matched the transcriptional profile over time for many of the tested cytokines for both sexes. The normalized expression values (FPKM values) for TNFα, IFNγ, and IL-12 had the highest levels in the infected mice at 21 days postinfection and decreased over time. Many immunological genes show a dip in transcriptional activity at 90 days postinfection, but the transcriptional change did not correlate to a reduction in serum cytokines tested. Gene expression of IL-6 and IL-10 showed low and unchanging levels throughout infection, and these levels were not significantly different from uninfected mice at any of the timepoints in the female mice. Expression for the receptors for many of the tested cytokines are increased in abundance, suggesting the host brain cells are responsive and active toward the immunological cytokine response.

Sex specific responses to infection

Because male and female mice had similar immunological GO term enrichment in response to *T. gondii* infection, we expected their survival to *T. gondii* would also be similar.

During an acute challenge with $1x10^5$ parasites/mouse, both male and female mice became moribund and required euthanasia at similar rates (Fig. 7A). When mice are infected with a lower dose of parasites ($1x10^4$ parasites/mouse) to allow survival into chronic infection, both sexes had 90% survival at the start of chronic infection (28 days) (Fig. 7B). Although male mice had a slightly lower survival percentage throughout chronic infection, the survival curve did not reach statistical significance between sexes. Although it has previously been seen that female mice are slightly more susceptible to *T. gondii* infection than male mice (16, 17), our studies contain many altered variables, including different parasite and mouse strains, than the earlier studies. Males had a statistically significant, 2-fold higher cyst count at 3 months postinfection (Fig. 7C). While the same trends were seen at 6 months postinfection, only about 20% of the mice survived to that timepoint, and the cyst counts in the remaining seven male mice were highly variable. Due to this low survival and variability, we were not able to adequately power the 6 month timepoint (Fig. 7C). These small differences in survival and cyst counts may be related to the slight reduction in key cytokines in males during chronic infection (Fig. 6). These results also indicate that cyst levels are not the only cause of mortality during chronic infection as male mice had slightly higher cyst counts but did not have increased mortality.

Although most differentially expressed genes were common between sexes, 11 genes (Table S7) were increased 20-fold in females but not in males (Fig. 8A). CXCL13 and CCR2 were two immunologically related genes from this set of 11, which showed a large difference between male and female. This trend of reduced expression in males was duplicated by qPCR (Fig. 8B), particularly for CCR2 at the 28 day timepoint ($p=0.036$). CCR2 is the receptor for MCP1, and 4 hour pretreatment with *T. gondii* PRF confers resistance to a secondary bacterial infection by recruiting monocytes in a CCR2 dependent manner (8). We tested the ability of *T. gondii* to confer resistance to *Listeria monocytogenes* in male mice during chronic infection (Fig. 8C) and found a 3.3 log reduction in CFU from the spleens of male mice chronically infected

with *T. gondii*. This was similar, to the 3.6 log reduction seen in chronically infected females (8). To directly compare male and females, and as PRF is the CCR2 stimulant, we treated mice with 10 ng PRF (as a proxy for chronically infected mice) prior to *L. monocytogenes* infection (Fig. 8D). The 3.2 log CFU reduction seen in male mice when treated with PRF was nearly identical as chronic infection, and female mice showed a 3.6 log reduction, similar to results seen previously (8). Although female mice had an overall higher CFU burden compared to males, the CFU reduction was slightly greater for female mice, but this difference was not statistically different. While female and male mice have similar protection against *T. gondii* (Fig. 7) and *L. monocytogenes* (Fig. 8), the precise molecules and their intensities of that protection are different, so mechanistic analyses should include both sexes in the studies.

Discussion

T. gondii can form a chronic infection in any warm-blooded animal, presumably for the life of the host. In mice, this chronic infection alters the host both physically and behaviourally. Mice show increased activity relative to uninfected controls (24, 25) and infected mice are no longer repulsed by feline urine (26). This type of host manipulation serves as a selective advantage for the feline/rodent cycle. However, the induced behavioural changes and their effects in humans is more controversial and less understood. Associations with *T. gondii* in humans range from personality changes, to increased risk of involvement in a traffic accident, to mental health disorders such as schizophrenia (27, 28). Because no drug treatments are effective against chronic *T. gondii* infection and there are no effective vaccine options, it is important for us to better understand the long-term effects on the host. Our current RNA-seq study of a long-term chronic infection time course will enhance our understanding of these behavioural studies and their effects on the brain.

Our transcriptional analysis of mouse genes during late chronic infection shows a continuous and robust immunological response to *T. gondii*. Host responses are reduced after the 21 day timepoint, but they are still significantly higher than the age-matched uninfected mice. Nearly half of all the genes that increased in abundance at 21 days post infection (start of chronic infection) were still increased 6 months postinfection (Fig 2). All the most enriched GO terms from this set of genes related to immunological responses (Fig. 5). Although the amplitude of expression for immunological genes during late-chronic infection may be reduced for some genes such as TNFα and IFNγ, they are still significantly more abundant than in the uninfected controls and many genes are >20-fold increased (Fig. 3). Given these results, it is not surprising that natural killer cells isolated from the peritoneal cavity of mice continue to be activated out to 6 months postinfection (29) and *T. gondii* infection maintains protection from secondary infection out to 7-months postinfection (2). This demonstrates a continual immunological response from the host and has been verified in our transcriptional analysis here.

Both sexes showed a major increase in the expression of several immunological genes. While the majority of the differentially expressed genes are shared, key factors showed differences between the sexes leading to altered responses to the infection. Levels of CCR2 expression was higher in females, along with a trend of increased serum cytokine concentrations, compared to male mice (Fig. 6). We previously found that CCR2 is essential for *T. gondii* chronic infection and PRF to confer resistance to *L. monocytogenes* in females, but these findings were not tested in male mice. In this current study, we found that both chronic infection and PRF treatment were effective to reduce the *L. monocytogenes* bacterial burden in male mice, similar to female mice. PRF treatment reduced bacterial burden in males by 3.2 logs compared to untreated males, related to the bacterial reduction of 3.6 logs for females (Fig. 8). These results emphasize that while there are some differences in the molecules induced by *T. gondii*, chronic infection with *T. gondii* can protect against *Listeria* in both sexes. Still, CXCL13

and CCR2 were increased 20-fold in females but not as much in males during chronic *T. gondii* infection, so females have may better protection against some co-infections than males. Future immune mechanistic analyses should include both female and male mice.

A striking difference between the sexes was seen in the number of genes with lowered abundance during infection. While female mice only had around one hundred genes with reduced abundance at each timepoint, male mice had over 2000 genes at 28 days postinfection and over 1000 at 6 months postinfection with lowered abundance (Fig. 4). Many of the most reduced genes have an unknown function (Table S4), but five of the most reduced genes are named genes: FCRLS, DLG2, PPIL6, SCEL, and MARCH10. These genes are all reduced specifically in males except for FCRLS which is reduced at in both sexes. Disks large homolog 2 (DLG2, transcript number ENSMUST00000207095) is a membrane-associated guanylate kinase that forms multimeric scaffolds at postsynaptic sites. While DLG2 knockout mice have normal synapse development (30), they have abnormal thermogenesis and bone density (31), suggesting male mice may have altered metabolism during *T. gondii* infection. Peptidylprolyl isomerase like 6 (PPIL6), is a gene enriched in olfactory sensory neurons (32); however, the biological function is unknown, as the PPIL6 catalytic site is inactive (33). As mice have altered perception of feline urine scent (26), PPIL6 may play a role in this mechanism for male mice.

Sciellin (SCEL), is a protein thought to function in the assembly or regulation of cornified envelope proteins in keratinocytes (34), and membrane associated ring-CH-type finger 10 (MARCH10) is a ubiquitin ligase (35). SCEL and MARCH10 are both linked to Alzheimer's disease. A specific type of keratin has been detected in cerebrospinal fluid of patients with Alzheimer's disease but not healthy individuals, which may be the result of blood brain barrier breakdown or dysregulation of the ubiquitin proteasome (36). Since SCEL is involved with cells which produce keratin and MARCH10 is a ubiquitin ligase, these genes may play a role in the mechanism of keratin accumulation in the CNS.

This current study highlights the importance of using male and female mice when studying the immune responses to *T. gondii*. Our previous studies of chronic *T. gondii* infection being protective against other pathogens were all performed exclusively in female mice (8, 37, 38). Our methods in the manuscript did not state the sex of the mice, but our records indicated that only female mice were used. The original studies on the effects of chronic infection being protective against other pathogens either did not say the sex of the animal (4) or they only used female mice (5–9), so this study is the first to show that the protective effects of *T. gondii* chronic infection are not exclusive to female mice. It is also been seen that sex hormones, especially estradiol, can affect the immune response to *T. gondii* as well as it's replication (39). In the rodent estrous cycle, ovulation occurs every 4–5 days and is characterized by increasing levels of estradiol. In proestrus, estradiol levels are triple that of estrus, so infection with *T. gondii* at these different stages of the estrous cycle may account for some of the variability seen during studies. Future studies using both male and female mice and documenting female estrus stage will increase our understanding of the host immune response to *T. gondii*.

Acknowledgements

We would like to thank Charles Czuprynski for *L. monocytogenes* EGD strain and Felix Yarovinsky for recombinant *T. gondii* profilin. This research was supported by the National Science Foundation fellowship DGE-1747503 (P.W.C), National Institutes of Health (NIH) National Research Service Award T32AI007414 (P.W.C) and T32AI55397 (A.L.G), Science and Medicine Graduate Research Scholars program (P.W.C), and NIH R21AI114277 (L.J.K.).

References

1. Cabral CM, Tuladhar S, Dietrich HK, Nguyen E, MacDonald WR, Trivedi T, Devineni A, Koshy AA. 2016. Neurons are the Primary Target Cell for the Brain-Tropic Intracellular Parasite *Toxoplasma gondii*. PLOS Pathog 12:e1005447.
2. Ruskin J, Remington JS. 1968. Immunity and Intracellular Infection: Resistance to Bacteria in Mice Infected with a Protozoan. Science 160:72–74.
3. Remington JS, Merigan TC. 1969. Resistance to Virus Challenge in Mice Infected with Protozoa or Bacteria. Proc Soc Exp Biol Med 131:1184–1188.
4. Gentry LO, Remington JS. 1971. Resistance against *Cryptococcus* Conferred by Intracellular Bacteria and Protozoa. J Infect Dis 123:22–31.
5. Mahmoud A a. F, Warren KS, Strickland GT. 1976. Acquired resistance to infection with *Schistosoma mansoni* induced by *Toxoplasma gondii*. Nature 263:56–57.
6. McLeod R, Estes RG, Cohen H. 1985. Influence of *Toxoplasma* on manifestations of Moloney virus infections. Trans R Soc Trop Med Hyg 79:781–787.
7. McLeod R, Remington JS. 1977. Studies on the specificity of killing of intracellular pathogens by macrophages. Cell Immunol 34:156–174.
8. Neal LM, Knoll LJ. 2014. *Toxoplasma gondii* Profilin Promotes Recruitment of Ly6Chi CCR2+ Inflammatory Monocytes That Can Confer Resistance to Bacterial Infection. PLOS Pathog 10:e1004203.
9. Plattner F, Yarovinsky F, Romero S, Didry D, Carlier M-F, Sher A, Soldati-Favre D. 2008. *Toxoplasma Profilin* Is Essential for Host Cell Invasion and TLR11-Dependent Induction of an Interleukin-12 Response. Cell Host Microbe 3:77–87.
10. Yarovinsky F, Zhang D, Andersen JF, Bannenberg GL, Serhan CN, Hayden MS, Hieny S, Sutterwala FS, Flavell RA, Ghosh S, Sher A. 2005. TLR11 Activation of Dendritic Cells by a Protozoan Profilin-Like Protein. Science 308:1626–1629.

11. Koblansky AA, Jankovic D, Oh H, Hieny S, Sungnak W, Mathur R, Hayden MS, Akira S, Sher A, Ghosh S. 2013. Recognition of Profilin by Toll-like Receptor 12 Is Critical for Host Resistance to *Toxoplasma gondii*. Immunity 38:119–130.
12. Andrade WA, Souza M do C, Ramos-Martinez E, Nagpal K, Dutra MS, Melo MB, Bartholomeu DC, Ghosh S, Golenbock DT, Gazzinelli RT. 2013. Combined Action of Nucleic Acid-Sensing Toll-like Receptors and TLR11/TLR12 Heterodimers Imparts Resistance to *Toxoplasma gondii* in Mice. Cell Host Microbe 13:42–53.
13. Suzuki Y, Conley FK, Remington JS. 1989. Importance of endogenous IFN-gamma for prevention of toxoplasmic encephalitis in mice. J Immunol 143:2045–2050.
14. Suzuki Y, Orellana MA, Schreiber RD, Remington JS. 1988. Interferon-gamma: the major mediator of resistance against *Toxoplasma gondii*. Science 240:516–518.
15. Frank O. Richards J, Kovacs JA, Luft BJ. 1995. Preventing Toxoplasmic Encephalitis in Persons Infected with Human Immunodeficiency Virus. Clin Infect Dis 21:S49–S56.
16. Roberts CW, Cruickshank SM, Alexander J. 1995. Sex-determined resistance to *Toxoplasma gondii* is associated with temporal differences in cytokine production. Infect Immun 63:2549–2555.
17. Roberts CW, Walker W, Alexander J. 2001. Sex-Associated Hormones and Immunity to Protozoan Parasites. Clin Microbiol Rev 14:476–488.
18. Zhang X, Liu J, Li M, Fu Y, Zhang T, Han Q, Liu Q. 2017. Role of an estradiol regulatory factor-hydroxysteroid dehydrogenase (HSD) in *Toxoplasma gondii* infection and pathogenicity. J Steroid Biochem Mol Biol 174:176–182.
19. Kittas C, Henry L. 1980. Effect of sex hormones on the response of mice to infection with *Toxoplasma gondii*. Br J Exp Pathol 61:590–600.
20. Pung OJ, Luster MI. 1986. *Toxoplasma gondii*: Decreased resistance to infection in mice due to estrogen. Exp Parasitol 61:48–56.

21. Pittman KJ, Aliota MT, Knoll LJ. 2014. Dual transcriptional profiling of mice and *Toxoplasma gondii* during acute and chronic infection. BMC Genomics 15:806.
22. Butovsky O, Jedrychowski MP, Moore CS, Cialic R, Lanser AJ, Gabriely G, Koeglsperger T, Dake B, Wu PM, Doykan CE, Fanek Z, Liu L, Chen Z, Rothstein JD, Ransohoff RM, Gygi SP, Antel JP, Weiner HL. 2014. Identification of a unique TGF-β–dependent molecular and functional signature in microglia. Nat Neurosci 17:131–143.
23. Magle CT, Pittman KJ, Moser LA, Boldon KM, Knoll LJ. 2014. A *Toxoplasma* Patatin-Like Protein Changes Localization and Alters the Cytokine Response during Toxoplasmic Encephalitis. Infect Immun 82:618–625.
24. Hutchinson WM, Bradley M, Cheyne WM, Wells BW, Hay J. 1980. Behavioural abnormalities in *Toxoplasma*-infected mice. Ann Trop Med Parasitol 74:337–345.
25. Hay J, Hutchison WM, Aitken PP, Graham DI. 1983. The effect of congenital and adult-acquired *Toxoplasma* infections on activity and responsiveness to novel stimulation in mice. Ann Trop Med Parasitol 77:483–495.
26. Vyas A, Kim S-K, Giacomini N, Boothroyd JC, Sapolsky RM. 2007. Behavioral changes induced by *Toxoplasma* infection of rodents are highly specific to aversion of cat odors. Proc Natl Acad Sci U S A 104:6442–6447.
27. Flegr J, Havlícek J, Kodym P, Malý M, Smahel Z. 2002. Increased risk of traffic accidents in subjects with latent toxoplasmosis: a retrospective case-control study. BMC Infect Dis 2:11.
28. Flegr J. 2007. Effects of *Toxoplasma* on Human Behavior. Schizophr Bull 33:757–760.
29. Hauser WE, Sharma SD, Remington JS. 1982. Natural killer cells induced by acute and chronic *Toxoplasma* infection. Cell Immunol 69:330–346.
30. McGee AW, Topinka JR, Hashimoto K, Petralia RS, Kakizawa S, Kauer F, Aguilera-Moreno A, Wenthold RJ, Kano M, Bredt DS. 2001. PSD-93 Knock-Out Mice Reveal That

Neuronal MAGUKs Are Not Required for Development or Function of Parallel Fiber Synapses in Cerebellum. J Neurosci 21:3085–3091.

31. Dickinson ME, Flenniken AM, Ji X, Teboul L, Wong MD, White JK, Meehan TF, Weninger WJ, Westerberg H, Adissu H, Baker CN, Bower L, Brown JM, Caddle LB, Chiani F, Clary D, Cleak J, Daly MJ, Denegre JM, Doe B, Dolan ME, Edie SM, Fuchs H, Gailus-Durner V, Galli A, Gambadoro A, Gallegos J, Guo S, Horner NR, Hsu C-W, Johnson SJ, Kalaga S, Keith LC, Lanoue L, Lawson TN, Lek M, Mark M, Marschall S, Mason J, McElwee ML, Newbigging S, Nutter LMJ, Peterson KA, Ramirez-Solis R, Rowland DJ, Ryder E, Samocha KE, Seavitt JR, Selloum M, Szoke-Kovacs Z, Tamura M, Trainor AG, Tudose I, Wakana S, Warren J, Wendling O, West DB, Wong L, Yoshiki A, Consortium TIMP, Wurst W, MacArthur DG, Tocchini-Valentini GP, Gao X, Flicek P, Bradley A, Skarnes WC, Justice MJ, Parkinson HE, Moore M, Wells S, Braun RE, Svenson KL, Angelis MH de, Herault Y, Mohun T, Mallon A-M, Henkelman RM, Brown SDM, Adams DJ, Lloyd KCK, McKerlie C, Beaudet AL, Bućan M, Murray SA. 2016. High-throughput discovery of novel developmental phenotypes. Nature 537:508–514.
32. McClintock TS, Glasser CE, Bose SC, Bergman DA. 2008. Tissue expression patterns identify mouse cilia genes. Physiol Genomics 32:198–206.
33. Davis TL, Walker JR, Campagna-Slater V, Jr PJF, Paramanathan R, Bernstein G, MacKenzie F, Tempel W, Ouyang H, Lee WH, Eisenmesser EZ, Dhe-Paganon S. 2010. Structural and Biochemical Characterization of the Human Cyclophilin Family of Peptidyl-Prolyl Isomerases. PLOS Biol 8:e1000439.
34. Champliaud M-F, Burgeson RE, Jin W, Baden HP, Olson PF. 1998. cDNA Cloning and Characterization of Sciellin, a LIM Domain Protein of the Keratinocyte Cornified Envelope. J Biol Chem 273:31547–31554.

35. Morokuma Y, Nakamura N, Kato A, Notoya M, Yamamoto Y, Sakai Y, Fukuda H, Yamashina S, Hirata Y, Hirose S. 2007. MARCH-XI, a novel transmembrane ubiquitin ligase implicated in ubiquitin-dependent protein sorting in developing spermatids. J Biol Chem 282:24806–24815.
36. Richens JL, Spencer HL, Butler M, Cantlay F, Vere K-A, Bajaj N, Morgan K, O'Shea P. 2016. Rationalising the role of Keratin 9 as a biomarker for Alzheimer's disease. Sci Rep 6:22962.
37. O'Brien KB, Schultz-Cherry S, Knoll LJ. 2011. Parasite-Mediated Upregulation of NK Cell-Derived Gamma Interferon Protects against Severe Highly Pathogenic H5N1 Influenza Virus Infection. J Virol 85:8680–8688.
38. Settles EW, Moser LA, Harris TH, Knoll LJ. 2014. *Toxoplasma gondii* Upregulates Interleukin-12 To Prevent *Plasmodium berghei*-Induced Experimental Cerebral Malaria. Infect Immun 82:1343–1353.
39. Galván-Ramírez M de la L, Gutiérrez-Maldonado AF, Verduzco-Grijalva F, Jiménez JMD. 2014. The role of hormones on *Toxoplasma gondii* infection: a systematic review. Front Microbiol 5.
40. Dobin A, Davis CA, Schlesinger F, Drenkow J, Zaleski C, Jha S, Batut P, Chaisson M, Gingeras TR. 2013. STAR: ultrafast universal RNA-seq aligner. Bioinforma Oxf Engl 29:15–21.
41. Li B, Dewey CN. 2011. RSEM: accurate transcript quantification from RNA-Seq data with or without a reference genome. BMC Bioinformatics 12:323.
42. Edgar R, Domrachev M, Lash AE. 2002. Gene Expression Omnibus: NCBI gene expression and hybridization array data repository. Nucleic Acids Res 30:207–210.
43. Schmittgen TD, Livak KJ. 2008. Analyzing real-time PCR data by the comparative C(T) method. Nat Protoc 3:1101–1108.

Figures

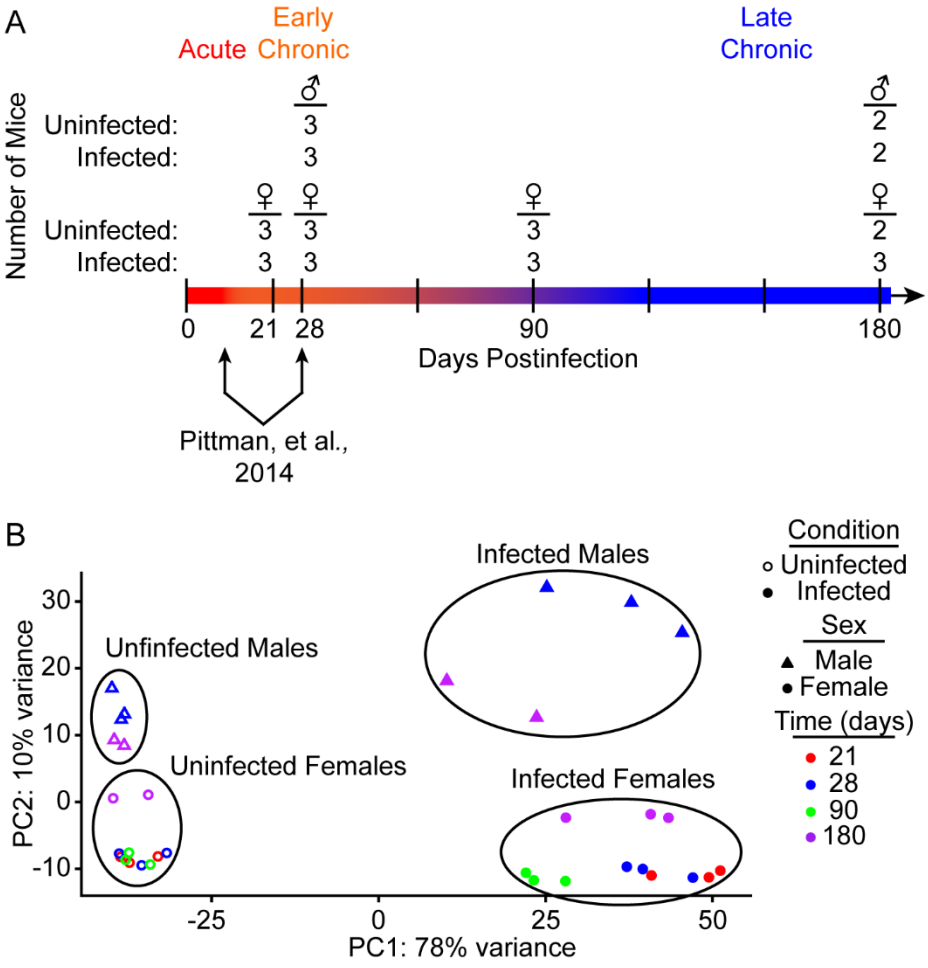

Figure 1. *RNA-seq of long-term chronic infection.* (A) Timeline of infection representing RNAseq timepoints, defining acute (<14 days), very early (21 days), early (28 days), mid (90 days) and late chronic (180 days) *T. gondii* infection. Female cerebral cortexes (♀) were harvested 21, 28, 90, and 180 days postinfection, and male cerebral cortexes (♂) were harvested 28 and 180 days postinfection. Numbers represent the number of individual mice used for each group in the RNAseq analysis. Arrows represent the timepoints used to compare acute and early chronic transcripts from the previous analysis (Pittman, et al., 2014). (B) PCA plot of samples used for RNA-seq analysis. Open symbols represent uninfected samples and closed symbols represent infected samples. Triangle represent males, and circles represent females. Colors correspond to timepoint of infection (red=21 days, blue=28 days, green=90 days, purple=180 days).

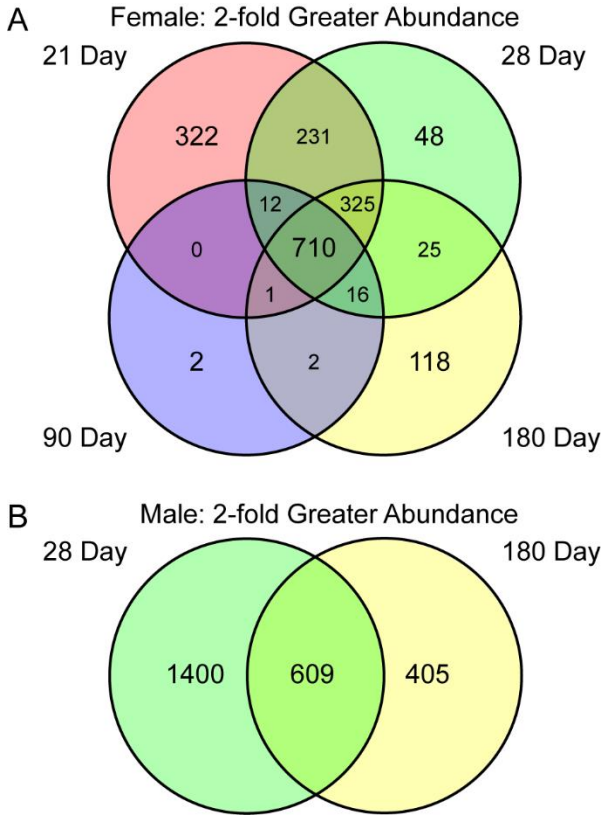

Figure 2. *Host genes with greater abundance after infection are shared throughout infection.* Number of female (A) and male (B) mouse genes with a greater than 2-fold increase from age-matched uninfected controls. Shared sets are represented by overlapping regions between the 21 day (red), 28 day (green), 90 day (blue), and 180 day (yellow) timepoints.

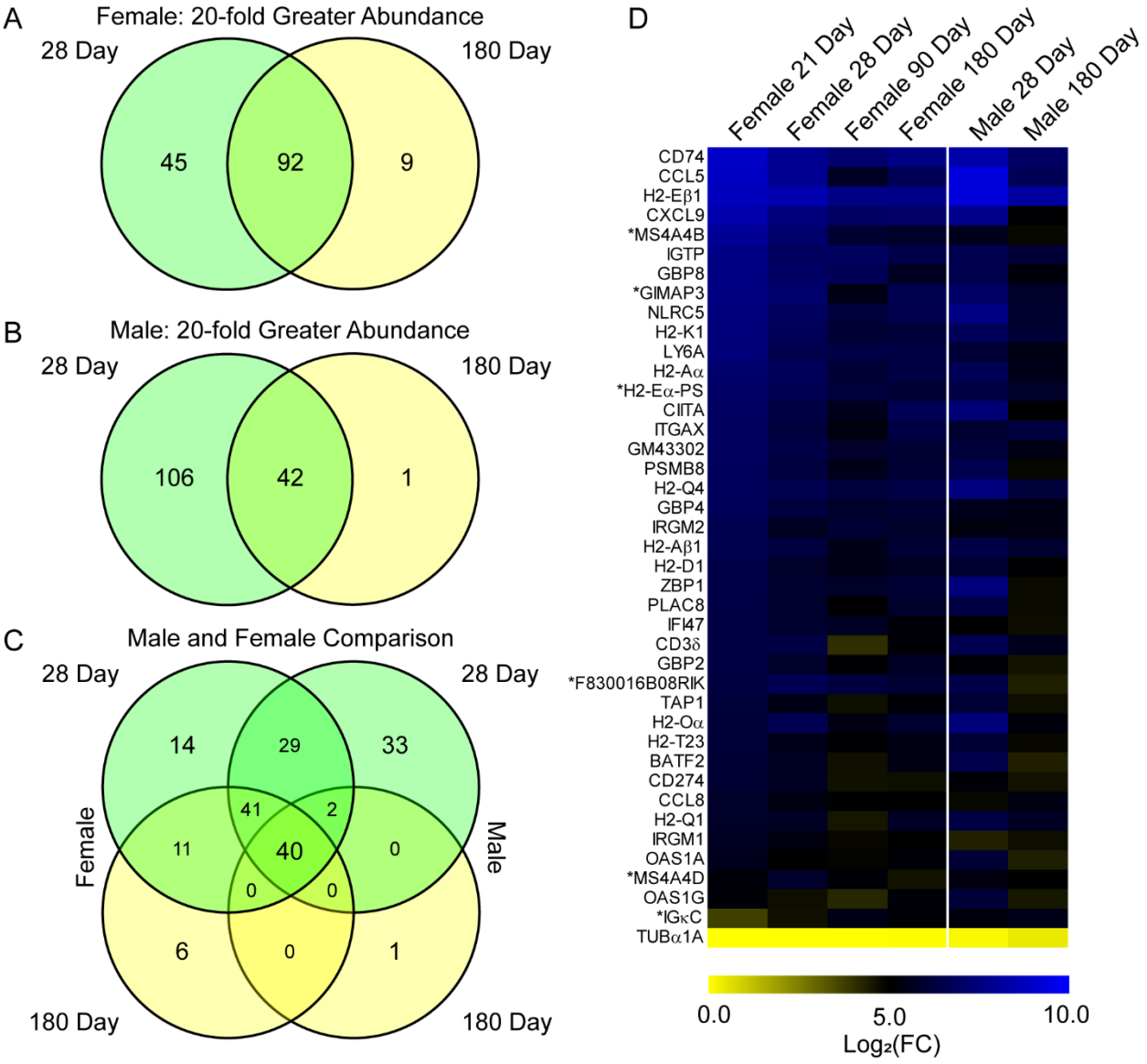

Figure 3. *Many enriched host genes are shared throughout infection and between sexes.* Number of female (A) and male (B) mouse genes with a 20-fold increase from uninfected controls. (C) Shared sets are represented by overlapping regions between the 28 day (green) and 180 day (yellow) timepoints. (D) Heatmap of differential expression compared to uninfected from the RNAseq data for the 40 mouse genes from panel C that are at least 20-fold more abundant in males and females at 28 and 180 days. Bright blue is 10.0 Log_2(FC) or 1024-fold

change. Yellow is no change, as seen for tubulin (Tubα1a) across the bottom. The six genes without an immune-relate GO term as marked with *.

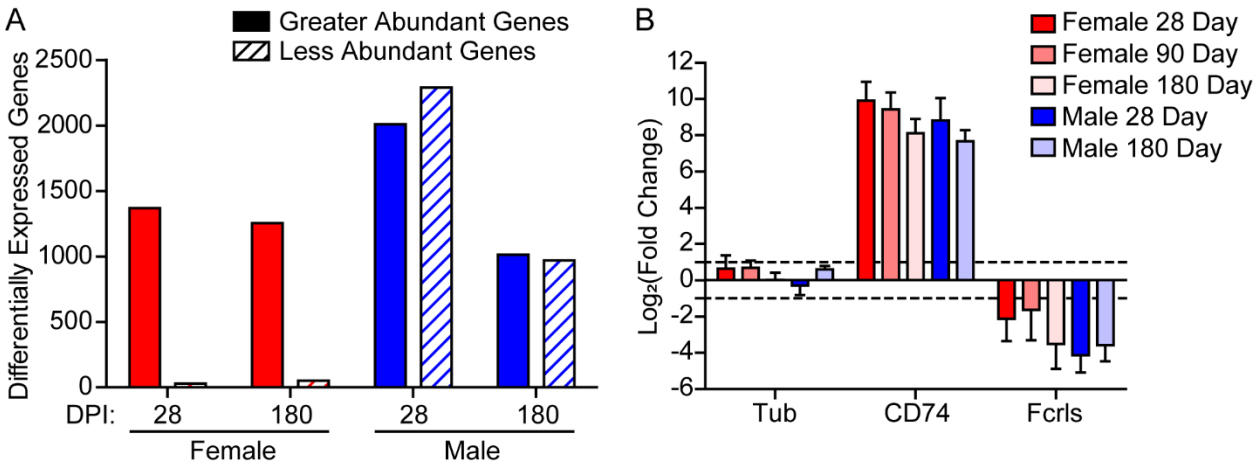

Figure 4. *Males have a greater number of less-abundant genes than females in response to infection.* (A) Total number of differentially express genes with both a FDR value <0.05 and a 2-fold increase (solid bars) or decrease (slashed bar) compared to uninfected controls for females (red) and males (blue) at 28 or 180 days postinfection (DPI). (B) qPCR analysis of one of the most differentially expressed genes with greater abundance (CD74) and one of the less abundant genes in both males and females (FCRLS), with tubulin as a control. Data from females is in shades of red, data from males is in shades of blue. Raw data was first normalized to housekeeping gene glyceraldehyde 3-phosphate dehydrogenase (GAPDH) before the fold change of infected versus uninfected was calculated.

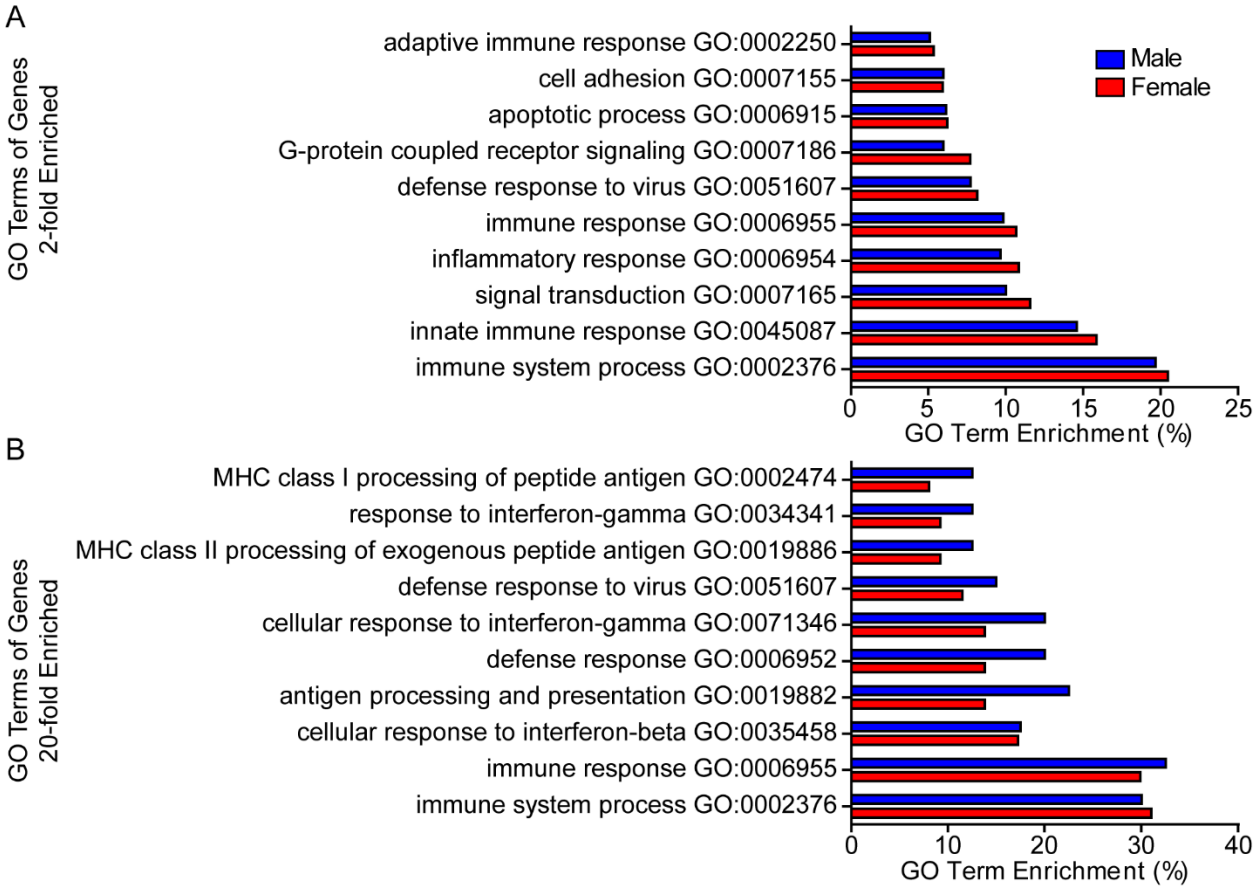

Figure 5. *Immunological gene ontology (GO) terms are highly enriched during infection.* (A) GO term enrichment was performed using the 710 genes with 2-fold greater abundance shared among the female timepoints (red) and the 609 genes with 2-fold greater abundance shared in the male timepoints (blue). (B) GO term enrichment for the >20-fold more abundant genes using the 92 genes shared among the female timepoints (red) and the 42 genes shared in the male timepoints (blue). Terms were sorted based on their q-value and the percent enrichment for the top ten most significant are shown.

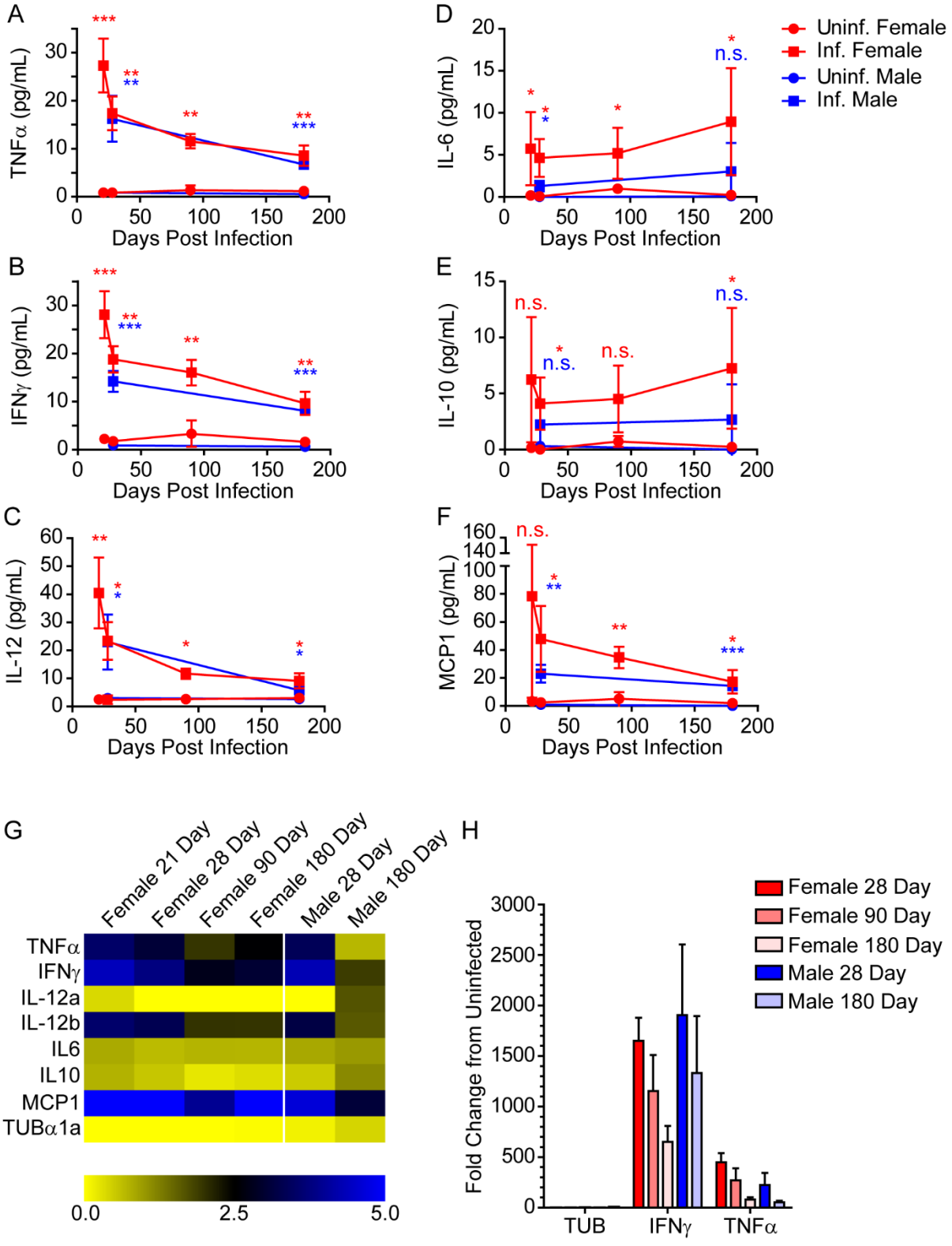

Figure 6. *Inflammatory cytokines are abundant throughout infection.* Serum TNF□□(A), IFN□□(B), IL-12 (C), IL-6 (D), IL-10 (E) and MCP1 (F) were quantified from the male (blue) and

female (red) mice used for the RNAseq analysis. Timepoints include 21, 28, 90 and 180 days postinfection. Circle symbols represent cytokines from infected mice and squares symbols represent uninfected mice. Data is the average concentration of three mice, except for infected and uninfected males at 180 days postinfection and uninfected females at 180 days postinfection, which had two mice each. Error bars represent the standard deviation between samples and asterisks indicate statistically significant differences between infected and uninfected samples by Student's t-test (n.s., not significant; *, $p<0.05$; **, $p<0.01$; ***, $p<0.001$). (G) Heatmap differential expression compared to uninfected, from the RNAseq data for the cytokine genes. Bright blue is 5.0 Log_2(FC) or 32-fold change. Yellow is no change as seen for tubulin (Tubα1a) across the bottom. The genes for the two subunits of IL-12 are shown, as the cytometric bead array quantified the dimeric form of IL-12 (IL-12p70). (H) qPCR analysis of the cytokine genes IFN□ and TNF□ □with tubulin as a control. Data from females is in shades of red, data from males is in shades of blue. Raw data was first normalized to housekeeping gene GAPDH before the fold change of infected versus uninfected was calculated.

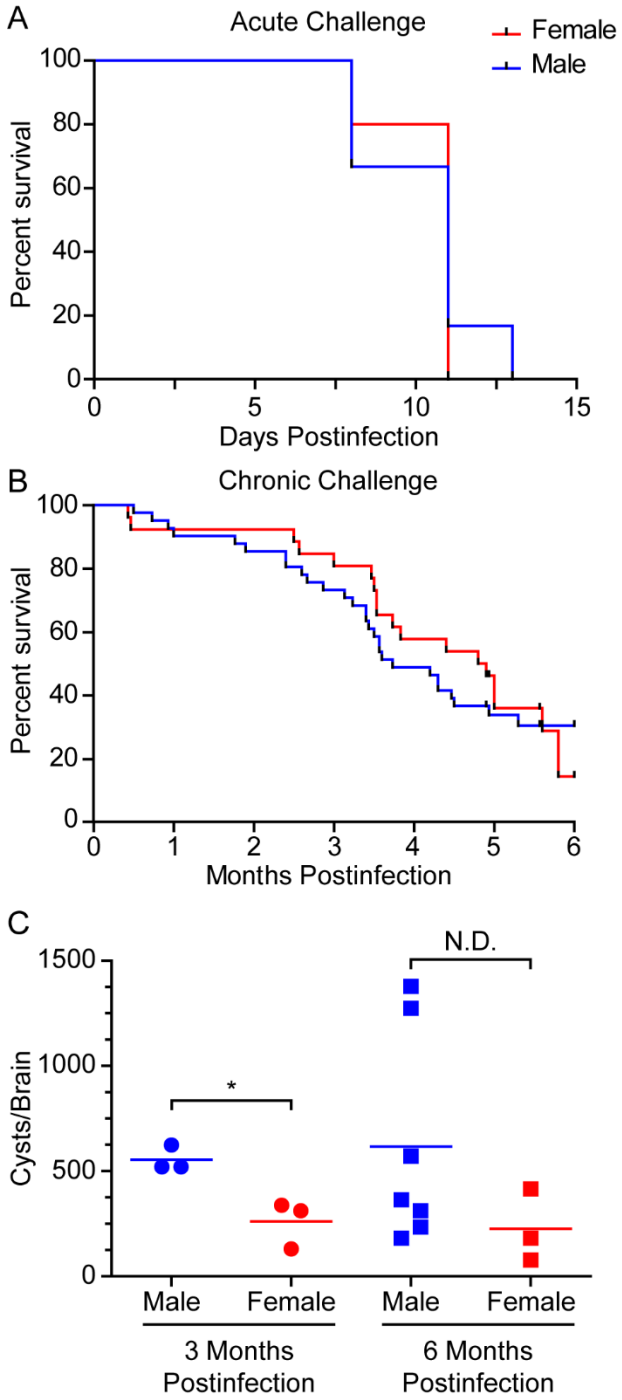

Figure 7. *Outcomes of T. gondii infection are similar in male and female mice.* (A) Acute survival curve of male (blue, n=6) and female (red, n=5) mice infected with $1x10^5$ parasites. (B) Chronic survival curve for male (n=28) and female (n=26) mice infected with $1x10^4$ parasites. (C) Cyst burden in brains of mice at 3 months (n=3 male, n=3 female) and of surviving mice at 6

months postinfection (from B; n=7 for males and n=3 female). Statistical differences between male and female survival curves was calculated using the Mantel Cox log-rank test, and differences between male and female cyst burdens was determined using Student's t-test (* $p<0.05$). N.D. = not determined because of inadequate power).

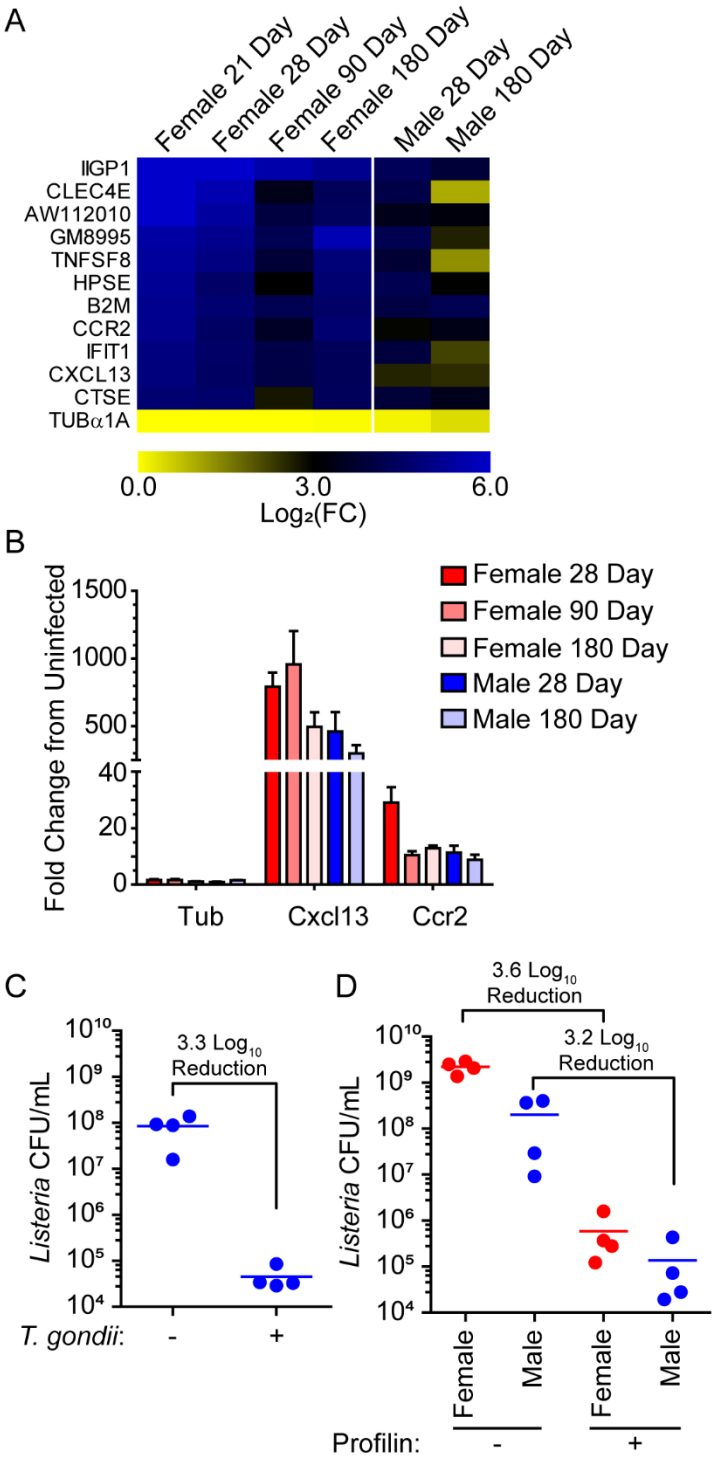

Figure 8. *Stimulation with T. gondii confers more resistance to L. monocytogenes in female mice.* (A) Heatmap of transcript abundance from the RNAseq data for the eleven genes that are more differentially expressed in females than males in response to *T. gondii* infection. Bright

blue is 6.0 Log_2(FC) or 64-fold change. Yellow is no change as seen for tubulin (Tubα1a) across the bottom. (B) qPCR analysis of CXCL13 and CCR2 with tubulin as a control. Data from females is in shades of red, data from males is in shades of blue. Raw data was first normalized to housekeeping gene GAPDH before the fold change of infected versus uninfected was calculated. (C) *L. monocytogenes* burden in spleens of male mice infected 28 days prior to *L. monocytogenes* with *T. gondii* (+, n=4) compared to uninfected male mice (-, n=4). (D) *L. monocytogenes* burden in spleens of female (red) and male (blue) mice (n=4/group) treated intravenously with saline (-) or 10 ng of recombinant *T. gondii* PRF (+) 4 hours prior to *L. monocytogenes* infection. Lines represent mean burden of each group.

Chapter 3

RIPK3 facilitates host and pathogen interactions after oral *Toxoplasma gondii* infection

Patrick W. Cervantes[1] and Laura J. Knoll[1*]

[1]Department of Medical Microbiology and Immunology, University of Wisconsin-Madison, Madison, Wisconsin, USA

*Corresponding author ljknoll@wisc.edu

Running Head: RIPK3 and host survival to oral *T. gondii* infection

Keywords: *Toxoplasma gondii,* Toxoplasmosis, ZBP1, RIPK3, cell death, necroptosis, pyroptosis

This chapter has been submitted to the journal of Infection and Immunity

Author contributions: PWC designed and performed all experiments.

Abstract

Toxoplasma gondii infection activates pattern recognition receptor (PRR) pathways that drive innate inflammatory responses to control infection. Necroptosis is a pro-inflammatory cell death pathway a part of the innate immune response that has evolved to control pathogenic infection. In this study we further defined the role of Z-DNA binding protein 1 (ZBP1) as a PRR and assessed its contribution to necroptosis as a host protection mechanism to *T. gondii* infection. We found that ZBP1 does not induce pro-inflammatory necroptosis cell death and ZBP1 null mice have reduced survival after oral *T. gondii* infection. In contrast, mice deleted in receptor-interacting serine/threonine-protein kinase 3 (RIPK3$^{-/-}$), a central mediator of necroptosis, have significantly improved survival after oral *T. gondii* infection even with higher parasite burden. The physiological consequences of RIPK3 activity did not show any differences in intestine villi immunopathology but RIPK3$^{-/-}$ mice showed higher immune cell infiltration and edema in the lamina propria. The contribution of necroptosis to host survival was clarified with mixed lineage kinase domain like pseudokinase null (MLKL$^{-/-}$) mice. We found MLKL$^{-/-}$ mice to succumb to oral *T. gondii* infection the same as wild type mice, indicating necroptosis-independent RIPK3 activity impacts host survival. These results provide new insights on the impacts of pro-inflammatory cell death pathways as a mechanism of host defense to oral *T. gondii* infection.

Introduction

Toxoplasma gondii is one of the most widespread parasitic infections in the world and is acquired by nearly 30% of the human population (1). The natural route of infection occurs by consuming food or water contaminated with tissue cysts from the asexual cycle or oocysts from the sexual cycle. Asexual cysts contain the bradyzoite stage, which differentiates into the tachyzoite stage after ingestion and invasion of the intestinal tract. Tachyzoites disseminate from the intestine throughout the body during acute infection. Host immune pressure causes tachyzoite parasites to differentiate into bradyzoite cysts that reside in the brain and muscle tissue. This stage constitutes a latent, chronic infection. Pathogen recognition and a balanced inflammatory immune response are necessary to survive an acute infection.

T. gondii elicits a strong T helper type 1 (Th1) response, characterized by interleukin-12 (IL-12) induced interferon-gamma (IFN-γ), which in turn orchestrates cell-mediated immunity important for intracellular-pathogen defense (2). Deficiencies in this pathway lead to uncontrolled parasite replication and host death (1, 3, 4), highlighted in mouse studies where IL-12, IFN-γ, toll-like receptors (TLR), and myeloid differentiation primary response 88 (MyD88) responses are perturbed (5-10). These signaling pathways, cytokines, and their downstream effectors are elevated throughout long-term chronic infection and must be maintained to prevent cyst reactivation and fatal encephalitis (11, 12).

In contrast to a weak Th1 response, a hyperactive and unregulated Th1 response results in severe tissue damage and host death (13, 14). Immune regulation by IL-10 is vital to host survival because IL-10 null mice succumb to oral *T. gondii* infection due to uncontrolled host immune response and not uncontrolled parasite replication (13, 14). Early studies in susceptible C57BL/6J mice used high dose oral *T. gondii* infections and showed mortality is caused by an excessive immune response that is accompanied by severe intestinal immunopathology and tissue necrosis (15-17). This fatal pathology is mediated by the

uncontrolled expression of IFN-γ, tumor necrosis factor (TNF), and nitric oxide (15, 16). Therefore, a balanced innate immune response is essential for a host to survive acute *T. gondii* infection.

The innate immune system employs pattern recognition receptors (PRRs) to identify pathogens. Common PRRs are TLRs, nucleotide oligomerization domain-like receptors (NLR), and DNA/RNA sensors like Z-DNA binding protein-1 (ZBP1). These PRRs induce programmed cell death pathways as a mechanism for host defense to infectious diseases (18, 19). Programmed cell death pathways include apoptosis, necroptosis, and pyroptosis. Apoptosis is a cell death pathway regarded as non-inflammatory, whereas necroptosis and pyroptosis are lytic forms of cell death that release highly pro-inflammatory damage associated molecular compounds (20, 21). Central to necroptosis is receptor-interacting serine/threonine-protein kinase 3 (RIPK3) and its downstream substrate mixed lineage kinase domain like pseudokinase (MLKL). Similarly, pyroptosis depends on caspase-1 activation that is mediated by NLR inflammasome components. The processes of necroptosis and pyroptosis ultimately induce cell membrane pores and lytic cell death that contribute to inflammatory immune responses, adaptive immunity, and host defense to pathogenic infection.

Our lab previously found *Zbp1* transcripts are highly expressed in the brains of mice chronically infected with *T. gondii* (22, 23). We also found ZBP1 to assist in host control of *T. gondii* infection *in vitro* and *in vivo* (24). Recently, IFN-γ has been shown to strongly induce ZBP1 to complex with RIPK3 to mediate inflammation and necroptosis as a host defense mechanism (25-28). Here, we tested the hypothesis that ZBP1-dependent necroptosis is protective for *T. gondii* infection.

Materials and methods

Ethics statement

All animal use was approved by and in agreement with the Institutional Animal Care and Use Committee (IACUC) at the University of Wisconsin-Madison (UW-Madison) (protocol #M005217). Cats were treated in compliance with the guidelines set by the IACUC of the United States Department of Agriculture, Beltsville Area (protocol #15-017). Both institutions adhere to the regulations and guidelines set by the National Research Council. All mice were monitored daily for clinical signs of disease and were euthanized if symptoms were severe.

Mouse experiments

All mice used were from the C57BL/6 background. Wild type (WT) were originally purchased from JAX but have been breed in the UW-Madison vivarium with all the other strains used for these studies. RIPK3 null (RIPK3$^{-/-}$) mice were provided from Genentech (29). MLKL null (MLKL$^{-/-}$) mice were provided by Dr. Doug Green at St. Jude Children's Research Hospital (30). The RIPK3$^{-/-}$ stain was genotyped by PCR with three primers: 5'-AGAAGATGCAGCAGCCTCAGCT, 5'-ACGGACCCAGGCTGACTTATCTC, and 5'-GGCACGTGCACAGGAAATAGC. The MLKL$^{-/-}$ strain was also genotyped by PCR with primers: 5'-TATGACCATGGCAACTCACG, 5'-ACCATCTCCCCAAACTGTGA, and 5'-TCCTTCCAGCACCTCGTAAT.

Z-DNA Binding Protein-1 CRISPR-Cas9 generated mouse knockout.

The ZBP1 null (ZBP1$^{-/-}$) mouse was generated at the UW-Madison Biotechnology Center. Two guide RNAs were designed to target the 5'-end (CGATCCCCTCTTACGTAATA; Chr:2 173219317-173219336) and 3'-end (TCAATCAATCGATCAACCGC; Chr:2 173207132-173207151) of *Zbp1*, removing 14KB of genomic DNA (gDNA) that included the promoter and all splice variants (Fig. S1A). The RNA guides were optimized for the least off-target effects

within the Zhang Laboratory CRISPR Design tool (crispr.mit.edu). The guides were cloned into the plasmids pX330 or pX548 (obtained from Zhang Laboratory via Addgene; Cambridge, MA) and the PCR products were transcribed with the T7 MEGAshortscript kit (Life Technologies). A mixture of 50 ng/μL guide RNAs and 40 ng/μL of Cas9 protein in injection buffer (5 mM Trizma Base, 5 mM Tris HCL, 0.1 mM EDTA, pH 7.4) was injected into the pronucleus of one-day old fertilized embryos isolated from C57BL/6 mice. The resulting pups were genotyped by PCR with a mixture of three *Zbp1* primers (5'-CAACGACTGCTGCTGTCTTGC, 5'-GAACTCTGTGAAAGCCCTGTGAGG, 5'-CCTCATCCCCTGGTTGGTGTTAC). Mice with a WT genotype produce a 376 base pair band and the ZBP1$^{-/-}$ genotype produce a 538 base pair band (Fig. S1B).

Necroptosis assay.

Lactate dehydrogenase (LDH) release was used as a measure of necroptosis in bone marrow derived macrophages (BMDM) from 2 independent experiments according to the manufacturer's instructions (Sigma-Aldrich, MAK066-1KT). Bone marrow derived macrophages were harvested from 8 – 10-week-old mice and grown in 20% L929 conditioned RPMI medium as described (31). Harvested BMDM were seeded in technical triplicate at 5 x 10^4 cells/well in a 96-well plate. Cells were infected with 2.5 x 10^5 ME49 tachyzoites or left uninfected for 3 hours. After infection, the cells were washed with PBS (Calcium and magnesium free) and stimulated with 50 ng/mL TNF (PMC3013) and 40 μM Z-VAD-FMK (ab120382) or left unstimulated for 24 hours. Necrostatin-1 (SC-200142) was added at 50 μM as a control to inhibit necroptosis. Media supernatant was used to measure LDH release at 450 nm every 5 minutes for 1 hour in a BioTek Synergy HT plate reader. An NADH standard curve was used to determine the amount of LDH activity for each sample by the colorimetric assay.

Parasites for in vitro and in vivo experiments

The ME49 type-2 *T. gondii* strain was used for all experiments and maintained in human foreskin fibroblast cells. The mCherry parasites were generated as follows: ME49 *T. gondii* strain (1×10^7) was electroporated with 25 µg tub-mCherry (32), linearized with KpnI, and selected with chloramphenicol. Clones were isolated by limiting dilution. Tachyzoites were injected into mice for at least 28 days and bradyzoites were collected from the brains for passage through a feline and mCherry oocysts were collected from the feces. Oocysts concentration was calculated using a hemocytometer. Brain tissue cysts were collected from chronically infected C57BL/6J mice and the number of brain tissue cysts for oral infection was determined by immunofluorescence as described previously (24).

Survival curve.

Male or female mice between 9 and 13 weeks old were used for oral and intraperitoneal (IP) challenges. Oral challenges were performed by gavage with mCherry oocysts or bradyzoite brain cysts. The mCherry oocyst oral challenge was done with 6×10^3 oocysts/mouse and the brain tissue cyst oral challenge was done with 2×10^3 or 4×10^3 brain tissue cysts/mouse. The IP infection was performed with 1×10^4 tachyzoites/mouse. All mice were monitored daily for clinical signs of disease and euthanized when moribund.

Intestine pathology

Intestine pathology was evaluated by histology and length. The Comparative Pathology Laboratory at UW-Madison scored blinded hematoxylin and eosin (H&E) stained ileum swiss rolls from female mice infected with 600 mCherry oocysts by oral gavage at day 7 post infection. The ileum (distal 1/3 of the small intestine) was washed with PBS and fixed in 10% buffered formalin in a swiss roll. Uninfected female mice ileum samples were processed as controls. The

slides were blinded and scored from 0 – 5 (0 = equivalent to control and 5 = severe) on inflammation, gland loss, smooth muscle vacuolation, and edema. The intestine length was measured in male and female mice at 7 – 10 weeks old that were gavage fed 1 x 10^4 mCherry oocysts. The small intestine was measured at 7 days post infection. Uninfected male and female mice 7 – 10 weeks old were used to normalize the intestine length of infected mice.

In vivo parasite quantification.

Parasite burden was determined in intestine samples by mCherry fluorescence and qPCR. The UW-Madison Small Animal Imaging and Radiotherapy Facility provided an *in vivo* imaging system (IVIS) to measure mCherry fluorescence. Male and female mice at 7 – 11 weeks old were gavage fed 1 x 10^4 mCherry oocysts/mouse in 2 independent experiments. At 7 days post infection the mice were sacrificed, their intestines were removed, and mCherry fluorescence was measured (excitation 587 and emission 610) by IVIS. The fluorescence of infected WT and RIPK3$^{-/-}$ mice was normalized to the average fluorescence in uninfected male and female mice. Parasite burden measured by qPCR was performed with parasite specific SAG1 primers (5'-TGCCCAGCGGGTACTACAAG and 5'-TGCCGTGTCGAGACTAGCAG) on gDNA from three intestine sections. Total gDNA was extracted from 1 cm sections from the duodenum, jejunum, and ileum tissues in female mice orally infected with 3 x 10^4 mCherry oocysts at 7 days post infection by Trizol following the manufacturer's instructions. A gDNA *T. gondii* standard curve was generated from a known concentration of parasites cultured in human foreskin fibroblast cells to calculate burden. A StepOne Real-Time PCR machine with iTaq Universal SYBR Green Supermix (Bio Rad, 1725120) was used to determine parasite number in each intestine section relative to a standard curve of parasite gDNA. Total parasite/ng was normalized across all 3 intestine tissue sections for each mouse sample.

Brain cyst quantification.

The number of brain cysts was determined by immunofluorescence at 28 days post oral infection with 3 x 10^3 mCherry oocysts in male mice. Each brain was homogenized separately with a Dounce homogenizer, fixed with 4% paraformaldehyde for 20 minutes, quenched with 0.1 M glycine for 2 minutes, and blocked for 1 hour at room temperature in blocking buffer (PBS with 3% BSA and 0.2% Triton-X 100). Brain cysts were stained with streptavidin conjugated Dolichos biflorus agglutinin (Vector laboratories, B-1035-5) for 1 hour at room temperature, washed in PBS with 0.1% Triton-X 100, followed by incubation with a biotinylated Alexa Flour 594 (Thermo Fisher, S11227) secondary antibody for 1 hour at room temperature in the dark. An aliquot of processed brains was mounted on glass coverslips, blinded and the number of cysts was counted on a Zeiss inverted Axiovert 200 motorized microscope with 10x objective.

In vitro parasite quantification.

The parasite burden *in vitro* was determined by immunofluorescence in BMDM. A total of 1 x 10^5 BMDM were seeded on glass coverslips and infected with 5 x 10^5 tachyzoite parasites for 3 hours. After infection, cells were stimulated with 25 ng/mL LPS and 25 U/mL IFN-γ for 24 and 48 hours. Cells were fixed with 3% formaldehyde for 20 minutes, quenched for 5 minutes with 0.1M glycine, and blocked for 1 hour at room temperature in blocking buffer (PBS with 3% BSA and 0.2% Triton-X 100). Parasites were stained with chronic infection serum for 1 hour at room temperature, followed by Alexa Flour 488 anti-mouse (Thermo Fisher, Z25002) secondary antibody for 1 hour. All slides were blinded before counting. The 24-hour timepoint included 7 WT and 5 RIPK3$^{-/-}$ coverslips, and the 48-hour timepoint included 6 WT and 6 RIPK3$^{-/-}$ coverslips. Total parasites were counted in 150 vacuoles and visualized using a Zeiss inverted Axiovert 200 motorized microscope with a 100x oil objective.

Intestine permeability assay.

Intestine permeability was determined by LPS and FITC-dextran concentration in mouse blood serum after oral infection. Serum LPS concentration was measured with the Pierce Chromogenic Endotoxin Quant Kit (Thermo Scientific, A39552) following the manufacture's protocol. Male and female mice were orally infected with 1 x 10^4 mCherry oocysts by gavage. As a positive control, male and female mice were treated with 3% dextran sodium sulfate (DSS) in drinking water. Paired blood serum was collected at days 0 (uninfected), 3, 5, and 7 post infection. Blood serum LPS concentration was measured spectrophotometrically at 405 nm in a 96-well BioTek Synergy HT plate reader. Intestine permeability was determined by FITC-dextran concentration in mouse blood serum after oral infection. Female mice were infected for 7 days with 600 mCherry oocysts by gavage. Mice were fasted overnight, gavage fed 0.44 mg/g FITC-dextran, and after 4 hours blood serum was collected at euthanasia. FITC-dextran was quantified spectrophotometrically (485 nm excitation and 528 nm emission) from blood serum.

Blood serum cytokine measurement.

The BD Cytometric Bead Array Mouse Inflammation Kit (BD Biosciences, 552364) was used to measure IL-6, IL-10, monocyte chemoattractant protein-1 (MCP-1), IFN-γ, TNF, and IL-12 from blood serum. Female mice at 8 – 13 weeks old were gavage fed 6 x 10^3 mCherry oocysts and euthanized at 7, 8, and 9 days post infection in 3 independent experiments. Blood serum was collected for cytokine analysis by flow cytometry with a ThermoFischer Attune at the UW-Madison Flow Cytometry Core.

Results

ZBP1$^{-/-}$ and RIPK3$^{-/-}$ mice show divergent phenotypes to necroptosis and host survival

The ZBP1 knockout mice used in Pittman *et al.* 2016 (24) originated from the Shizuo Akira lab and appear to have a mixed genetic background (33). This mixed background in the Akira knockout has complicated comparisons to WT mice (33). To rectify this, we created a new ZBP1 null (ZBP1$^{-/-}$) mouse in the C57BL/6 background using CRISPR-Cas9 technology to remove the entire *Zbp1* genomic locus, including the promoter and all mRNA splice variants (Fig. S1). We then evaluated the role of ZBP1 in host protection during *T. gondii* infection.

Necroptosis is a pro-inflammatory cell death pathway where cells become permeable and release damage associated molecular compounds that enhance inflammatory responses (20). Because ZBP1 has been shown to drive RIPK3-dependent necroptosis (34), we tested whether ZBP1 could activate this pathway during *T. gondii* infection. We included RIPK3 null (RIPK3$^{-/-}$) mice as a negative control for necroptosis because RIPK3 kinase and scaffold domains are essential for necroptosis (35, 36). Necroptosis was measured in WT, ZBP1$^{-/-}$, and RIPK3$^{-/-}$ bone marrow derived macrophages (BMDM) by lactate dehydrogenase (LDH) release. LDH release was reduced in all genotypes treated with necrostatin-1, a necroptosis inhibitor (Fig. 1A). Infection with *T. gondii* alone caused little LDH release in each BMDM genetic background, but stimulation with TNF and Z-VAD-FMK (a pan caspase inhibitor that drives necroptosis) caused a similar increase in LDH release in WT and ZBP1$^{-/-}$ BMDM. The LDH release in WT and ZBP1$^{-/-}$ BMDM was amplified when stimulation with TNF and Z-VAD-FMK was combined with *T. gondii* infection (Fig. 1A). In contrast, RIPK3$^{-/-}$ BMDM showed no LDH release above background in any condition. This outcome indicates that ZBP1 does not promote cell permeability, a process apart of necroptosis, while RIPK3 influences cell membrane integrity during *T. gondii* infection.

Pro-inflammatory cell death pathways, like necroptosis, have evolved to protect the host from pathogenic infections (18). An acute host survival challenge is a simple assay to determine a gene's contribution to host protection during infection. We established host protection against *T. gondii* by intraperitoneal (IP) and oral infection. Similar to previous observations (20), there was no significant difference between WT and ZBP1$^{-/-}$ mouse survival after IP inoculation (Fig. 1B), but the ZBP1$^{-/-}$ mice were more susceptible to oral *T. gondii* challenges with oocysts and brain tissue cysts (Fig. 1C&D, S2 - 4). Along with ZBP1$^{-/-}$ mice, the RIPK3$^{-/-}$ mice also showed no difference in survival after IP inoculation with *T. gondii* tachyzoites (Fig. 1B). However, unlike ZBP1$^{-/-}$ mice, the RIPK3$^{-/-}$ mice had significantly improved survival after oral infection with both *T. gondii* oocysts and brain tissue cysts (Fig. 1C & D). These results suggest that while ZBP1 and RIPK3 both play roles during oral *T. gondii* infection, they are likely working in different pathways.

RIPK3$^{-/-}$ mice have higher parasite burdens

We sought to understand the role of RIPK3 in host defense responses given the striking survival phenotype to oral infection. Genetic evidence supports RIPK3-dependent necroptosis clears viral, bacterial, and parasitic infections which can affect host susceptibility (25, 26, 36-40). We determined the *T. gondii* parasite burden at the peak acute infection by measuring mCherry parasite fluorescence and by qPCR in intestine sections. A significantly higher mCherry signal was present in RIPK3$^{-/-}$ intestines compared to WT (Fig. 2A) which correlated with a greater parasite load by qPCR (Fig. 2B). Oral infection with a sub-lethal mCherry oocyst dose also showed an increased parasite burden in RIPK3$^{-/-}$ small intestine and livers during acute infection (Fig. S5) and mouse brains at chronic infection (Fig. 2C). Moreover, RIPK3$^{-/-}$ BMDM exhibited increased total parasite burden by immunofluorescence *in vitro* after infection and stimulation (25 ng/mL LPS and 25 U/mL IFN-γ) (Fig. 2D). These results reinforce previous evidence for

RIPK3 control of pathogenic infections, and more importantly, these results suggest that fatality in WT mice is not a consequence of increased parasite replication.

WT and RIPK3$^{-/-}$ mice do not have differences in intestinal villi pathology

As RIPK3 is associated with mucosal immune pathology (41, 42) and oral *T. gondii* infection causes intestinal inflammation (43-46), we assessed intestinal villi immunopathology. At day 7 post oral *T. gondii* infection, H&E stained ileum swiss rolls were blinded and assessed for villi integrity. While we saw signs of villi damage due to oral *T. gondii* infection, there were no differences in villi damage between WT and RIPK3$^{-/-}$ mice (Fig. 3). We further examined villi integrity by measuring intestine permeability because it was previously seen that oral *T. gondii* infection causes lipopolysaccharide (LPS) from the bacterial microbiome as well as gavage fed FITC-dextran to enter the circulation (47). Using a dextran sulfate sodium-induced colitis model as a positive control, we measured LPS in the blood at 3, 5, and 7 days after oral *T. gondii* infection. There were no significant differences in serum LPS (Fig. 4A) or gavage fed FITC-dextran concentration in blood serum between WT and RIPK3$^{-/-}$ mice (Fig. S6). These results suggest that intestine permeability induced by oral *T. gondii* infection is equivalent in both strains and the increased survival seen in RIPK3$^{-/-}$ mice after oral *T. gondii* infection is not due to decrease intestinal villi pathology.

RIPK3$^{-/-}$ mice have more immune cell infiltration and edema in the lamina propria

After oral infection, *T. gondii* parasites can be found largely in the lamina propria of the ileum (48-50). We noticed that large patches of immune cells tended to be more common in the lamina propria of RIPK3$^{-/-}$ mice after oral *T. gondii* infection (Fig. 3), so we submitted the H&E stained ileum swiss rolls to the UW-Madison Comparative Pathology Laboratory for analysis. They scored gland loss, immune cell infiltration, edema in the lamina propria, and vacuolation of

the muscularis mucosa (Fig. 4B-E). While none of these scores reached statistical significance, there was a trend for the RIPK3$^{-/-}$ mice to have increased inflammatory measures compared to WT mice. We then measured the length of the entire infected small intestine because intestine shortening is associated with tissue damage and pathology from oral *T. gondii* infections (43-46). The difference in intestine length was significant (Fig. 4F) as WT mice lost 17% intestine length compared to a 10% loss in RIPK3$^{-/-}$ mice. The longer RIPK3$^{-/-}$ intestine length could be due to swelling from increased edema, immune cell infiltration, and muscularis vacuolation or it could be due to decreased immunopathology.

RIPK3$^{-/-}$ mice have higher IFN-γ and lower IL-10

As inflammatory cytokines are critical for the control of *T. gondii* infection, we compared serum cytokine levels between WT and RIPK3$^{-/-}$ mice using the cytometric bead array mouse inflammation kit. There were no differences in MCP-1, IL-6, IL-12, and TNF systemic cytokines levels between WT and RIPK3$^{-/-}$ mice at any of the time points examined (Fig. S7A-D). However, at day 9 post oral infection, RIPK3$^{-/-}$ mice had significantly higher IFN-γ (Fig. 5A) and reduced IL-10 levels (Fig. 5B). IFN-γ and IL-10 are both essential for mice to survive acute *T. gondii* infection, but IFN-γ is necessary to control parasitemia (9, 10) and IL-10 is necessary to control the host immune response (13, 14). These results may be due to the higher parasitemia in the RIPK3$^{-/-}$ mice (Fig. 2).

MLKL$^{-/-}$ and RIPK3$^{-/-}$ mice show divergent host survival phenotypes

Necroptotic induced cell death and inflammation are dependent on RIPK3, but RIPK3 activity is not limited to necroptosis (51). The necroptosis executioner, MLKL, is the downstream substrate of RIPK3 that ultimately compromises cell membranes, fulfilling the necroptotic pathway (52). We specifically examined RIPK3-dependent necroptosis in host survival to oral *T.*

gondii infection with MLKL null (MLKL$^{-/-}$) mice. After oral infection, MLKL$^{-/-}$ mice succumb to infection similar to WT mice, whereas RIPK3$^{-/-}$ mice showed improved survival (Fig. 6, S8). This data provides evidence that RIPK3-independent necroptosis contributes to severe intestine pathology and host death.

Discussion

Innate immune activation and its role in host defense to pathogenic infections depend on PRR driven inflammation. ZBP1 has recently come to light as a PRR involved in innate immunity and programmed cell death (34). Mechanisms of programmed cell death include apoptosis, necroptosis, and pyroptosis. *T. gondii* has evolved mechanisms to inhibit apoptosis to promote fitness (53). However, the host maintains cellular cross-talk between each programmed cell death pathway to subvert apoptosis inhibition and guard against pathogenic infection via necroptosis and pyroptosis (18). ZBP1 was found to mediate the interferon-induced necroptosis pathway in response to viral infection (27, 28). ZBP1 as a PRR that induces immunity could fit within the realm of bacterial and parasitic infection (24, 54-56). The fact that IFN-γ and ZBP1 are highly expressed and maintained throughout *T. gondii* infection (22, 23), make *T. gondii* a thought-provoking target to investigate the role of ZBP1 in non-viral infections. Our lab previously found ZBP1 to be important for oral but not IP infection (24). Here, we sought to determine the potential role of ZBP1 in host induced necroptosis in response to *T. gondii* infection by comparing ZBP1$^{-/-}$ and RIPK3$^{-/-}$ mice.

We tested ZBP1 induced necroptosis by LDH release in BMDM and found ZBP1 to be independent of necroptosis in *T. gondii* infection. We also found ZBP1$^{-/-}$ and RIPK3$^{-/-}$ mice to have opposing responses to oral *T. gondii* infection, with ZBP1$^{-/-}$ mice being more susceptible (24) and RIPK3$^{-/-}$ mice being more resistant (Fig. 1). Studies using high dose oral *T. gondii* infection have linked excessive Th1 immunity and intestinal pro-inflammatory cell death as the

culprit in host mortality (15-17). The physiological role of RIPK3-dependent necroptosis can drive immunopathology and impair host fitness (35, 36, 41, 42). These findings support the fact that RIPK3$^{-/-}$ mice have improved survival to oral *T. gondii* infection even with a higher parasite burden (Fig. 2). While there were no differences between WT and RIPK3$^{-/-}$ mice in intestinal villi damage, there was a trend for the RIPK3$^{-/-}$ mice to have increased inflammatory measures in the lamina propria (Fig. 3, 4), as well as a reduction in IL-10 (Fig. 5). IL-10 is up-regulated to control excessive Th1 cells and prevent immunopathology (57) and has previously been seen to be key in host survival after *T. gondii* infection (13, 14). All of these factors contradict a model where RIPK3$^{-/-}$ mice survive oral *T. gondii* infection better than WT mice because of reduced immunopathology. RIPK3$^{-/-}$ mice have reduced intestinal length loss after oral *T. gondii* infection compared to WT mice (Fig. 4F). This difference could be due to the WT mice having RIPK3-dependent activity causing more severe intestinal immunopathology, or more likely, it could be that the small intestine in the RIPK3$^{-/-}$ mice is more swollen and longer with the increased edema, immune cell infiltration, and muscularis vacuolation (Fig. 4B-D).

Gut bacteria drive an unregulated immune response that results in early host death, cellular necrosis, and severe tissue pathology in susceptible C57BL/6 WT mice in high dose oral *T. gondii* infections (44, 58). The inflammatory response reduces antimicrobial compound secretion and compromises the epithelial barrier, which allows greater interaction with gut bacteria to promote Th1 immunity and pathogen control (47). Gnotobiotic and antibiotic treated mice are one of the few models that have also shown improved survival and higher parasite burdens after lethal oral *T. gondii* infections (44), similar to our RIPK3$^{-/-}$ mice. Therefore, we examined intestine permeability by measuring bacterial LPS or gavage-fed FITC-dextran concentration in blood serum after oral *T. gondii* infection. There was no difference in LPS or FITC-dextran concentration in blood serum between WT and RIPK3$^{-/-}$ mice (Fig. 4A, S6), which

suggests intestine permeability and the degree of immune activation by gut bacteria is equivalent.

The biological function of RIPK3 appears to be only important for the natural route of *T. gondii* infection as there is not a difference in susceptibility between WT and RIPK3$^{-/-}$ mice after IP infections. This implicates the importance of exposure route when studying host responses to pathogenic infections. The difference in RIPK3$^{-/-}$ mouse survival between IP and oral infection likely contrast in pathogen recognition pathways that lead to immune stimulation. This result was evident in TLR-11 null (TLR-11$^{-/-}$) mice that also have improved survival to oral but not IP *T. gondii* infection (59). TLR-11 in mice is a PRR that recognizes *T. gondii* profilin which activates MyD88 dependent signaling pathways to induce IL-12 and IFN-γ, two critical cytokines for host survival to *T. gondii* infection (60). When TLR-11$^{-/-}$ mice are challenged with *T. gondii* by IP infection, the host is unable to recognize the pathogen, mount an appropriate immune response, and as a consequence, is overcome by uncontrolled parasite replication. In contrast, oral infection generates a TLR-11-independent protective immune response from gut bacteria that improves host survival. This study points towards an important role for gut bacteria to stimulate PRRs and immunity in the intestine to help fight pathogenic infections.

The role of RIPK3 is not limited to necroptosis. RIPK3 can activate pyroptosis as an alternative cell death mechanism that releases the pro-inflammatory effectors, IL-1β and IL-18. Pyroptosis and its pro-inflammatory effectors are activated upon *T. gondii* infection and have been shown to control parasite burden in *in vitro* and *in vivo* oral infection models (61, 62). The proportion of RIPK3 activity in necroptosis or pyroptosis in host survival to oral *T. gondii* infection was clarified with MLKL$^{-/-}$ mice. The observation that MLKL$^{-/-}$ mice succumb to oral infection with WT mice indicated that necroptosis does not play a major role in the survival difference between WT and RIPK3$^{-/-}$ mice. The difference in survival between RIPK3$^{-/-}$ and MLKL$^{-/-}$ mice could be attributed to their ability to initiate pyroptosis because RIPK3 can activate

pyroptosis in an MLKL-dependent or -independent manner (63, 64). This result agrees with previous findings that show inhibition of pyroptosis effectors IL-1β and IL-18 improve host survival to oral *T. gondii* infection (17, 65-67). However, genetic knockouts in other inflammasome and pyroptosis components have shown conflicting results in host susceptibility from IP *T. gondii* infection (68-70). Our study provides further evidence that supports inflammasome activation in oral *T. gondii* infection affects the host immune response.

Our CRISPR-Cas9 ZBP1$^{-/-}$ mouse had no significant effect on host survival to IP infection and reduced survival to oral challenge. This result corresponded with our previous findings, where the Akira ZBP1 knockout mice also showed no significant difference to IP infection but reduced survival to oral infection (24). Although independent groups have linked ZBP1 function to necroptosis, they have reported opposing susceptibility phenotypes to viral infection with the Akira ZBP1 knockouts (26, 37). Thus, the relevance of ZBP1 to host vulnerability in infectious diseases could be remedied by our clean CRISPR-Cas9 ZBP1$^{-/-}$ mouse.

Acknowledgments

We sincerely thank JP Dubey for oocyst production of mCherry expressing parasites, Sarah Wilson for assistance with IVIS, Laura Lettenberg for assistance with parasite replication assays, Wynne Moss for the creation of the ME49 strain expressing mCherry, and Melissa Graham for blinded histopathological analysis. We also thank Genentech for providing RIPK3$^{-/-}$ mice and Dr. Doug Green at St. Jude Children's Research Hospital for providing (MLKL$^{-/-}$) mice. This work was supported by the National Institutes of Health grants T32 AI007414 (PWC) and R01AI144016-01(LJK) as well as the National Science Foundation Graduate Research Fellowship Program grant DGE-1747503 (PWC). Any opinions, findings, and conclusions or

recommendations expressed in this material are those of the authors and do not necessarily reflect the views of the funding agencies.

References

1. Pittman KJ, Knoll LJ. 2015. Long-Term Relationships: the Complicated Interplay between the Host and the Developmental Stages of Toxoplasma gondii during Acute and Chronic Infections. Microbiol Mol Biol Rev 79:387-401.
2. Cosmi L, Maggi L, Santarlasci V, Liotta F, Annunziato F. 2014. T helper cells plasticity in inflammation. Cytometry A 85:36-42.
3. Sasai M, Pradipta A, Yamamoto M. 2018. Host immune responses to Toxoplasma gondii. Int Immunol 30:113-119.
4. Cohen SB, Denkers EY. 2015. The gut mucosal immune response to Toxoplasma gondii. Parasite Immunology 37:108-117.
5. Egan CE, Sukhumavasi W, Butcher BA, Denkers EY. 2009. Functional aspects of Toll-like receptor/MyD88 signalling during protozoan infection: focus on Toxoplasma gondii. Clin Exp Immunol 156:17-24.
6. Scanga CA, Aliberti J, Jankovic D, Tilloy F, Bennouna S, Denkers EY, Medzhitov R, Sher A. 2002. Cutting edge: MyD88 is required for resistance to Toxoplasma gondii infection and regulates parasite-induced IL-12 production by dendritic cells. J Immunol 168:5997-6001.
7. Gazzinelli RT, Hayashi S, Wysocka M, Carrera L, Kuhn R, Muller W, Roberge F, Trinchieri G, Sher A. 1994. Role of IL-12 in the initiation of cell mediated immunity by Toxoplasma gondii and its regulation by IL-10 and nitric oxide. J Eukaryot Microbiol 41:9S.
8. Khan IA, Matsuura T, Kasper LH. 1994. Interleukin-12 enhances murine survival against acute toxoplasmosis. Infect Immun 62:1639-42.
9. Scharton-Kersten TM, Wynn TA, Denkers EY, Bala S, Grunvald E, Hieny S, Gazzinelli RT, Sher A. 1996. In the absence of endogenous IFN-gamma, mice develop unimpaired

IL-12 responses to Toxoplasma gondii while failing to control acute infection. J Immunol 157:4045-54.

10. Deckert-Schlüter M, Rang A, Weiner D, Huang S, Wiestler OD, Hof H, Schlüter D. 1996. Interferon-gamma receptor-deficiency renders mice highly susceptible to toxoplasmosis by decreased macrophage activation. Lab Invest 75:827-41.
11. Garfoot AL, Cervantes PW, Knoll LJ. 2019. Transcriptional Analysis Shows a Robust Host Response to *Toxoplasma gondii* during Early and Late Chronic Infection in Both Male and Female Mice. Infect Immun 87.
12. Suzuki Y, Joh K. 1994. Effect of the strain of Toxoplasma gondii on the development of toxoplasmic encephalitis in mice treated with antibody to interferon-gamma. Parasitol Res 80:125-30.
13. Suzuki Y, Sher A, Yap G, Park D, Neyer LE, Liesenfeld O, Fort M, Kang H, Gufwoli E. 2000. IL-10 is required for prevention of necrosis in the small intestine and mortality in both genetically resistant BALB/c and susceptible C57BL/6 mice following peroral infection with Toxoplasma gondii. J Immunol 164:5375-82.
14. Roers A, Siewe L, Strittmatter E, Deckert M, Schlüter D, Stenzel W, Gruber AD, Krieg T, Rajewsky K, Müller W. 2004. T cell-specific inactivation of the interleukin 10 gene in mice results in enhanced T cell responses but normal innate responses to lipopolysaccharide or skin irritation. J Exp Med 200:1289-97.
15. Liesenfeld O, Kosek J, Remington JS, Suzuki Y. 1996. Association of CD4+ T cell-dependent, interferon-gamma-mediated necrosis of the small intestine with genetic susceptibility of mice to peroral infection with Toxoplasma gondii. J Exp Med 184:597-607.
16. Liesenfeld O, Kang H, Park D, Nguyen TA, Parkhe CV, Watanabe H, Abo T, Sher A, Remington JS, Suzuki Y. 1999. TNF-alpha, nitric oxide and IFN-gamma are all critical for

development of necrosis in the small intestine and early mortality in genetically susceptible mice infected perorally with Toxoplasma gondii. Parasite Immunol 21:365-76.

17. Vossenkämper A, Struck D, Alvarado-Esquivel C, Went T, Takeda K, Akira S, Pfeffer K, Alber G, Lochner M, Förster I, Liesenfeld O. 2004. Both IL-12 and IL-18 contribute to small intestinal Th1-type immunopathology following oral infection with Toxoplasma gondii, but IL-12 is dominant over IL-18 in parasite control. Eur J Immunol 34:3197-207.
18. Jorgensen I, Rayamajhi M, Miao EA. 2017. Programmed cell death as a defence against infection. Nat Rev Immunol 17:151-164.
19. Amarante-Mendes GP, Adjemian S, Branco LM, Zanetti LC, Weinlich R, Bortoluci KR. 2018. Pattern Recognition Receptors and the Host Cell Death Molecular Machinery. Front Immunol 9:2379.
20. Kaczmarek A, Vandenabeele P, Krysko DV. 2013. Necroptosis: the release of damage-associated molecular patterns and its physiological relevance. Immunity 38:209-23.
21. Jorgensen I, Miao EA. 2015. Pyroptotic cell death defends against intracellular pathogens. Immunol Rev 265:130-42.
22. Pittman KJ, Aliota MT, Knoll LJ. 2014. Dual transcriptional profiling of mice and Toxoplasma gondii during acute and chronic infection. BMC Genomics 15:806.
23. Garfoot AL, Cervantes PW, Knoll LJ. 2019. Transcriptional Analysis Shows a Robust Host Response to. Infect Immun 87.
24. Pittman KJ, Cervantes PW, Knoll LJ. 2016. Z-DNA Binding Protein Mediates Host Control of Toxoplasma gondii Infection. Infect Immun 84:3063-70.
25. Upton JW, Kaiser WJ, Mocarski ES. 2012. DAI/ZBP1/DLM-1 complexes with RIP3 to mediate virus-induced programmed necrosis that is targeted by murine cytomegalovirus vIRA. Cell Host Microbe 11:290-7.

26. Kuriakose T, Man SM, Malireddi RK, Karki R, Kesavardhana S, Place DE, Neale G, Vogel P, Kanneganti TD. 2016. ZBP1/DAI is an innate sensor of influenza virus triggering the NLRP3 inflammasome and programmed cell death pathways. Sci Immunol 1.

27. Yang D, Liang Y, Zhao S, Ding Y, Zhuang Q, Shi Q, Ai T, Wu SQ, Han J. 2020. ZBP1 mediates interferon-induced necroptosis. Cell Mol Immunol 17:356-368.

28. Rebsamen M, Heinz LX, Meylan E, Michallet MC, Schroder K, Hofmann K, Vazquez J, Benedict CA, Tschopp J. 2009. DAI/ZBP1 recruits RIP1 and RIP3 through RIP homotypic interaction motifs to activate NF-kappaB. EMBO Rep 10:916-22.

29. Newton K, Sun X, Dixit VM. 2004. Kinase RIP3 is dispensable for normal NF-kappa Bs, signaling by the B-cell and T-cell receptors, tumor necrosis factor receptor 1, and Toll-like receptors 2 and 4. Mol Cell Biol 24:1464-9.

30. Murphy JM, Czabotar PE, Hildebrand JM, Lucet IS, Zhang JG, Alvarez-Diaz S, Lewis R, Lalaoui N, Metcalf D, Webb AI, Young SN, Varghese LN, Tannahill GM, Hatchell EC, Majewski IJ, Okamoto T, Dobson RC, Hilton DJ, Babon JJ, Nicola NA, Strasser A, Silke J, Alexander WS. 2013. The pseudokinase MLKL mediates necroptosis via a molecular switch mechanism. Immunity 39:443-53.

31. Tobin C, Pollard A, Knoll L. 2010. Toxoplasma gondii cyst wall formation in activated bone marrow-derived macrophages and bradyzoite conditions. J Vis Exp.

32. Chtanova T, Schaeffer M, Han SJ, van Dooren GG, Nollmann M, Herzmark P, Chan SW, Satija H, Camfield K, Aaron H, Striepen B, Robey EA. 2008. Dynamics of neutrophil migration in lymph nodes during infection. Immunity 29:487-96.

33. Upton JW, Kaiser WJ, Mocarski ES. 2019. DAI/ZBP1/DLM-1 Complexes with RIP3 to Mediate Virus-Induced Programmed Necrosis that Is Targeted by Murine Cytomegalovirus vIRA. Cell Host Microbe 26:564.

34. Kuriakose T, Kanneganti TD. 2018. ZBP1: Innate Sensor Regulating Cell Death and Inflammation. Trends Immunol 39:123-134.

35. He S, Wang L, Miao L, Wang T, Du F, Zhao L, Wang X. 2009. Receptor interacting protein kinase-3 determines cellular necrotic response to TNF-alpha. Cell 137:1100-11.

36. Cho YS, Challa S, Moquin D, Genga R, Ray TD, Guildford M, Chan FK. 2009. Phosphorylation-driven assembly of the RIP1-RIP3 complex regulates programmed necrosis and virus-induced inflammation. Cell 137:1112-23.

37. Thapa RJ, Ingram JP, Ragan KB, Nogusa S, Boyd DF, Benitez AA, Sridharan H, Kosoff R, Shubina M, Landsteiner VJ, Andrake M, Vogel P, Sigal LJ, tenOever BR, Thomas PG, Upton JW, Balachandran S. 2016. DAI Senses Influenza A Virus Genomic RNA and Activates RIPK3-Dependent Cell Death. Cell Host Microbe 20:674-681.

38. Nogusa S, Thapa RJ, Dillon CP, Liedmann S, Oguin TH, Ingram JP, Rodriguez DA, Kosoff R, Sharma S, Sturm O, Verbist K, Gough PJ, Bertin J, Hartmann BM, Sealfon SC, Kaiser WJ, Mocarski ES, López CB, Thomas PG, Oberst A, Green DR, Balachandran S. 2016. RIPK3 Activates Parallel Pathways of MLKL-Driven Necroptosis and FADD-Mediated Apoptosis to Protect against Influenza A Virus. Cell Host Microbe 20:13-24.

39. Kitur K, Wachtel S, Brown A, Wickersham M, Paulino F, Peñaloza HF, Soong G, Bueno S, Parker D, Prince A. 2016. Necroptosis Promotes Staphylococcus aureus Clearance by Inhibiting Excessive Inflammatory Signaling. Cell Rep 16:2219-2230.

40. Luz NF, Khouri R, Van Weyenbergh J, Zanette DL, Fiuza PP, Noronha A, Barral A, Boaventura VS, Prates DB, Chan FK, Andrade BB, Borges VM. 2018. *Leishmania braziliensis* Subverts Necroptosis by Modulating RIPK3 Expression. Front Microbiol 9:2283.

41. Chen J, Wang S, Fu R, Zhou M, Zhang T, Pan W, Yang N, Huang Y. 2018. RIP3 dependent NLRP3 inflammasome activation is implicated in acute lung injury in mice. J Transl Med 16:233.

42. Hansen LW, Jacob A, Yang WL, Bolognese AC, Prince J, Nicastro JM, Coppa GF, Wang P. 2018. Deficiency of receptor-interacting protein kinase 3 (RIPK3) attenuates inflammation and organ injury in neonatal sepsis. J Pediatr Surg 53:1699-1705.

43. von Klitzing E, Ekmekciu I, Kühl AA, Bereswill S, Heimesaat MM. 2017. Intestinal, extra-intestinal and systemic sequelae of Toxoplasma gondii induced acute ileitis in mice harboring a human gut microbiota. PLoS One 12:e0176144.

44. Heimesaat MM, Bereswill S, Fischer A, Fuchs D, Struck D, Niebergall J, Jahn HK, Dunay IR, Moter A, Gescher DM, Schumann RR, Göbel UB, Liesenfeld O. 2006. Gram-negative bacteria aggravate murine small intestinal Th1-type immunopathology following oral infection with Toxoplasma gondii. J Immunol 177:8785-95.

45. Heimesaat MM, Dunay IR, Alutis M, Fischer A, Möhle L, Göbel UB, Kühl AA, Bereswill S. 2014. Nucleotide-oligomerization-domain-2 affects commensal gut microbiota composition and intracerebral immunopathology in acute Toxoplasma gondii induced murine ileitis. PLoS One 9:e105120.

46. Heimesaat MM, Dunay IR, Schulze S, Fischer A, Grundmann U, Alutis M, Kühl AA, Tamas A, Toth G, Dunay MP, Göbel UB, Reglodi D, Bereswill S. 2014. Pituitary adenylate cyclase-activating polypeptide ameliorates experimental acute ileitis and extra-intestinal sequelae. PLoS One 9:e108389.

47. Burger E, Araujo A, López-Yglesias A, Rajala MW, Geng L, Levine B, Hooper LV, Burstein E, Yarovinsky F. 2018. Loss of Paneth Cell Autophagy Causes Acute Susceptibility to Toxoplasma gondii-Mediated Inflammation. Cell Host Microbe 23:177-190.e4.

48. Dubey JP, Speer CA, Shen SK, Kwok OC, Blixt JA. 1997. Oocyst-induced murine toxoplasmosis: life cycle, pathogenicity, and stage conversion in mice fed Toxoplasma gondii oocysts. J Parasitol 83:870-82.

49. Gregg B, Taylor BC, John B, Tait-Wojno ED, Girgis NM, Miller N, Wagage S, Roos DS, Hunter CA. 2013. Replication and distribution of Toxoplasma gondii in the small intestine after oral infection with tissue cysts. Infect Immun 81:1635-43.

50. Speer CA, Dubey JP. 1998. Ultrastructure of early stages of infections in mice fed Toxoplasma gondii oocysts. Parasitology 116 (Pt 1):35-42.

51. Moriwaki K, Chan FK. 2017. The Inflammatory Signal Adaptor RIPK3: Functions Beyond Necroptosis. Int Rev Cell Mol Biol 328:253-275.

52. Wang H, Sun L, Su L, Rizo J, Liu L, Wang LF, Wang FS, Wang X. 2014. Mixed lineage kinase domain-like protein MLKL causes necrotic membrane disruption upon phosphorylation by RIP3. Mol Cell 54:133-146.

53. Mammari N, Halabi MA, Yaacoub S, Chlala H, Dardé ML, Courtioux B. 2019. Modulates the Host Cell Responses: An Overview of Apoptosis Pathways. Biomed Res Int 2019:6152489.

54. Pearson JS, Giogha C, Mühlen S, Nachbur U, Pham CL, Zhang Y, Hildebrand JM, Oates CV, Lung TW, Ingle D, Dagley LF, Bankovacki A, Petrie EJ, Schroeder GN, Crepin VF, Frankel G, Masters SL, Vince J, Murphy JM, Sunde M, Webb AI, Silke J, Hartland EL. 2017. EspL is a bacterial cysteine protease effector that cleaves RHIM proteins to block necroptosis and inflammation. Nat Microbiol 2:16258.

55. Takaoka A, Wang Z, Choi MK, Yanai H, Negishi H, Ban T, Lu Y, Miyagishi M, Kodama T, Honda K, Ohba Y, Taniguchi T. 2007. DAI (DLM-1/ZBP1) is a cytosolic DNA sensor and an activator of innate immune response. Nature 448:501-5.

56. Wang Z, Choi MK, Ban T, Yanai H, Negishi H, Lu Y, Tamura T, Takaoka A, Nishikura K, Taniguchi T. 2008. Regulation of innate immune responses by DAI (DLM-1/ZBP1) and other DNA-sensing molecules. Proc Natl Acad Sci U S A 105:5477-82.

57. Couper KN, Blount DG, Riley EM. 2008. IL-10: the master regulator of immunity to infection. J Immunol 180:5771-7.

58. Heimesaat MM, Fischer A, Jahn HK, Niebergall J, Freudenberg M, Blaut M, Liesenfeld O, Schumann RR, Göbel UB, Bereswill S. 2007. Exacerbation of murine ileitis by Toll-like receptor 4 mediated sensing of lipopolysaccharide from commensal Escherichia coli. Gut 56:941-8.

59. Benson A, Pifer R, Behrendt CL, Hooper LV, Yarovinsky F. 2009. Gut commensal bacteria direct a protective immune response against Toxoplasma gondii. Cell Host Microbe 6:187-96.

60. Plattner F, Yarovinsky F, Romero S, Didry D, Carlier MF, Sher A, Soldati-Favre D. 2008. Toxoplasma profilin is essential for host cell invasion and TLR11-dependent induction of an interleukin-12 response. Cell Host Microbe 3:77-87.

61. Ewald SE, Chavarria-Smith J, Boothroyd JC. 2014. NLRP1 is an inflammasome sensor for Toxoplasma gondii. Infect Immun 82:460-8.

62. Chu JQ, Shi G, Fan YM, Choi IW, Cha GH, Zhou Y, Lee YH, Quan JH. 2016. Production of IL-1β and Inflammasome with Up-Regulated Expressions of NOD-Like Receptor Related Genes in *Toxoplasma gondii*-Infected THP-1 Macrophages. Korean J Parasitol 54:711-717.

63. Conos SA, Chen KW, De Nardo D, Hara H, Whitehead L, Núñez G, Masters SL, Murphy JM, Schroder K, Vaux DL, Lawlor KE, Lindqvist LM, Vince JE. 2017. Active MLKL triggers the NLRP3 inflammasome in a cell-intrinsic manner. Proc Natl Acad Sci U S A 114:E961-E969.

64. Lawlor KE, Khan N, Mildenhall A, Gerlic M, Croker BA, D'Cruz AA, Hall C, Kaur Spall S, Anderton H, Masters SL, Rashidi M, Wicks IP, Alexander WS, Mitsuuchi Y, Benetatos CA, Condon SM, Wong WW, Silke J, Vaux DL, Vince JE. 2015. RIPK3 promotes cell death and NLRP3 inflammasome activation in the absence of MLKL. Nat Commun 6:6282.

65. Melchor SJ, Saunders CM, Sanders I, Hatter JA, Byrnes KA, Coutermarsh-Ott S, Ewald SE. 2020. IL-1R Regulates Disease Tolerance and Cachexia in *Toxoplasma gondii* Infection. J Immunol 204:3329-3338.

66. Villeret B, Brault L, Couturier-Maillard A, Robinet P, Vasseur V, Secher T, Dimier-Poisson I, Jacobs M, Zheng SG, Quesniaux VF, Ryffel B. 2013. Blockade of IL-1R signaling diminishes Paneth cell depletion and Toxoplasma gondii induced ileitis in mice. Am J Clin Exp Immunol 2:107-16.

67. Guiton R, Vasseur V, Charron S, Arias MT, Van Langendonck N, Buzoni-Gatel D, Ryffel B, Dimier-Poisson I. 2010. Interleukin 17 receptor signaling is deleterious during Toxoplasma gondii infection in susceptible BL6 mice. J Infect Dis 202:427-35.

68. Gorfu G, Cirelli KM, Melo MB, Mayer-Barber K, Crown D, Koller BH, Masters S, Sher A, Leppla SH, Moayeri M, Saeij JP, Grigg ME. 2014. Dual role for inflammasome sensors NLRP1 and NLRP3 in murine resistance to Toxoplasma gondii. mBio 5.

69. Coutermarsh-Ott SL, Doran JT, Campbell C, Williams TM, Lindsay DS, Allen IC. 2016. Caspase-11 Modulates Inflammation and Attenuates Toxoplasma gondii Pathogenesis. Mediators Inflamm 2016:9848263.

70. López-Yglesias AH, Camanzo E, Martin AT, Araujo AM, Yarovinsky F. 2019. TLR11-independent inflammasome activation is critical for CD4+ T cell-derived IFN-γ production and host resistance to Toxoplasma gondii. PLoS Pathog 15:e1007872.

Figures

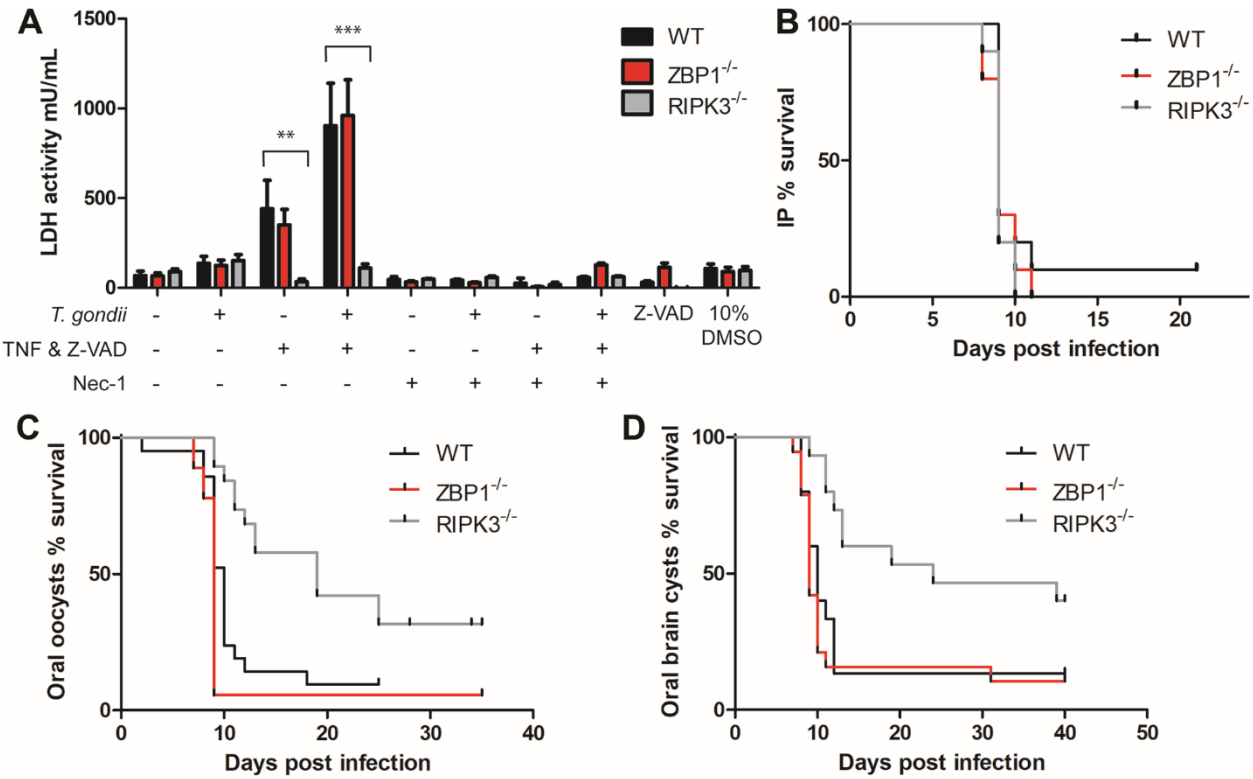

Figure 1. *ZBP1 and RIPK3 show divergent phenotypes to necroptosis and host survival.* (A) Necroptosis was measured by LDH release in BMDM. Cells were seeded at 5 x 10^4 cells/well in triplicate in a 96-well plate and infected with 2.5 x 10^5 parasites/well or left uninfected for 3 hours. Stimulated cells received 50 ng/mL TNF and 40 μM Z-VAD-FMK and unstimulated cells received fresh media. After 24 hours, the media supernatant was used to measure LDH release by absorption. Necrostatin-1 was added upon stimulation at 50 μM as a negative control for necroptosis. These results are from 2 independent experiments. A 2-way ANOVA with Bonferroni post-test was used for statistical analysis in LDH release. ** P-value < 0.01, *** P-value < 0.001. (B) Host survival from IP inoculation with *T. gondii* tachyzoites. Female (WT n = 10, $ZBP1^{-/-}$ n = 10, $RIPK3^{-/-}$ n = 10) mice were IP infected with 1 x 10^4 tachyzoites/mouse. This data combines 2 independent experiments. Significance was

determined by a Log-rank (Mantel-Cox) test and the P-value between each genotype was not significant. (C) Host survival from an oral infection with oocysts. Male (WT n = 17, ZBP1$^{-/-}$ n = 12, RIPK3$^{-/-}$ n = 15) and female (WT n = 9, ZBP1$^{-/-}$ n = 6, RIPK3$^{-/-}$ n = 8) mice were orally infected by gavage with 6 x 10^3 mCherry oocysts/mouse in 3 independent experiments. Significance was determined by a Log-rank (Mantel-Cox) test. The P-value = 0.001 for WT compared to RIPK3$^{-/-}$ mice and the P-value was not significant between WT and ZBP1$^{-/-}$ mice. (D) Host survival from an oral infection with brain tissue cysts. Female (WT n = 15, ZBP1$^{-/-}$ n = 17, RIPK3$^{-/-}$ n = 15) mice were orally infected by gavage with 4 x 10^3 brain tissue cysts in 3 independent experiments. Significance was determined by a Log-rank (Mantel-Cox) test. The P-value = 0.003 between WT and RIPK3$^{-/-}$ mice and the P-value was not significant between WT and ZBP1$^{-/-}$ mice.

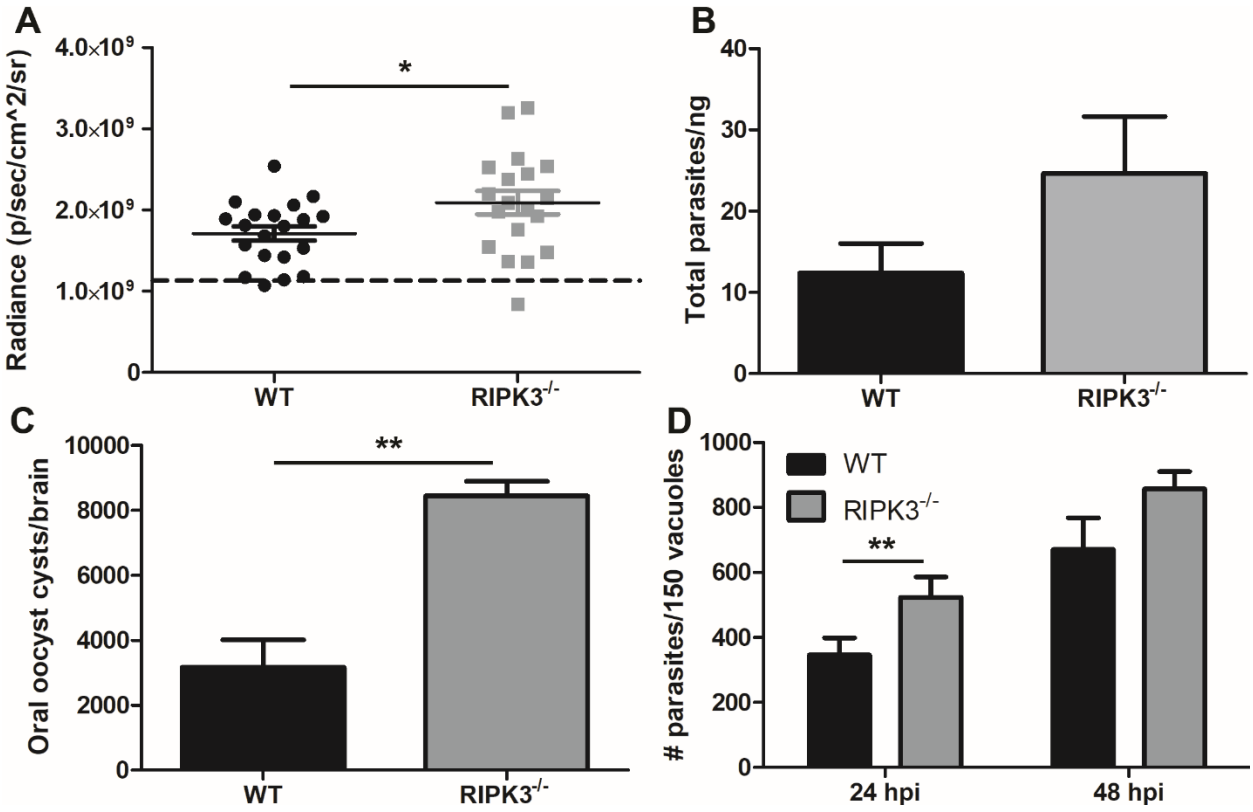

Figure 2. *RIPK3$^{-/-}$ mice have higher parasite burdens.* (A) Intestine parasite burden determined by mCherry fluorescence with IVIS. Male (WT n = 10, RIPK3$^{-/-}$ n = 9) and female (WT n = 10, RIPK3$^{-/-}$ n= 10) mice were gavage fed 1 x 10^4 mCherry oocysts and mCherry fluorescence was measured (excitation 587 and emission 610) in extracted intestines at 7 days post infection. The dotted line indicates the average background mCherry fluorescence of uninfected male (WT n = 2, RIPK3$^{-/-}$ n = 2) and female (WT n = 4, RIPK3$^{-/-}$ n = 3) mouse intestines. (B) Parasite burden measured by qPCR in intestines with parasite specific SAG1 primers. Total gDNA was extracted from 1 cm intestine sections (duodenum, jejunum, and ileum) in female (WT n = 3, RIPK3$^{-/-}$ n = 3) mice orally infected with 3 x 10^4 mCherry oocysts. A standard curve was generated from a known concentration of tachyzoite parasites to calculate the burden. The intestine parasite burden was normalized across all 3 intestine tissue sections for each mouse. P-value was not significant for the intestine qPCR. (C) Brain cyst burden in male (WT n = 5, RIPK3$^{-/-}$ n = 3) mice 28 days post oral infection with 3 x 10^3 mCherry oocysts. (D) Parasite burden in WT and RIPK3^{-}

$^{/-}$ BMDM. Total parasites in 150 vacuoles were counted by IFA on blinded glass coverslips at 24 (WT n = 7, RIPK3$^{-/-}$ n = 5) and 48 (WT n = 6, RIPK3$^{-/-}$ n = 6) hour post infection and stimulation (25 ng/mL LPS and 25 U/mL IFN-γ). A 2-tailed independent Student's T-test was used to calculate significance. * P-value < 0.05, ** P-value < 0.01.

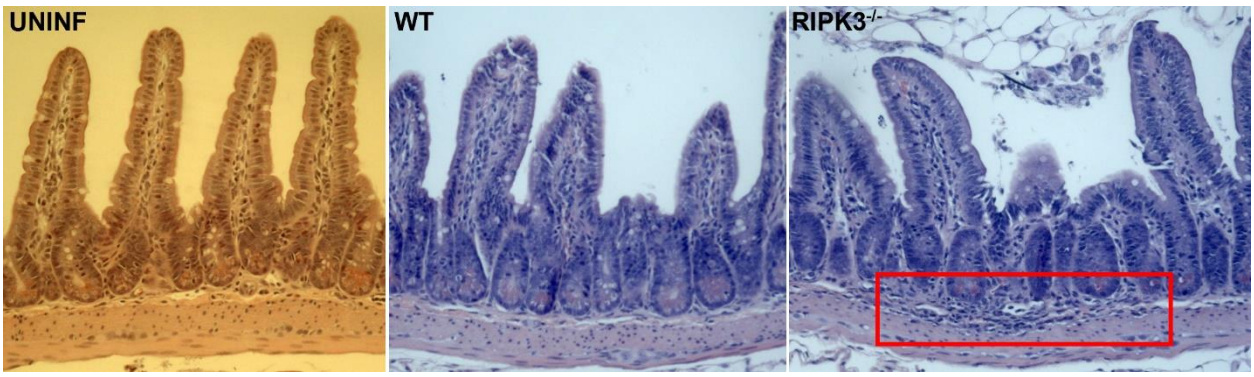

Figure 3. *Intestinal histopathology shows similar villi damage in WT and RIPK3$^{-/-}$ mice.* Female mice were left uninfected (UNINF, left panel) or were infected with 600 mCherry oocysts by oral gavage and sacrificed at day 7 post infection (WT, middle panel and RIPK3$^{-/-}$, right panel). The ileum (distal 1/3 of the small intestine) was washed with PBS and fixed in 10% buffered formalin in a swiss roll, sectioned, then stained with H&E and imaged using Zeiss light microscopy. The red box indicates dark nuclei of inflammatory cells that have infiltrated in the lamina propria and submucosa of this tissue.

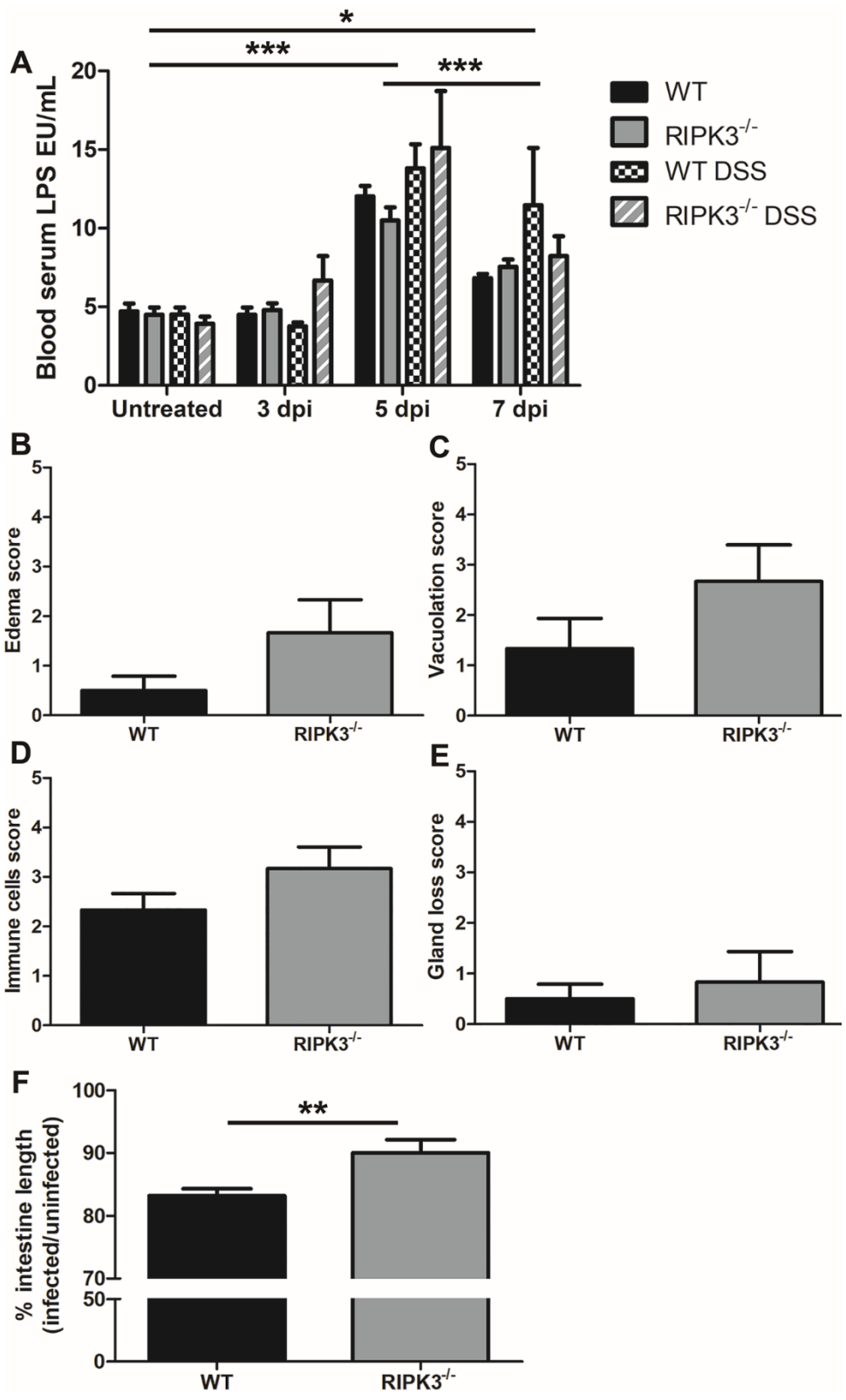
A
Blood serum LPS EU/mL
20
15
10
5
0
*
***
***
Untreated
3 dpi
5 dpi
7 dpi
WT
RIPK3-/-
WT DSS
RIPK3-/- DSS
B
Edema score
C
Vacuolation score
D
Immune cells score
E
Gland loss score
F
% intestine length (infected/uninfected)
100
90
80
70
50
0
**
WT
RIPK3-/-

Figure 4. *RIPK3 does not affect intestinal permeability but lamina propria pathology after oral T. gondii infection.* (A) Intestine permeability by LPS concentration in blood serum. Male (WT n = 4, RIPK3$^{-/-}$ n =3) and female (WT n = 5, RIPK3$^{-/-}$ n = 5) mice were orally infected with 1 x 10^4 mCherry oocysts by gavage. As a positive control, male (WT n = 4, RIPK3$^{-/-}$ n = 5) and female (WT n = 4, RIPK3$^{-/-}$ n = 3) mice were treated with 3% DSS in the drinking water. Paired blood serum was collected at days 0 (uninfected), 3, 5, and 7 post oral infection. Statistical significance was calculated by 2-way ANOVA with Bonferroni post-test. *** P-value < 0.001 for uninfected compared to 5 dpi, and 5 dpi compared to 7 dpi. * P-value < 0.05 for uninfected compared to 7 dpi. There was no significant difference within each group. (B-E) Intestine pathology scores by H&E in ileum swiss rolls. Female mice (WT n = 3, RIPK3$^{-/-}$ n = 3) were infected with 600 mCherry oocysts by oral gavage and sacrificed at day 7 post infection. The ileum (distal 1/3 of the small intestine) was washed with PBS and fixed in 10% buffered formalin in a swiss roll. Uninfected female mice (WT n = 2, RIPK3$^{-/-}$ n = 3) ileum samples were processed the same as controls. The slides were blinded and scored from 0 – 5 (0 = equivalent to control and 5 = severe) for (B) edema, (C) smooth muscle vacuolation, (D) immune cell infiltration, and (E) gland loss. (F) Intestine length was measured in male (WT n = 6, RIPK3$^{-/-}$ n = 6) and female (WT n = 6, RIPK3$^{-/-}$ n = 6) mice at 7 days post oral infection by gavage with 1 x 10^4 mCherry oocysts. A 2-tailed independent Student's T-test was used to calculate significance from 2 independent experiments. ** P-value < 0.01.

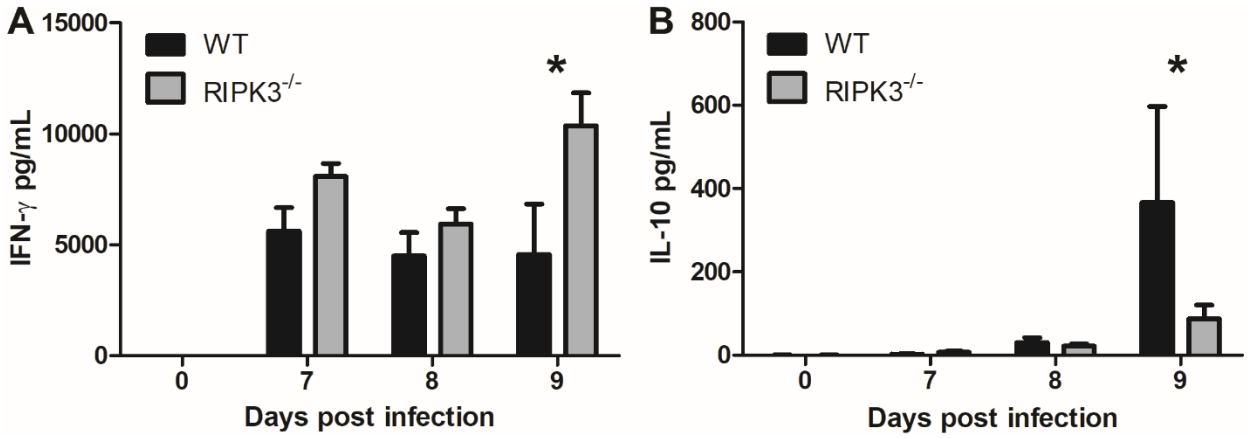

Figure 5. *RIPK3 activity affects IFN-γ and IL-10 serum cytokine levels.* Blood serum cytokines in female (WT n = 14, RIPK3$^{-/-}$ n = 15) mice gavage fed 6 x 10^3 mCherry oocysts. Serum samples were collected at 7, 8, and 9 days post infection in 3 independent experiments. IFN-γ (A) and IL-10 (B) were significantly different. A 2-way ANOVA with Bonferroni post-test was used to calculate significance. * P-value < 0.05.

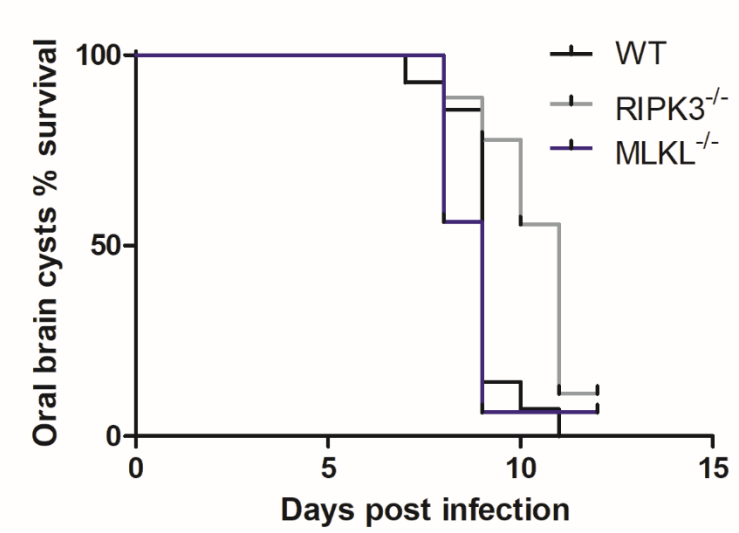

Figure 6. *RIPK3-independent necroptosis activity influences host survival to oral infection.* Female (WT n = 25, RIPK3$^{-/-}$ n = 16, MLKL$^{-/-}$ n = 16) mice were orally infected with 4 x 10^3 brain tissue cysts by gavage. A Log-rank (Mantel-Cox) test was used to calculate significance between each genotype. ** P-value <0.01. The results are a compilation of 3 independent experiments.

Supplementary figures

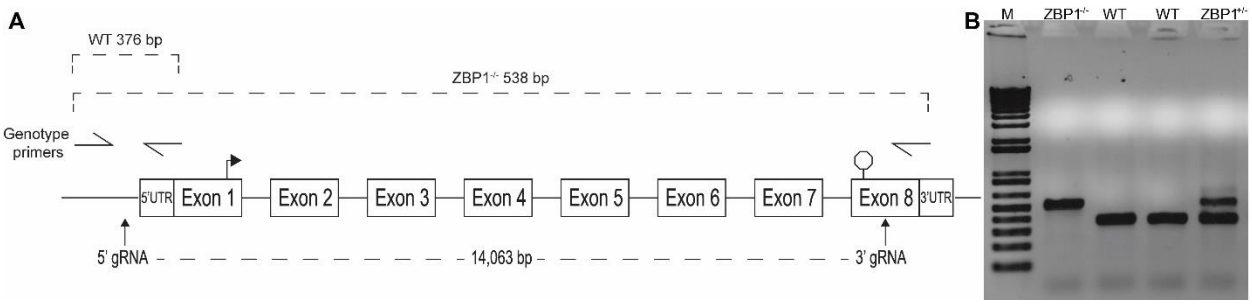

Figure S1. *Generation of CRISPR-Cas9 ZBP1$^{-/-}$ mice.* (A) Two guide RNAs were designed to target the 5'-end (CGATCCCCTCTTACGTAATA; Chr:2 173219317-173219336) and 3'-end (TCAATCAATCGATCAACCGC; Chr:2 173207132-173207151) of *Zbp1*, removing 14KB of genomic DNA that included the promoter and all splice variants. Relative genotype primer locations are shown and the expected band sizes for WT (376 bp) and ZBP1$^{-/-}$ (538 bp) genotypes after PCR. (B) Genotype PCR of WT and ZBP1$^{-/-}$ mice. Lane M is a 1 Kb reference ladder. The ZBP1$^{-/-}$ lane shows a single 538 bp band and the WT lanes show a single 376 bp band for homozygous null and WT genotypes, respectively. The ZBP1$^{+/-}$ lane shows two bands, 538 bp and 376 bp, to indicate a heterozygous genotype.

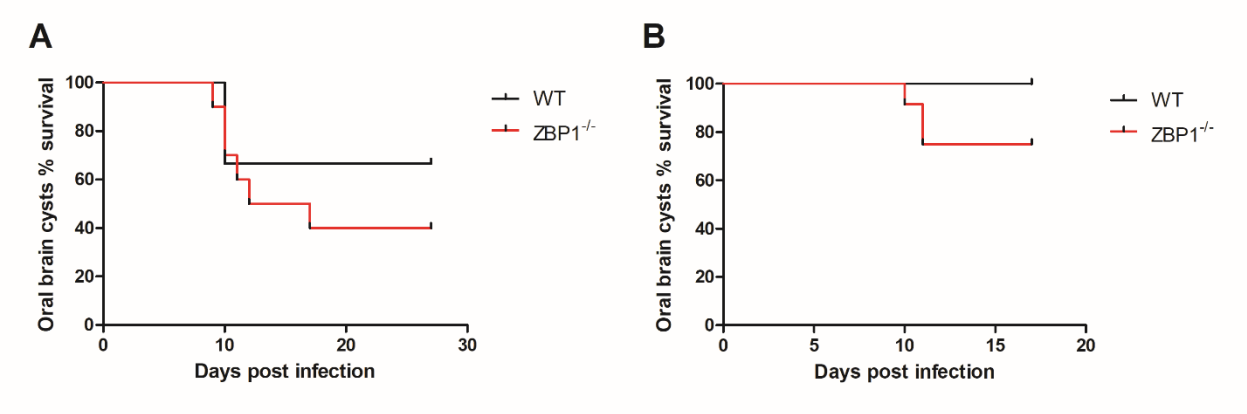

Figure S2. *Independent experiments for oral brain tissue cyst survival challenges with WT and ZBP1$^{-/-}$ mice.* (A) Experiment 1. Female (WT n = 6, ZBP1$^{-/-}$ n = 10) mice were gavage fed 4 x 10^3 brain tissue cysts by gavage. (B) Experiment 2. Female (WT n = 11, ZBP1$^{-/-}$ n = 12) mice were gavage fed 2 x 10^3 brain tissue cysts by gavage.

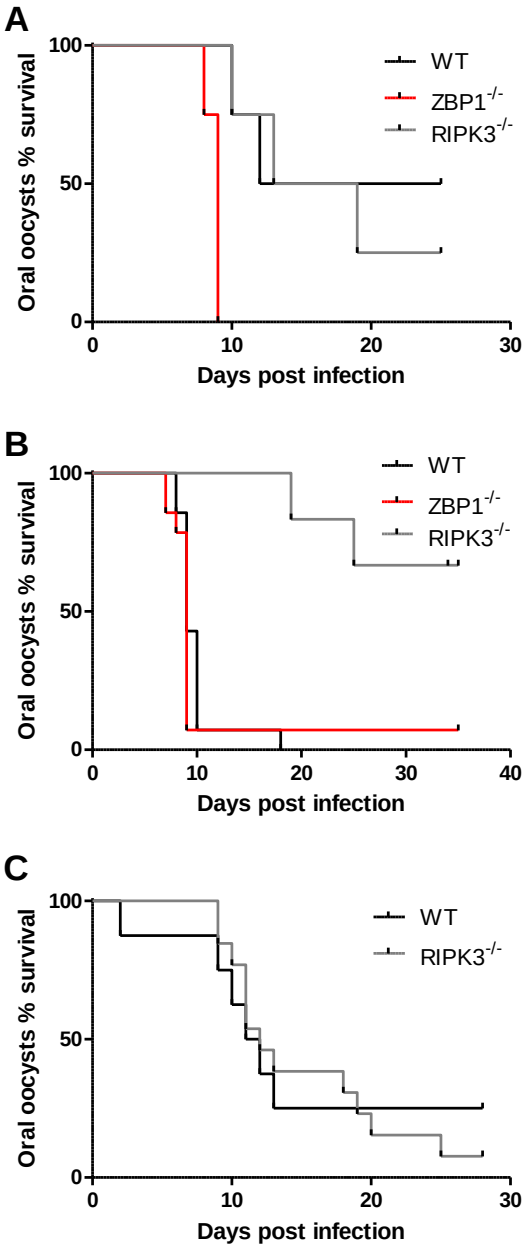

Figure S3. *Independent experiments for oral oocyst survival challenges.*

Mice were gavage fed 6 x 10^3 mCherry oocysts. (A) Oocyst survival challenge experiment 1. Male (WT n = 4, ZBP1$^{-/-}$ n = 4, RIPK3$^{-/-}$ n = 4) mice. (B) Oocyst survival challenge experiment 2. Male and female (WT n = 14, ZBP1$^{-/-}$ n = 14, RIPK3$^{-/-}$ n = 6) mice. (C) Oocysts survival challenge experiment 3. Male and female (WT n = 8, RIPK3$^{-/-}$ n = 13) mice.

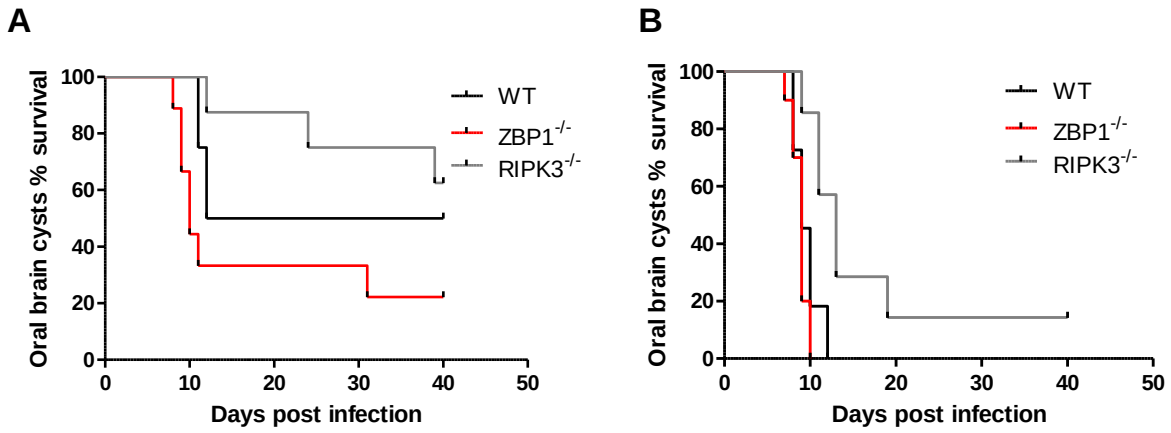

Figure S4. *Independent experiments for oral brain tissue cyst survival challenges.* Mice were fed 4x10^3 brain tissue cysts. (A) Experiment 1. Female (WT n = 4, ZBP1$^{-/-}$ n = 7, RIPK3$^{-/-}$ n = 8) mice. (B) Experiment 2. Female (WT n = 11, ZBP1$^{-/-}$ n = 10, RIPK3$^{-/-}$ n = 7) mice.

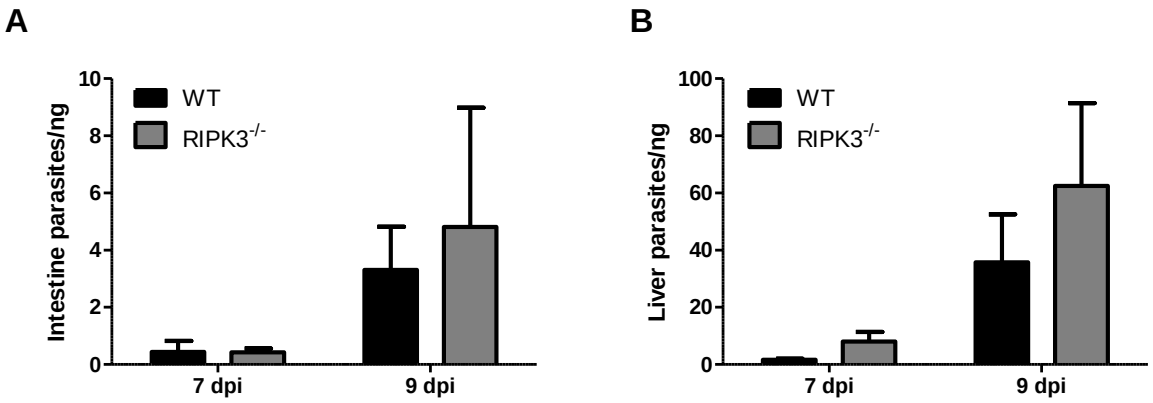

Figure S5. *RIPK3$^{-/-}$ mice have elevated parasite burden in the intestine and liver.* Female (WT n = 6, RIPK3$^{-/-}$ n = 6) mice were orally infected with 6 x 10^3 mCherry oocysts and parasite burden was measured by qPCR with parasite specific SAG1 primers at 7 and 9 dpi. (A) Intestine gDNA was extracted from 1 cm tissue sections (duodenum, jejunum, ileum) and parasite burden was normalized across all 3 sections for each mouse. (B) Liver gDNA was extracted from 50 mg samples. A standard curve was generated from a known concentration of tachyzoite parasites to calculate burden in the intestine and liver.

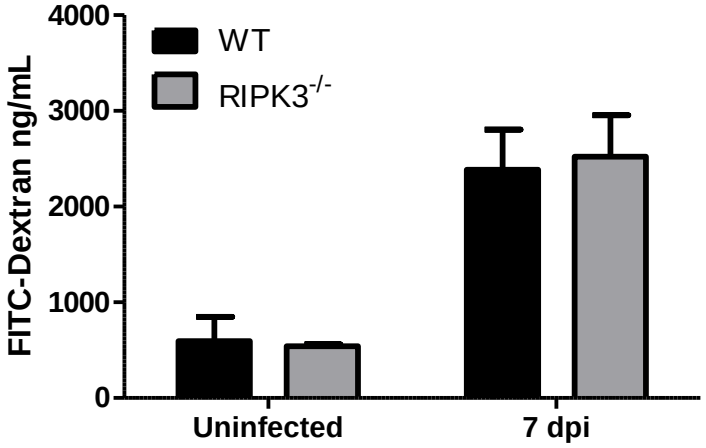

Figure S6. *T. gondii infection creates leaky intestinal villi in both WT and RIPK3$^{-/-}$ mice.* FITC-dextran concentration in blood serum from female (WT n = 9, RIPK3$^{-/-}$ n = 7) mice fed 600 mCherry oocysts by gavage. At 7 days post infection, mice were fasted over night then gavage fed 0.44 mg/g FITC-dextran. Blood serum was collected after 4 hours and FITC-dextran was measured (485 nm excitation and 528 nm emission).

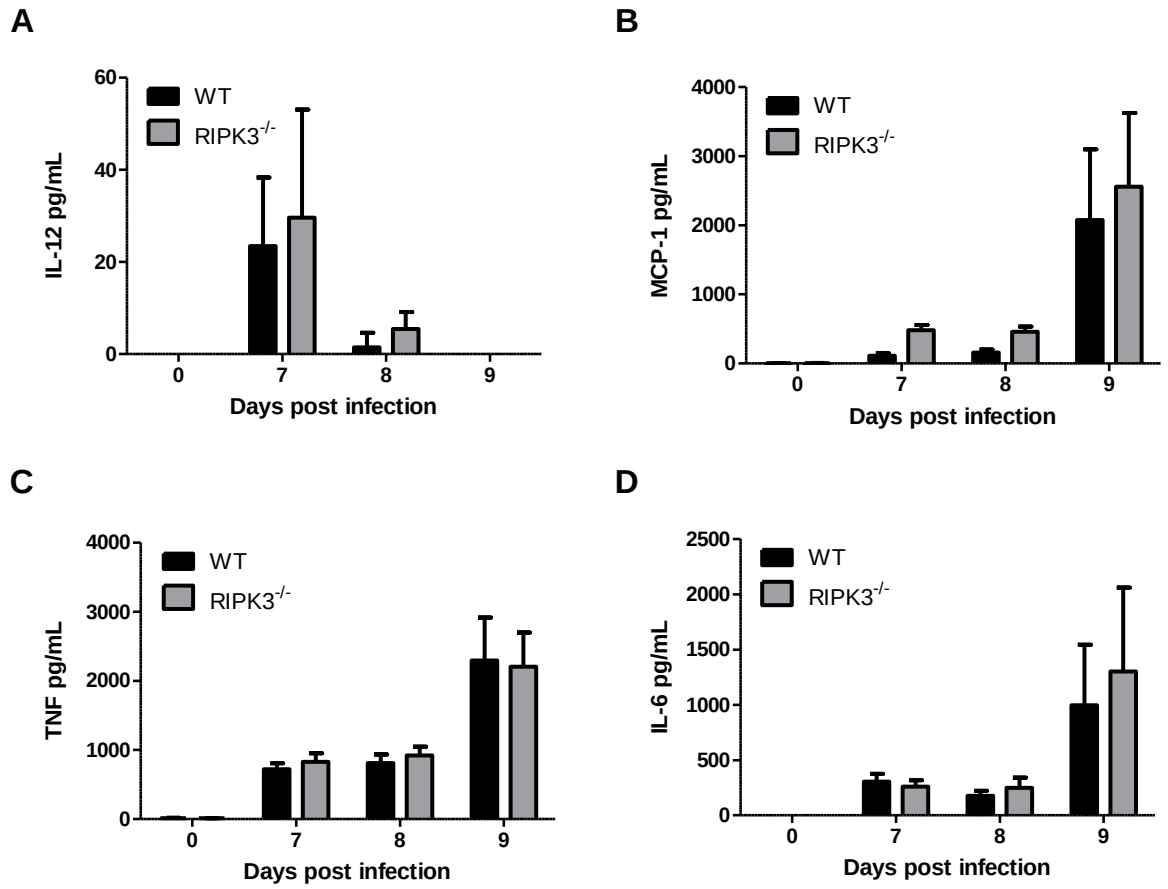

Figure S7. *Inflammatory cytokines in blood serum.* Blood serum cytokines in female (WT n = 14, RIPK3-/- n = 15) mice gavage fed 6 x 10^3 mCherry oocysts. Samples were collected at 7, 8, and 9 days post infection used to measure (A) IL-12, (B) MCP-1, (C) TNF, and (D) IL-6. Each time point has at least 3 biological replicates from 3 independent experiments. A 2-way ANOVA with Bonferroni post-test was used to calculate significance. There was no statistical significance between any of these cytokines.

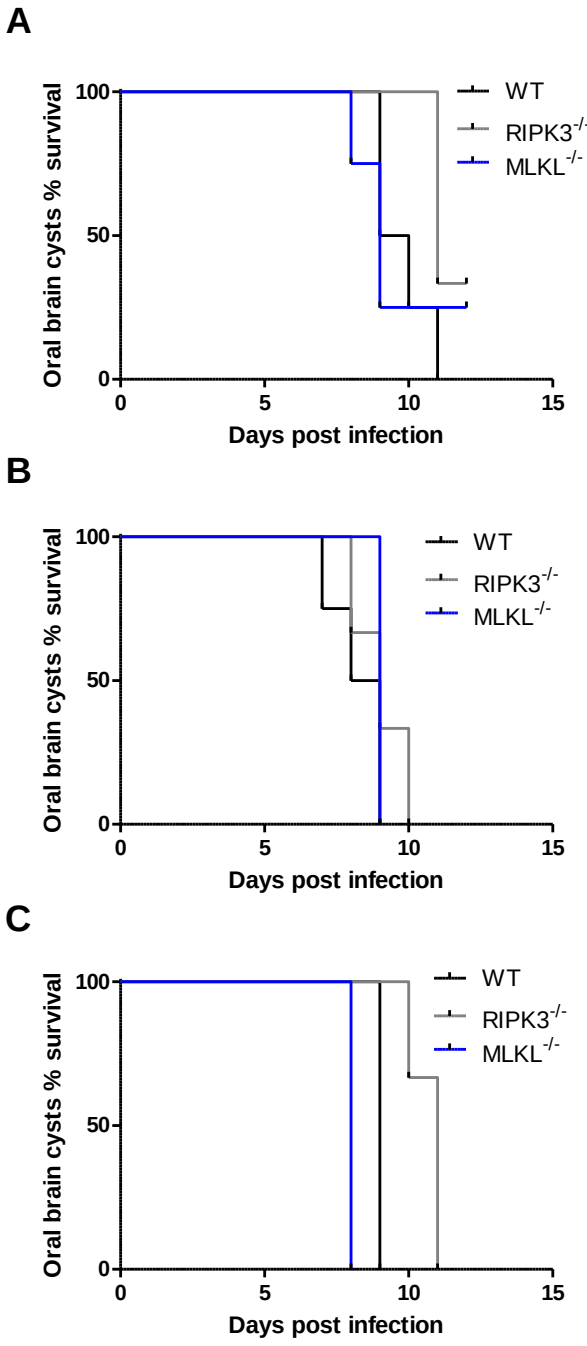

Figure S8. *Independent MLKL$^{-/-}$ survival experiments to oral brain tissue cyst infection.*

(A) MLKL$^{-/-}$ brain tissue cyst survival challenge experiment 1. Female (WT n = 4, RIPK3$^{-/-}$ n = 3, MLKL$^{-/-}$ n = 4) mice. (B) MLKL$^{-/-}$ brain tissue cysts survival challenge experiment 2. Female (WT

n = 3, RIPK3$^{-/-}$ n = 3, MLKL$^{-/-}$ n = 6) mice. (C) MLKL$^{-/-}$ brain tissue cyst survival challenge experiment 3. Female (WT n = 6, RIPK3$^{-/-}$ n = 3, MLKL$^{-/-}$ n = 6) mice.

Chapter 4

Conclusions and Future Directions

Conclusion

The protozoan, *Toxoplasma gondii,* is an obligate intracellular parasite that infects about 30% of the human population and is naturally acquired from food or water contaminated with infectious cysts. Acute infection progresses with tachyzoite parasite dissemination from the intestine throughout the body. Meanwhile, host immune and inflammatory responses cause tachyzoites to differentiate into bradyzoite cysts that persist in brain and muscle tissue, a phase that constitutes chronic infection. The central objective of this thesis was to characterize the host transcriptional response to long-term chronic *T. gondii* infection in the brain and to understand the role programmed lytic cell death plays in host protection to a natural peroral *T. gondii* exposure.

Bradyzoite cysts can presumably persevere in the brain of a healthy host for the lifetime of the host, and host gender can influence immune responses to protozoan infections (1). The long-term effects and sex-specific responses to chronic *T. gondii* infection are poorly understood. In Chapter 2, we characterized the host transcriptional response to long-term chronic infection in the brains of both male and female mice. We discovered that key transcripts for the immune response were similar in both biological sexes. Also, for both male and female mice, the same transcripts that were more abundant in early chronic infection were still increased in late chronic infection. However, the less abundant transcripts were significantly different between the two sexes. Males had 10-fold more genes with reduced abundance compared to females. Additionally, *T. gondii* infected males were less resistant to *Listeria monocytogenes*, as a secondary infection, further suggesting sex-specific responses.

Our study showed that the host sex is limiting the immune response in the case of *T. gondii* and secondary infections. Moreover, it provided additional evidence that hosts with a latent *T. gondii* infection display a state of chronic inflammation, which can have significant effects on weight gain and commensal bacteria populations (2-4). The host transcriptome

throughout long-term chronic infection generated in this study will be useful in future studies to identify the molecular factors affected by chronic inflammation and develop hypotheses for their physiological impact on the host.

Host survival is key to reach the state of a latent *T. gondii* infection after oral exposure. Normally the intestine mucosal immune system generates a protective pro-inflammatory response that controls parasite growth, and this response is counterbalanced by anti-inflammatory mechanisms to prevent severe tissue damage and host death. Interestingly, in high dose oral *T. gondii* infection models, the host conjures an excessive and unregulated pro-inflammatory response that causes severe tissue damage and host death (5-7). Necroptosis and pyroptosis are two lytic cell death pathways that can enhance innate immunity and potentially drive harmful pro-inflammatory responses (8). The receptor-interacting serine/threonine-protein kinase 3 (RIPK3) is an essential component of the necroptosis pathway, and it also plays a dispensable role in pyroptosis (9). Previous *in vivo* reports have shown that mice with RIPK3 inhibition have attenuated mucosal tissue damage and organ injury after a viral or bacterial ligand challenge (10-12). Therefore, we hypothesized that RIPK3-dependent activity could be the tipping point that contributes to unregulated pro-inflammatory responses in high dose oral *T. gondii* infection.

In Chapter 3, our data show RIPK3 null ($RIPK3^{-/-}$) mice have improved survival over wild type (WT) counterparts, even with a higher intestine parasite burden, after a high dose oral *T. gondii* infection. The extended survival phenotype observed in $RIPK3^{-/-}$ mice suggests that RIPK3 activity during acute toxoplasmosis is detrimental to the host. Additionally, the parasite load was significantly higher in $RIPK3^{-/-}$ mice, further suggesting that the difference in survival was due to the RIPK3 activity itself and not directed related to the parasite burden. Given RIPK3 is involved in two lytic cell death mechanisms, we tested the hypothesis that RIPK3-dependent necroptosis specifically prolonged host survival. We obtained mice deficient in mixed lineage

kinase domain-like protein (MLKL) which is the downstream substrate of RIPK3 and ultimately causes necroptosis. The MLKL$^{-/-}$ mice presented similar survival as WT mice. This data shows that disruption of necroptosis does not increase host survival, and further suggests that the phenotype observed in the RIPK3$^{-/-}$ mice survival is not related to necroptosis. Thus, we can hypothesize that RIPK3 involvement in pyroptosis could be the mechanism that drives host death after a high dose oral *T. gondii* infection.

Future directions

Our data in Chapter 3 suggest that RIPK3 activity affects host susceptibility to oral *T. gondii* infection in a necroptosis-independent fashion. Future studies will focus on how cell specific RIPK3 activity affects host responses, and they will investigate the potential role for RIPK3 regulated pyroptosis in mucosal defenses against *T. gondii* infection.

Why do RIPK3$^{-/-}$ mice have improved survival?

Previous reports have established that host death from a high dose oral *T. gondii* infection is due to hyperimmune stimulation from gram-negative bacterial translocation into the intestine (13). This translocation resulting from an increase of intestine permeability causes severe tissue damage from excess IFN-γ, TNF-α, and NO production (5, 7, 13). When gut bacteria and pro-inflammatory cytokines are suppressed by treatment with antibiotic prophylactics or cytokine-specific antibodies, intestine pathology is reduced and host survival is improved (5, 7, 13). Improved survival and pathology are present in these treated animals despite there being no difference in parasite burden between groups. These observations support the hypothesis that host death is due to unregulated pro-inflammatory cytokine production and not uncontrolled parasite growth.

From the organismal level, RIPK3$^{-/-}$ mice have improved survival despite a higher intestinal parasite burden. It remains unclear whether intestine pathology is the primary cause of death for these animals. Our data show no difference in intestine histopathology score between WT and RIPK3$^{-/-}$ mice. However, RIPK3$^{-/-}$ mice exhibit intestinal shortening, and therefore intestinal pathology, to a lesser degree than WT counterparts. Intestine shortening is an established indicator for pathology in oral *T. gondii* infection models (13-17). Moreover, RIPK3$^{-/-}$ mice show no difference in intestine permeability or systemic levels of IFN-γ and TNF-α than WT mice. These results seemingly contradict the hypothesis that host death is due to excess pro-inflammatory cytokine production and tissue damage. The intestine histopathology scores and degree of intestinal shortening also appear contradictory, as these methods both indicate pathology severity and yet support different conclusions. Given these apparent discrepancies, it seems possible that intestine length and intestine histopathology scores capture distinct endpoints, i.e. intestine length is an objective measure of overall tissue health and histopathology scores can have pitfalls determined by tissue preservation quality, section quality, and histologist training. Importantly, the histopathology experiments were underpowered and would benefit from the evaluation of additional mice. Also, as both WT and RIPK3$^{-/-}$ mice presented similar intestinal pathology scores but different survival, we can hypothesize that intestinal pathology is not the primary cause of death. In this case, it would be useful to perform necropsies on recently deceased animals to better survey the health of the animal and the consequences of genetic deletion of RIPK3 in mice treated with a high dose oral *T. gondii* infection. Also, by day 7 post-infection, *T. gondii* parasites are present in many other organs, such as the lungs and liver. It would be informative to assess pathology scores in other infection sites and compare them between RIPK3$^{-/-}$ and WT mice. While the results presented here provide a baseline indication of intestinal health, it is clear that more exhaustive characterization of this genetic model is required.

What cell type does RIPK3 activity contribute to host susceptibility after oral *T. gondii* infection?

The intestine mucosal immune system is the first line of defense against luminal microorganisms and pathogenic infections. Intestine epithelial cells and resident immune cells sense invading pathogens and produce inflammatory cytokines to coordinate innate and adaptive immune responses (18). The RIPK3$^{-/-}$ mouse used in Chapter 3 was a global knockout, so the detrimental effects of RIPK3-dependent activity could be attributed to events in certain cell types such as intestine epithelial cells or immune cells. Therefore, classifying the specific cell type that RIPK3 activity contributes to host susceptibility could be beneficial to understanding the mechanism by which RIPK3 affects host survival following oral *T. gondii* infection.

Irradiation and adoptive bone marrow transplant experiments could clarify if the deleterious effects of RIPK3 activity on the host are specific to immune cells. Total body irradiation is a method used to ablate host immune cells and allow for hematopoietic stem cell reconstitution by bone marrow transplant with a genetically disparate donor (19). In our case, irradiation and adoptive transfer experiments provide a means to study the effects of RIPK3 activity in myeloid and lymphoid cell populations on the host. Preliminary results show improved survival in WT mice that received RIPK3$^{-/-}$ bone marrow compared to RIPK3$^{-/-}$ mice that received WT bone marrow (Fig. 1). Although this experiment did not reach statistical significance, it suggests that RIPK3 activity in immune cells negatively affects host susceptibility to oral *T. gondii* infection. One caveat to this experiment is that a successful bone marrow adoption was determined by a genotyping PCR from tail bleeds. A genotype PCR does not determine the percent retention of native immune cells compared to donor immune cells, and the residual non-irradiated cells could skew host susceptibility and affect observations. This potential retention of host cells may not be represented in a genotyping PCR. Flow cytometry is one method that could be used to measure the percent retention of native immune cells and provide a better

overview of immune cell genotype. This could be performed on peripheral blood mononuclear cells labeled with monoclonal antibodies specific for RIPK3, anti-B220 (B cells), anti-CD4 (T cells), anti-CD8 (T cells), anti-GR1 (granulocytes), and anti-F4/80 (macrophages). The percentage of donor cell engraftment would be calculated for these lymphocyte and myeloid cell populations.

A conditional RIPK3$^{-/-}$ mouse model could be an effective complement to the adoptive transfer model in the effort to delineate the cell type in which RIPK3 activity influences host susceptibility to oral *T. gondii* infection. There are many mouse models that harbor cell specific *Cre* recombinase transgenes that could be crossed with a conditional floxed RIPK3 mouse model to generate the conditional deletion of RIPK3 in the desired cell type. In particular, a villin-cre mouse could be crossed with a floxed RIPK3 mouse to generate a conditional RIPK3 deletion in intestine epithelial cells. This would help identify whether RIPK3 activity in intestine epithelial cells leads to differences in host survival. Our adoptive transfer preliminary results point towards hematopoietic cells as an important candidate cell type to follow up with a RIPK3 conditional knockout. A hematopoietic RIPK3 conditional deletion could be achieved by crossing a floxed RIPK3 mouse with BAB-Cre mice. Activity of RIPK3 could further be assessed down the hematopoietic developmental pathway to dendritic cells or inflammatory monocytes by crossing floxed RIPK3 mice with CD11c-Cre or CCR2-Cre mice, respectively.

Preliminary data suggests potential mechanisms of action for RIPK3 in a candidate cell type, inflammatory macrophages. Inflammatory macrophages play a versatile and important role in immunity to oral *T. gondii* infections through pro-inflammatory functions (20-22). Nitric oxide (NO) production from inducible nitric oxide synthase (iNOS) is one effector mechanism by which inflammatory macrophages can induce intestine dysbiosis and cause host death after oral *T. gondii* infection (23). We observed elevated monocyte chemoattractant protein 1 (MCP-1) in RIPK3$^{-/-}$ mouse intestines after oral infection which corresponded to a percent increase in an

F4/80+ macrophage cell population by flow cytometry (Fig. 2A & B). In addition, RIPK3$^{-/-}$ bone marrow-derived macrophages (BMDM) produce less nitric oxide after *T. gondii* infection and stimulation with LPS and IFN-γ (Fig. 2C). These preliminary results suggest that RIPK3 activity influences inflammatory macrophage recruitment and NO production in macrophages. Therefore, RIPK3$^{-/-}$ mice could have improved survival from reduced NO production in inflammatory macrophages.

A RIPK3 conditional knockout in inflammatory macrophages could be generated to determine how RIPK3 activity affects host survival in these cells after oral infection. This would be achieved by crossing floxed RIPK3 mice with CCR2-Cre mice. Alternatively, flow cytometry could be used to measure iNOS expressing intestine inflammatory macrophages in WT and the global RIPK3$^{-/-}$ mice after an oral challenge. Briefly, immune cells can be isolated from the intestine by filtering collagenase treated tissue through a 100 μm mesh. A detailed protocol for immune cell isolation from the intestine can be found here (24). After isolation, flow cytometry could be used to identify NO producing inflammatory macrophages, which would be positive for antibodies against Ly6C+, F4/80+, and iNOS. If RIPK3-mediated NO production in inflammatory macrophages affects host survival, then we would expect NO to be reduced in the RIPK3$^{-/-}$ cells.

Does RIPK3-mediated pyroptosis drive host susceptibility to oral *T. gondii* infection?

Pyroptosis is another lytic cell death pathway that elicits a pro-inflammatory response mediated by IL-1β and IL-18 (25). In the context of oral *T. gondii* infection, inhibition of IL-1β and IL-18, as well as their downstream effectors, improves host survival (3, 6, 26, 27). Since RIPK3 can activate pyroptosis (9) and our data in Chapter 3 suggest that RIPK3 activity affects host survival in a necroptosis-independent manner, it would be interesting to determine if pyroptosis effectors are differentially regulated in RIPK3$^{-/-}$ mice after oral *T. gondii* infection. IL-1β and IL-18 transcripts could be measured by quantitative-PCR in intestine tissue sections. However, local

or systemic cytokine concentration might be more biologically relevant due to their widespread physiological impact. Cytokine production could be measured by a cytometric bead array or an ELISA assay. If RIPK3 mediated pyroptosis affects host survival, then we would expect IL-1β and IL-18 production to be reduced compared to WT mice. In addition, active forms of IL-1β and IL-18 in MLKL$^{-/-}$ mice would be expected to be similar to WT mice since RIPK3 can drive pyroptosis in an MLKL-independent manner (28, 29). If RIPK3$^{-/-}$ mice produce less pyroptosis effectors, then we could determine if supplementation with IL-1β or IL-18 in RIPK3$^{-/-}$ mice decreases survival similar to WT survival levels. This data would support the hypothesis that RIPK3 activity influences the host response to oral *T. gondii* infection through pyroptosis effectors.

While there is much to be discovered about the mechanisms by which RIPK3 facilitates host death, this work has established a significant role for RIPK3 in host survival to a protozoan infection. The experiments described above could be a starting point to uncover the cause of such a profound phenotype in RIPK3$^{-/-}$ mice.

References

1. Roberts CW, Walker W, Alexander J. 2001. Sex-associated hormones and immunity to protozoan parasites. Clin Microbiol Rev 14:476-88.
2. Prandovszky E, Li Y, Sabunciyan S, Steinfeldt CB, Avalos LN, Gressitt KL, White JR, Severance EG, Pletnikov MV, Xiao J, Yolken RH. 2018. Induced Long-Term Changes in the Upper Intestinal Microflora during the Chronic Stage of Infection. Scientifica (Cairo) 2018:2308619.
3. Melchor SJ, Saunders CM, Sanders I, Hatter JA, Byrnes KA, Coutermarsh-Ott S, Ewald SE. 2020. IL-1R Regulates Disease Tolerance and Cachexia in *Toxoplasma gondii* Infection. J Immunol 204:3329-3338.
4. Hatter JA, Kouche YM, Melchor SJ, Ng K, Bouley DM, Boothroyd JC, Ewald SE. 2018. Toxoplasma gondii infection triggers chronic cachexia and sustained commensal dysbiosis in mice. PLoS One 13:e0204895.
5. Liesenfeld O, Kang H, Park D, Nguyen TA, Parkhe CV, Watanabe H, Abo T, Sher A, Remington JS, Suzuki Y. 1999. TNF-alpha, nitric oxide and IFN-gamma are all critical for development of necrosis in the small intestine and early mortality in genetically susceptible mice infected perorally with Toxoplasma gondii. Parasite Immunol 21:365-76.
6. Vossenkämper A, Struck D, Alvarado-Esquivel C, Went T, Takeda K, Akira S, Pfeffer K, Alber G, Lochner M, Förster I, Liesenfeld O. 2004. Both IL-12 and IL-18 contribute to small intestinal Th1-type immunopathology following oral infection with Toxoplasma gondii, but IL-12 is dominant over IL-18 in parasite control. Eur J Immunol 34:3197-207.
7. Liesenfeld O, Kosek J, Remington JS, Suzuki Y. 1996. Association of CD4+ T cell-dependent, interferon-gamma-mediated necrosis of the small intestine with genetic

susceptibility of mice to peroral infection with Toxoplasma gondii. J Exp Med 184:597-607.

8. Jorgensen I, Rayamajhi M, Miao EA. 2017. Programmed cell death as a defence against infection. Nat Rev Immunol 17:151-164.

9. Moriwaki K, Chan FK. 2017. The Inflammatory Signal Adaptor RIPK3: Functions Beyond Necroptosis. Int Rev Cell Mol Biol 328:253-275.

10. Sai K, Parsons C, House JS, Kathariou S, Ninomiya-Tsuji J. 2019. Necroptosis mediators RIPK3 and MLKL suppress intracellular *Listeria* replication independently of host cell killing. J Cell Biol 218:1994-2005.

11. Chen J, Wang S, Fu R, Zhou M, Zhang T, Pan W, Yang N, Huang Y. 2018. RIP3 dependent NLRP3 inflammasome activation is implicated in acute lung injury in mice. J Transl Med 16:233.

12. Hansen LW, Jacob A, Yang WL, Bolognese AC, Prince J, Nicastro JM, Coppa GF, Wang P. 2018. Deficiency of receptor-interacting protein kinase 3 (RIPK3) attenuates inflammation and organ injury in neonatal sepsis. J Pediatr Surg 53:1699-1705.

13. Heimesaat MM, Bereswill S, Fischer A, Fuchs D, Struck D, Niebergall J, Jahn HK, Dunay IR, Moter A, Gescher DM, Schumann RR, Göbel UB, Liesenfeld O. 2006. Gram-negative bacteria aggravate murine small intestinal Th1-type immunopathology following oral infection with Toxoplasma gondii. J Immunol 177:8785-95.

14. Heimesaat MM, Dunay IR, Schulze S, Fischer A, Grundmann U, Alutis M, Kühl AA, Tamas A, Toth G, Dunay MP, Göbel UB, Reglodi D, Bereswill S. 2014. Pituitary adenylate cyclase-activating polypeptide ameliorates experimental acute ileitis and extra-intestinal sequelae. PLoS One 9:e108389.

15. Heimesaat MM, Dunay IR, Alutis M, Fischer A, Möhle L, Göbel UB, Kühl AA, Bereswill S. 2014. Nucleotide-oligomerization-domain-2 affects commensal gut microbiota

composition and intracerebral immunopathology in acute Toxoplasma gondii induced murine ileitis. PLoS One 9:e105120.

16. von Klitzing E, Ekmekciu I, Kühl AA, Bereswill S, Heimesaat MM. 2017. Intestinal, extra-intestinal and systemic sequelae of Toxoplasma gondii induced acute ileitis in mice harboring a human gut microbiota. PLoS One 12:e0176144.
17. Burger E, Araujo A, López-Yglesias A, Rajala MW, Geng L, Levine B, Hooper LV, Burstein E, Yarovinsky F. 2018. Loss of Paneth Cell Autophagy Causes Acute Susceptibility to Toxoplasma gondii-Mediated Inflammation. Cell Host Microbe 23:177-190.e4.
18. Hooper LV. 2015. Epithelial cell contributions to intestinal immunity. Adv Immunol 126:129-72.
19. Duran-Struuck R, Dysko RC. 2009. Principles of bone marrow transplantation (BMT): providing optimal veterinary and husbandry care to irradiated mice in BMT studies. J Am Assoc Lab Anim Sci 48:11-22.
20. Park J, Hunter CA. 2020. The role of macrophages in protective and pathological responses to Toxoplasma gondii. Parasite Immunol 42:e12712.
21. Detavernier A, Azouz A, Shehade H, Splittgerber M, Van Maele L, Nguyen M, Thomas S, Achouri Y, Svec D, Calonne E, Fuks F, Oldenhove G, Goriely S. 2019. Monocytes undergo multi-step differentiation in mice during oral infection by Toxoplasma gondii. Commun Biol 2:472.
22. Desalegn G, Pabst O. 2019. Inflammation triggers immediate rather than progressive changes in monocyte differentiation in the small intestine. Nat Commun 10:3229.
23. Wang S, El-Fahmawi A, Christian DA, Fang Q, Radaelli E, Chen L, Sullivan MC, Misic AM, Ellringer JA, Zhu XQ, Winter SE, Hunter CA, Beiting DP. 2019. Infection-Induced

Intestinal Dysbiosis Is Mediated by Macrophage Activation and Nitrate Production. mBio 10.

24. Couter CJ, Surana NK. 2016. Isolation and Flow Cytometric Characterization of Murine Small Intestinal Lymphocytes. J Vis Exp.

25. Guo H, Callaway JB, Ting JP. 2015. Inflammasomes: mechanism of action, role in disease, and therapeutics. Nat Med 21:677-87.

26. Villeret B, Brault L, Couturier-Maillard A, Robinet P, Vasseur V, Secher T, Dimier-Poisson I, Jacobs M, Zheng SG, Quesniaux VF, Ryffel B. 2013. Blockade of IL-1R signaling diminishes Paneth cell depletion and Toxoplasma gondii induced ileitis in mice. Am J Clin Exp Immunol 2:107-16.

27. Guiton R, Vasseur V, Charron S, Arias MT, Van Langendonck N, Buzoni-Gatel D, Ryffel B, Dimier-Poisson I. 2010. Interleukin 17 receptor signaling is deleterious during Toxoplasma gondii infection in susceptible BL6 mice. J Infect Dis 202:427-35.

28. Conos SA, Chen KW, De Nardo D, Hara H, Whitehead L, Núñez G, Masters SL, Murphy JM, Schroder K, Vaux DL, Lawlor KE, Lindqvist LM, Vince JE. 2017. Active MLKL triggers the NLRP3 inflammasome in a cell-intrinsic manner. Proc Natl Acad Sci U S A 114:E961-E969.

29. Lawlor KE, Khan N, Mildenhall A, Gerlic M, Croker BA, D'Cruz AA, Hall C, Kaur Spall S, Anderton H, Masters SL, Rashidi M, Wicks IP, Alexander WS, Mitsuuchi Y, Benetatos CA, Condon SM, Wong WW, Silke J, Vaux DL, Vince JE. 2015. RIPK3 promotes cell death and NLRP3 inflammasome activation in the absence of MLKL. Nat Commun 6:6282.

Figures

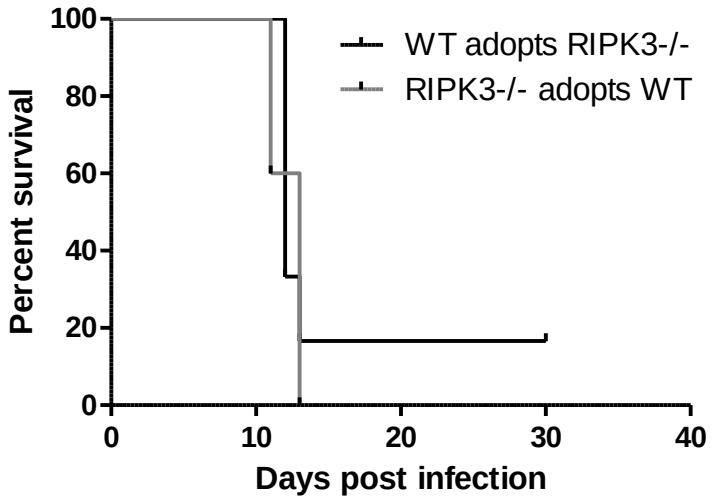

Figure 1. Irradiation and adoptive bone marrow transfer.

Susceptible C57BL/6 WT mice and RIPK3$^{-/-}$ mice were subject to two rounds of X-ray irradiation at 550 cGy for 8 minutes each. The following day irradiated mice were reconstituted by retroorbital injection with 1.5 x 10^6 bone marrow cells from WT and RIPK3$^{-/-}$ donor mice. Irradiated and adoptive transfer mice were maintained on medicated diet (275 ppm trimethoprim and 1365 ppm sulfadiazine) for 6 weeks. Tail bleeds were performed, and successful adoptive transfers were determined by genotype PCR with three RIPK3 primers (5'AGAAGATGCAGCAGCCTCAGCT, 5'ACGGACCCAGGCTGACTTATCTC, 5'GGCACGTGCACAGGAAATAGC). Mice (WT adopts RIPK3$^{-/-}$ n = 7, RIPK3$^{-/-}$ adopts WT n = 9) were gavage fed 6 x 10^3 mCherry oocysts and monitored for clinical signs of disease. A Log-rank (Mantel-Cox) test was performed to calculated significance.

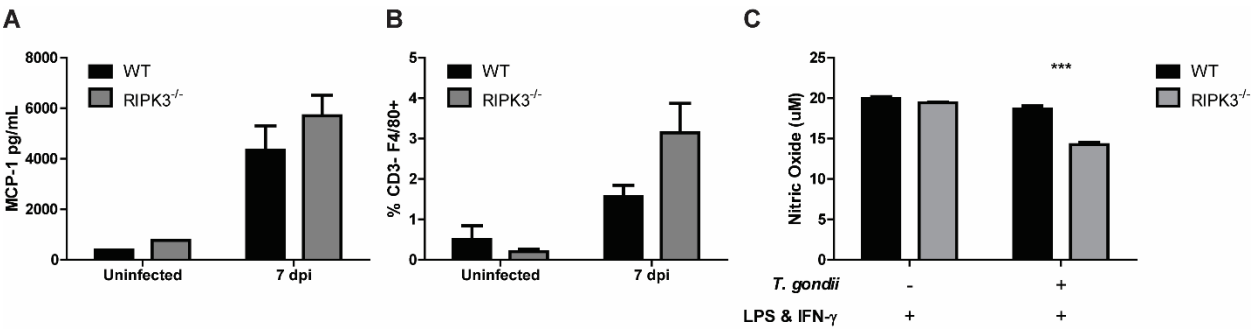

Figure 2. RIPK3$^{-/-}$ mice show phenotypic differences in inflammatory macrophage recruitment and effector capacity. (A) Cytometric bead array was used to measure MCP-1 in blood serum from female (WT n = 3, RIPK3$^{-/-}$ n = 3) mice gavage fed 6 x 10^3 mCherry oocysts at 7 days post infection. (B) Lamina propria cells were isolated from female (WT n = 3, RIPK3$^{-/-}$ n = 3) mice gavage fed 6 x 10^3 mCherry oocysts at 7 days post infection. The percent CD3-F4/80+ positive cells was determined with an Attune flow cytometer. (C) Nitric oxide was measured by Griess reaction in WT (n = 3) and RIPK3$^{-/-}$ (n = 3) BMDM. Cells were seeded in a 4 well plate at 1 x 10^4 cells/well in a 4-well plate and infected with 2 x 10^4 tachyzoite parasites. After 3 hours of infection, cells were stimulated with 25 ng/mL LPS and 25 U/mL IFN-γ for 24 hours. Statistical significance was determined by 2-way ANOVA with Bonferroni post-test. *** P-value < 0.001.

Appendix 1

Z-DNA binding protein mediates host control of *Toxoplasma gondii* infection

Kelly J. Pittman[1], Patrick W. Cervantes[2], and Laura J. Knoll[2]*

[1]Department of Molecular Genetics and Microbiology, Duke University, Durham, NC 27708

[2]Department of Medical Microbiology and Immunology, University of Wisconsin-Madison, Madison, WI 53706

*Corresponding author ljknoll@wisc.edu

Running title: ZBP1 mediates *T. gondii* infection

Appendix A was accepted for publication in the Journal of Infection and Immunity, on July 27. 2016.

Pittman KJ, Cervantes PW, Knoll LJ. Z-DNA Binding Protein Mediates Host Control of Toxoplasma gondii Infection. *Infect Immun*. 2016;84(10):3063-3070. Published 2016 Sep 19. doi:10.1128/IAI.00511-16

Author contributions: KJP performed the parasite replication assays *in vitro* and the quantitative-PCR experiments. KJP and PWC measured brain cyst burden, percent survival, and inflammatory cytokine levels. KJP wrote the manuscript and was proofed by PWC.

Abstract

Intrinsic to *Toxoplasma gondii* infection is the parasite-induced modulation of the host immune response, which ensures establishment of a chronic life-long infection. This manipulation of the host immune response allows *T. gondii* to not only dampen the ability of the host to eliminate the parasite, but also to trigger parasite differentiation to the slow growing, encysted bradyzoite form. We previously used RNAseq to profile the transcriptomes of mice and *T. gondii* during acute and chronic stages of infection. One of the most abundant host transcripts during acute and chronic infection was Z-DNA binding protein 1 (ZBP1). Here, we determined that ZBP1 functions to control *T. gondii* growth. In activated macrophages isolated from ZBP1 deletion mice (ZBP1$^{-/-}$), *T. gondii* has an increased rate replication and a decreased rate of degradation. We also identified a novel function for ZBP1 as a regulator of NO production in activated macrophages, even in the absence of *T. gondii* infection. Upon stimulation, *T. gondii* infected ZBP1$^{-/-}$ macrophages display increased pro-inflammatory cytokines compared to wild type macrophages under the same conditions. These In vitro phenotypes recapitulated in vivo with ZBP1$^{-/-}$ mice having increased susceptibility to oral challenge, higher cyst burdens during chronic infection and an evaluated inflammatory cytokine response. Taken together, these results highlight a role for ZBP1 in assisting host control of *T. gondii* infection.

Introduction

Toxoplasma gondii is an obligate intracellular parasite capable of infecting any nucleated cell in warm-blooded animals. With such a large host range, *T. gondii* has become one of the most prevalent eukaryotic parasites in the world, with approximately 30 percent of the human population infected (1). *T. gondii* has both a sexual and asexual cycle, with the sexual cycle occurring only in the feline intestine, and asexual cycle existing in all warm-blooded hosts. Two asexual forms of the parasite exist in infected animals, the rapidly replicating tachyzoite and the slower growing encysted bradyzoite. During acute infection, the tachyzoite disseminates throughout the host until pressure from the immune system trigger differentiation to the slower growing encysted bradyzoite, which signifies the establishment of a chronic life-long infection. Cysts containing bradyzoites only occur in cells of the central nervous system and striated muscle (2). Cysts persist for the lifetime of the host and remain infectious if contaminated tissue is consumed. The most common route of exposure to *T. gondii* is ingestion of undercooked meat containing bradyzoite cysts or consumption of unwashed food contaminated with environmentally stable oocysts (3).

Infection with *T. gondii* is typically asymptomatic, but does present issues in the immune compromised and unborn fetuses when acquired congenitally. In immune competent hosts, a multitude of defenses to combat *T. gondii* infection are present with the majority involved in production of interferon-gamma (IFN-γ). The significance of IFN-γ during infection is attributed to its ability to stimulate hundreds of genes (4). These genes initiate an array of responses necessary for control of parasite growth and dissemination including host immune cell proliferation, differentiation, and destruction of infected cells. *T. gondii* has developed strategies to evade these host immune responses. An interesting example of *T. gondii* modulation of host cell responses lies in the ability of *T. gondii* to block its degradation by activated macrophages (5, 6). At least part of this block is due to the ability of *T. gondii* to suppress NO production by limiting the availability of intracellular arginine (5, 7, 8). Type I strain parasites initiate arginine

starvation by secreting ROP16, a kinase that activates STAT6 resulting in expression of host arginase-1(5). Arginase-1 degrades available host cell arginine thus limiting the availability for NO (9). A decrease in NO synthesis would appear to be beneficial to the parasite, but *T. gondii* is an arginine auxotroph and exhibits decreased growth in media lacking arginine (5). Another example of *T. gondii* triggered host response is the MyD88 dependent production of IL-12 and subsequent expression of IFN-γ. The downstream effector of the MyD88 pathway that triggers IL-12 transcription is NF-κB. Type II strains of *T. gondii* actually promote expression and translocation of NF-κB to the nucleus via secretion of GRA15 (10). The promotion of pro-inflammatory signal would seem detrimental to the parasite, but stimulation of this mechanism may be adapted by the parasite to ensure survival of the host, establishment of a stable chronic infection and subsequent persistence of the parasite.

Our laboratory has sought to determine other mechanisms of host and parasite interactions through dual transcriptome analysis of mice infected with *T. gondii* (11). From this dataset, host Z-DNA binding protein 1 (ZBP1) was shown to be highly abundant in acute and chronic time points when compared to uninfected samples. ZBP1 also had a fold change difference of approximately 240 in a similar study where *T. gondii* infected mice were compared at 30 days post infection to uninfected mice (12). Since its initial identification, ZBP1 has been implicated in the cytosolic sensing of foreign bacterial and viral DNA and subsequent activation of type I interferon pathways (13-15). Known binding partners are RIPK3 and RIPK1 through the RHIM binding domain of ZBP1 and can activate NF-κB through IRF3 and TBK1 recruitment (13-16). In more recent years ZBP1 has been studied in the context of viral induced necroptosis through RIPK3, in the absence of RIPK1 (17). It has been demonstrated that ZBP1 and RIPK3 form a complex that triggers necroptosis of infected cells with viruses lacking the M45 gene responsible for blocking the interaction of RIPK3 and ZBP1 with the RHIM domain (17). ZBP1 also initiates type I interferon production in response to viral infection, which is a critical response for clearance. Although it has been implicated in multiple host defense pathways,

ZBP1 was deemed indispensable for the innate and adaptive immune response to B-DNA and DNA vaccine (18), possibly due to redundancy in DNA sensing proteins. The role of ZBP1 during parasitic infection has yet to be elucidated. In this paper, we address the significance of ZBP1 expression during *T. gondii* infection.

Materials and methods

qPCR

Using Invitrogen Superscript III Reverse Transcriptase cDNA synthesis kit, cDNA was generated from the same RNA samples used for the previous RNAseq analysis (11). qPCR primers were IDT PrimeTime primers designed to targeting ZBP1 and GAPDH as a house keeping control. Fold changes were determined using the ΔΔCT method and normalized to GAPDH, then compared to uninfected samples. For qPCR measurements in macrophages, wild type and ZBP1$^{-/-}$ macrophages were plated and infected at an MOI of 5. Two hours post-infection, macrophages were stimulated with 5ng/mL of LPS and 25U/mL of IFN-γ, and 48 hours post-infection, RNA was extracted using TRIzol. cDNA was synthesized using Invitrogen Superscript III Reverse Transcriptase cDNA synthesis kit. PrimeTime qPCR primers from IDT targeting GAPDH (control), iNOS, ZBP1, and ARG1 were used in these experiments. ZBP1, iNOS, and ARG1 transcript levels were normalized to GAPDH levels and then compared to uninfected wild type and ZBP1$^{-/-}$ naïve macrophages using the ΔΔCT method.

Determination of parasites per vacuole and the percent degraded parasites

Bone marrow-derived macrophages were isolated and grown in RPMI media containing 20% L929 cell conditioned medium as previously described (19). 1x10^5 wild type or ZBP1$^{-/-}$ macrophages were plated on glass cover slips in RPMI media. Cells were infected with 5x10^5 parasites per well. Two hours post-infection, the media was changed and RPMI containing 5ng/mL LPS and 25U/mL IFN-γ or fresh untreated RPMI was added to the cells. For the

replication assay, cells were fixed at 24 hours post-infection, and for the degradation assay, cells were fixed at 48 hours post-infection. Cells were incubated with chronic infection serum, followed by Alexa Flour 488 anti-mouse secondary antibody. Parasites were visualized using a Zeiss inverted Axiovert 200 motorized microscope with a 100X objective (PlanApo 1.4 na oil PH3 objective). Slides were blinded prior to the counting. For the replication assay, a total of 6 slides for wild type and 6 slides for ZBP1$^{-/-}$ cells were quantified with 150 vacuoles counted on each slide. The percent of vacuoles containing 1, 2, 4, and 8 parasites were calculated based on number of total vacuoles counted on each slide. For the degradation assay, a total of 4 slides for wild type and 4 slides for ZBP1$^{-/-}$ cells were quantified with 100 vacuoles counted on each slide. The percent of vacuoles containing degraded parasites were calculated based on number of total vacuoles counted on each slide as described in (20).

NO assay

Wild type and ZBP1$^{-/-}$ macrophages were seeded at 1x10^4 cells per well in a 96-well plate. Three hours after plating, macrophages were infected with *T. gondii* at an MOI of 0, 2, 5, and 20. Two hours post-infection, the media was changed and RPMI containing 5ng/mL LPS and 25U/mL IFN-γ or fresh untreated RPMI. Supernatants from the cells were removed 48 and 72 hours post-infection and transferred to a new 96 well plate. NO levels were determined using the Promega Griess reagent system according to the manufacturer's protocol. Absorbance was measured at 530 nm using a Synergy HT plate reader. Concentrations were determined using a standard curve generated for each reaction. Experiments were conducted with three technical replicates and three biological replicates. Statistical significance was determined using GraphPad Prism's two-way ANOVA analysis.

Mouse experiments

All animal use was approved by and in accordance with the policies of the Institutional Animal Care and Use Committee at the University of Wisconsin-Madison. ZBP1$^{-/-}$ mice were backcrossed 6 times to C57BL/6 mice, therefore to generate ZBP1$^{+/+}$ and ZBP1$^{-/-}$ mice we established heterozygous ZBP1$^{+/-}$ breeding colonies. ZBP1$^{+/-}$ mice were bred to produce wild type, heterozygous, and knockout mice. Primers used for genotyping were, WT Forward: GCTCTGGGAATGACGACAGC. Knockout Forward: CTAAAGCGCATGCTCCAGACTG. Reverse: CACTTCGTCTGCCCCTCAATTAGA.

Six to eight-week old ZBP1$^{+/+}$ and ZBP1$^{-/-}$ mice were used for all studies. For acute infection, mice were infected with 5x10^3 tachyzoites by intraperitoneal (i.p.) injection. Animals were monitored daily for clinical signs of disease (ruffled fur, hunched posture, paralysis, etc.) and were euthanized if moribund. For quantification of the cyst burden, mice were infected with 1x10^3 tachyzoites by i.p. injection. Mice were sacrificed at 24 days post-infection, their brains were removed, and ground with a mortar and pestle in 1.3 ml of phosphate buffered saline (PBS). 250 µl of the homogenized brain was spun at 3000 x g for 5 min, then the supernatant removed for cytokine analysis and the pellet fixed with 3.0% formaldehyde. Tissue cysts were stained with fluorescein-labeled *Dolichos biflorus* agglutinin (Vector Labs, Burlingame, CA, USA) and 3- 5 µL samples were mounted and cyst numbers counted by fluorescence microscopy. Samples were blinded to ensure no counting bias.

For oral infection studies, eight-week old CBA/J mice from JAX labs were infected with 2x10^4 tachyzoites by i.p.. Cyst burden was quantified as described above for 2-4 mice at 27 days post-infection. Then at 28 days post-infection, the brains were removed from the rest of the mice, pooled, ground with a mortar and pestle, and fed to ZBP1$^{+/+}$, ZBP1$^{+/-}$ and ZBP1$^{-/-}$ mice at approximately 4000 cysts/mouse. Mice were monitored daily for clinical signs of disease (ruffled fur, hunched posture, paralysis, etc.) and were euthanized if moribund.

Cytokine quantification

Wild type and ZBP1$^{-/-}$ bone marrow-derived macrophages were infected with *T. gondii* at an MOI of 5, then stimulated with LPS and IFN-γ after 2 hours. At 48 hours post-infection, media was removed and the cytokines quantified using a mouse inflammation cytokine bead array (CBA) kit (BD Biosciences), which measures IL-12p70, IFNγ, TNFα, MCP-1, IL-6 and IL-10 in the same sample. Alternatively, cytokines were measure in the supernatants of the 24 day post-infection brain preparations described above. Events were collected and gated using the BD LSR II flow cytometer and FACsDIVA software (BD Biosciences).

Results

ZBP1 is highly abundant during acute and chronic T. gondii infection

Our laboratory previously generated an in vivo RNAseq time course of the forebrains of mice during acute and chronic *T. gondii* infection (11). Differential expression analysis was conducted and comparisons made between uninfected, 10 and 28 days post infection. One of the highest differentially expressed transcripts between uninfected and infected time points was ZBP1. The average fold change between acute versus uninfected and chronic versus uninfected time points were 300 and 1000, respectively (Table 1). qPCR was conducted on these samples to verify the increase in abundance of ZBP1 transcripts between each experimental time point. Fold changes of ZBP1 transcript levels were similar between qPCR and RNAseq analysis (Table 1).

ZBP1 expression is altered by T. gondii in activated macrophages

ZBP1 was originally described as a highly up-regulated product of IFN-γ stimulation in macrophages (21). To characterize the expression of ZBP1 in macrophages, qPCR was performed on wild type and ZBP1$^{-/-}$ (18) bone marrow-derived macrophages with and without *T. gondii* infection. In wild type uninfected macrophages stimulated with LPS and IFN-γ, a 11.5-fold increase in ZBP1 expression was detected when compared to uninfected naive macrophages

(Fig. 1A). In wild type macrophages infected with *T. gondii* and stimulated, only a 5-fold increase in expression of ZBP1 was observed. As expected, there was no expression of ZBP1 in macrophages from ZBP1$^{-/-}$ mice. These results confirm that ZBP1 is up-regulated by IFN-γ in macrophages and that macrophages do not initiate expression of ZBP1 in response to *T. gondii* infection alone. The decrease in ZBP1 transcript levels between infected and uninfected macrophages was significant, suggesting that while IFN-γ induces expression of ZBP1, *T. gondii* infection can counteract that induction.

Absence of ZBP1 leads to increased parasite replication and decreased parasite degradation in activated macrophages

To determine if ZBP1 contributes to *T. gondii* growth in macrophages, a replication assay was conducted. Bone marrow-derived macrophages were plated on glass cover slips, infected with *T. gondii* at an MOI of 5 and stimulated with LPS and IFN-γ two hours post-infection. After 24 hours, cells were fixed and an immunofluorescence was used to determine the number of parasites per vacuole. The number of total parasites within the 150 random vacuoles was quantified, and ZBP1$^{-/-}$ stimulated macrophages contained significantly more parasites than wild type stimulated macrophages (Fig. 1B). In wild type macrophages, there was a statistically higher percentage of single parasite vacuoles, 44%, compared to 28% *ZBP1*$^{-/-}$ cells. Only 13% of wild type cells contained vacuoles with 4 parasites whereas 24% in ZBP1$^{-/-}$ cells contained vacuoles with 4 parasites. To analyze whether the difference in parasite numbers was intrinsic to stimulation, we compared the number of parasites per vacuole in naïve wild type and ZBP1$^{-/-}$ macrophages. There was no statistical difference between the number of parasites per vacuole between wild type and ZBP1$^{-/-}$ naïve macrophages (data not shown). These data suggests that ZBP1 has an influence on parasite growth and/or stability in activated, but not naïve macrophages.

Because we had previously determined that decreased parasite growth in activated macrophages could be directly related to parasite degradation (20), we assessed the ability of stimulated wild type and ZBP1$^{-/-}$ macrophages to degrade intracellular *T. gondii*. Using differential interference contrast (DIC) and immunofluorescence to visualize *T. gondii* within stimulated macrophages, parasites were verified as being intracellular and classified as degraded based on the lack of consistent staining around the membrane of the parasites (20). A total of 100 vacuoles were counted and the percentage of degradation was quantified. Over 60% of parasites within wild type activated macrophages appeared degraded, whereas only 30% of parasites were degraded in activated ZBP1$^{-/-}$ macrophages (Fig. 1C). This data suggests ZBP1 has a key role in the pathway that leads to *T. gondii* degradation in activated macrophages.

NO production is decreased in ZBP1$^{-/-}$ activated macrophages

Generation of reactive nitrogen species, such as nitric oxide (NO), by macrophages is critical for control of *T. gondii* infection (22, 23). Macrophage production of NO induces degradation of intracellular *T. gondii*, with detectable levels of NO at 48 hours post-stimulation (24). Because of the enhanced degradation of *T. gondii* in stimulated wild type macrophages, compared to ZBP1$^{-/-}$, we assessed NO production in *T. gondii* infected cells. Wild type and ZBP1$^{-/-}$ bone marrow-derived macrophages were infected with *T. gondii* at an MOI of 0, 2 or 5. Two hours post-infection, macrophages were primed and stimulated with LPS and IFN-γ, and 48 hours post-infection, a Griess reaction was performed to quantify production of NO. Wild type cells produced significantly higher levels of NO in response to stimulation, compared to ZBP1$^{-/-}$ cells (Fig. 2A). There was a significant decrease in NO production ZBP1$^{-/-}$ macrophages, even in the absence of *T. gondii* infection (MOI 0), indicating the role of ZBP1 in the NO production pathways.

To evaluate whether the decrease in NO production in ZBP1$^{-/-}$ macrophages is due to a difference in transcriptional expression of inducible nitric oxide synthase (iNOS), the enzyme that catalyzes the conversion of L-arginine into NO, qPCR was performed. Uninfected and infected wild type and ZBP1$^{-/-}$ macrophages, with and without stimulation, were grown for 48 hours prior to RNA extraction. No difference in iNOS transcript expression was observed between wild type and ZBP1$^{-/-}$ infected or uninfected stimulated macrophages (Fig. 2B). A decrease in iNOS transcript levels was seen between infected and uninfected wild type and ZBP1$^{-/-}$ macrophages, indicating that *T. gondii* infection can inhibit transcription of iNOS independently of ZBP1.

A decrease in NO production can also be attributed to reduction in the availability of the substrate of iNOS, L-arginine. *T. gondii* up-regulates expression of Arginase-1 (ARG1), an enzyme that competes with iNOS for L-arginine in the cell, in order to decrease the ability of cells to produce nitric oxide (54). qPCR was also performed to determine if the decrease in NO production in ZBP1$^{-/-}$ macrophages was due to an increase of ARG1 expression (Fig. 2C). Infected ZBP1$^{-/-}$ macrophages increased ARG1 expression at similar levels to wild type macrophages, indicating the reduced NO levels in ZBP1$^{-/-}$ macrophages is not due to ZBP1 influence on ARG1 expression.

Increased levels of pro-inflammatory cytokines in ZBP1$^{-/-}$ macrophages

To assess whether lack of ZBP1 lead to defects in cytokine production after stimulation with LPS and IFN-γ, the mouse inflammation CBA was used to determine levels of IL-12, TNF-α, IL-10, MCP-1, and IL-6. Wild type and ZBP1$^{-/-}$ bone marrow-derived macrophages were infected with *T. gondii* at an MOI of 5, then stimulated with LPS and IFN-γ 2 hours post-infection. At 48 hours post-infection, ZBP1$^{-/-}$ macrophages had increased levels of TNF-α, MCP-1, and IL-6 compared to wild type cells (Fig. 3). There was no difference in IL-12 or IL-10 levels between stimulated wild type and ZBP1$^{-/-}$ macrophages. While IFN-γ is part of the mouse

inflammation array, levels were saturated due to the activation of the macrophages with IFN-γ. These results indicate that pro-inflammatory molecules TNF-α, MCP-1, and IL-6 are higher in ZBP1$^{-/-}$ macrophages.

ZBP1$^{-/-}$ mice have increased inflammatory cytokines and cyst counts during chronic infection

Because ZBP1 was highly abundant in mouse brains, compared to uninfected controls (Table 1), we determined whether ZBP1 influences outcome of *T. gondii* acute and chronic infection. To examine acute infection, wild type and ZBP1$^{-/-}$ mice were infected with 5x10^3 parasites by i.p. intraperitoneal inoculation. No significant differences were seen in the susceptibility of wild type and ZBP1$^{-/-}$ mice to this high dose of parasites (data not shown).

We then compared the cyst burden during chronic infection of wild type and ZBP1$^{-/-}$ mice infected with a lower 1x10^3 dose. ZBP1$^{-/-}$ mice had a statistically higher cyst burden at 28 days post-infection than wild type mice (Fig. 5A). When we measure the cytokine levels in these brains, we saw results similar to the macrophages, where ZBP1$^{-/-}$ mice had increased levels of TNF-α, MCP-1, and IL-6 compared to wild type mice (Fig. 4). We also saw higher levels of IFN-γ in the ZBP1$^{-/-}$ mice, which we were not able to measure in our stimulated macrophages.

ZBP1$^{-/-}$ mice have a decreased resistance to T. gondii after oral challenge

ZBP1 was highly abundant in the small intestine of mice (21, 25), possibly to assist in the control of oral pathogens. To test this hypothesis, we fed wild type and ZBP1$^{-/-}$ mice approximately *T. gondii* 4000 cysts each and monitored their health. ZBP1$^{-/-}$ showed an increase in susceptibility to lethal oral doses of *T. gondii* compared to wild type mice. Overall, these animal studies mirror the results seen in tissue culture, namely increased parasite growth and cytokine production in the absence of ZBP1. They suggest ZBP1$^{-/-}$ mice have increase in pro-inflammatory cytokines (Figs. 3 and 4) but are not able to control the parasite burden, or that increased parasite burden leads to higher cytokine levels.

Discussion

We previously used RNAseq to determine the host and parasite transcriptome during *T. gondii* acute and chronic infection (11), with the ultimate goal of understanding the mechanisms involved in establishment and maintenance of infection. From this dataset, the host specific gene ZBP1 was highly expressed in the brains of mice during acute and chronic infection (11). ZBP1 was described over a decade ago as a gene up-regulated in macrophages in response to LPS and IFN-γ (21). Since its discovery, the function in activated macrophages has not been elucidated. In this paper we have identified ZBP1 as another IFN-γ product that is manipulated by *T. gondii* upon infection because the IFN-γ induction of ZBP1 is reduced in *T. gondii* infected macrophages (Fig 1A). We determined that absence of ZBP1 in activated macrophages leads to a defect in parasite degradation and an increase in parasite growth. We have also identified a novel function for ZBP1 as a regulator of NO production in activated macrophages, even in the absence of infection. Finally, we have demonstrated that these in vitro phenotypes translate to increased parasite numbers and mortality in ZBP1$^{-/-}$ mice. Overall, we have found that *T. gondii* has increased survival in ZBP1$^{-/-}$ macrophages through lack of degradation. As macrophages are manipulated by *T. gondii* for use in dissemination throughout the host, we hypothesize that this increase in parasites survival leads to higher parasitemia in many organs including those in immunoprivileged areas (26).

ZBP1 has been shown to initiate transcription of type-I interferons; however, type-1 interferons are not critical for survival during *T. gondii* infection. Mice lacking the IFN-α/IFN-β receptor do not succumb to *T. gondii* infection as severely as IFN-γ$^{-/-}$ mice. (27-29). Our data supports the nonessential role of type-I interferons during *T. gondii* as no IFN-α transcripts were detected in stimulated wild type or ZBP1$^{-/-}$ macrophages (data not shown). These data suggest that ZBP1 is not functioning in the type-I interferons response during *T. gondii* infection.

The reduced degradation of *T. gondii* in ZBP1$^{-/-}$ activated macrophages lead us to investigate the role of the NO production pathways during infection. NO production during *T.*

gondii infection has dichotomous roles. Absence of NO has been deemed dispensable for survival of *T. gondii* during acute infection, but tight regulation of NO production is critical as too much can lead to substantial tissue damage (30, 31). These studies focus on comparison of iNOS$^{-/-}$ mice to IL-12$^{-/-}$ and IFN-γ$^{-/-}$ mice, which rapidly succumb to *T. gondii* infection at low doses. The role of iNOS has not been studied in the context of lethal doses of *T. gondii* as the wild type controls from this study did not begin to die of infection until 12 weeks post-inoculation. iNOS$^{-/-}$ mice showed an intermediate phenotype between the severely compromised IL-12$^{-/-}$ and IFN-γ$^{-/-}$ mice and the wild type controls, dying at the beginning of chronic infection (20 days post-infection). While this study suggests that NO production during early infection is less critical than IL-12 or IFN-γ, these data do not address the potential role of NO during lethal oral challenge of *T. gondii* infection. We conducted experiments in wild type and ZBP1$^{-/-}$ mice that were orally fed 4000 cysts from the brains of mice infected with *T. gondii* for 4 weeks, simulating ingestion of a lethal challenge of *T. gondii*. Our data suggest a role for NO production in response to acute toxoplasmosis. Future experiments will elucidate the precise role of ZBP1 in the production of NO in activated macrophages as well as determining the contributions of ZBP1 during chronic *T. gondii* infection.

T. gondii blocks parasite degradation by reducing NO production in activated macrophages (5, 6). *T. gondii* accomplishes this through multiple strategies including down-regulating transcription of the enzyme iNOS, which is required for NO production (32). *T. gondii* also suppresses NO production by limiting the availability of the substrate required for NO production, L-arginine (5, 7, 8). This limitation is accomplished through *T. gondii* mediated up-regulation of ARG1, an enzyme that degrades intracellular arginine. The mechanism of action has been studied in type I strains, where parasites initiate arginine starvation by secreting ROP16, a kinase that activates STAT6 resulting in expression of ARG1 (5). ARG1 up-regulation leads to limiting the availability of L-arginine and thus NO synthesis (9). The mechanism of ARG1 up-regulation and iNOS down-regulation in cells infected with type II parasites is currently

unknown. A decrease in NO synthesis would appear to be beneficial to the parasite, but *T. gondii* is an arginine auxotroph and exhibits decreased growth in media lacking arginine (5). This is an example of *T. gondii* triggering a response that leads to reduction in parasite growth for the purpose of long-term survival of the parasite within the host. While NO plays a role during acute infection, it is most important during chronic infection, as iNOS knockout mice succumb to *T. gondii* in the early stages of chronic infection (20-25 days) (33).

Our data shows the down-regulation of NO in ZBP1$^{-/-}$ macrophages is not due to transcriptional differences in iNOS or ARG1 (Fig. 4B-C). However, iNOS expression is induced by TNF-α (34), which shows a statistically significant increase in ZBP1$^{-/-}$ in both infected macrophages and mouse brains. We hypothesize that this increase in TNF-α seen in ZBP1$^{-/-}$ macrophages is in response to the increased number of *T. gondii* in the absence of ZBP1, perhaps due to the decrease in parasite degradation. ZBP1$^{-/-}$ cells produce higher levels of IFN-γ, TNF-α, IL-6 and MCP-1 possibly as a means to initiate antimicrobial actions against *T. gondii* infection. The higher levels of IL-6, which can act in either pro or anti-inflammatory mechanisms, in stimulated ZBP1$^{-/-}$ macrophages will need to be studied further to elucidate whether it is acting to stimulate or dampen the cytokine response.

Acknowledgements

We sincerely thank Jason Upton for helpful discussions and ZBP1$^{-/-}$ mice (originally provided by Ken Ishii). This research was supported by the National Institutes of Health (NIH) National Research Service Award T32 AI007414 (K.J.P.), and NIH R21AI114277 (L.J.K.).

References

1. Pappas G, Roussos N, Falagas ME. 2009. Toxoplasmosis snapshots: global status of Toxoplasma gondii seroprevalence and implications for pregnancy and congenital toxoplasmosis. International journal for parasitology 39:1385-1394.
2. Dubey JP, Lindsay DS, Speer CA. 1998. Structures of Toxoplasma gondii tachyzoites, bradyzoites, and sporozoites and biology and development of tissue cysts. Clinical microbiology reviews 11:267-299.
3. Jones JL, Dubey JP. 2012. Foodborne toxoplasmosis. Clinical infectious diseases : an official publication of the Infectious Diseases Society of America 55:845-851.
4. de Veer MJ, Holko M, Frevel M, Walker E, Der S, Paranjape JM, Silverman RH, Williams BR. 2001. Functional classification of interferon-stimulated genes identified using microarrays. J Leukoc Biol 69:912-920.
5. Butcher BA, Fox BA, Rommereim LM, Kim SG, Maurer KJ, Yarovinsky F, Herbert DR, Bzik DJ, Denkers EY. 2011. Toxoplasma gondii rhoptry kinase ROP16 activates STAT3 and STAT6 resulting in cytokine inhibition and arginase-1-dependent growth control. PLoS Pathog 7:e1002236.
6. Butcher BA, Kim L, Johnson PF, Denkers EY. 2001. Toxoplasma gondii tachyzoites inhibit proinflammatory cytokine induction in infected macrophages by preventing nuclear translocation of the transcription factor NF-kappa B. J Immunol 167:2193-2201.
7. Chao CC, Anderson WR, Hu S, Gekker G, Martella A, Peterson PK. 1993. Activated microglia inhibit multiplication of Toxoplasma gondii via a nitric oxide mechanism. Clin Immunol Immunopathol 67:178-183.
8. Peterson PK, Gekker G, Hu S, Chao CC. 1995. Human astrocytes inhibit intracellular multiplication of Toxoplasma gondii by a nitric oxide-mediated mechanism. J Infect Dis 171:516-518.

9. Green SJ, Mellouk S, Hoffman SL, Meltzer MS, Nacy CA. 1990. Cellular mechanisms of nonspecific immunity to intracellular infection: cytokine-induced synthesis of toxic nitrogen oxides from L-arginine by macrophages and hepatocytes. Immunol Lett 25:15-19.

10. Rosowski EE, Lu D, Julien L, Rodda L, Gaiser RA, Jensen KD, Saeij JP. 2011. Strain-specific activation of the NF-kappaB pathway by GRA15, a novel Toxoplasma gondii dense granule protein. J Exp Med 208:195-212.

11. Pittman KJ, Aliota MT, Knoll LJ. 2014. Dual transcriptional profiling of mice and Toxoplasma gondii during acute and chronic infection. BMC Genomics 15:806.

12. Tanaka S, Nishimura M, Ihara F, Yamagishi J, Suzuki Y, Nishikawa Y. 2013. Transcriptome Analysis of Mouse Brain Infected with Toxoplasma gondii. Infection and immunity 81:3609-3619.

13. Takaoka A, Wang Z, Choi MK, Yanai H, Negishi H, Ban T, Lu Y, Miyagishi M, Kodama T, Honda K, Ohba Y, Taniguchi T. 2007. DAI (DLM-1/ZBP1) is a cytosolic DNA sensor and an activator of innate immune response. Nature 448:501-505.

14. Wang Z, Choi MK, Ban T, Yanai H, Negishi H, Lu Y, Tamura T, Takaoka A, Nishikura K, Taniguchi T. 2008. Regulation of innate immune responses by DAI (DLM-1/ZBP1) and other DNA-sensing molecules. Proc Natl Acad Sci U S A 105:5477-5482.

15. Kaiser WJ, Upton JW, Mocarski ES. 2008. Receptor-interacting protein homotypic interaction motif-dependent control of NF-kappa B activation via the DNA-dependent activator of IFN regulatory factors. J Immunol 181:6427-6434.

16. Rebsamen M, Heinz LX, Meylan E, Michallet MC, Schroder K, Hofmann K, Vazquez J, Benedict CA, Tschopp J. 2009. DAI/ZBP1 recruits RIP1 and RIP3 through RIP homotypic interaction motifs to activate NF-kappaB. EMBO Rep 10:916-922.

17. Upton JW, Kaiser WJ, Mocarski ES. 2012. DAI/ZBP1/DLM-1 complexes with RIP3 to mediate virus-induced programmed necrosis that is targeted by murine cytomegalovirus vIRA. Cell Host Microbe 11:290-297.

18. Ishii KJ, Kawagoe T, Koyama S, Matsui K, Kumar H, Kawai T, Uematsu S, Takeuchi O, Takeshita F, Coban C, Akira S. 2008. TANK-binding kinase-1 delineates innate and adaptive immune responses to DNA vaccines. Nature 451:725-729.

19. Tobin C, Pollard A, Knoll L. 2010. Toxoplasma gondii cyst wall formation in activated bone marrow-derived macrophages and bradyzoite conditions. J Vis Exp doi:10.3791/2091.

20. Mordue DG, Scott-Weathers CF, Tobin CM, Knoll LJ. 2007. A patatin-like protein protects Toxoplasma gondii from degradation in activated macrophages. Mol Microbiol 63:482-496.

21. Fu Y, Comella N, Tognazzi K, Brown LF, Dvorak HF, Kocher O. 1999. Cloning of DLM-1, a novel gene that is up-regulated in activated macrophages, using RNA differential display. Gene 240:157-163.

22. Adams LB, Hibbs JB, Jr., Taintor RR, Krahenbuhl JL. 1990. Microbiostatic effect of murine-activated macrophages for Toxoplasma gondii. Role for synthesis of inorganic nitrogen oxides from L-arginine. J Immunol 144:2725-2729.

23. Murray HW, Teitelbaum RF. 1992. L-arginine-dependent reactive nitrogen intermediates and the antimicrobial effect of activated human mononuclear phagocytes. J Infect Dis 165:513-517.

24. Lowry MA, Goldberg JI, Belosevic M. 1998. Induction of nitric oxide (NO) synthesis in murine macrophages requires potassium channel activity. Clin Exp Immunol 111:597-603.

25. Rothenburg S, Schwartz T, Koch-Nolte F, Haag F. 2002. Complex regulation of the human gene for the Z-DNA binding protein DLM-1. Nucleic Acids Res 30:993-1000.

26. Courret N, Darche S, Sonigo P, Milon G, Buzoni-Gatel D, Tardieux I. 2006. CD11c- and CD11b-expressing mouse leukocytes transport single Toxoplasma gondii tachyzoites to the brain. Blood 107:309-316.

27. Beiting DP. 2014. Protozoan parasites and type I interferons: a cold case reopened. Trends Parasitol 30:491-498.

28. Suzuki Y, Orellana MA, Schreiber RD, Remington JS. 1988. Interferon-gamma: the major mediator of resistance against Toxoplasma gondii. Science 240:516-518.

29. Yap GS, Sher A. 1999. Effector cells of both nonhemopoietic and hemopoietic origin are required for interferon (IFN)-gamma- and tumor necrosis factor (TNF)-alpha-dependent host resistance to the intracellular pathogen, Toxoplasma gondii. J Exp Med 189:1083-1092.

30. Khan IA, Matsuura T, Fonseka S, Kasper LH. 1996. Production of nitric oxide (NO) is not essential for protection against acute Toxoplasma gondii infection in IRF-1-/- mice. J Immunol 156:636-643.

31. Scharton-Kersten TM, Yap G, Magram J, Sher A. 1997. Inducible nitric oxide is essential for host control of persistent but not acute infection with the intracellular pathogen Toxoplasma gondii. J Exp Med 185:1261-1273.

32. Luder CG, Algner M, Lang C, Bleicher N, Gross U. 2003. Reduced expression of the inducible nitric oxide synthase after infection with Toxoplasma gondii facilitates parasite replication in activated murine macrophages. Int J Parasitol 33:833-844.

33. Scharton-Kersten TM, Yap G, Magram J, Sher A. 1997. Inducible nitric oxide is essential for host control of persistent but not acute infection with the intracellular pathogen Toxoplasma gondii. The Journal of experimental medicine 185:1261-1273.

34. Yamada K, Otabe S, Inada C, Takane N, Nonaka K. 1993. Nitric oxide and nitric oxide synthase mRNA induction in mouse islet cells by interferon-gamma plus tumor necrosis factor-alpha. Biochem Biophys Res Commun 197:22-27.

Figures and tables

Table 1. *Comparison of ZBP1 transcripts as determined by RNAseq and qPCR.*

	Acute vs Uninfected	Chronic vs uninfected
RNAseq	300	1000
qPCR	480	1500

Fold change of ZBP1 transcript levels between acute vs uninfected and chronic vs uninfected mouse forebrains was analyzed through RNAseq analysis, as descripted previously (11). To verify the dramatic increase in ZBP1 transcripts between each sample, qPCR using the same cDNA samples was performed. Primers targeting ZBP1 and GAPDH were used. qPCR fold change was determined by normalization to GAPDH and then comparing to uninfected samples using the ΔΔCT method.

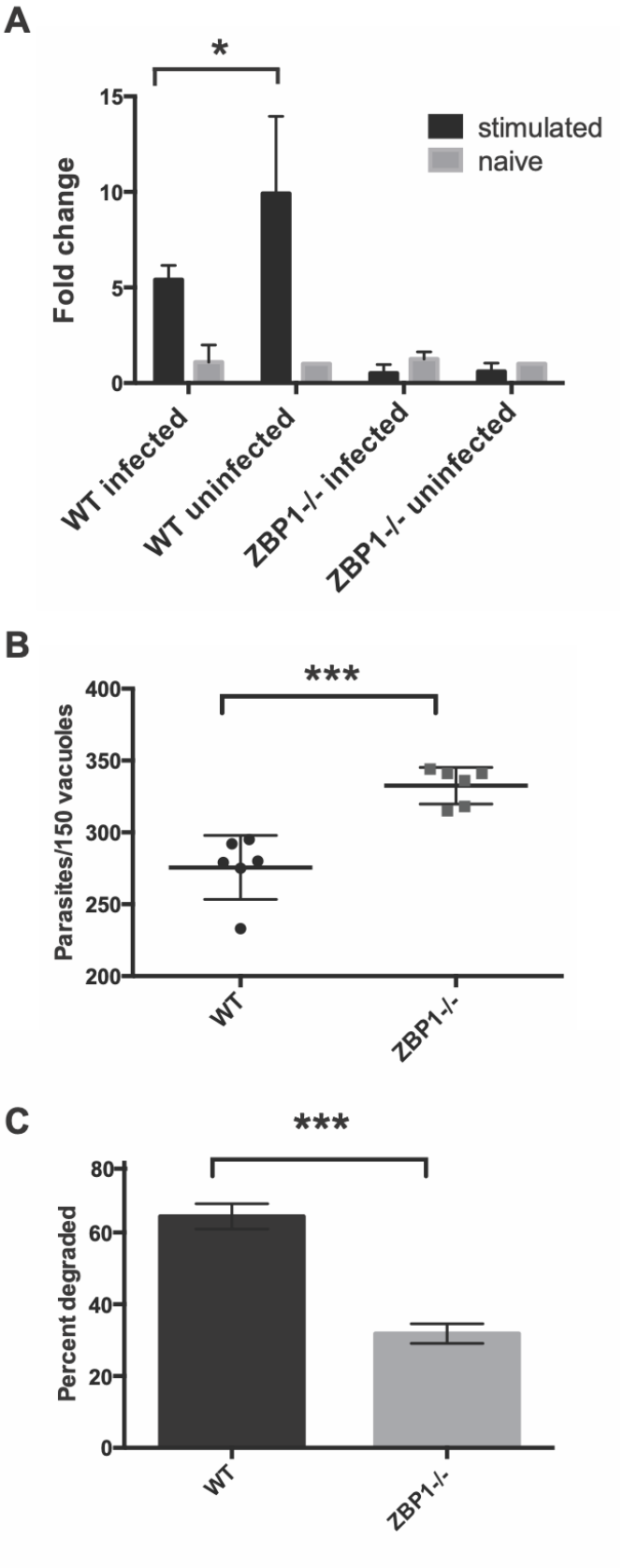
A
*
15
10
5
0
Fold change
stimulated
naive
WT infected
WT uninfected
ZBP1-/- infected
ZBP1-/- uninfected
B
***
400
350
300
250
200
Parasites/150 vacuoles
WT
ZBP1-/-
C
***
80
60
40
20
0
Percent degraded
WT
ZBP1-/-

Figure 1. *ZBP1 is up-regulated and influences parasite replication in activated macrophages.* (A) Wild type and ZBP1$^{-/-}$ macrophages were infected with *T. gondii* at an MOI of 5 (infected) or left uninfected. Two hours later, media was changed with no additives (gray bars, naïve) or 5ng/mL LPS and 25U/mL IFN-γ (black bars, stimulated). At 48 hours post-infection, RNA was extracted, cDNA was synthesized and qPCR was performed using primers targeting ZBP1 and GAPDH. ZBP1 transcript levels were normalized to GAPDH transcripts and then compared to uninfected naïve cells for both wild type and ZBP1$^{-/-}$ cells using the ΔΔCT method. qPCR was performed in duplicate and RNA was collected from 3 independent experiments. P-value <0.05 as determined by 2-way ANOVA of stimulated vs naïve samples. (B) *T. gondii* was cultured in macrophages from wild type (WT, black circles) and ZBP1$^{-/-}$ (gray squares) and stimulated with LPS and IFN-γ. At 24 hours post-infection, the number of total parasites was determined by adding together the number of 1, 2, and 4 parasites per vacuole from a total of 150 vacuoles. Three technical replicates were collected from two independent experiments. (C) Degradation of *T. gondii* is decreased in stimulated ZBP1$^{-/-}$ macrophages. WT and ZBP1$^{-/-}$ macrophages were infected with *T. gondii* (MOI 5), stimulated with LPS and IFN-γ 2 hours later, and fixed 48 hours post-infection. Degradation was determined based on presence of intact vacuole staining by IFA as described in (20). 100 vacuoles were counted and the percentage of intact vs degraded parasites was counted in duplicate in three independent experiments. Significance was determined by student's t-test.

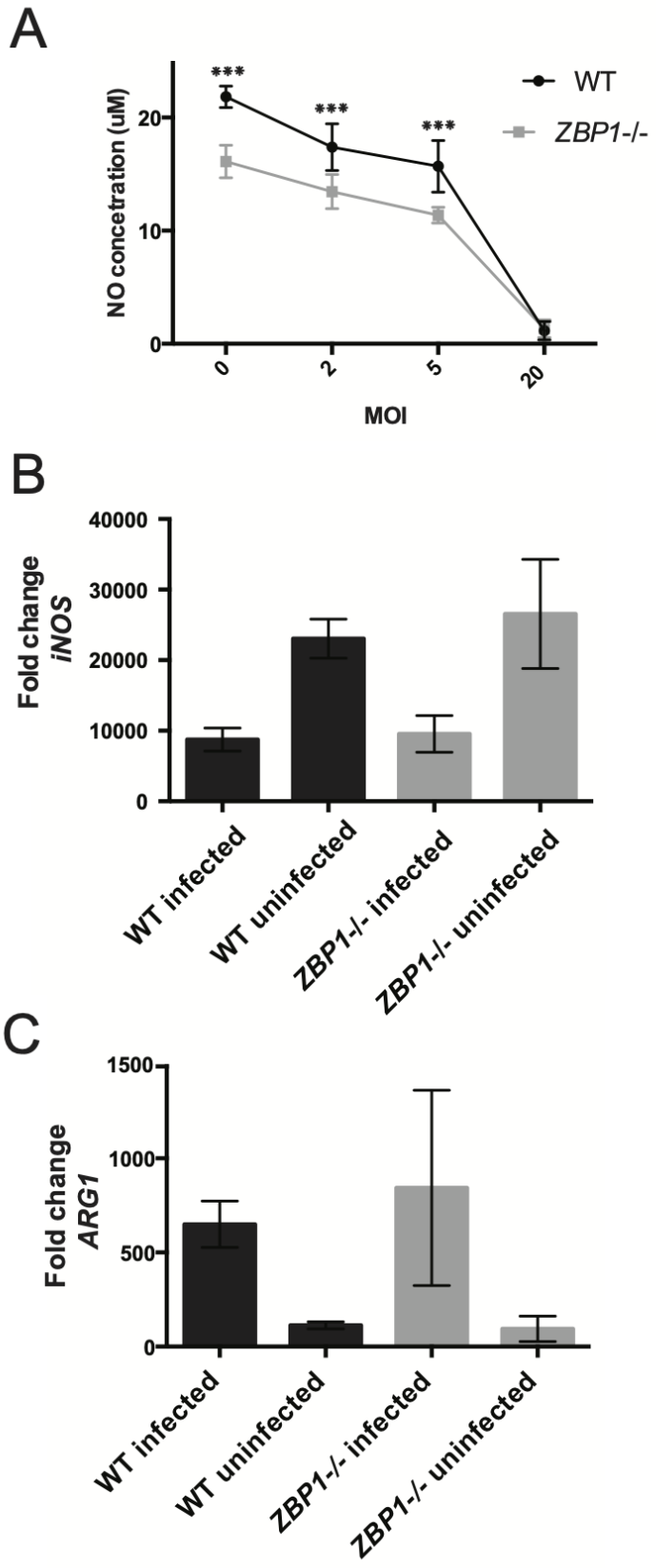
A
***
***
***
WT
ZBP1-/-
NO concetration (uM)
20
10
0
0
2
5
20
MOI
B
Fold change
iNOS
40000
30000
20000
10000
0
WT infected
WT uninfected
ZBP1-/- infected
ZBP1-/- uninfected
C
Fold change
ARG1
1500
1000
500
0
WT infected
WT uninfected
ZBP1-/- infected
ZBP1-/- uninfected

Figure 2. *NO production is decreased in stimulated ZBP1$^{-/-}$ macrophages.* (A) Wild type (WT, black circles) and ZBP1$^{-/-}$ (gray squares) macrophages were infected with *T. gondii* at an MOI of 0, 2, 5, 20. At 2 hours post-infection, cells were stimulated and at 48 hours post-infection, NO levels in cell supernatants were determined by Griess reaction. Three technical replicates were collected from three independent experiments. P-value < 0.0005 as determined by 2-way ANOVA of all data. (B and C) To determine the mechanism of NO reduction in ZBP1$^{-/-}$ cells, qPCR was performed targeting iNOS (B) and ARG1 (C) transcripts. Expression between wild type (WT, black) and ZBP1$^{-/-}$ (gray) macrophages was compared between stimulated infected and uninfected samples using GAPDH as a control and the ΔΔCT method. All samples were compared to uninfected naïve samples. qPCR was performed in duplicate from two independent experiments.

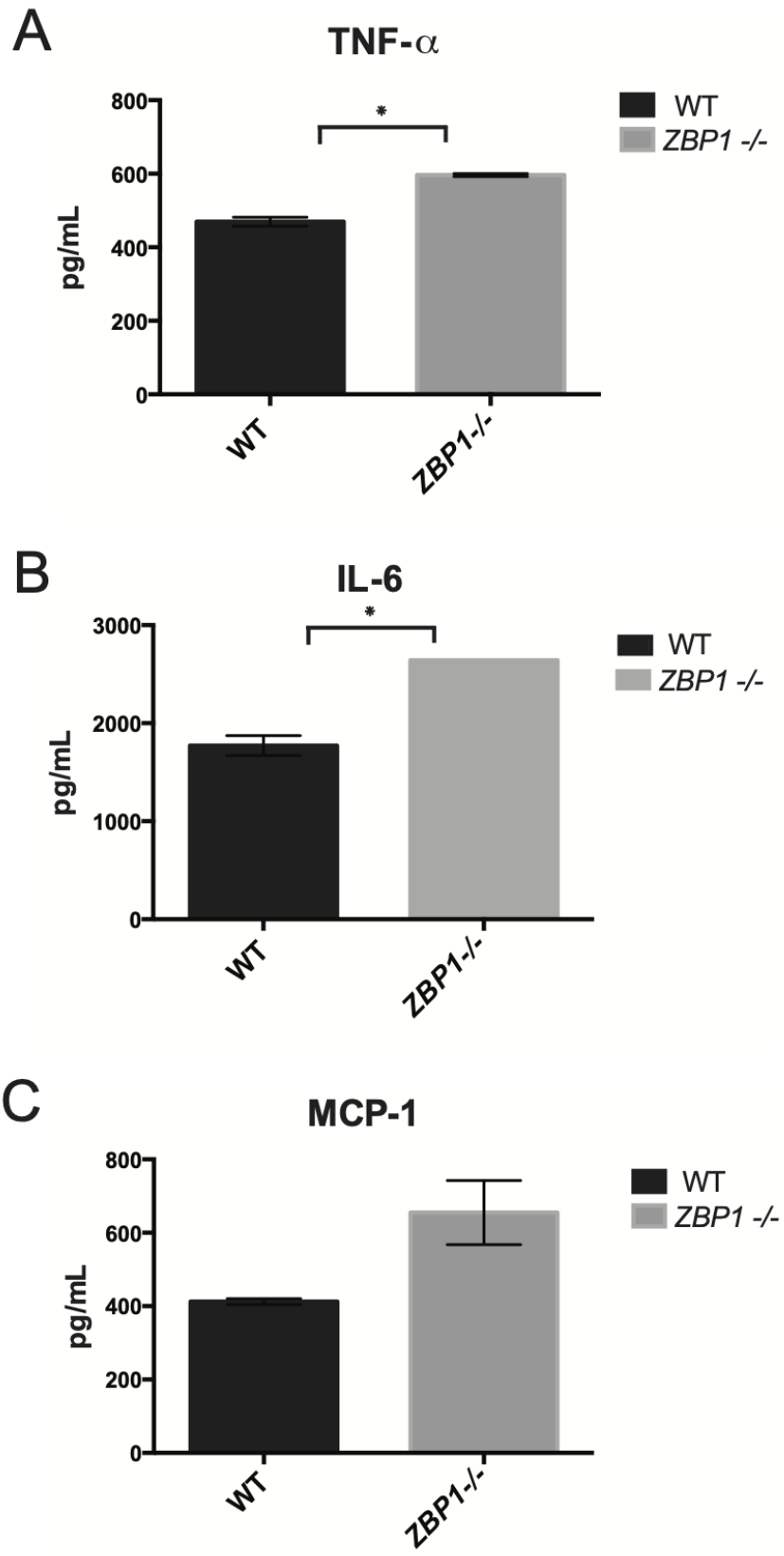
A
TNF-α
800
600
400
200
0
pg/mL
*
WT
ZBP1 -/-
WT
ZBP1-/-
B
IL-6
3000
2000
1000
0
pg/mL
*
WT
ZBP1 -/-
WT
ZBP1-/-
C
MCP-1
800
600
400
200
0
pg/mL
WT
ZBP1 -/-
WT
ZBP1-/-

Figure 3. *Expression of pro-inflammatory cytokines is increased in ZBP1$^{-/-}$ macrophages.* Wild type (WT, black) and ZBP1$^{-/-}$ (gray) macrophages infected with *T. gondii* at an MOI of 5, stimulated after 2 hours with LPS and IFN-γ, and grown for an additional 48 hours. Cytometric bead arrays were used to determine levels of IL-12, IFN-γ, TNF-α, IL-10, MCP-1, and IL-6 from supernatants. Two biological replicates were used for the analysis. TNF-α and IL-6 levels were significantly higher in ZBP1$^{-/-}$ supernatants. P-value=0.029 and 0.035, respectively as determined by t-test.

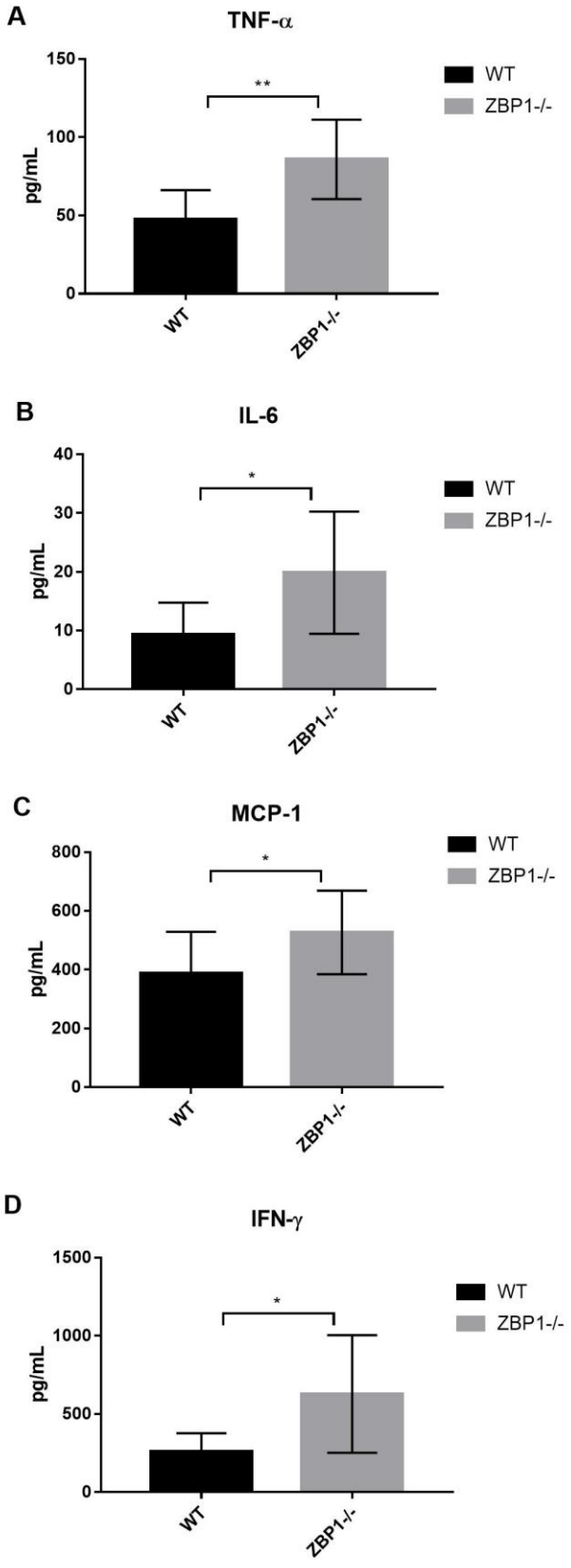
A
TNF-α
150
100
50
0
pg/mL
**
WT
ZBP1-/-
WT
ZBP1-/-
B
IL-6
40
30
20
10
0
pg/mL
*
WT
ZBP1-/-
WT
ZBP1-/-
C
MCP-1
800
600
400
200
0
pg/mL
*
WT
ZBP1-/-
WT
ZBP1-/-
D
IFN-γ
1500
1000
500
0
pg/mL
*
WT
ZBP1-/-
WT
ZBP1-/-

Figure 4. *Expression of pro-inflammatory cytokines is increased in the brains of ZBP1$^{-/-}$ infected mice.* Wild type (WT, black) and ZBP1$^{-/-}$ (gray) mice were infected with 1x10^{3} *T. gondii*, sacrificed at 28 days post-infection and the cytokine levels measured from the supernatant of brain homogenates. Shown is the pooled results from two independent experiments, with wild type n=8 and ZBP1$^{-/-}$ n=12. Statistical significance was determined by a two-tailed, independent t-test and the p-values were TNF-α = 0.0018, IL-6 = 0.0172, MCP-1 = 0.0461, IFN-γ = 0.0161.

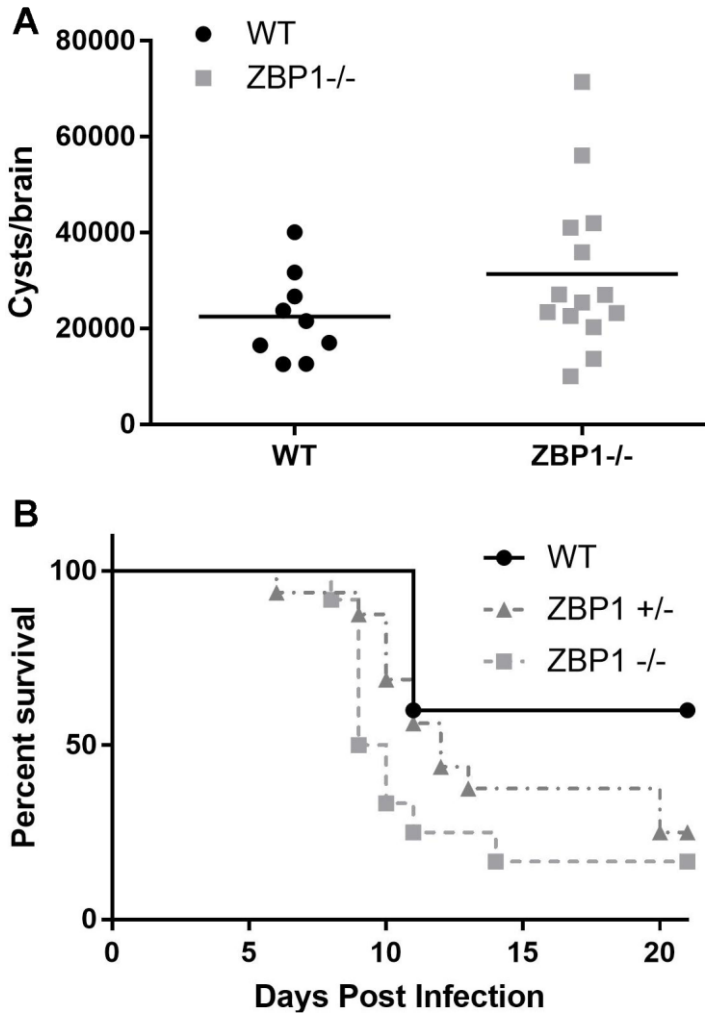

Figure 5. *ZBP1$^{-/-}$ mice have higher cyst burdens and are more susceptible to oral T. gondii infection.* ZBP1$^{+/-}$ mice were bred to each other to produce ZBP1$^{+/+}$(wild type), ZBP1$^{+/-}$, and ZBP1$^{-/-}$ used in these studies. (A) Wild type (WT, black circles) and ZBP1$^{-/-}$ (gray squares) mice infected were infected with 1x10^{3} *T. gondii*, sacrificed at 28 days post-infection and the cyst burden quantified in brain homogenates. Shown is the pooled results from two independent experiments, with wild type n=9 and ZBP1$^{-/-}$ n=14. (B) Wild type (WT, black circles), ZBP1$^{+/-}$ (dark gray triangles) and ZBP1$^{-/-}$ (gray squares) mice were fed brains of mice chronically infected with *T. gondii* for 28 days, receiving approximately 4000 cysts each, and time to death was determined. Shown is the pooled results from two independent experiments, with wild type

n=6, ZBP1$^{+/-}$ n=16, and ZBP1$^{-/-}$ n=12. Statistical significance was determined by log-rank test, which has a p-value of 0.0504 for WT vs. KO.

Appendix 2

A Gene Expression Biomarker Predicts Heat Shock Factor 1 (HSF1) Activation in a Gene Expression Compendium

Patrick W. Cervantes[1,2] and J. Christopher Corton[1*]

1Center for Computational Toxicology and Exposure, US Environmental Protection Agency, Research Triangle Park, NC 27711

[2] Department of Medical Microbiology and Immunology, University of Wisconsin-Madison, Madison, Wisconsin

*Corresponding author chris@epa.gov

Running title**:** A biomarker approach to identify activators of HSF1

Key words**:** heat shock; heat shock factor 1; biomarker; transcript profiling; microarray compendium; NRF2; oxidative stress

Appendix B will be submitted to the journal of Computational Toxicology

Author contributions: PWC designed and generated the HSF1 biomarker. PWC performed IPA analysis and determined predictive accuracy. PWC and JCC wrote the manuscript. PWC generated all tables and figures.

Abstract

Environmental chemical screening programs such as those carried out at the US EPA are increasingly using high throughput transcriptomics (HTTr) to identify molecular targets that can be linked to adverse outcomes. Here, we describe a method that uses a gene expression biomarker to predict chemical activation of heat shock factor 1 (HSF1), a transcription factor critical for proteome maintenance. The HSF1 biomarker was built from transcript profiles derived from A375 cells exposed to a HSF1-activating HSP90 inhibitor in the presence or absence of HSF1 expression. The resultant 44 identified genes included those 1) dependent on HSF1 for regulation, 2) that have direct interactions with HSF1 assessed by ChIP-Seq, and 3) in the molecular chaperone family. To test for accuracy, the biomarker was compared in a pair-wise manner to gene lists derived from treatments with known HSF1 activity (HSP and proteasomal inhibitors) using the correlation-based Running Fisher test; the balanced accuracy for prediction was 96%. A microarray compendium consisting of 12,092 microarray comparisons from human cells exposed to 2,670 individual chemicals was screened using our approach; 112 and 19 chemicals were identified as putative HSF1 activators or suppressors, respectively and most appear to be novel modulators. A large percentage of the chemical treatments that induced HSF1 also induced oxidant-activated NRF2 (~46%). For 5 compounds or mixtures, we found that NRF2 activation occurred at lower concentrations or at earlier times than HSF1 activation supporting a tiered cellular protection system based on stress response levels. The approach described here could be used to identify environmentally-relevant chemical HSF1 activators in HTTr datasets. (258 words)

Introduction

The heat shock response is a highly conserved major stress pathway that protects cells from diverse physical and chemical insults (1). Activation of this pathway by heat or chemical toxicants triggers the rapid transcriptional expression of a family of genes known as “heat shock” proteins that include members of the heat shock protein (HSP) family, some of which bind to unfolded proteins to minimize denaturation, prevent protein aggregate formation and facilitate the refolding of denatured proteins. Under basal conditions, the major transcriptional regulator of the inducible HSPs is called heat shock factor 1 (HSF1) which typically exists as a monomer in the cytoplasm through interactions with primary negative regulators, the molecular chaperones HSP70 and HSP90 (2). Exposure to a multitude of stressors can activate HSF1 leading to formation of transcriptionally active trimers that accumulate in the nucleus and bind to heat shock elements (HSE, inverted nGAAn repeats) in the upstream regulatory regions of target genes (3, 4).

The mechanisms by which HSF1 is activated are not entirely understood given that a great number of stressors of varied nature can trigger the heat shock response. The classical model frequently described in the literature posits that when cells are subjected to heat shock or other proteotoxic conditions, the increased levels of protein misfolding releases HSP90 from HSF1 monomers allowing HSF1 activation and increased transcription of the genes encoding HSP90 proteins (*HSP90AA1, HSP90AA2*) (2). Upon return to conditions in which protein denaturation is eliminated, increased levels of HSP90 protein binds to HSF1, providing a negative feedback mechanism. This mechanism ensures coordination between the overall condition of the protein folding environment and the level of expression of HSF1 target genes. Another (possibly) parallel mechanism of activation is the intrinsic ability of HSF1 itself to detect and respond to proteotoxic stimuli. Purified recombinant HSF1 becomes trimeric in a cell free system by a number of stressors including high temperature, low pH, oxidative stress or increasing concentrations of calcium (5, 6). The Arg 250 and Ser 247 residues in the DNA-

binding domain of HSF1 are critical for DNA binding, since mutations in either residue significantly alters HSF1 trimer formation and HSE recognition (7). In a third proposed mechanism, rapid activation of HSF1 by heat is facilitated in the early stages by a ribonucleoprotein complex consisting of translation elongation factor-1α (eEF1A) and a constitutively expressed non-coding RNA called heat-shock RNA-1 (HSR-1)(8). It is proposed that HSF1 is activated by the heat-sensing HSR-1 complexed with eEF1A, leading to translational inhibition observed during heat shock. The identification of this 'RNA temperature sensor' suggests that HSF1 activation by heat occurs when temperatures surpass the thermometer threshold.

A number of studies indicate that HSF1 plays an important role in tumor initiation, development and maintenance. Eliminating a functional HSF1 protected mice from tumors induced by mutation of the RAS oncogene or a hot spot mutation in tumor suppressor p53 as well as from diethylnitrosomine-induced hepatocellular carcinoma (HCC) formation (9-11). Loss of the tumor suppressor Neurofibromatosis Type 1 (NF1) activates HSF1 to promote carcinogenesis through dysregulated MAPK signaling (12). In a wide variety of human cancer cell lines, depletion of a functional HSF1 markedly reduces growth, survival, and metastatic potential (13-17)The cancer HSF1 program supports malignant cancer cell phenotypes through direct effects on cell cycle, DNA repair, anabolic metabolism, and proliferation (11, 14, 15, 18). The HSF1 program within the tumor stroma cells drives pathways that support malignant elements within the tumor. These pathways facilitate angiogenesis, extracellular matrix organization, adhesion, and migration. Surprisingly, the transcriptional program activated by HSF1 in cancer cells is different from the program activated by classical heat shock , and there is increasing evidence that tumors co-opt the ancient survival functions of HSF1 to orchestrate malignancy in both a cell-autonomous and non-cell-autonomous manner (14). In particular, the HSF1 tumor transcriptional program acts to support the malignant state by promoting pathways that facilitate anabolic metabolism, protein folding, proliferation, invasion, and metastasis as well

as blunting apoptotic responses (11, 12, 14, 15, 17-19). Activation of this program by HSF1 in cancer cells is strongly associated with disease progression in patients with breast, colon, lung, and hepatocellular carcinoma (14, 16, 19).

High-throughput transcriptomic (HTTr) technologies are being increasingly used to screen chemicals in human cell lines. The Environmental Protection Agency's (EPA) Toxicity Forecaster (ToxCast) screening program is now using HTTr to replace the battery of individual ToxCast screening assays (20) with a targeted RNA-Seq technique called TempO-Seq (21). HTTr has the advantage over individual assays by examining the effects of environmental chemicals on essentially all pathways simultaneously, many of which are not examined by the battery of ToxCast assays (20). A major challenge for any transcript profiling strategy including HTTr is how to make linkages between chemical exposure and modulation of molecular targets. A number of approaches have been used to interpret the HTTr profiles, and these include typical pathway analysis as well as comparisons to archived profiles of reference chemicals (e.g., (22)). While these approaches can lead to testable hypotheses as to what the chemical targets are, they do not allow prediction with known accuracy. Gene expression biomarkers have emerged as a complementary approach to accurately identify specific molecular targets. Biomarkers are sets of genes known or predicted to be regulated by a particular transcription factor (23). The biomarker gene expression pattern is compared to gene expression profiles derived from human cells exposed to chemicals using a number of computational techniques that include correlation analysis (24). Gene expression biomarkers that predict modulation of estrogen receptor (25), androgen receptor (26), metal-induced transcription factor 1 (27), and the oxidant-induced transcription factor NRF2 (28) have been described. In addition, a biomarker that identifies chemical exposure conditions that lead to DNA damage has been extensively characterized (29, 30) and is currently undergoing review by the Food and Drug Administration to be used as a tool to identify potential DNA damaging agents in human cells. A methodical analysis of gene expression profiles from cells exposed to reference chemicals as

well as perturbations of the gene encoding the chemical target will eventually lead to a battery of highly predictive biomarkers that can be used to interpret HTTr data streams (23). The large quantity of microarray data that already exists in commercial databases and in public repositories will provide for *in silico* high-throughput screening (HTS) identification of chemical agents that activate or suppress human molecular targets. Approaches to assess HSF1 modulation in a large microarray compendium have not been previously described.

In the present study, we developed procedures for predicting HSF1 perturbation in HTTr data. The biomarker was constructed from microarray profiles derived from cells treated with a HSP90 inhibitor in the presence or absence of HSF1 expression. The derived 44 genes were enriched for those involved in proteome maintenance, most of which were shown to be directly regulated by HSF1. The biomarker was used to screen a library of microarray profiles from cells treated with ~2600 organic chemicals to identify modulators of HSF1. The biomarker approach can readily identify chemical treatments known to activate HSF1, including inhibitors of HSP family members and the proteasome. Almost half of the chemical treatments that activated HSF1 also activated NRF2. Five chemicals were shown to activate NRF2 at lower doses or earlier times than HSF1, pointing to a tiered cellular protection system. Our approach not only greatly expands the identification of chemicals that activate HSF1 but provides a proof of principle approach that can be used to identify environmental chemicals that activate stress responses linked to human diseases.

Materials and methods

Use of a gene expression microarray experiment compendium.

As described previously in Rooney *et al.* 2018 (31), information from BaseSpace Correlation Engine (BSCE) (https://www.illumina.com/products/by-type/informatics-products/basespace-correlationengine.html; formerly NextBio) was used to build and test the HSF1 biomarker as well as to screen for HSF1 modulators. The database consists of lists of statistically-filtered gene expression comparisons (called biosets) from experiments carried out using human cell lines and tissues. Each bioset is derived from a pairwise comparison (i.e. treated vs. untreated, or mutant vs. wildtype). The master list was annotated to include information on bioset name, study accession information, cell line, tissue, chemical name, chemical concentration, genetic perturbation (e.g., *HSF1* shRNA treatment), treatment time, and predicted HSF1 activity. Of the biosets included, > 12,000 biosets were derived from experiments from chemically-treated cells. Methods used to derive the statistically-filtered gene lists generated by different microarray platforms or by RNA-Seq are described in detail in Kuperschmidt *et al.* 2010 (24).

HSF1 biomarker generation.

One study was selected to derive a set of HSF1-regulated genes that could be used for HSF1 modulation prediction. Out of our database, there was only one study in which gene expression was perturbed by both a chemical known to activate HSF1 and in which the expression of the *HSF1* gene was inhibited. In this case, a short hairpin (sh) RNA inhibitor was used to knockdown the expression of the *HSF1* gene (9). Malignant melanoma A375 cells were treated for 3 hrs with 100 nM NVP-HSP990, known to activate HSF1. Exposures to NVP-HSP990 occurred in the presence or absence of induced levels of the shHSF1 or control shRNA. The final dataset consisted of 3 comparisons of NVP-HSP990 treatment and 4 comparisons of *HSF1* gene knockdown. The 7 biosets selected to build the HSF1 biomarker are described in **Table 1**. Starting with lists of statistically-filtered genes, the candidate biomarker genes were identified in

two steps. In the first step, genes were selected that exhibited consistent directional changes in at least 2 of 3 NVP-HSP990 treatments. Any genes that exhibited inconsistent directional changes were removed. In the second step, a genetic filter was used to identify those genes that require HSF1 for expression changes and that exhibited opposite directional expression in at least 2 of 4 shHSF1 vs. wild-type biosets. Thus for the genes that were positively regulated by HSP990, the genes had to also exhibit down-regulation when HSF1 was knocked down. Conversely for the genes that were negatively regulated by HSP990, the genes had to also exhibit up-regulation when HSF1 was knocked down. These filters resulted in a set of 44 genes (33 genes with increased expression and 11 genes with decreased expression). The gene fold-change values were then averaged across the 3 NVP-HSP990 treatment biosets to create the final biomarker of 44 genes. The list of genes and associated fold-change values was uploaded into BSCE for further analysis. The genes in the biomarker are found in **Table S1.**

Comparison of the biomarker to biosets in the database.

The HSF1 biomarker was compared to all other biosets in the database using the Running Fisher algorithm. This method provides an assessment of the statistical significance of the overlapping genes between the biomarker and each bioset by assessing correlation and providing a summary p-value. A complete description of the Running Fisher test is provided in Kuperschmidt *et al*. 2010 (24). The statistical significance of the pair-wise comparisons were exported and each *p*-value was converted to a -log(*p*-value), with negative values used to indicate negative correlation between the biomarker and the bioset. Biosets with -log(*p*-value) ≥ |4| were considered significant based on prior studies using this threshold (25, 32, 33). A column in the human gene expression spreadsheet was populated with the -log(*p*-value) for each bioset. Biosets that were positively correlated with the biomarker (-log(*p*-value) ≥ 4) were predicted to exhibit activation of HSF1, while biosets that were negatively correlated (-log(*p*-value) ≤ -4) were predicted to exhibit suppression of HSF1.

Ingenuity pathway analysis.

The HSF1 biomarker genes were analyzed using the canonical pathway and upstream analysis functions of Ingenuity Pathway Analysis (IPA, Qiagen Bioinformatics, Redwood City, California). IPA uses a right-tailed Fisher's Exact test to calculate a significant overlap between the HSF1 biomarker genes and the IPA pathway gene list. The upstream analysis uses the number of differentially expressed genes to predict upstream regulators of the biomarker genes. The p-values for the canonical pathway analysis and upstream regulator were converted to -log(p-value)s. The results are found in **Table S2** and **Table S3**.

Selection of positive and negative controls and calculation of biomarker accuracy.

The HSF1 predictive accuracy was calculated separately for human HSF1 activation by chemical treatments or by heat shock treatments. In the database of human gene expression comparisons, biosets were identified that examined the effects of different factors on HSF1 modulation. These included chemical (87), genetic (12), and heat shock (37) treatments known or suspected to modulate HSF1. Information about the biosets used in these two analyses is found in **Table S4** and **Table S5** including reference citations supporting HSF1 activity (or lack thereof). The biosets used to create the biomarker were not included in the analysis. The -log(p-value) correlations of each bioset to the HSF1 biomarker was used to analyze the predictive accuracy. HSF1 predictive accuracy for chemical activation was calculated from 74 biosets treated with chemicals known to activate HSF1 and 18 biosets from chemical and genetic perturbation treatments known to not increase HSF1 activity. The sensitivity for human HSF1 activation by heat shock treatment was determined using 37 biosets subjected to heat shock treatment. Accuracy to predict HSF1 activation in mice was carried out using all 25 and 8 biosets from mouse cells undergoing either heat shock or treatment with known HSF1-activating chemicals, respectively. Additionally, there was only one bioset from the livers of intact mice subjected to heat shock. Bioset information is provided in **Table S6**. The predictive accuracy for

the HSF1 biomarker was calculated as follows: sensitivity (true positive rate) = TP/(TP+FN); specificity (true negative rate) = TN/(TN+FP); positive predictive value (PPV) = TP/(TP+FP); negative predictive value (NPV) = TN/(TN+FN); balanced accuracy = (sensitivity + specificity)/2.

Results and discussion

HSF1 biomarker generation

The HSF1 biomarker was generated and tested for predictive accuracy using gene expression comparisons (biosets) with known HSF1 activity. (Each bioset consists of a list of statistically-significant genes from a pairwise comparison in a gene expression study). The biosets included chemical (87), genetic (12), and heat shock (37) perturbations known or assumed to modulate HSF1 activity. One study was selected to derive a core set of HSF1-regulated genes that could be used for HSF1 modulation prediction. Out of our database, the selected study was the only one in which gene expression was perturbed by both a chemical known to activate HSF1 and a genetic approach using a short hairpin (sh) RNA inhibitor targeted to knockdown the expression of the *HSF1* gene (9). The 7 biosets selected to build the HSF1 biomarker are found in **Table 1**. In this study, malignant melanoma A375 cells were treated for 3 hrs with 100 nM NVP-HSP990, a compound that inhibits HSP90 leading indirectly to activation of HSF1. Exposures to NVP-HSP990 occurred in the presence or absence of induced levels of the shHSF1. The final dataset consisted of 3 comparisons of NVP-HSP990 treatment and 4 comparisons of HSF1 genetic perturbation. First, genes were identified that exhibited consistent directional changes in at least 2 of 3 NVP-HSP990 treatments. Then a genetic filter was used to identify genes under control of HSF1 that exhibited opposite directional expression in at least 2 of 4 shHSF1 vs. wild-type biosets. The gene fold-change values were averaged across the 3 NVP-HSP990 treatment biosets to create the final biomarker of 44 genes (33 genes with increased expression and 11 genes with decreased expression).

The expression of the 44 genes across the 7 biosets is represented in a heat map (**Figure 1A**). The biomarker genes are listed in **Table S1**.

The correlation between the biomarker and each of the biosets used in its construction was determined. The Running Fisher algorithm was used to calculate the statistical significance of each pair-wise correlation. Statistically-significant correlations were defined as those with a -log(p-value) ≥ |4|, where negative values indicated a negative correlation. Conditions that resulted in positively-correlated biosets were predicted to activate HSF1, while those conditions that resulted in negatively-correlated biosets were predicted to suppress HSF1. As expected, all 3 biosets from the NVP-HSP990 treatments exhibited very significant positive correlation (**Figure 1B**). All 4 of the biosets in which HSF1 expression was suppressed exhibited negative correlation with three of them being significant and one approaching significance (-log(p-value) = -2.92).

Characterization of HSF1 biomarker genes

The HSF1 biomarker gene list was analyzed by canonical pathway and upstream regulator analysis in IPA. The top 7 canonical pathways most significantly affected by the HSF1 biomarker genes are shown in **Figure 2A** and **Table S2** and included pathways that are known to affect HSF1 activity including protein ubiquitination, unfolded protein response, and oxidative stress. The relationships between HSF1 activation and NRF2-mediated oxidative stress response is addressed in detail below. Additional pathways identified have less clear linkages with regulation of the HSF1 genes. Mineralocorticoid receptors as well as other nuclear receptors are held in an inactive state in the cytoplasm by a complex of HSPs (34). Deregulation of HSF activity has been linked to a number of neurological diseases including Huntington disease and Parkinson disease in which the pathology arises from protein misfolding including that associated with compromised activation of HSF1, which further exacerbates protein misfolding (35). Bcl2-associated athanogene 2 (BAG2) functions as a co-chaperone and

interacts with the ATPase domain of HSP70 (36). In vascular endothelial cells, increases in the expression of human HSF1 corresponded with elevated steady-state levels of eNOS (37).

The top 10 upstream transcription factors predicted to regulate the biomarker genes are shown in **Figure 2B** and **Table S3**. The most significant factor was HSF1 followed by HSF2. HSF1 and HSF2 bind to both distinct and overlapping sites in the genome and can form hetero-oligomers, increasing the breadth of the regulatory control mechanisms imposed on each HSF subtype in a combinatorial manner (35). HSF2 has a different expression pattern than HSF1 and is highly expressed in the testis and brain (38, 39). The other transcription factors predicted included KMT2A, a histone lysine methyltransferase (2A); MYC proto-oncogene; H2AFX, the DNA-dependent protein kinase catalytic subunit, H2A histone family member X; KLF4, Kruppel-like factor 4; and CREB1, cAMP Responsive Element Binding Protein 1. While not KMT2A, another histone H3K3 methyltransferase called mixed lineage leukemia 1 (MLL1) functions as a coactivator of HSF1 in response to HSP90 inhibition. MLL1 is recruited to the promoters of HSF1 target genes and regulates their expression in response to HSP90 inhibition (40). Ablation of HSF1 restrains the growth of c-Myc-derived mouse hepatocellular carcinoma (HCC) cell lines, in parallel with downregulation of c-Myc levels. Conversely, silencing of the c-Myc gene in human and mouse HCC cells led to downregulation of HSF1 expression. Most importantly, overexpression of a dominant negative form of HSF1 in the mouse liver resulted in complete inhibition of mouse hepatocarcinogenesis driven by overexpression of c-Myc (41). HSF1 induces DNA-PKcs including H2AFX upregulation through the activation of the MAPK/JNK/AP-1 axis (42). Overexpression of KLF4 was found to promote the basal expression of HSP90 (HSP84 and HSP86) but not inducible expression in the C2C12 cells and RAW264.7 cells (43). HSF1 interacted with members of the ATF1/CREB family involved in metabolic homeostasis and recruited them to the HSP70 promoter in response to heat shock (44). There was no information about the linkage between HSF1 and ONECUT1, FERD3L, and PML.

Additional evidence was examined to determine if the biomarker genes are regulated by HSF1. In a comparison of the biomarker genes with those identified by ChIP-Seq, there was a significant overlap with those identified as HSF1 targets (p-value = 1.3E-18) but not two other transcription factors (E2F4 or C/EBPα; p-values > 0.05) in human adipocytes derived from mesenchymal stem cells (data from GSE24326;(45)). Out of the 20 biomarker genes identified as direct targets, all but 3 were positively regulated by NVP-HSP990. Furthermore, in a direct comparison between NVP-HSP990 treatments of A375 cells with and without expression of the shRNA against HSF1, the 32 biomarker genes with significant expression were all partially or completely dependent on HSF1 for altered expression (**Figure S1**). Between the two sets of genes, there were 35/44 (80%) that exhibited either direct interactions with HSF1 by ChIP-Seq and/or were regulated by HSF1 as assessed by the wild-type vs. HSF1 knockdown comparison.

The genes in the biomarker included those in various HSP families known to be regulated by HSF1. These included HSP27 *(HSPB1),* a number of DNAJ family members that are known as HSP40 subfamily members (*DNAJA1, DNAJB1, DNAJB4, DNAJB6*), a HSP47 family member (*SERPINH1*; serpin peptidase inhibitor, clade H (heat shock protein 47), member 1, (collagen binding protein 1)), HSP70 family members (*HSPA1A, HSPA1B, HSPA6),* and HSP105/110 *(HSPH1*). There were other genes associated with proteome maintenance including a cochaperone of HSP90 (*AHSA2*; AHA1, activator of heat shock 90kDa protein ATPase homolog 2 (yeast)), ubiquitin B (*UBB*), ubiquitin specific peptidase like 1 (*USPL1*), and BCL2-associated athanogene 3 (*BAG3*), which serves as a co-chaperone with heat shock proteins in facilitating autophagy. All of these genes were included in the 35 genes discussed above with linkages to HSF1. Thus, our unbiased weight of evidence method identified a set of genes enriched in those involved in proteome maintenance and regulated by HSF1.

Biomarkers predictive of human MIE modulation in vitro have been described that were built in a fashion similar to that used to make the HSF1 biomarker in which genetic perturbation of the factor was incorporated into the gene filtering procedures. Androgen receptor (AR)

biomarker genes were first identified as those with consistent regulation by a set of AR agonists and opposite regulation by a set of AR antagonists (26). The genes were then filtered for those with concordant directional changes in cells expressing a set of constitutively-active ARs and opposite regulation in cells treated with siRNA against the AR gene. The gene set behaved similarly to agonists or when AR was constitutively-activated and opposite of AR antagonists and after AR knockdown. NRF2 biomarker genes were identified by first identifying those with concordant directional changes across NRF2 activators followed by genetic filters (Keap1 siRNA and NRF2 siRNA knockdown)(31). The NF-kB biomarker genes were identified as those that were responsive to TNFα in wild-type cells but not in cells that overexpressed the inhibitor of NF-kB (IkB). In each of these approaches, the resultant gene lists were generally in the range of 46-144 genes.

Similar to approaches taken here, the resultant gene lists of the biomarkers have been evaluated a number of ways to confirm that the genes were in fact regulated by the factor to be predicted. Approaches that have been used included literature mining for studies showing direct or indirect regulation of the target gene by the factor, pathway based analysis, prediction of regulators using the upstream analysis function (Ingenuity Pathway Analysis) which identifies potential transcriptional regulators of the group of biomarker genes, and performing a reexamination of archived chromatin immunoprecipitation (ChIP)-Seq datasets in which genes were identified that were physically associated with the TF (26, 31, 46). The p53-dependence of genes in the TGx-DDI biomarker, the ER-dependence of genes in the ER biomarker, and the MTF-1-dependence of genes in the MTF-1 biomarker were confirmed by comparing transcriptional responses in wild-type cells to those in cells in which the expression of the factor was knocked down by factor-specific siRNAs (27, 29, 46). These analyses increase the confidence that relevant gene sets were identified and are appropriate for further analyses.

The HSF1 biomarker accurately identifies known HSF1-activating chemicals

For a biomarker to be useful in HTTr screening of environmentally-relevant chemicals, the methods using the biomarker must have known high accuracy. To test accuracy, the biomarker was compared to biosets that examined factors with known HSF1 activity. In the compendium there were 74 biosets comprising exposure to 26 chemicals that were putative true positives. The chemicals included those known to 1) inhibit HSP90 (17-(allylamino)-17-demethoxygeldanamycin, 17-(dimethylaminoethylamino)-17-demethoxygeldanamycin, 5-(2,4-dihydroxy-5-isopropylphenyl)-4-(4-morpholin-4-ylmethylphenyl)isoxazole-3-carboxylic acid ethylamide, alvespimycin, gamitrinib-G4, gedunin, geldanamycin, hypericin, monorden, NMS-E973, PU-H71, sanguinarine, withaferin A), 2) inhibit HSP70 family members (MAL3-101, parthenolide), 3) act as proteasomal inhibitors that lead to HSF1 activation (bortezomib, MG262, MG132, Thiostrepton), and 4) increase oxidative stress (pyrrolidine dithiocarbamic acid, sapphyrin). A number of other chemicals were selected that are known to activate HSF1 but through unknown mechanisms (4-hydroxy-2-nonenal, arsenic trioxide, disulfiram). Using the Running Fisher test, the biomarker was compared to these 74 chemical treatment biosets. (It should be noted that these biosets did not include those used to make the biomarker (essentially the training set)). The HSF1 biomarker successfully predicted 71 true positives with 3 false negatives resulting in a 96% biomarker sensitivity for HSF1 chemical activation (**Figure 3A**). The 3 false negatives had -log(p-values) close to the cutoff used (2.3-2.9). To test for specificity, true negatives were selected as they included treatment by chemicals known not to activate HSF1 and also included comparisons between HSF1 knockdown vs. wild-type. The biomarker effectively identified all 10 true negative biosets for 100% specificity. Overall, the balanced accuracy for HSF1 chemical activation was 98% (**Table 2)**. The gene expression fold changes for the 44 biomarker genes across all 84 biosets are shown in a heat map (**Figure 3B**). For those biosets that were positively correlated with the biomarker, the expression of the biomarker genes was remarkably similar to the biomarker itself. Literature citations supporting

HSF1 activity and in some cases, mechanisms of action for the biosets used are found in **Table S4**.

For a biomarker to be useful, predictive accuracy must be high in the tissue or cell line in which chemicals will be screened. The balanced accuracies for characterized biomarkers used for in vitro screening ranged from 87-97% for activators. Only two of the biomarkers (AR, ER) have been characterized for prediction of suppression (98%) (26, 46). In a number of cases, the biomarkers were shown to be accurate independent of the platform used to generate the gene expression profiles and included a variety of microarray types (mostly Affymetrix, Illumina and Agilent) as well as RNA-Seq. The accuracy of the TGx-DDI biomarker was similar across many platforms including microarrays, RT-qPCR, and direct digital nCounter technology (29). In the case of the HSF1 biomarker, the biosets used to determine predictive accuracy came mostly from different Affymetrix chip types, but also came from microarrays from Agilent and Illumina as well as a custom chip. This indicates that the biomarkers described so far are relatively insensitive to the platform used to assess gene expression. The biomarkers predicting hormone receptor-mediated effects are highly cell context-dependent due to the cell-specific expression patterns of these receptors. In contrast, biomarkers that predict the activation of factors involved in generalized stress responses (TGx-DDI, NRF2, NF-kB, MTF-1) are useful for prediction in many cell lines but are still dependent on expression of the factor. For example, the TGx-DDI biomarker cannot identify genotoxic agents in cells with inactivating mutations in the *TP53* gene. While we did not systematically determine the context of use of the HSF1 biomarker, the biomarker appears to be able to identify HSF1 activation in >30 cell lines or cell contexts (**Table S4**), consistent with HSF1 being expressed and the HSF1 regulon being responsive in a wide variety of cell lines, typical for a generalized stress factor.

The HSF1 biomarker identifies conditions undergoing the heat shock response in multiple species

The ability of the biomarker to predict activation of HSF1 by heat shock was carried out using 37 biosets derived from human cells subjected to heat shock treatments. The HSF1 biomarker identified 20 true positive biosets but failed to classify 17 biosets resulting in a 54% sensitivity (**Figure 4A,B; Table 2**). The ability to detect HSF1 activation appears to be specific to a group of 10 different cell lines or primary cells (**Figure 4C**). Most of the false negatives (13) were from one study examining the effects of heat shock in HeLa cells or primary lung fibroblasts (GSE4301;(47)). Three of the false negatives came from three different breast cancer cell lines. It is unlikely that these breast cancer cell lines are not responsive to HSF1 activation, as there are examples of chemical-induced HSF1 biomarker gene alteration by true positive chemicals in HeLa and MCF-7 cells (**Table S5, Table S7**). The lack of predicted activation of HSF1 in the GSE4301 study for the two cell lines is in contrast to the robust induction of HSF1 in the leukocyte cell line K-562 generated in the same study. In this cell line, there was significant biomarker correlation from 1 hr that peaked at 4 hrs and was maintained until the last time point measured (24 hrs) (**Figure 4D**). The lack of robust induction of HSF1 in these other two cell lines remains to be determined.

Given the strong conservation of the HSF1 regulon in mammals, we hypothesized that the biomarker could identify conditions in which HSF1 was activated in mice and rats. Out of the >13,000 biosets examined in rat tissues, there were only 4 examples in which the effects of induced heat shock (hyperthermia) were examined within a time frame of expected HSF1 activation (3 hrs) (from GSE29733 and GSE23093). There was significant activation of HSF1 in three of the comparisons: 1) choroid plexus (GSE23093), 2) blood (GSE23093), and 3) meninges and associated vasculature (GSE29733). Activation of HSF1 in the parietal cortex approached significance (-log(p-value) = 2.62) (GSE23093). A larger group of biosets derived from mouse tissues or cells with known effects on HSF1 were evaluated. These included 25

heat shock treatments in wild-type tissues or in tissues with HSF1 expression either knocked down or knocked out. There were also three chemicals (NVP-HSP990, AUY992, MG132) in 8 biosets known to activate HSF1 and 12 comparisons which examined the transcriptional effects of knocking down or knocking out *Hsf1*. **Figure 4E** shows that out of the 25 biosets predicted to exhibit HSF1 activation, 8 did not pass the statistical threshold (false negatives). Out of these 8, there were 3 biosets that approached significance (-log(p-value) > 2.5). Some of the false negatives came from a study in which there was significant activation of HSF1 at 2 and 3 hrs but not at 1, 4 and 6 hrs (from GSE3074). There were 20 true negatives and none exhibited activation. Overall, the balanced accuracy was 84%. Thus, the biomarker identified mouse conditions in which HSF1 was activated.

This is the first example of the ability of a biomarker designed to predict effects in human tissues demonstrating predictive effects in rodents. The ability of the biomarker to identify effects in mouse tissues is most likely due not only to the conservation of the responsive genes between species but the degree to which each gene responds to HSF1 activation between species. Thus, while there were outliers in mouse tissues (*Hspb1, Hspa1a, Hsph1, Dnaja1*; **Figure S2**), most of the genes exhibited the relative order of the fold-change responses observed in human tissues. However, the fact that not all genes overlapped or that orthologs could be found in mice may at least partially explain the diminished range of the correlations in the mouse tissues (-log(p-value)s < 9) compared to those in humans (-log(p-value)s < 16). This diminishment would potentially impact sensitivity of the response resulting in increases in false negatives. However, this prediction would have to be validated by an independent set of biosets derived from HSF1 activators that cause a spectrum of responses. Future work could focus on identification and characterization of chemicals that modulate HSF1 in the rat and mouse microarray chemical compendia.

An in silico screen identified novel chemical modulators of HSF1

Given the high predictive accuracy of the biomarker for identifying HSF1 chemical activators, an *in-silico* screen was performed of our human microarray chemical compendium. Using the Running Fisher test, the HSF1 biomarker was compared to all gene expression biosets derived from 12,089 treatments in human cells of 2670 chemicals. The significance of each bioset correlation to the HSF1 biomarker was ranked by -log(p-value) (**Figure 5**). Using a statistical cutoff of -log(p-value) ≥ |4|, we identified 202 biosets including 112 chemicals that were putative HSF1 activators and 19 chemicals in 20 biosets that were putative HSF1 suppressors. The chemicals that resulted in HSF1 suppression are discussed in **Supplemental File 2**. The biosets which exhibited significant correlation to the biomarker are found in **Table S7**.

Characterization of chemicals predicted to activate HSF1

We examined the chemicals that were potential novel activators of HSF1. The distribution of the -Log(p-value)s across the identified positive chemicals is shown in (**Figure S3A**). These chemicals exhibited an expression pattern of the biomarker genes very similar to that of the biomarker itself (**Figure S3B**). The top 20 ranking biosets that resulted in HSF1 activation are shown in **Table 3**. The top 20 hits included exposure to 9 mixtures or individual chemicals including tobacco smoke, diesel exhaust, iron(III) meso-tetramesitylporphyrin, metals (sodium arsenite, zinc oxide nanoparticles), albendazole, sulforafan, allyl alcohol, and furosemide. There were also five chemicals in 7 biosets from the CMAP collection (discussed below). For most of these exposures, there is only limited evidence that HSF1 is activated. Pro-oxidative diesel exhaust particle chemicals induce heat shock proteins and an unfolded protein response in a bronchial epithelial cell line (48).One-month exposure of rats to cigarette smoke/air mixture led to increased expression of HSP70 and HSF1 in airway smooth muscle in rats (49). Sulforaphane activated the heat shock response and enhanced proteasome activity

through up-regulation of HSP27 (50). Allyl alcohol, furosemide, iron(III) meso-tetramesitylporphyrin, and albendazole appear to be novel HSF1 activators.

We next asked whether there were any chemicals that activated HSF1 in multiple cell lines under similar or identical exposure conditions. The 1078 chemicals profiled in HL-60, MCF-7, and PC3 cells for 6 hrs were examined and ranked based on significance of the correlation and number of cell lines in which the chemical activated HSF1 (**Figure S3C**). There were three chemicals that activated HSF1 in all three cell lines (15-deoxy-delta(12,14)-prostaglandin J2, ebselen, securinine), 6 that activated in two cell lines (1,4-chrysenequinone, diethylstilbestrol, menadione, oxyphenbutazone, phenoxybenzamine, piperlonguminine), and 16 that activated in only one (5182598, 5224221, 5253409, carbamazepine, celastrol, chelidonine, clotrimazole, cyproheptadine, ethacrynic acid, fenbendazole, mometasone furoate, nifedipine, oxaprozin, resveratrol, scoulerine, trichostatin A). Very little information exists that links exposure of these compounds to HSF1 activation. Prostaglandin 15-deoxy-delta12,14-prostaglandin (PG) J2 was shown to have anti-inflammatory properties in carrageenin-induced hind-paw edema, an acute model of inflammation, and this effect was associated with HSF1-induced HSP72 expression in vivo suggesting that the use of cyclopentenone derivatives such as PGJ2 may represent a novel therapeutic approach for the treatment of inflammatory diseases (51). Treatment of cultured cardiac myocytes with ebselen for 24 hr increased the expression of stress proteins such as HSP70 in cardiac myocytes (52). Securinine, a GABAA receptor antagonist, has been reported to enhance monocyte cell killing of *Coxiella burnetii* without obvious adverse effects in vivo; HSPs (60, 70, and 90), including seven HSP70 isoforms were observed to be up-regulated in a monocyte cell line (53). A gene expression-based analysis was used to classify HSP90 inhibitors as having similar transcriptional profiles to celastrol which was found to inhibit HSP90 activity and the HSP90 client, androgen receptor (54). In summary, we have identified a number of potential novel HSF1 activators. Identification of the mechanisms of how these compounds might induce HSF1 requires further study.

Relationships between oxidative stress and activation of HSF1

We tested the hypothesis that in many cases, chemical exposure leads to HSF1 activation through increases in oxidative stress, subsequent damage to proteins, and induction of the unfolded protein response. To test this hypothesis, biosets in which HSF1 was activated were examined for NRF2 activation using a recently characterized gene expression biomarker that can predict the modulation of oxidant-induced NRF2. **Figure 6A** shows the relationships between activation of HSF1 and NRF2 across the 2670 chemical treatments examined in this study. The correlation to the HSF1 biomarker generally increased with increasing correlation to the NRF2 biomarker. (It should be noted that co-occurrence of activation was not due to overlap of the biomarker genes, as there was only one gene (*SLC7A11*) that overlapped between the biomarkers.) Remarkably, for 124 of the 276 biosets (45%) representing 64 chemicals or mixtures in which there was significant activation of HSF1, there was significant activation of NRF2.

We examined the relationships between different functional classes of HSF1 inducers and NRF2 activation. Only 3 out of the 42 biosets from treatments of HSP70, HSP72, and HSP90 inhibitors exhibited NRF2 activation, supporting the classical activation of HSF1 by a mechanism that does not involve oxidative stress (**Figure 6B**). Similar to inhibition of HSP family members, none of the 20 biosets from heat shock-treated biosets in which there was activation of HSF1 was there also activation of NRF2 (**Figure 6C**). In contrast, 15 out of the 21 biosets from proteasomal inhibitors (bortezomib, MG132, thiostrepton) exhibited NRF2 activation (**Figure 6D**), indicating that inhibition of protein degradation can lead to oxidative stress and activation of both factors. There were a number of compounds described previously as being dual activators of NRF2 and HSF1 that overlapped with those examined in our compendium (15-deoxy-delta(12,14)-prostaglandin J2, 4-hydroxy-2-nonenal, acrolein, celastrol, curcumin, gedunin, resveratrol, sulforafan, withaferin A) (55). The ability of these compounds to

activate both factors is shown in **Figure 6E**. Four of the chemicals activated both factors (celastrol, PGJ2, sulforafan, withaferin A).

We next tested the hypothesis that chemical exposure leads first to NRF2 activation followed by activation of HSF1 (55, 56) 25465722. We found a number of studies to determine if this hypothesis is true as the studies involved 3 or more concentrations or treatment times of the chemical. Primary human hepatocytes were exposed to three concentrations of two chemicals (azathioprin, propylthiourea) for 24 hrs (data from the TG-GATES study) (**Figure 7A**). Each compound activated NRF2 with increasing significance of correlation at increasing concentration, with HSF1 activation achieving significance at either the two highest doses (propylthiourea) or highest dose only (azathioprine). **Figure 7B** shows the effects of 15% tobacco smoke in bronchial epithelial AIR-100 cells. In these experiments, cells were exposed to the 15% tobacco smoke for 7, 14, 21, or 28 min and then after replacement with synthetic air, gene expression was evaluated at 5 different times (0.5 – 48 hrs) (data from MTAB-874). Under each of the 4 treatment times, NRF2 activation preceded activation of HSF1. **Figure 7C** shows the effects of three concentrations of the Chinese herbal supplement si-wu-tang on gene expression in MCF-7 cells (data from GSE23610). NRF2 activation occurred at the two highest doses whereas HSF1 occurred only at the highest dose. **Figure 7D** shows the effects of exposure to hemin, an iron-containing porphyrin with chlorine in K-562 cells at 5 times of exposure (data from GSE1036). Activation of NRF2 occurred at all time points examined, whereas HSF1 activation only occurred at the two latest time points. These studies examining the effects of 5 chemicals or mixtures indicate that oxidative stress produced by chemical exposure leads first to activation of NRF2 followed by HSF1 in a concentration- and time-dependent manner.

Naturally occurring and synthetic small molecules have been identified that can activate both HSF1 and NRF2 including endogenous chemicals, phytochemicals and synthetic compounds (55). In line with the diverse cytoprotective functions of HSF1- and NRF2-regulated

proteins, numerous studies have described the protective effects of many inducers in various cell culture and animal models of chronic disease, including neurodegenerative and cardiovascular disease, as well as cancer (55). Here, we identified 64 compounds or mixtures that activate both HSF1 and NRF2, and most of these appear to be novel. A common feature of many of these compounds is their ability (or that of their metabolites) to react with sulfhydryl groups (55). For example, the active electrophilic cyclopentenone 15d-PGJ2, which contains an α,β-unsaturated carbonyl moiety is active while other arachidonic acid metabolites which lack this electrophilic functional group, are inactive (57). Similarly, in sharp contrast to the electrophilic nitro-oleic acid, the non-electrophilic oleic acid counterpart is devoid of inducer activity (58). The importance of sulfhydryl reactivity for inducer activity is a well-established property of NRF2 activators which react with cysteine sensors of Keap1 (59, 60) resulting in blocking degradation of NRF2 (61). Although the sensor protein(s) in the mammalian cell for HSF1 activators is often unknown, the fact that many of the HSF1 chemical inducers possess sulfhydryl reactivity suggests that these proteins contain reactive nucleophilic amino acids. For example, the sulfoxythiocarbamate inducer (STCA) which activates both NRF2 and HSF1 conjugates to HSP90 in experiments performed in human HEK293 cells (56). Thus, chemical-induced modifications of HSP90 and/or HSP70 independent of specific inhibitors may trigger release of HSF1 and activation of gene expression. Some activators can be directly sensed by HSF1 itself as cysteine oxidation by H_2O_2 affects HSF1-dependent transcription (62, 63). Additionally, sulfhydryl-reactive compounds could cause transient depletion of the intracellular GSH and reduced thioredoxin pools, and it is therefore possible that, in certain cases, global protein oxidation, rather than, or in addition to, direct target protein modifications, activates HSF1 and NRF2.

In our compendium, we identified microarray experiments which allowed us to test the hypothesis that NRF2 is activated at lower concentrations of chemical inducers than HSF1 (55, 56). The hypothesis was based on experiments with a tricyclic bis(cyanoenone)-31 (TBE-31)

that protects against peroxynitrite-induced cytotoxicity carried out in mouse embryonic fibroblasts that were either wild-type or knocked out for *Nfe2l2* or *Hsf1*. In our experiments, all 4 chemicals examined at least 3 concentrations exhibited activation of NRF2 at concentrations lower than those that activated HSF1. Additionally, hemin activated NRF2 at earlier times than HSF1. Thus for the limited number of compounds and mixtures examined with appropriate experimental conditions, our findings support the earlier hypothesis that the KEAP1/NRF2/ARE regulon is at the forefront of cellular defense, protecting against low levels of oxidative stress while HSF1 and regulator response closely follows under more adverse exposure conditions to resolve subsequent potentially devastating damage in efforts to save the proteome. This duality contributes to the effects of cytoprotective molecules in models of carcinogenesis, cardiovascular disease, and neurodegeneration (56).

What are the implications for identifying HSF1 modulation in HTTr chemical screening studies using the HSF1 biomarker?

Large numbers of environmentally-relevant chemicals are currently being tested by the EPA and other organizations for transcriptional effects in human cell lines using HTTr. Here, using our biomarker and the Running Fisher test to determine correlation, we can readily identify HSF1 activators. How will we interpret these findings in terms of the underlying mechanistic basis? The biomarker approach can identify HSF1 activated by two major mechanisms: selective inhibition of HSPs and increases in proteotoxicity. Based on profiles in our compendium, chemical-induced HSF1 activation occurs mainly through inhibition of HSP90, but a few chemicals could activate by inhibiting HSP70 family members. Increases in proteotoxicity could occur through multiple mechanisms including specific inhibition of the ubiquitin-dependent 19S (thiostrepton) or ubiquitin-independent 20S (MG132, MG262, bortezomib) proteasome. There were no compounds in the compendium to determine if selective inhibition of the immunoproteasome would lead to activation of HSF1. HSF1 can also

be activated by protein unfolding or damage caused by a number of mechanisms that include oxidative stress. To gain insights into the underlying mechanism of induction, concentration-dependent activation of HSF1 could be compared to the activity of other stress factors. These comparisons would help to distinguish between HSF1 coactivated with other stress factors as part of the cytotoxic burst attributed to a (nonspecific) generalized stress response (64). Under these exposure scenarios, the prediction would be that in many cases NRF2 activation would occur at chemical concentrations lower than the burst itself. If activation of HSF1 occurs at concentrations that are below the cytotoxic burst, then there may be more specific mechanisms in play including inhibition of one or more of the HSP family members. However, it remains to be determined the relationships between exposure to inhibitors of HSPs and cytotoxicity. While there were compounds in the compendium that have been previously characterized as direct HSF1 activators, none of these activated HSF1. In a previous study, a strong transcriptional linkage was found as part of the alteration of a cancer transcriptional program between perturbations that inhibit protein translation and HSF1 suppression (18). In our studies, we did not find as many chemicals that suppressed HSF1 as those that activated and for the most part they did not include translation inhibitors (except one instance). How those chemicals suppress HSF1 requires further study. Additionally, how we put chemical-induced HSF1 activation into the context of human health requires further study.

Summary

Chemical screening programs are increasingly relying on high throughput transcriptomics (HTTr) to identify extrapolated doses that would be predicted to not cause effects in humans and to identify molecular targets that can be linked to adverse outcomes (20). Prior work using cellular assays in ToxCast and Tox21 screening programs have shown that chemicals often activate one or more cellular stress response pathways especially at high concentrations. Using HTTr screening, there are opportunities to move from reliance on a set of

single assays with limited coverage of potential biological targets to essentially characterize all molecular events simultaneously. These individual findings could be assembled to identify a specific pattern or bio-signature attributable to compound and/or tissue-specific toxicity. It is hoped but not yet realized that identification of the biomolecular changes and signaling pathway alterations that precede a toxic phenotype will allow for better classification and earlier prediction of compound toxicity (20). At the very least, the approach will allow the identification of chemicals of greater concern for human exposure that can be further evaluated.

The major toxicologically-relevant stress factor-governed molecular pathways include those that are activated by chemical-induced oxidative, genotoxic and proteotoxic stress, which induce coordinated responses in an effort to restore homoeostasis. These response pathways include those regulated by NRF2, NRF1, p53, HSF1, HIF1, regulators of the unfolded protein response (ATF4, ATF6, XBP1), MTF-1, and the immunomodulatory transcription factor NF-κB. The biochemical characteristics of these stress response pathways, their common architecture that enables rapid activation during stress, their participation in cell fate decisions, the essential nature of these pathways to the organism, and the biochemical basis of their cross-talk have been extensively reviewed (65, 66).

We describe here a method that uses a gene expression biomarker and a correlation-based comparison approach to predict chemical activation of heat shock factor 1 (HSF1), a transcription factor implicated in a number of human diseases. The HSF1 biomarker can now be added to a growing number of gene expression biomarkers for different stress pathways that include DNA damage, NRF2, MTF1, and NF-kB. Like the biomarker for HSF1, biomarkers for NRF2 and NF-kB utilized profiles in which the factor itself was perturbed either directly by knocking down the expression of the factor or indirectly by knocking down or overexpressing positive or negative effectors of response. Efforts are underway to create biomarkers of the other common stress pathways allowing a comprehensive assessment of how environmentally-relevant chemicals cause perturbations in homeostasis that using future models can be linked to

key events in adverse outcome pathways. The balanced accuracy for identification of HSF1 chemical activators was 96%. The high accuracy was similar to the other biomarkers characterized and ranged from 87 to 97%. These biomarkers have been shown to identify chemical modulators in human cell lines derived from a wide range of tissues as long as the factor being predicted is expressed and not mutated. This is in contrast to more tissue-specific biomarkers that can only be used in the context of a limited number of tissues (i.e., the androgen receptor biomarker used in AR positive prostate cancer cell lines; the estrogen receptor biomarker used in ER positive breast cancer cell lines). All of the biomarkers have been used to screen a microarray compendium consisting of >12,000 microarray comparisons from human cells exposed to >2,600 individual chemicals providing a rich catalog of chemical-key event interactions for future assembly into networks of AOPs. It is anticipated that with a complete set of biomarkers that predict the major stress pathways there will be opportunities to uncover cell-agnostic as well as cell-specific network interactions that would help to catalog and prioritize chemicals for further testing. One example of a greater systems biology understanding of stress responses is the identification of sequential activation of NRF2 followed by HSF1 based on level of chemical-induced stress. Lastly, the fact that these biomarkers did not require any specialized computational techniques to build and use provides the impetus to reconstruct a similar architecture that is publicly-available possibly similar to CMAP that would allow a greater number of investigators to build predictive biomarkers and used them for screening in publicly-available datasets.

References

1. Westerheide SD, Morimoto RI. 2005. Heat shock response modulators as therapeutic tools for diseases of protein conformation. J Biol Chem 280:33097-100.
2. Dayalan Naidu S, Dinkova-Kostova AT. 2017. Regulation of the mammalian heat shock factor 1. FEBS J 284:1606-1627.
3. Trinklein ND, Murray JI, Hartman SJ, Botstein D, Myers RM. 2004. The role of heat shock transcription factor 1 in the genome-wide regulation of the mammalian heat shock response. Mol Biol Cell 15:1254-61.
4. Jaeger AM, Makley LN, Gestwicki JE, Thiele DJ. 2014. Genomic heat shock element sequences drive cooperative human heat shock factor 1 DNA binding and selectivity. J Biol Chem 289:30459-69.
5. Hentze N, Le Breton L, Wiesner J, Kempf G, Mayer MP. 2016. Molecular mechanism of thermosensory function of human heat shock transcription factor Hsf1. Elife 5.
6. Jarosz DF, Lindquist S. 2010. Hsp90 and environmental stress transform the adaptive value of natural genetic variation. Science 330:1820-4.
7. Littlefield O, Nelson HC. 1999. A new use for the 'wing' of the 'winged' helix-turn-helix motif in the HSF-DNA cocrystal. Nat Struct Biol 6:464-70.
8. Shamovsky I, Ivannikov M, Kandel ES, Gershon D, Nudler E. 2006. RNA-mediated response to heat shock in mammalian cells. Nature 440:556-60.
9. Chen Y, Chen J, Loo A, Jaeger S, Bagdasarian L, Yu J, Chung F, Korn J, Ruddy D, Guo R, McLaughlin ME, Feng F, Zhu P, Stegmeier F, Pagliarini R, Porter D, Zhou W. 2013. Targeting HSF1 sensitizes cancer cells to HSP90 inhibition. Oncotarget 4:816-29.
10. Dai C, Whitesell L, Rogers AB, Lindquist S. 2007. Heat shock factor 1 is a powerful multifaceted modifier of carcinogenesis. Cell 130:1005-18.

11. Jin X, Moskophidis D, Mivechi NF. 2011. Heat shock transcription factor 1 is a key determinant of HCC development by regulating hepatic steatosis and metabolic syndrome. Cell Metab 14:91-103.

12. Dai C, Santagata S, Tang Z, Shi J, Cao J, Kwon H, Bronson RT, Whitesell L, Lindquist S. 2012. Loss of tumor suppressor NF1 activates HSF1 to promote carcinogenesis. J Clin Invest 122:3742-54.

13. Scherz-Shouval R, Santagata S, Mendillo ML, Sholl LM, Ben-Aharon I, Beck AH, Dias-Santagata D, Koeva M, Stemmer SM, Whitesell L, Lindquist S. 2014. The reprogramming of tumor stroma by HSF1 is a potent enabler of malignancy. Cell 158:564-78.

14. Mendillo ML, Santagata S, Koeva M, Bell GW, Hu R, Tamimi RM, Fraenkel E, Ince TA, Whitesell L, Lindquist S. 2012. HSF1 drives a transcriptional program distinct from heat shock to support highly malignant human cancers. Cell 150:549-62.

15. Meng L, Gabai VL, Sherman MY. 2010. Heat-shock transcription factor HSF1 has a critical role in human epidermal growth factor receptor-2-induced cellular transformation and tumorigenesis. Oncogene 29:5204-13.

16. Santagata S, Hu R, Lin NU, Mendillo ML, Collins LC, Hankinson SE, Schnitt SJ, Whitesell L, Tamimi RM, Lindquist S, Ince TA. 2011. High levels of nuclear heat-shock factor 1 (HSF1) are associated with poor prognosis in breast cancer. Proc Natl Acad Sci U S A 108:18378-83.

17. Scott KL, Nogueira C, Heffernan TP, van Doorn R, Dhakal S, Hanna JA, Min C, Jaskelioff M, Xiao Y, Wu CJ, Cameron LA, Perry SR, Zeid R, Feinberg T, Kim M, Vande Woude G, Granter SR, Bosenberg M, Chu GC, DePinho RA, Rimm DL, Chin L. 2011. Proinvasion metastasis drivers in early-stage melanoma are oncogenes. Cancer Cell 20:92-103.

18. Santagata S, Mendillo ML, Tang YC, Subramanian A, Perley CC, Roche SP, Wong B, Narayan R, Kwon H, Koeva M, Amon A, Golub TR, Porco JA, Whitesell L, Lindquist S. 2013. Tight coordination of protein translation and HSF1 activation supports the anabolic malignant state. Science 341:1238303.

19. Fang F, Chang R, Yang L. 2012. Heat shock factor 1 promotes invasion and metastasis of hepatocellular carcinoma in vitro and in vivo. Cancer 118:1782-94.

20. Thomas RS, Bahadori T, Buckley TJ, Cowden J, Deisenroth C, Dionisio KL, Frithsen JB, Grulke CM, Gwinn MR, Harrill JA, Higuchi M, Houck KA, Hughes MF, Hunter ES, Isaacs KK, Judson RS, Knudsen TB, Lambert JC, Linnenbrink M, Martin TM, Newton SR, Padilla S, Patlewicz G, Paul-Friedman K, Phillips KA, Richard AM, Sams R, Shafer TJ, Setzer RW, Shah I, Simmons JE, Simmons SO, Singh A, Sobus JR, Strynar M, Swank A, Tornero-Valez R, Ulrich EM, Villeneuve DL, Wambaugh JF, Wetmore BA, Williams AJ. 2019. The Next Generation Blueprint of Computational Toxicology at the U.S. Environmental Protection Agency. Toxicol Sci 169:317-332.

21. Yeakley JM, Shepard PJ, Goyena DE, VanSteenhouse HC, McComb JD, Seligmann BE. 2017. A trichostatin A expression signature identified by TempO-Seq targeted whole transcriptome profiling. PLoS One 12:e0178302.

22. De Abrew KN, Kainkaryam RM, Shan YK, Overmann GJ, Settivari RS, Wang X, Xu J, Adams RL, Tiesman JP, Carney EW, Naciff JM, Daston GP. 2016. Grouping 34 Chemicals Based on Mode of Action Using Connectivity Mapping. Toxicol Sci 151:447-61.

23. Corton JC, Kleinstreuer NC, Judson RS. 2019. Identification of potential endocrine disrupting chemicals using gene expression biomarkers. Toxicol Appl Pharmacol:114683.

24. Kupershmidt I, Su QJ, Grewal A, Sundaresh S, Halperin I, Flynn J, Shekar M, Wang H, Park J, Cui W, Wall GD, Wisotzkey R, Alag S, Akhtari S, Ronaghi M. 2010. Ontology-based meta-analysis of global collections of high-throughput public data. PLoS One 5.

25. Ryan N, Chorley B, Tice RR, Judson R, Corton JC. 2016. Moving Toward Integrating Gene Expression Profiling Into High-Throughput Testing: A Gene Expression Biomarker Accurately Predicts Estrogen Receptor alpha Modulation in a Microarray Compendium. Toxicol Sci 151:88-103.

26. Rooney JP, Chorley B, Kleinstreuer N, Corton JC. 2018. Identification of Androgen Receptor Modulators in a Prostate Cancer Cell Line Microarray Compendium. Toxicol Sci 166:146-162.

27. Jackson AC LJ, Vallanat B, Jones C, Nelms MD, Patlewicz G, Corton JC. 2020. Identification of Novel Activators of the Metal Responsive Transcription Factor (MTF-1) Using a Gene Expression Biomarker in a Microarray Compendium. Submitted.

28. Rooney J, Chorley, B, Corton JC. 2020. Mining a human transcriptome database for chemical modulators of Nrf2. TBD.

29. Cho E, Buick JK, Williams A, Chen R, Li HH, Corton JC, Fornace AJ, Aubrecht J, Yauk CL. 2019. Assessment of the performance of the TGx-DDI biomarker to detect DNA damage-inducing agents using quantitative RT-PCR in TK6 cells. Environ Mol Mutagen 60:122-133.

30. Corton JC, Williams A, Yauk CL. 2018. Using a gene expression biomarker to identify DNA damage-inducing agents in microarray profiles. Environ Mol Mutagen 59:772-784.

31. Rooney J, Oshida K, Vasani N, Vallanat B, Ryan N, Chorley BN, Wang X, Bell DA, Wu KC, Aleksunes LM, Klaassen CD, Kensler TW, Corton JC. 2018. Activation of Nrf2 in the liver is associated with stress resistance mediated by suppression of the growth hormone-regulated STAT5b transcription factor. PLoS One 13:e0200004.

32. Oshida K, Vasani N, Jones C, Moore T, Hester S, Nesnow S, Auerbach S, Geter DR, Aleksunes LM, Thomas RS, Applegate D, Klaassen CD, Corton JC. 2015. Identification of chemical modulators of the constitutive activated receptor (CAR) in a gene expression compendium. Nucl Recept Signal 13:e002.

33. Oshida K, Vasani N, Thomas RS, Applegate D, Rosen M, Abbott B, Lau C, Guo G, Aleksunes LM, Klaassen C, Corton JC. 2015. Identification of modulators of the nuclear receptor peroxisome proliferator-activated receptor alpha (PPARalpha) in a mouse liver gene expression compendium. PLoS One 10:e0112655.

34. Yang J, Young MJ. 2009. The mineralocorticoid receptor and its coregulators. J Mol Endocrinol 43:53-64.

35. Gomez-Pastor R, Burchfiel ET, Thiele DJ. 2018. Regulation of heat shock transcription factors and their roles in physiology and disease. Nat Rev Mol Cell Biol 19:4-19.

36. Qin L, Guo J, Zheng Q, Zhang H. 2016. BAG2 structure, function and involvement in disease. Cell Mol Biol Lett 21:18.

37. Uchiyama T, Atsuta H, Utsugi T, Oguri M, Hasegawa A, Nakamura T, Nakai A, Nakata M, Maruyama I, Tomura H, Okajima F, Tomono S, Kawazu S, Nagai R, Kurabayashi M. 2007. HSF1 and constitutively active HSF1 improve vascular endothelial function (heat shock proteins improve vascular endothelial function). Atherosclerosis 190:321-9.

38. Goodson ML, Park-Sarge OK, Sarge KD. 1995. Tissue-dependent expression of heat shock factor 2 isoforms with distinct transcriptional activities. Mol Cell Biol 15:5288-93.

39. Wang G, Zhang J, Moskophidis D, Mivechi NF. 2003. Targeted disruption of the heat shock transcription factor (hsf)-2 gene results in increased embryonic lethality, neuronal defects, and reduced spermatogenesis. Genesis 36:48-61.

40. Chen Y, Chen J, Yu J, Yang G, Temple E, Harbinski F, Gao H, Wilson C, Pagliarini R, Zhou W. 2014. Identification of mixed lineage leukemia 1(MLL1) protein as a coactivator

of heat shock factor 1(HSF1) protein in response to heat shock protein 90 (HSP90) inhibition. J Biol Chem 289:18914-27.

41. Cigliano A, Pilo MG, Li L, Latte G, Szydlowska M, Simile MM, Paliogiannis P, Che L, Pes GM, Palmieri G, Sini MC, Cossu A, Porcu A, Vidili G, Seddaiu MA, Pascale RM, Ribback S, Dombrowski F, Chen X, Calvisi DF. 2017. Deregulated c-Myc requires a functional HSF1 for experimental and human hepatocarcinogenesis. Oncotarget 8:90638-90650.

42. Evert M, Frau M, Tomasi ML, Latte G, Simile MM, Seddaiu MA, Zimmermann A, Ladu S, Staniscia T, Brozzetti S, Solinas G, Dombrowski F, Feo F, Pascale RM, Calvisi DF. 2013. Deregulation of DNA-dependent protein kinase catalytic subunit contributes to human hepatocarcinogenesis development and has a putative prognostic value. Br J Cancer 109:2654-64.

43. Liu Y, Liu M, Liu J, Zhang H, Tu Z, Xiao X. 2010. KLF4 is a novel regulator of the constitutively expressed HSP90. Cell Stress Chaperones 15:211-7.

44. Takii R, Fujimoto M, Tan K, Takaki E, Hayashida N, Nakato R, Shirahige K, Nakai A. 2015. ATF1 modulates the heat shock response by regulating the stress-inducible heat shock factor 1 transcription complex. Mol Cell Biol 35:11-25.

45. Okuno M, Muto Y, Kato M, Moriwaki H, Noma A, Tagaya O, Tanabe Y. 1991. Changes in serum and hepatic levels of immunoreactive prolyl hydroxylase in two models of hepatic fibrosis in rats. J Gastroenterol Hepatol 6:271-7.

46. Ryan N, Chorley B, Tice RR, Judson R, Corton JC. 2016. Moving Toward Integrating Gene Expression Profiling Into High-Throughput Testing: A Gene Expression Biomarker Accurately Predicts Estrogen Receptor α Modulation in a Microarray Compendium. Toxicol Sci 151:88-103.

47. Murray JI, Whitfield ML, Trinklein ND, Myers RM, Brown PO, Botstein D. 2004. Diverse and specific gene expression responses to stresses in cultured human cells. Mol Biol Cell 15:2361-74.

48. Jung EJ, Avliyakulov NK, Boontheung P, Loo JA, Nel AE. 2007. Pro-oxidative DEP chemicals induce heat shock proteins and an unfolding protein response in a bronchial epithelial cell line as determined by DIGE analysis. Proteomics 7:3906-18.

49. Xie J, Zhao J, Xiao C, Xu Y, Yang S, Ni W. 2010. Reduced heat shock protein 70 in airway smooth muscle in patients with chronic obstructive pulmonary disease. Exp Lung Res 36:219-26.

50. Gan N, Wu YC, Brunet M, Garrido C, Chung FL, Dai C, Mi L. 2010. Sulforaphane activates heat shock response and enhances proteasome activity through up-regulation of Hsp27. J Biol Chem 285:35528-36.

51. Ianaro A, Ialenti A, Maffia P, Di Meglio P, Di Rosa M, Santoro MG. 2003. Anti-inflammatory activity of 15-deoxy-delta12,14-PGJ2 and 2-cyclopenten-1-one: role of the heat shock response. Mol Pharmacol 64:85-93.

52. Hoshida S, Aoki K, Nishida M, Yamashita N, Igarashi J, Hori M, Kuzuya T, Tada M. 1997. Effects of preconditioning with ebselen on glutathione metabolism and stress protein expression. J Pharmacol Exp Ther 281:1471-5.

53. Shipman M, Lubick K, Fouchard D, Guram R, Grieco P, Jutila M, Dratz EA. 2012. Proteomic and systems biology analysis of monocytes exposed to securinine, a GABA(A) receptor antagonist and immune adjuvant. PLoS One 7:e41278.

54. Hieronymus H, Lamb J, Ross KN, Peng XP, Clement C, Rodina A, Nieto M, Du J, Stegmaier K, Raj SM, Maloney KN, Clardy J, Hahn WC, Chiosis G, Golub TR. 2006. Gene expression signature-based chemical genomic prediction identifies a novel class of HSP90 pathway modulators. Cancer Cell 10:321-30.

55. Dayalan Naidu S, Kostov RV, Dinkova-Kostova AT. 2015. Transcription factors Hsf1 and Nrf2 engage in crosstalk for cytoprotection. Trends Pharmacol Sci 36:6-14.

56. Zhang Y, Ahn YH, Benjamin IJ, Honda T, Hicks RJ, Calabrese V, Cole PA, Dinkova-Kostova AT. 2011. HSF1-dependent upregulation of Hsp70 by sulfhydryl-reactive inducers of the KEAP1/NRF2/ARE pathway. Chem Biol 18:1355-61.

57. Elia G, Polla B, Rossi A, Santoro MG. 1999. Induction of ferritin and heat shock proteins by prostaglandin A1 in human monocytes. Evidence for transcriptional and post-transcriptional regulation. Eur J Biochem 264:736-45.

58. Kansanen E, Jyrkkänen HK, Volger OL, Leinonen H, Kivelä AM, Häkkinen SK, Woodcock SR, Schopfer FJ, Horrevoets AJ, Ylä-Herttuala S, Freeman BA, Levonen AL. 2009. Nrf2-dependent and -independent responses to nitro-fatty acids in human endothelial cells: identification of heat shock response as the major pathway activated by nitro-oleic acid. J Biol Chem 284:33233-41.

59. Dinkova-Kostova AT, Holtzclaw WD, Cole RN, Itoh K, Wakabayashi N, Katoh Y, Yamamoto M, Talalay P. 2002. Direct evidence that sulfhydryl groups of Keap1 are the sensors regulating induction of phase 2 enzymes that protect against carcinogens and oxidants. Proc Natl Acad Sci U S A 99:11908-13.

60. McMahon M, Lamont DJ, Beattie KA, Hayes JD. 2010. Keap1 perceives stress via three sensors for the endogenous signaling molecules nitric oxide, zinc, and alkenals. Proc Natl Acad Sci U S A 107:18838-43.

61. Baird L, Llères D, Swift S, Dinkova-Kostova AT. 2013. Regulatory flexibility in the Nrf2-mediated stress response is conferred by conformational cycling of the Keap1-Nrf2 protein complex. Proc Natl Acad Sci U S A 110:15259-64.

62. Ahn SG, Thiele DJ. 2003. Redox regulation of mammalian heat shock factor 1 is essential for Hsp gene activation and protection from stress. Genes Dev 17:516-28.

63. Lu M, Kim HE, Li CR, Kim S, Kwak IJ, Lee YJ, Kim SS, Moon JY, Kim CH, Kim DK, Kang HS, Park JS. 2008. Two distinct disulfide bonds formed in human heat shock

transcription factor 1 act in opposition to regulate its DNA binding activity. Biochemistry 47:6007-15.

64. Judson R, Houck K, Martin M, Richard AM, Knudsen TB, Shah I, Little S, Wambaugh J, Woodrow Setzer R, Kothiya P, Phuong J, Filer D, Smith D, Reif D, Rotroff D, Kleinstreuer N, Sipes N, Xia M, Huang R, Crofton K, Thomas RS. 2016. Editor's Highlight: Analysis of the Effects of Cell Stress and Cytotoxicity on In Vitro Assay Activity Across a Diverse Chemical and Assay Space. Toxicol Sci 152:323-39.

65. Simmons SO, Fan CY, Ramabhadran R. 2009. Cellular stress response pathway system as a sentinel ensemble in toxicological screening. Toxicol Sci 111:202-25.

66. Jennings P, Limonciel A, Felice L, Leonard MO. 2013. An overview of transcriptional regulation in response to toxicological insult. Arch Toxicol 87:49-72.

67. Zemore R, Shepel LF. 1987. Information seeking and adjustment to cancer. Psychol Rep 60:874.

Figures and tables

Table 1. Biosets used to make HSF1 biomarker.

Bioset number	Bioset name (from BSCE)	Perturbant	Mode	Exposure time	Cell line
1	Malignant melanoma A375 cells uninduced HSF1 shRNA - 100nM HSP990 3hr _vs_ DMSO treatment	NVP-HSP990	HSF1 activation	3 hours	A-375
2	Malignant melanoma A375 cells uninduced control shRNA - 100nM HSP990 3hr _vs_ DMSO treatment	NVP-HSP990	HSF1 activation	3 hours	A-375
3	Malignant melanoma A375 cells induced control shRNA 3d - 100nM HSP990 3hr _vs_ DMSO treatment	NVP-HSP990	HSF1 activation	3 hours	A-375
4	Malignant melanoma A375 cells DMSO treatment - induced HSF1 shRNA 3d _vs_ uninduced	HSF1 shRNA	HSF1 suppression	3 days	A-375
5	Malignant melanoma A375 cells DMSO treatment - induced HSF1 shRNA 3d _vs_ induced control shRNA	HSF1 shRNA	HSF1 suppression	3 days	A-375

6	Malignant melanoma A375 cells 100nM HSP990 3hr - induced HSF1 shRNA 3d _vs_ uninduced	HSF1 shRNA	HSF1 suppression	3 days	A-375
7	Malignant melanoma A375 cells 100nM HSP990 3hr - induced HSF1 shRNA 3d _vs_ induced control shRNA	HSF1 shRNA	HSF1 suppression	3 days	A-375

All biosets were from GSE44867.

Table 2. HSF1 biomarker predictive accuracy for HSF1 activation by chemicals and heat shock.

	HSF1 chemical activation	**HSF1 heat shock activation**
True positives	71	20
False negatives	3	17
True negatives	18	
False positives	0	
Sensitivity	0.96	0.54
Specificity	1	
Balanced accuracy	0.98	
Positive predictive value	1	
Negative predictive value	0.86	

Table 3. Top 20 biosets with positive correlation to the HSF1 biomarker.

Bioset Name (from BSCE)	Factor	Cell line	Public id	HSF1 biomarker (-Log(p-value))
Monocytes exposed to diseal exhaust particles in vitro _vs_ saline control	Diesel Exhaust	Monocytes	GSE34025	16.1
T cell Jurkat A3 cells treated 6hr with 10ug/mL ZnO particles _vs_ 6hr untreated	Zinc Oxide Nanoparticles	Jurkat A3	GSE39444	15.0
PC3 cells + 15-delta prostaglandin J2, 10uM _vs_ DMSO vehicle	15-Deoxy-Delta(12,14)-Prostaglandin J2	PC-3	GSE5258	14.9
PC3 cells + 1,4-chrysenequinone, 15.4uM _vs_ DMSO vehicle	1,4-Chrysenequinone	PC-3	GSE5258	13.9
MCF7 cells + piperlongumine, 12.6uM _vs_ DMSO vehicle	Piperlonguminine	MCF7	GSE5258	13.7
Leukemic cells (K562) 20uM Fe(III) mesoporphyrin treated for 20hr _vs_ DMSO control	Iron(III) Meso-Tetramesitylporphyrin	K-562	GSE52087	13.6
MCF7 cells + celastrol, 2.5uM _vs_ DMSO vehicle	Celastrol	MCF7	GSE5258	12.7

Prostate cancer androgen-independent PC3 cells + 15uM sulforaphane for 6hr _vs_ vehicle (DMSO)	Sulforafan	PC-3	GSE48812	11.7
Bronchial epithelial cells 2hr post-15min cigarette smoke exposure _vs_ air exposure	Tobacco Smoke	Bronchial epithelial	GSE10718	11.3
HL60 cells + piperlongumine, 12.6uM _vs_ DMSO vehicle	Piperlonguminine	HL-60	GSE5258	11.2
Prostate cancer androgen-dependent LnCaP cells + 15uM sulforaphane for 6hr _vs_ vehicle (DMSO)	Sulforafan	LNCaP	GSE48812	11.2
Hepatocytes of female donors treated 24hr with 2500uM furosemide _vs_ 0uM	Furosemide	Hepatocytes	TG-GATES	11.2
NHBE cells 4hr post-exposure to 15min of light cigarette smoke _vs_ mock exposure	Tobacco Smoke	Bronchial epithelial	GSE10700	10.9
Bronchial epithelial cells 4hr post-15min cigarette smoke exposure _vs_ air exposure	Tobacco Smoke	Bronchial epithelial	GSE10718	10.9

Lymphoblastoid B cells treated 2hr with 5uM sodium arsenite _vs_ untreated controls	Sodium Arsenite	B-Lymphocytes	GSE51454	10.8
Monocytes from lymphatic filariasis patients - 8mo post albendazole treatment _vs_ pretreatment	Albendazole	Monocytes	GSE2135	10.7
Hepatocytes of female donors treated 24hr with 70uM allyl alcohol _vs_ 0uM	Allyl Alcohol	Hepatocytes	TG-GATES	10.6
HL60 cells + 15-delta prostaglandin J2, 10uM _vs_ DMSO vehicle	15-Deoxy-Delta(12,14)-Prostaglandin J2	HL-60	GSE5258	10.4
Monocytes from lymphatic filariasis patients 8mo post albendazole treatment _vs_ healthy controls	Albendazole	Monocytes	GSE2135	10.4
PC3 cells + scoulerine, 12.2uM _vs_ DMSO vehicle	Scoulerine	PC-3	GSE5258	10.3

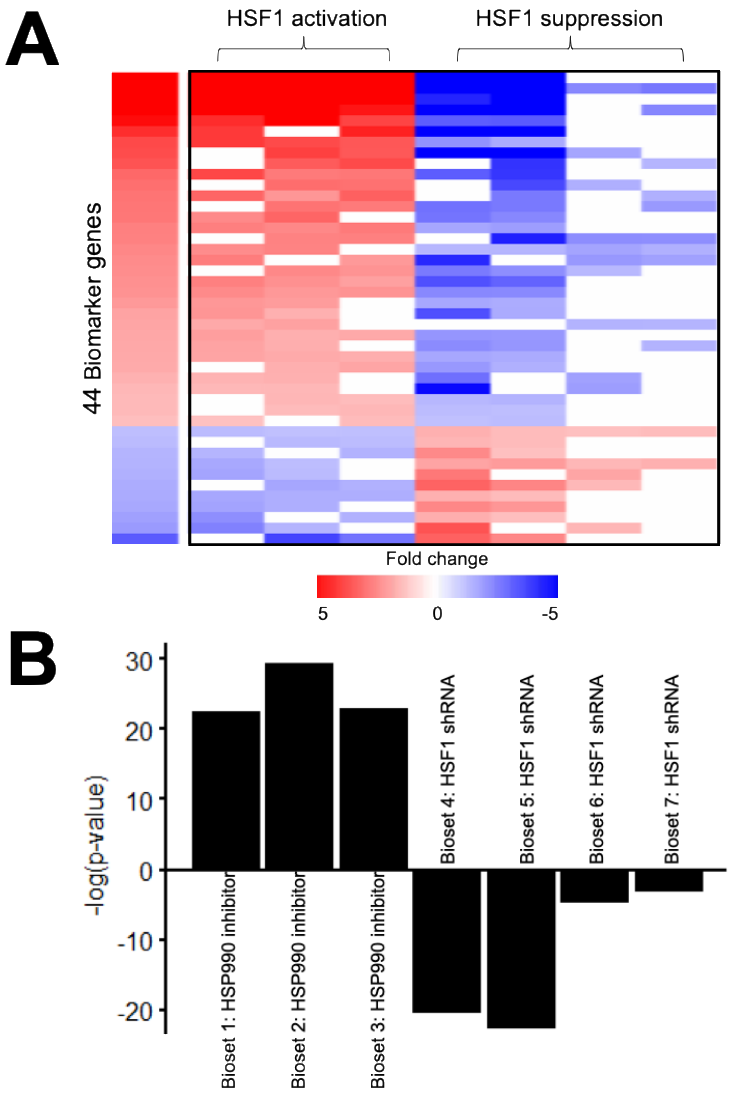

Figure 1. *Identification of HSF1 biomarker genes.* Genes were derived from comparisons between A375 cells treated with the HSP90 inhibitor NVP-HSP990 for 3 hrs in wild-type cells and cells in which HSF1 expression was knocked down by targeted shRNA (67). Two filters were used to identify HSF1 biomarker genes. (1) Consistent up- or down-regulation in at least 2 of the 3 HSF1 activation biosets. (2) Opposite regulation in at least 2 of the 4 HSF1 suppression biosets. The biomarker gene fold-changes were derived from the average fold-change values across the HSF1 activation biosets. The list of biosets used are found in **Table 1**. (A) Heat map

of the fold-changes of the 44 HSF1 biomarker genes across each bioset used to build the biomarker. (B) Correlation of each bioset to the biomarker genes. The 44 HSF1 biomarker genes were compared to each bioset using the Running Fisher test and the significance is indicated by the -log(p-value). The compound used to modulate HSF1 in each bioset is indicated.

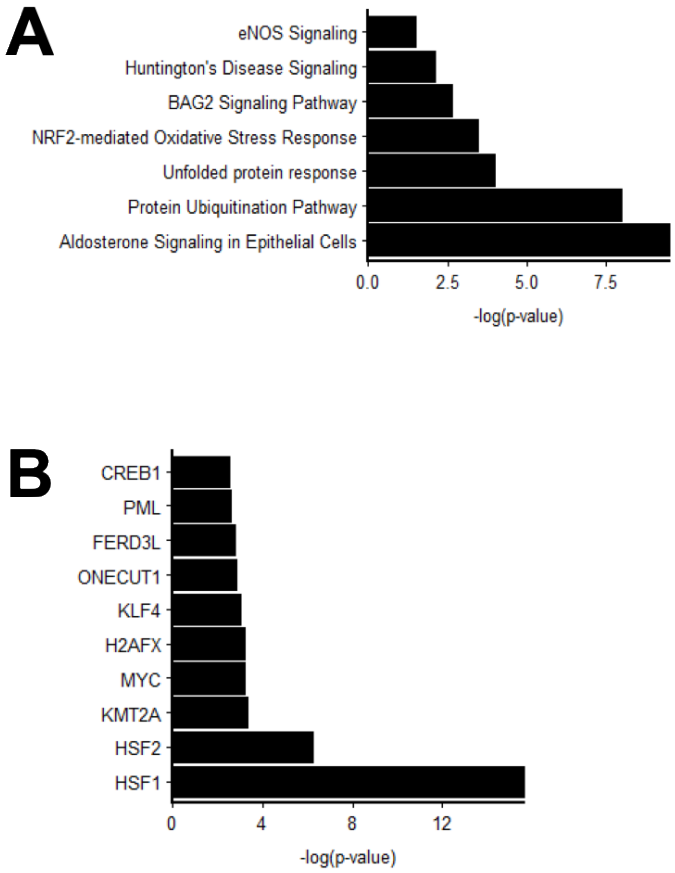

Figure 2. *Characterization of the HSF1 biomarker genes.* The HSF1 biomarker genes and their associated fold-changes were analyzed in Ingenuity Pathway Analysis. (A) List of top canonical pathways. (B) List of top transcription factors predicted to regulate the expression of HSF1 biomarker genes.

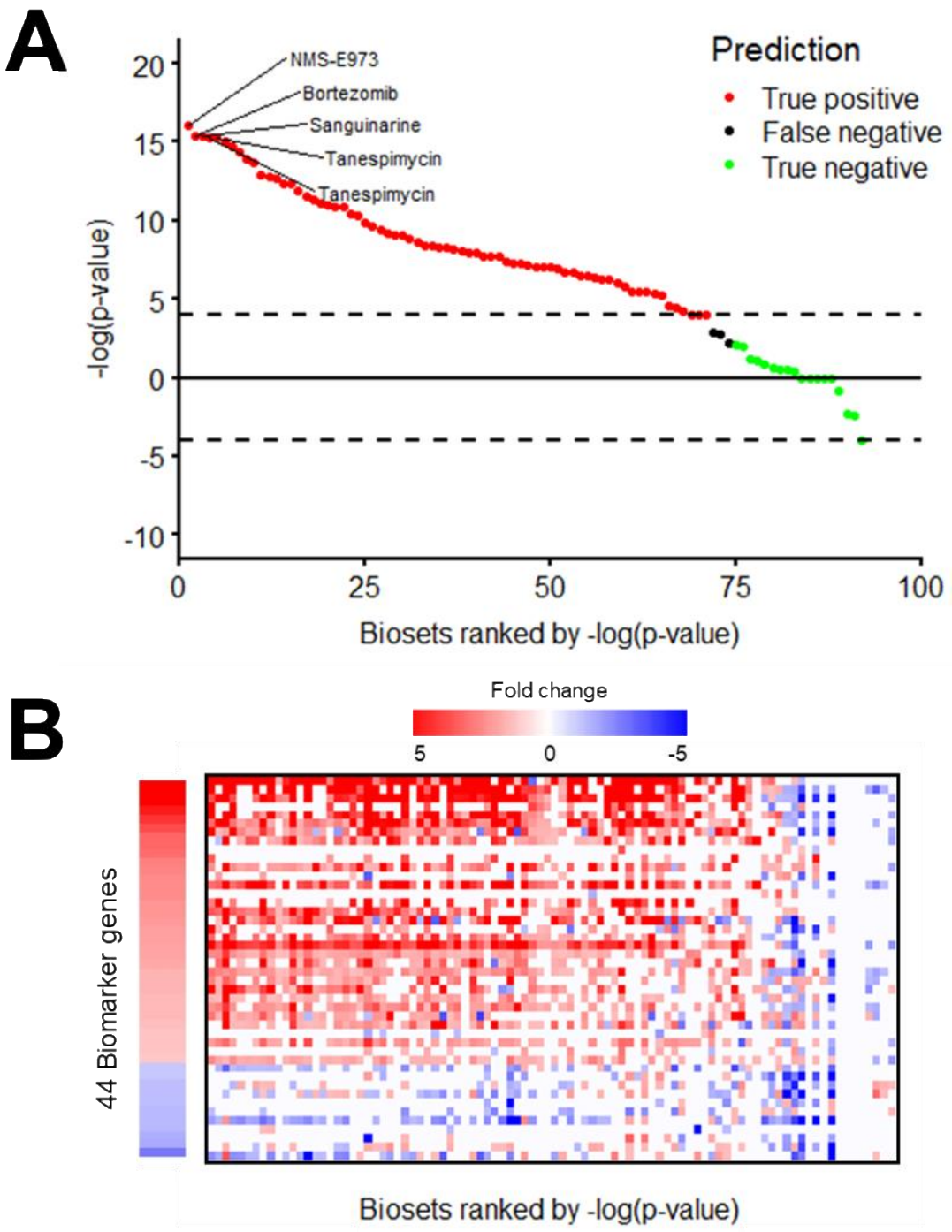

Figure 3. *The biomarker accurately predicts HSF1 chemical activation.* (A) The HSF1 biomarker was compared to 87 chemical and 12 genetic treatment biosets known to activate or suppress HSF1 using the Running Fisher test. The significance of correlation to the HSF1 biomarker for each bioset is ordered by -log(p-value)s. Biosets included those known to activate HSF1 (true

positives; red), biosets that do not activate HSF1 (true negatives; green), and false negative biosets predicted to activate HSF1 but did not meet the cut off (-log(p-value) ≥ 4; black). The top 5 biosets of 4 chemical treatments with the highest -Log(p-value)s are shown.

(B) The fold changes for the biomarker genes across the biosets are represented as a heat map in the same order as those found in A.

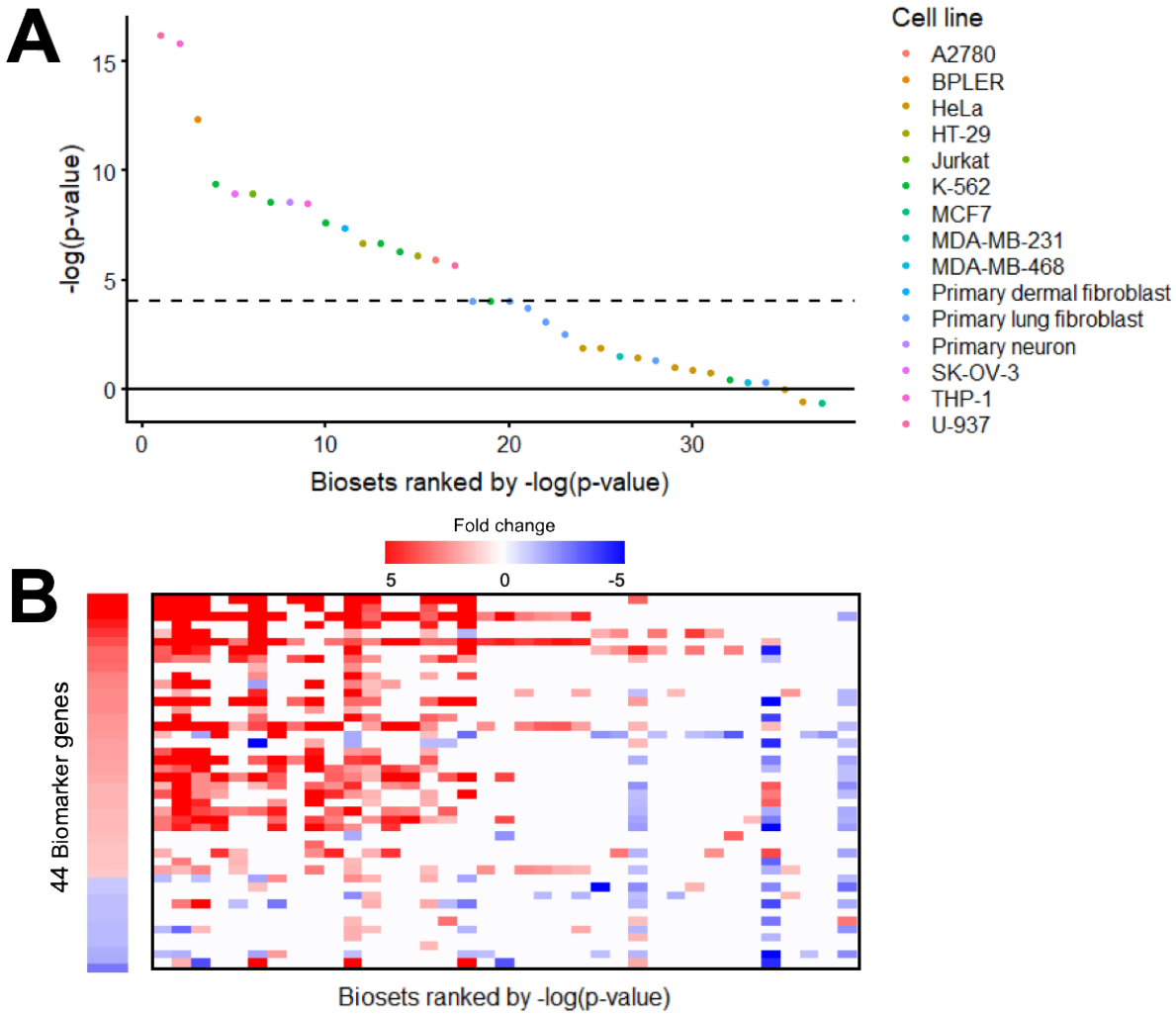
A
-log(p-value)
15
10
5
0
0
10
20
30
Biosets ranked by -log(p-value)
Cell line
A2780
BPLER
HeLa
HT-29
Jurkat
K-562
MCF7
MDA-MB-231
MDA-MB-468
Primary dermal fibroblast
Primary lung fibroblast
Primary neuron
SK-OV-3
THP-1
U-937
B
Fold change
5
0
-5
44 Biomarker genes
Biosets ranked by -log(p-value)

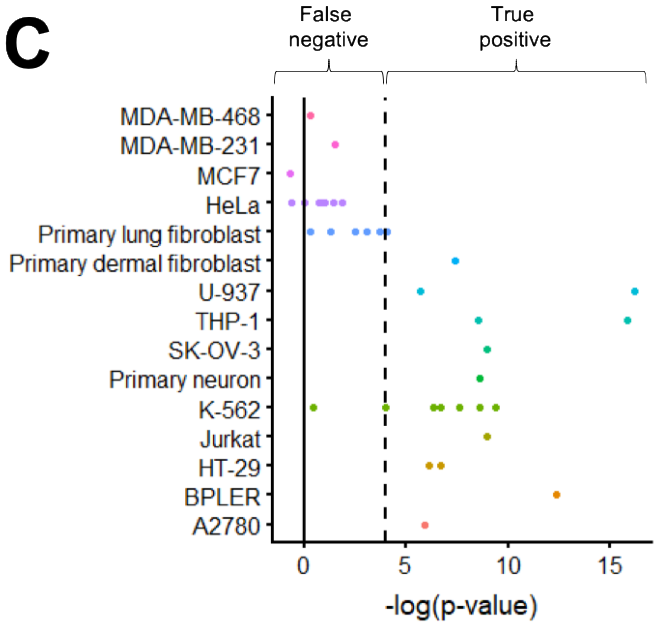
C
False negative
True positive
MDA-MB-468
MDA-MB-231
MCF7
HeLa
Primary lung fibroblast
Primary dermal fibroblast
U-937
THP-1
SK-OV-3
Primary neuron
K-562
Jurkat
HT-29
BPLER
A2780
0
5
10
15
-log(p-value)

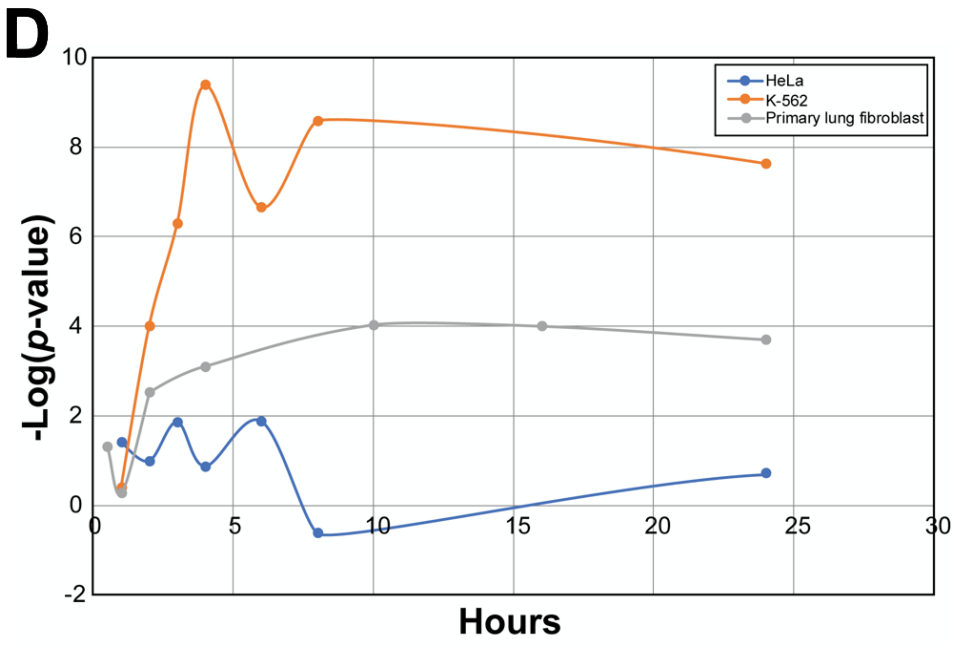
D
HeLa
K-562
Primary lung fibroblast
-Log(p-value)
10
8
6
4
2
0
-2
0
5
10
15
20
25
30
Hours

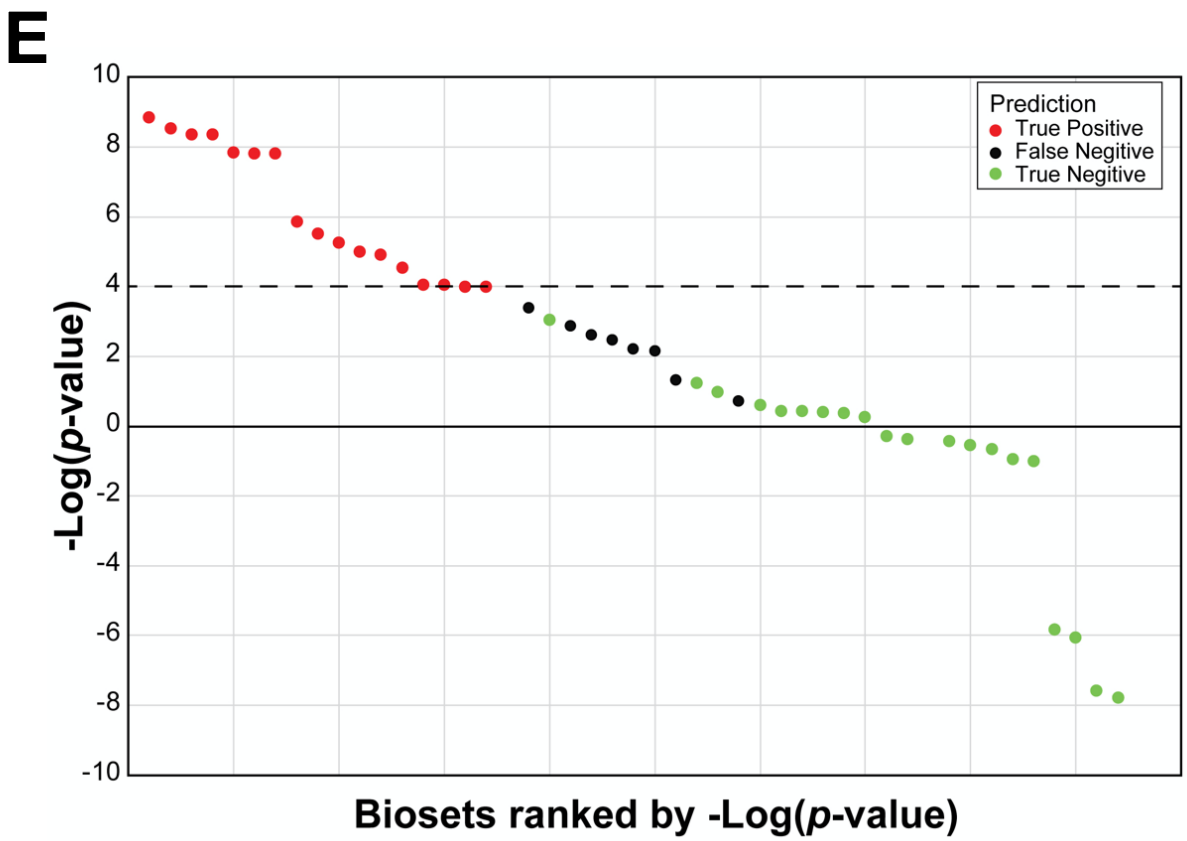

Figure 4. *The HSF1 biomarker can predict heat shock conditions in humans and mice.* The biomarker was compared to a list of 37 heat shock treated biosets from various human cell-lines using the Running Fisher test. (A) The bioset significance of correlation to the HSF1 biomarker is ordered by the -log(p-value). The cell line or cell source used is indicated. (B) The fold changes for the biomarker genes across the biosets are represented as a heat map in the same order as those found in A. (C) The biosets were grouped by cell line and the significance of biomarker correlation to each bioset is indicated by a -log(p-value). Biosets with ≥ 4 -log(p-value) were considered true positives for heat shock and biosets below < 4 -log(p-value) were considered false negatives. (D) Time course of heat shock response in three human cell lines. HeLa, K-562, and primary lung fibroblasts were exposed to 42 degrees heat for 30 min and then analyzed for gene expression changes after the indicated time at 37 degrees (data from GSE3074). Each treatment was compared to the corresponding control at time 0 and the

indicated biosets were compared to the biomarker using the Running Fisher test. (E) The HSF1 biomarker was compared to 45 heat shock or hsp activator chemical exposure conditions derived from mouse cells or tissues. The significance of correlation of each bioset to the HSF1 biomarker is ordered by the -log(p-value). Biosets included those known to activate HSF1 (true positives; red) and false negative biosets predicted to activate HSF1 but did not meet the cut off (-log(p-value) ≥ 4; black).

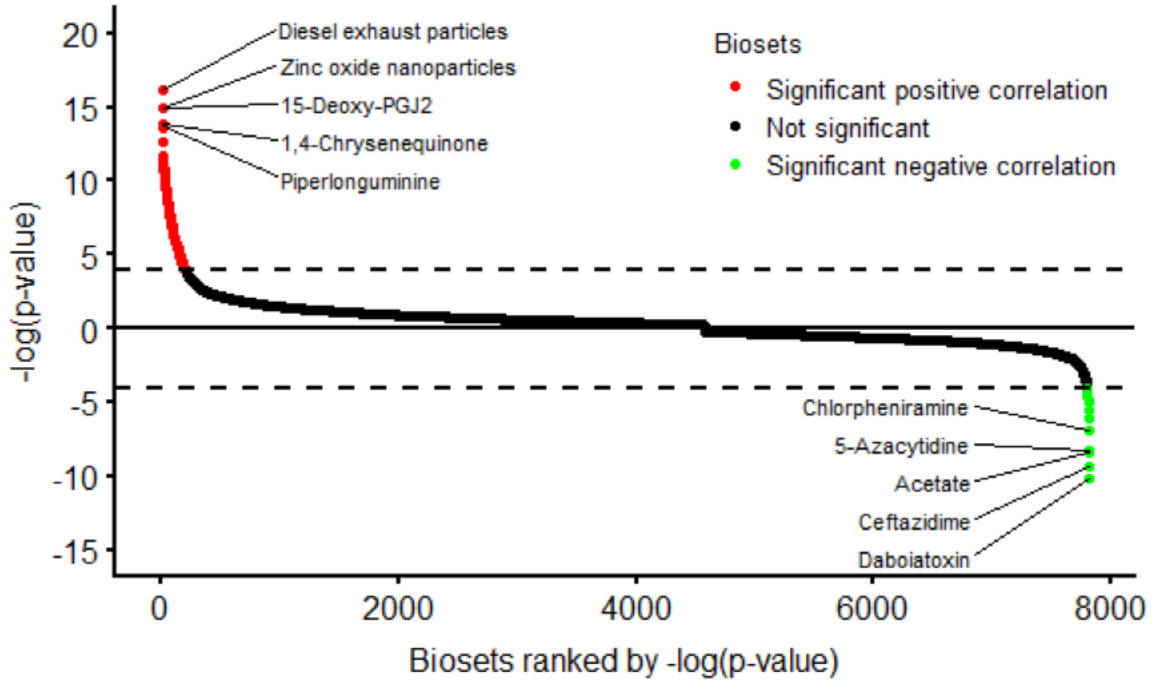

Figure 5. *HSF1 biomarker identifies novel chemicals that activate or suppress HSF1.*

The HSF1 biomarker was compared to a list of 7,823 chemical treatment biosets using the Running Fisher test. The resulting correlation -Log(p-value)s were ranked ordered. Biosets were considered significantly correlated to the HSF1 biomarker if the -log(p-value) was ≥ |4|. Biosets with a significant positive correlation are colored red and biosets with a significant negative correlation are colored green. Biosets that did not meet the significance cutoff are colored black. The chemicals from the top 5 positively and negatively correlated biosets are indicated. The biosets used to make the HSF1 biomarker and the biosets from chemical treatments used to determine biomarker accuracy were not included in this analysis.

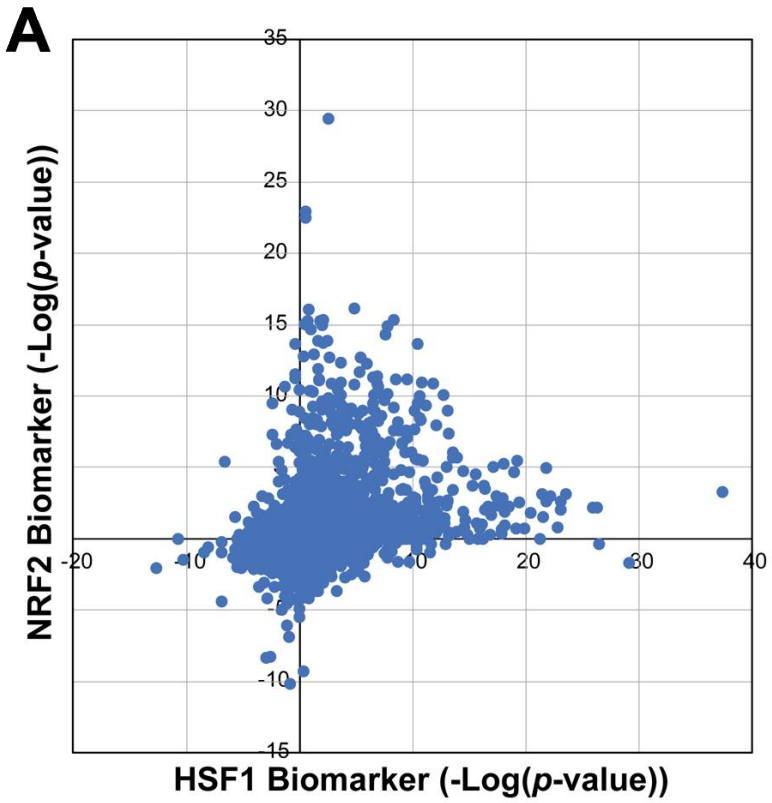
A
NRF2 Biomarker (-Log(p-value))
HSF1 Biomarker (-Log(p-value))
35
30
25
20
15
10
-10
-15
-20
-10
0
20
30
40

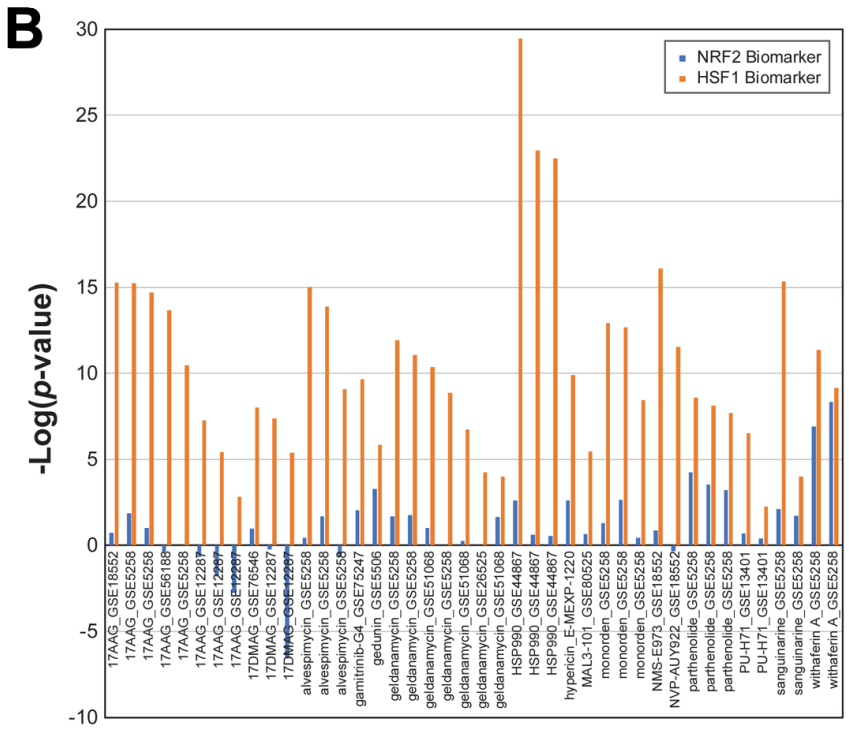
B
-Log(p-value)
NRF2 Biomarker
HSF1 Biomarker
30
25
20
15
10
5
0
-5
-10
17AAG_GSE18552
17AAG_GSE5258
17AAG_GSE5258
17AAG_GSE56188
17AAG_GSE5258
17AAG_GSE12287
17AAG_GSE12287
17AAG_GSE12287
17DMAG_GSE76546
17DMAG_GSE12287
17DMAG_GSE12287
alvespimycin_GSE5258
alvespimycin_GSE5258
alvespimycin_GSE5258
gamitrinib-G4_GSE75247
geldunin_GSE5506
geldanamycin_GSE5258
geldanamycin_GSE5258
geldanamycin_GSE51068
geldanamycin_GSE5258
geldanamycin_GSE51068
geldanamycin_GSE26525
geldanamycin_GSE51068
HSP990_GSE44867
HSP990_GSE44867
HSP990_GSE44867
hypericin_E-MEXP-1220
MAL3-101_GSE80525
monorden_GSE5258
monorden_GSE5258
monorden_GSE5258
NMS-E973_GSE18552
NVP-AUY922_GSE18552
parthenolide_GSE5258
parthenolide_GSE5258
parthenolide_GSE5258
PU-H71_GSE13401
PU-H71_GSE13401
sanguinarine_GSE5258
sanguinarine_GSE5258
withaferin A_GSE5258
withaferin A_GSE5258

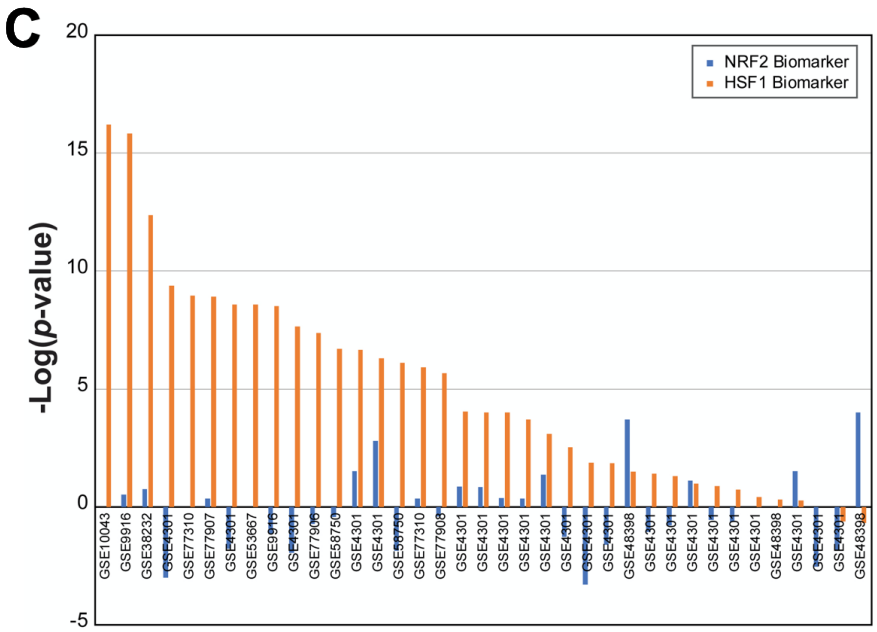
C
NRF2 Biomarker
HSF1 Biomarker
-Log(p-value)
20
15
10
5
0
-5
GSE10043
GSE9916
GSE38232
GSE4301
GSE77310
GSE77907
GSE4301
GSE53667
GSE9916
GSE4301
GSE77907
GSE58750
GSE4301
GSE4301
GSE58750
GSE77310
GSE77908
GSE4301
GSE4301
GSE4301
GSE4301
GSE4301
GSE4301
GSE4301
GSE48398
GSE4301
GSE4301
GSE4301
GSE4301
GSE4301
GSE4301
GSE48398
GSE4301
GSE4301
GSE48398

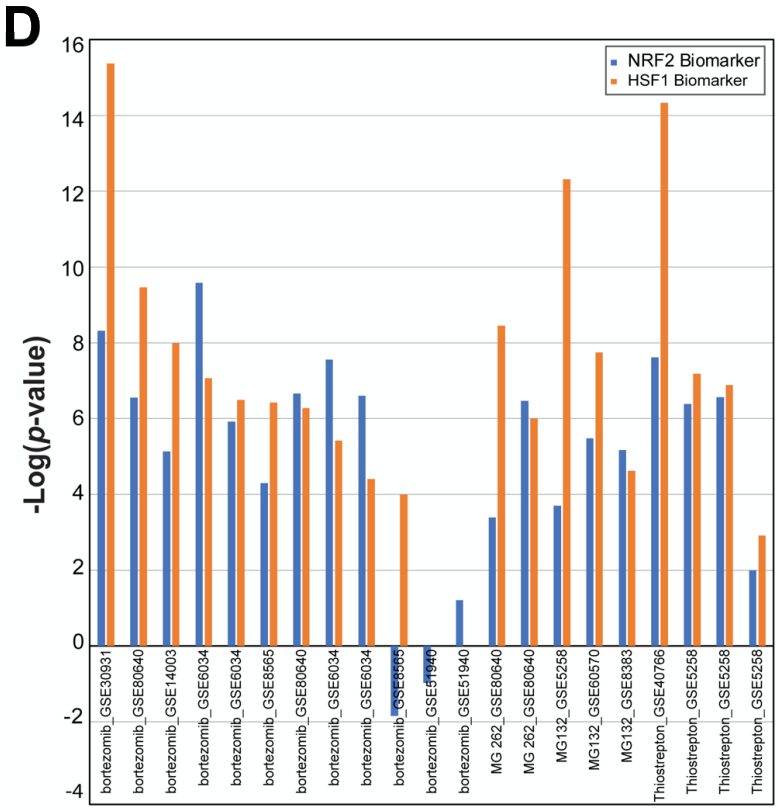
D
NRF2 Biomarker
HSF1 Biomarker
-Log(p-value)
16
14
12
10
8
6
4
2
0
-2
-4
bortezomib_GSE30931
bortezomib_GSE80640
bortezomib_GSE14003
bortezomib_GSE6034
bortezomib_GSE6034
bortezomib_GSE8565
bortezomib_GSE80640
bortezomib_GSE6034
bortezomib_GSE6034
bortezomib_GSE8565
bortezomib_GSE51940
bortezomib_GSE51940
MG 262_GSE80640
MG 262_GSE80640
MG132_GSE5258
MG132_GSE60570
MG132_GSE8383
Thiostrepton_GSE40766
Thiostrepton_GSE5258
Thiostrepton_GSE5258
Thiostrepton_GSE5258

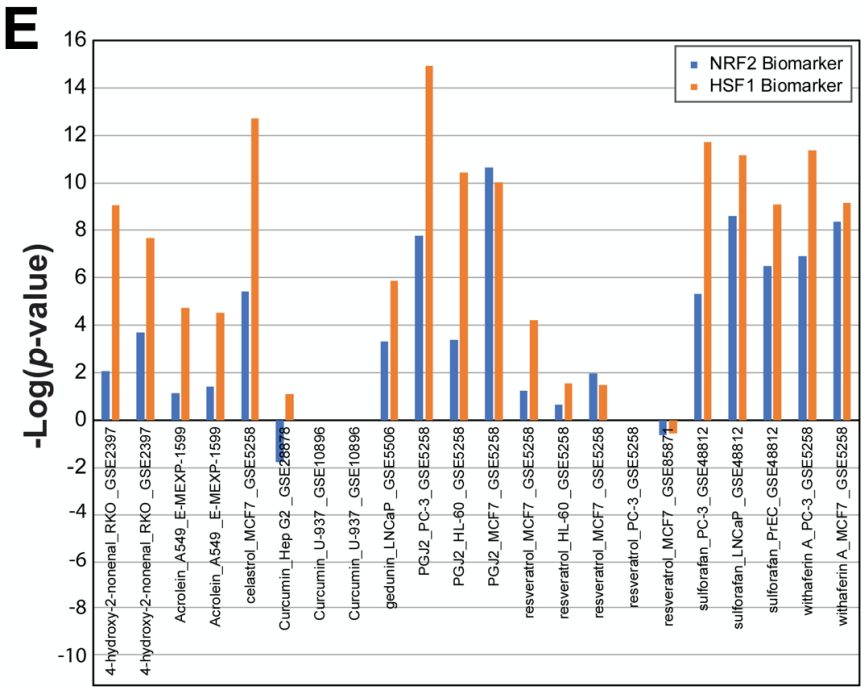

Figure 6. *Relationships between oxidative stress and activation of HSF1.* (A) All chemical biosets with significant HSF1 activation were compared to the NRF2 biomarker. The graph shows the relationship for each bioset between the significance of the activation of HSF 1 and the significance of the activation of NRF2. (B) Lack of NRF2 activation by HSP inhibitors. (C) Lack of NRF2 activation by heat shock. (D) Proteasomal inhibitors activate NRF2. (E) Activation of HSF1 and nrf by chemicals known to activate both factors. Chemicals were selected from those in Naidu et al. (55).

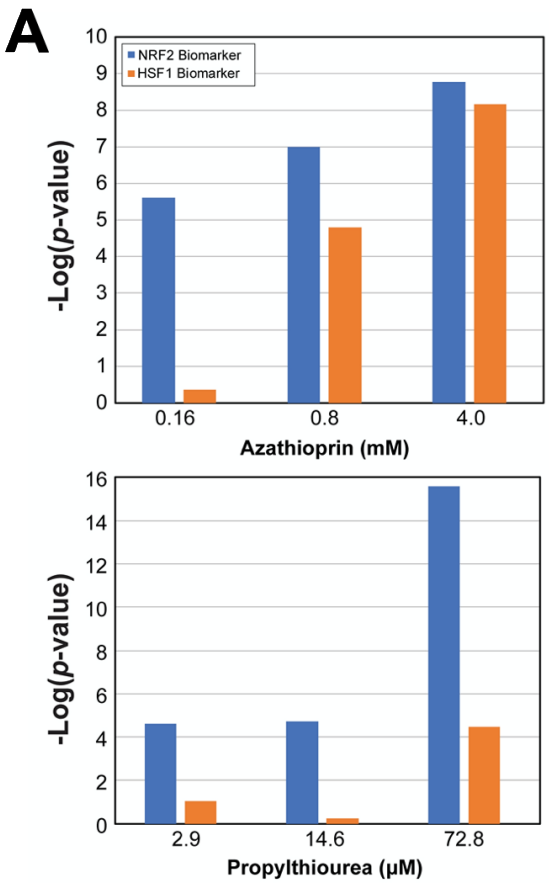
A
NRF2 Biomarker
HSF1 Biomarker
-Log(p-value)
0.16
0.8
4.0
Azathioprin (mM)
2.9
14.6
72.8
Propylthiourea (µM)

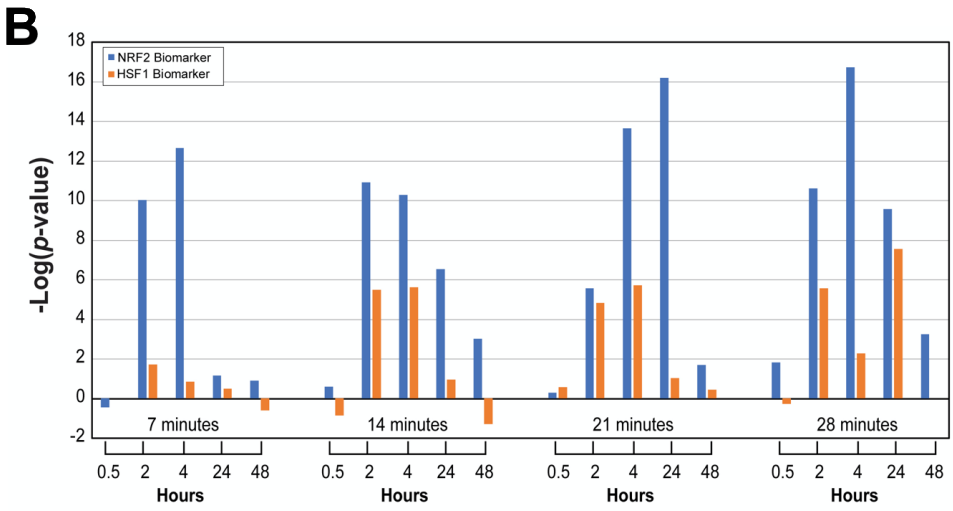
B
NRF2 Biomarker
HSF1 Biomarker
-Log(p-value)
7 minutes
14 minutes
21 minutes
28 minutes
0.5 2 4 24 48
Hours

C

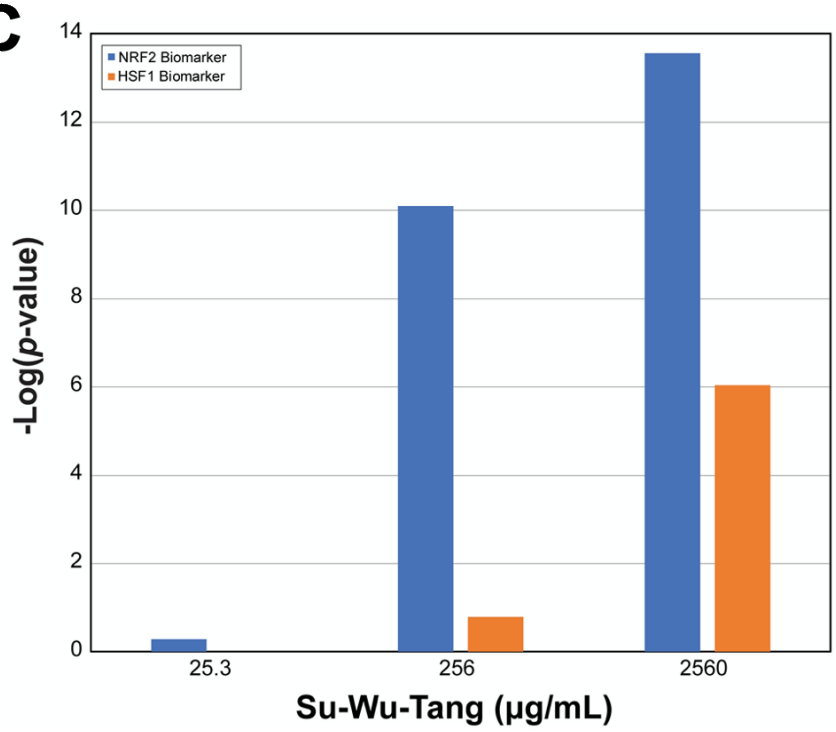
NRF2 Biomarker
HSF1 Biomarker
-Log(p-value)
14
12
10
8
6
4
2
0
25.3
256
2560
Su-Wu-Tang (µg/mL)

D

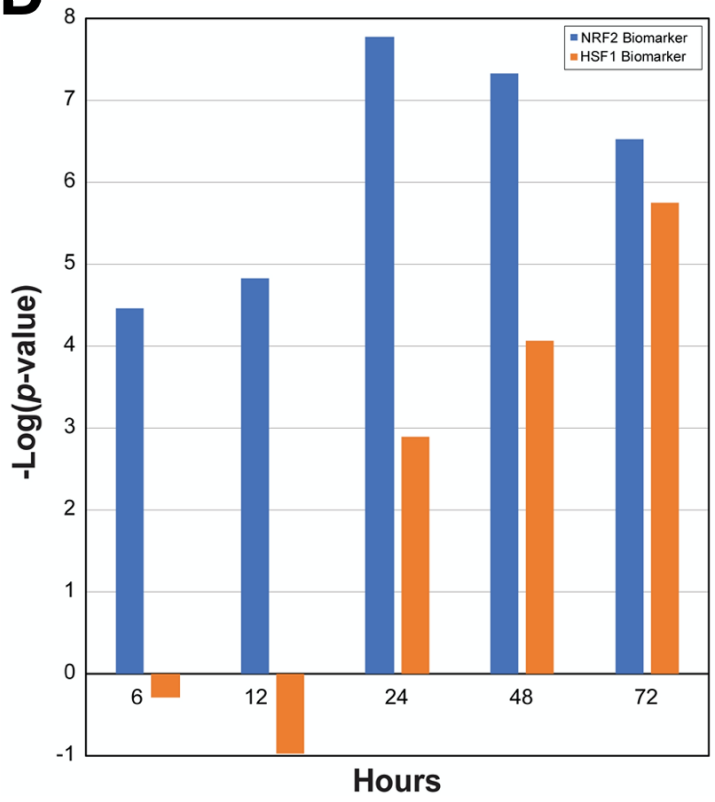
NRF2 Biomarker
HSF1 Biomarker
-Log(p-value)
8
7
6
5
4
3
2
1
0
-1
6
12
24
48
72
Hours

Figure 7. *Chemicals induce NRF2 at lower concentrations and at earlier times than HSF1.* A number of microarray experiments were examined to determine the relationships between activation of NRF2 and HSF1. Statistically-filtered gene lists were compared in a pair-wise manner to the biomarkers for NRF2 or HSF1 using the Running Fisher test. (A) Primary human hepatocytes were exposed to three concentrations of two chemicals (azathioprin, propylthiourea) for 24 hrs (data from the TG-GATES study). (B) Effects of 15% tobacco smoke in bronchial epithelial AIR-100 cells. Cells were exposed to 15% tobacco smoke for 7, 14, 21, or 28 min and then after replacement with synthetic air, gene expression was evaluated at 5 different times (0.5 – 48 hrs) (data from MTAB-874). (C) Effects of the Chinese herbal supplement si-wu-tang in MCF-7 cells (data from GSE23610). (D) Effects of hemin (50 uM) on K-562 cells at increasing times of exposure (data from GSE1036).

Supplementary figures and tables

Table S1. Top 20 biosets with negative correlation to the HSF1 biomarker.

Bioset Name (from BSCE)	Factor	Cell Line	Public id	HSF1 biomarker (-Log(p-value))
THP-1 cell line infected with B. pseudomallei and Daboiatoxin treated _vs_ untreated	Daboiatoxin	THP-1	GSE7577	-10.2
THP-1 cell line infected with B. pseudomallei and ceftazidime treated _vs_ untreated	Ceftazidime	THP-1	GSE7577	-9.3
Glioblastoma LN229 cells 1mM glucose and 5mM acetate treated 24hr _vs_ glucose only	Acetate	LN229	GSE57488	-8.3
MM1 cell line + 5-aza-2-deoxycytidine 0.5uM _vs_ control	5-Azacytidine	MM1	E-MEXP-1269	-8.3
Hepatocytes of female donors treated 24hr with 90uM chlorpheniramine _vs_ 0uM	Chlorpheniramine	Primary hepatocytes	TG-GATES	-6.9
MM1 cell line + trichostatin A 100 ng per mL _vs_ control	Trichostatin A	MM1	E-MEXP-1269	-6.1
Hepatocytes of female donors treated 24hr with 35uM promethazine _vs_ 0uM	Promethazine	Primary hepatocytes	TG-GATES	-5.5
Melanoma Me23682 cells control siRNA for 24hr then 500nM PLX4720 treated 8hr _vs_ untreated	Plx4720	Me23682	GSE34686	-5.0
Hepatocytes of female donors treated 24hr with 15uM imipramine _vs_ 0uM	Imipramine	Primary hepatocytes	TG-GATES	-4.9
Prostate cancer VCaP cells control siRNA - R1881 treated _vs_ ethanol control	R1881	VCaP	GSE60836	-4.5
HepG2 human hepatocyte cell line cultured with 25mM (high) glucose _vs_ 2.7mM (low)	Glucose	HepG2	GSE22074	-4.4
Hepatocytes of female donors treated 24hr with 150uM diltiazem _vs_ 0uM	Diltiazem	Primary hepatocytes	TG-GATES	-4.3
Pancreatic progenitors (INS+) derived from HES-3 ES cells treated 8d with 10uM H-1152 _vs_ DMSO	H 1152	Pancreatic progenitors	GSE84325	-4.2
Rectal mucosal biopsies of ulcerative colitis non-inflamed - ex vivo 50mM 5-ASA 6hr _vs_ untreated	Mesalamine	Rectal mucosal biopsies	GSE46451	-4.2

Melanoma Me23682 cells control siRNA for 24hr then 5nM PD0235901 treated 8hr _vs_ untreated	Pd 0325901	Me2368 2	GSE 3468 6	-4.2
Glioblastoma LN229 cells 10mM glucose treated 24hr _vs_ 1nM	Glucose	LN229	GSE 5748 8	-4.1
MCF7 cells + cicloheximide, 14.2uM _vs_ DMSO vehicle	Cyclohexi mide	MCF-7	GSE 5258	-4.1
Bronchial epithelial BEAS-2B cells treated 3wk - 10nM TCDD _vs_ acetone controls	Tetrachloro dibenzodio xin	BEAS-2B	GSE 8388 6	-4.0
Ovarian cancer cell line MCAS 1uM NVP-BEZ235 treated 6hr _vs_ DMSO control	Nvp Bez235	MCAS	GSE 2899 2	-4.0
Prostate cancer LNCaP cells treated 6hr with 35uM PPC _vs_ DMSO	Phenproco umon	LNCaP	GSE 9478 3	-4.0

Figure S1. *HSF1-dependence of expression of HSF1 biomarker genes.* Heatmap showing the expression of the biomarker genes after exposure to NVP-HSP990 in A375 cells expressing a control short hairpin RNA (shRNA) (no induction) or expressing a shRNA targeting the *HSF1* gene (induction).

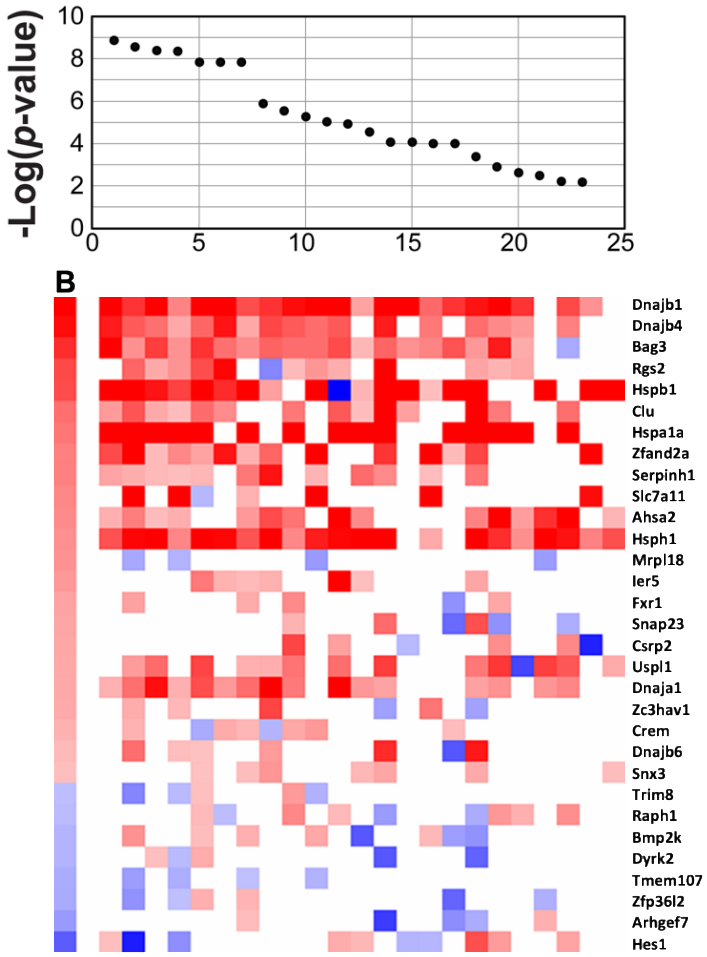

Figure S2. *Comparison of heat shock biosets from mouse tissues to the HSF1 biomarker.* The top 23 most significant biosets were examined. (Top) Bioset -Log(p-value). (Bottom) Heat map of expression of genes in the biomarker for the corresponding 23 biosets.

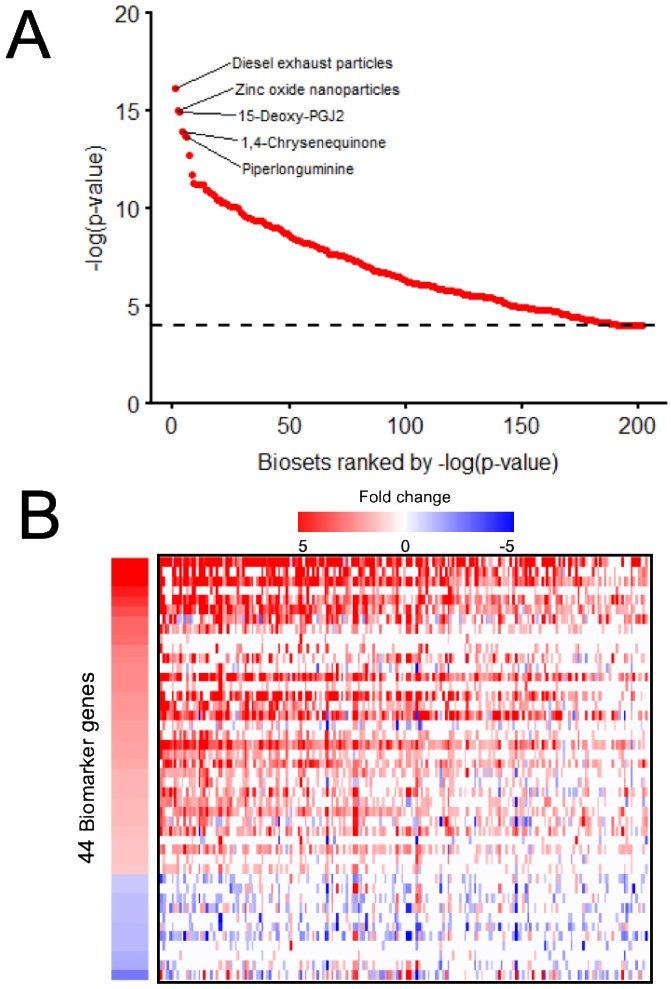

Figure S3. *Biosets with significant positive correlation to the HSF1 biomarker including those from CMAP.* (A) The HSF1 biomarker was compared to all human gene expression biosets using the Running Fisher. There were 202 biosets from chemical treatments with a significant positive correlation. The significance of each correlated bioset is ranked by -log(p-value). (B) The fold change values for the 44 HSF1 biomarkers genes across the 202 biosets with a significant positive correlation are shown in a heat map. (C) Activation of HSF1 by CMAP chemicals across three cell lines. Chemicals were ordered based on number of cell lines the chemical activated HSF1 and the significance of the correlation to the biomarker. Bright red in the heat map indicates activation of HSF1 by the chemical in that cell line.